Durham E-Theses

A spectroscopic study of sunscreens

Allison Elizabeth Jones

A

SPECTROSCOPIC

STUDY OF

SUNSCREENS

Allison Elizabeth Jones

Department of Chemistry, University of Durham, Durham.

Submitted in partial fulfilment of the requirements for the degree of

Doctor of Philosophy, University of Durham.

November 2000
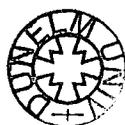
DECLARATION

The work described in this thesis was carried out at the Department of Chemistry, University of Durham between October 1997 and September 2000, unless otherwise stated. This thesis is the work of the author except where acknowledged by reference, and has not been submitted for any other degree.

STATEMENT OF COPYRIGHT

ABSTRACT

Exposure to UV radiation is known to result in the development of skin cancer and the use of protectants in the form of topically applied sunscreens is becoming widespread. The compounds used within sunscreen formulations are subject to stringent tests and must be approved for use by such bodies as COLIPA (EC), or the FDA (U.S.). Despite these testing procedures the photochemical and photophysical properties of many of the active ingredients are poorly understood and not well documented.

This study presents the results of detailed photophysical investigations of two sunscreen agents. Menthyl anthranilate is currently approved for use in commercially available formulations by the FDA, and N-acetyl-menthyl anthranilate has been synthesised as an analogue of N-acetyl-homomenthyl anthranilate, a compound approved for use by COLIPA until 1989. This work has highlighted some disturbing properties of these compounds. Following absorption of light both compounds fluoresce in UV-A region. Population of the triplet state also occurs to a significant extent, producing long lived species which are readily quenched by oxygen generating singlet oxygen, a potentially damaging species that has been linked to DNA damage. Furthermore, the triplet state energy of N-acetyl-menthyl anthranilate has been shown to be ~315 kJmol^{-1}, high enough to sensitise the formation of thymine dimers in the skin, another potential source of DNA damage.

A thorough understanding of the behaviour of sunscreen formulations in contact with skin is vital. *In vivo* studies are made difficult due to restrictions in the sampling methods for currently used spectroscopic techniques such as UV and fluorescence. This work demonstrates the use of infrared spectroscopy, utilising an ATR probe and a flat ATR crystal, to analyse sunscreen formulations present on skin at normal usage levels. The technique has been used successfully to identify the individual active components within the formulations, probe the water-resistance properties and monitor changes that occur within the formulations following irradiation. A relationship between the IR absorbance values and Sun Protection Factor (SPF) values of any given formulation has been demonstrated and this has been used to test the water resistance claims of the manufacturers.

<u>*ACKNOWLEDGEMENTS*</u>

CONTENTS

Chapter One – Introduction

Chapter Two – Experimental Techniques

Chapter Three - The Photophysical Properties of Menthyl and Methyl Anthranilate

Chapter Four - The Photophysical Properties of N-acetyl-menthyl Anthranilate

Chapter Five – Detection and Analysis of Sunscreens using Infrared Spectroscopy

Chapter Six - Water resistance testing of Sunscreens using Infrared Spectroscopy

*Appendix A - Photochemistry of the π-Extended 9,10-Bis(1,3-dithiol-2-ylidene)-9,10-
dihydroanthracene System: Generation and Characterisation of the
Radical Cation, Dication and Derived Products*

Appendix B - Publications, Presentations, Courses and Seminars

LIST OF FIGURES

Chapter Three   *Title of Figure*   *Page*

13

Chapter Six   *Title of Figure*   *Page*

14

LIST OF TABLES

ABBREVIATIONS

General

DNA	Deoxyribonucleic acid
EC	European Community
FDA	Food and Drug Administration (U.S.)
FWHM	Full width at half maximum
IR	Infrared
MED	Minimal erythemal dose
SPF	Sun protection factor
U.S.	United States
UV	Ultraviolet
UV-A	Ultraviolet-A (320 nm < λ < 400 nm)
UV-B	Ultraviolet-B (290 nm < λ < 320 nm)
UV-C	Ultraviolet-A (190 nm < λ < 290 nm)

Solvents

EPA	Solvent mixture consisting of a 5:5:2 mixture of diethyl ether : iso-pentane : ethanol
EtOH	Ethanol
i-P	*iso*-pentane
MCH	Methylcyclohexane
MeOH	Methanol

Symbols

ε	Molar absorption coefficient/ $dm^3 mol^{-1} cm^{-1}$
λ_{em}	Emission wavelength/ nm
λ_{ex}	Excitation wavelength/ nm
λ_{max}	Wavelength of maximum absorbance or emission/ nm

Φ_f Fluorescence quantum yield

τ_ϕ Fluorescence lifetime/ ns

E_T Triplet state energy/ kJmol^{-1}

τ_T Triplet state lifetime/ ms

k_{O_2} Oxygen-quenching rate constant/ dm^{3}mol^{-1}s^{-1}

k_{self} Self-quenching rate constant/ dm^{3}mol^{-1}s^{-1}

Φ_Δ Singlet oxygen generation quantum yield

k_Δ Rate constant for the quenching of singlet oxygen/ dm^{3}mol^{-1}s^{-1}

Constants

c Speed of light, 2.998×10^8 ms^{-1}

h Planck constant, 6.626×10^{-34} Js^{-1}

N_A Avogadro constant, 6.022×10^{23} mol^{-1}

Chapter 1

Introduction

1.1. UV radiation and the need for protection

1.1.1. UV Radiation

Life on Earth depends both directly and indirectly on light (electromagnetic radiation) and its influence on chemistry[1]. The electromagnetic spectrum is shown in figure 1.1. The boundaries between the regions are arbitrary and different values are often quoted in the literature.
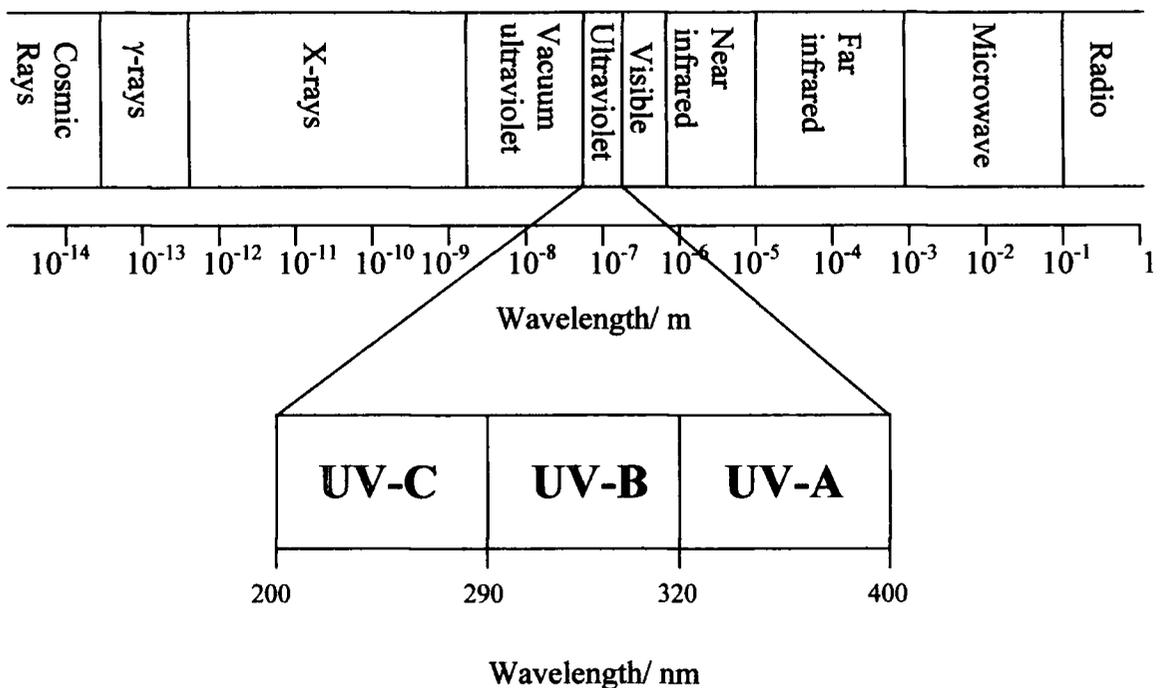
Figure 1.1. The Electromagnetic Spectrum.

A wide range of electromagnetic radiation from the sun reaches the earth's surface. The ultraviolet region can be sub-divided into three sections, as shown in figure 1.1. The harmful solar rays come from the short wavelength end of the sunlight spectrum. Exposure to solar UV radiation is the most important cause of non-melanoma skin cancers, the most common human cancer[2].

1.1.2. Penetration of UV radiation into the skin

UV-C rays are the most dangerous of the ultraviolet rays but are absorbed by the ozone layer and other gases in the earth's atmosphere. However, the partial destruction of the earth's protective ozone layer has raised concerns about the impact of increased UV radiation on the earth's biological systems. As pollution depletes the ozone layer, more UV-C radiation will penetrate to the earth's surface[3]. The estimated number of cases of non-melanoma skin cancer in North America in 1994 was 1.2 million[4]. A 1% depletion in the ozone layer may lead to 30,000 new cases of skin cancer a year in North America alone, and it has been suggested that, if ozone depletion continues at the present rate the lifetime risk of skin cancer for children living in the UK today will increase by 10-15%[5].

UV-B rays represent less than 1% of the sun's energy that reaches the earth's surface, but they act directly on biological molecules, causing skin cancer, skin ageing and the familiar delayed sunburn that arises 12-24 hours after exposure[6].

UV-A rays were once thought to be harmless and early sunscreen products were designed to absorb only UV-B rays, allowing UV-A rays to filter through for a 'safe tan'. Recent research has shown that UV-A rays may in fact be more harmful than UV-B rays. UV-A is 100-1000 times more abundant than UV-B (depending on the season) and penetrates deeper into the skin where it can alter the position of elastin fibres, and damage both blood vessels and DNA[7].

1.1.3. Biological effects of UV radiation[8,9]

The incidence of UV radiation on the skin can have both beneficial and harmful effects. Vitamin D, essential for healthy bones, is synthesised in the skin following irradiation by light. Over-production of Vitamin D is harmful but is prevented by the natural UV attenuating mechanisms of the skin such as pigmentation and keratinisation.

Tanning, or the increase of pigmentation in the skin, is the most common biological reaction following exposure to UV radiation. There are two types of tanning reactions. Immediate tanning reaches a maximum 1 hour after exposure and fades after 3 hours, and is due to photochemical oxidation of melanin granules. Delayed tanning appears 2 days after exposure, reaches a maximum after 2-3 weeks and fades within 10-12 months. It is due to the formation of new melanin pigment cells deep in the skin and the subsequent migration of these cells to the surface.

The melanin formed acts to absorb the incident UV radiation, thus protecting the skin. It can also act as a free-radical scavenger, further limiting the potential UV-induced damage.

Keratinisation, like pigmentation is a natural defensive response of the skin to UV radiation. UV radiation promotes the formation of highly scattering keratin in the skin which acts to reduce the amount of UV radiation reaching the lower layers.

Erythema, or sunburn, is often the most noticeable reaction to UV radiation, particularly in fair-skinned people. It develops 2-3 hours after initial exposure and reaches a maximum 10-24 hours later. The mechanism is thought to involve the photochemical generation of unstable radical species which combine to form irritants such as peroxides, which subsequently give rise to erythema.

Carcinogenesis, or skin cancer, is the most serious consequence of UV exposure. It has been shown that long term exposure of the skin to UV light can result in the formation of non-melanoma and melanoma skin cancers. Whilst the former is less serious than the latter, skin cancer is now the second most common cancer behind lung cancer in the U.S.

The role of exposure to UV radiation resulting in 'photoageing' is a relatively recent discovery. Exposure to UV causes a thickening of the skin, elastosis and a reduction in collagen. These cause the skin to sag and wrinkle, and take on a dry and leathery appearance.

1.2. Sunscreen formulations

1.2.1. Active ingredients

As evidence concerning the harmful consequences of the action of UV radiation on human skin increased sunscreens were developed. These fall into two categories – physical sunscreens and chemical sunscreens. Physical sunscreens contain compounds such as titanium dioxide and zinc oxide in particulate form, which **scatter** and **reflect** the UV light, preventing the radiation from reaching the skin. Chemical sunscreens **absorb** the incident UV radiation and then dissipate the energy in a variety of ways. This may be as vibrational relaxation giving rise to heat or via other deactivation pathways such as photoisomerisation of the active species.

The ideal chemical sunscreen ingredient should have the following properties:

1.   It should have a strong, broad absorption band in the UV region of the spectrum which is unaffected by solvent.

2.   It must not be toxic, sensitising nor phototoxic.

3.   For water-resistant formulations it should ideally be insoluble in water, but soluble in the vehicle of choice.

4.   It must be photostable over the expected exposure time.

5.   Following absorption of radiation, it should revert quickly to its original form, via safe, non-radiative pathways without producing any toxic intermediates.

6.   For cosmetic reasons it should not absorb light in the visible region of the spectrum.

There are many compounds currently being used in sunscreen formulations across the world, but their photophysical and photochemical properties are poorly understood and in many cases not well documented. The techniques used to analyse the final formulations are far from ideal. Current methods rely upon the determination of sun protection factors by volunteer studies which are invasive, involve exposing volunteers to potentially large doses of UV radiation and are notoriously unreliable.

The growing awareness of the capabilities of sunlight to cause skin cancer and degenerative skin changes such as ageing has resulted in a sharp increase in the sales of sun-protective and accessory products in recent years.

Recent surveys have shown that 57% of the British public had bought sunscreens in the two to three years up to summer 1996[10], and 53% of the respondents to an American National Health Survey reported that they were "very likely" to use sunscreen if they were outside on a sunny day for more than 1 hour[4].

As cosmetic manufacturers are now using UV-A and UV-B filters in many of their products, not just those specifically designed to prevent sunburn, such chemical UV filters will become even more important in reducing the risk of premature ageing and skin cancer. Such filters are subjected to stringent testing prior to their acceptance by bodies such as the European Cosmetic, Toiletry and Perfume Association (COLIPA) and the U.S. Food and Drug Administration (FDA) for use in commercially available products.

1.2.2. Sun Protection Factors

At present the UV-B protection provided by a given sunscreen formulation is expressed as the sun protection factor (SPF). The SPF is defined as the ratio of the time of UV radiation exposure necessary to produce minimally detectable erythema in sunscreen protected skin to that time for unprotected skin i.e.

$$SPF = \frac{MED\ (protected\ skin)}{MED\ (unprotected\ skin)} \qquad Equation\ 1.1$$

where MED is the minimal erythemal dose, i.e. the amount of UV radiation that produces the first detectable erythemal response 24 hours after exposure. It can be expressed in terms of either a time of exposure or a dose of radiation in Jm^{-2}.[11]

A typical protocol for the determination of the SPF value involves covering a 'non-exposed' area of skin, such as the lower back with lightproof foil and irradiating with a standard UV source. 1 cm^2 areas of foil are then removed sequentially, usually following a geometrical progression, so that each area receives a defined dose of UV radiation.

The sunscreen formulation under study is usually assessed at the same time as the determination of the unprotected MED. It is applied uniformly at a surface density of 2 mgcm^{-2} and allowed to dry for 15 minutes before the subject is irradiated again for incrementally increasing times (based on an estimation of the SPF value of the sunscreen determined spectrophotometrically). The following day the volunteer returns and the exposed areas of skin are examined and assessed for erythema to determine the MEDs, and the SPF value calculated from the ratio of the protected MED to the unprotected MED[12]. Clearly this is a highly subjective measurement, but one that the industry relies upon.

Depending on the irradiation source used the SPF value can also give an indication of the protection offered by the formulation against UV-A radiation. This can also be assessed using the Phototoxic Protection Factor[13], the Ultraviolet-A Erythema Protection Factor[14], the Pigment-Darkening Protection Factor[15], the *In Vitro* Transmission Protection Factor[16,17,18] or the Sunburn Cell Protection Factor[17, 18]. Currently there is no consensus of opinion as to the ideal *in vivo* assay to assess protection against UV-A. The main drawbacks with using the UV-B *in vivo* assay are the much larger doses of radiation that are needed to produce detectable erythema by UV-A radiation and the unknown action spectra of other UV-A induced phenomena such as photoageing, photosensitivity dermatitis and development of melanoma and non-melanoma skin cancer.

Although these *in vivo* techniques give reliable and meaningful data as far as the protection offered by the sunscreen to the skin is concerned, the major disadvantage is the exposure of the volunteers to UV radiation. Such *in vivo* assays are particularly problematic for high protection sunscreens (SPF>25) due to the impractically long UV irradiation times needed to achieve erythema on the sunscreen protected skin.

The other main property of any sunscreen formulation is its substantivity. This is the characteristic of a sunscreen that reflects how effectively the advertised degree of protection is maintained under adverse conditions, including abrasion, repeated water exposure or sweating[12, 19]. Diffey and Grice[20] have shown that the protection afforded by topical sunscreens depends very much on how they are applied and activities subsequent to application. They conducted studies to examine the influence of different application techniques and post-application activities on the protective ability of the formulation. Rhodes and Diffey[21, 22] have used fluorescence spectroscopy to quantify the application thickness of topically applied agents and demonstrated its application for monitoring

application techniques and substantivity. Stokes and Diffey[23] have also used this technique to study the application and substantivity of sunscreen formulations on skin. However, despite the success of the technique, it is not globally applicable since it is limited to the few formulations that are inherently fluorescent. There is currently no universally accepted method for monitoring the performance of sunscreen formulations on skin under these conditions and this remains a challenge for the industry as a whole.

1.3. Photochemistry of Sunscreen agents

The relationship between chemical structure and the efficacy of ultraviolet filters is clearly recognised and understood. Most of the chemical UV filters in use throughout the world can be classified as derivatives of the following[24]: -

> PABA (p-Aminobenzoic acid) and p-aminobenzoates
>
> Salicylates
>
> Cinnamates
>
> Benzophenones
>
> Anthranilates
>
> Dibenzoylmethanes
>
> Camphors

Although these chemicals are subjected to rigorous testing and must be approved by either the U.S. FDA or COLIPA little is known about their photochemical and photophysical properties. A summary of the properties of the main groups of sunscreen compounds is given below.

1.3.1. Photochemistry of PABA

PABA was the first sunscreen patented from this family of UV filters. It has an absorption maximum at 296 nm and a corresponding molar absorption coefficient of 13600 $dm^3mol^{-1}cm^{-1}$. The chemical structure is shown in figure 1.2.
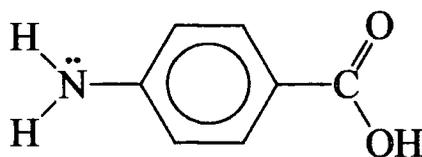
Figure 1.2. p-Aminobenzoic acid (PABA).

When this compound is exposed to UV radiation it undergoes electron delocalisation to form the zwitterion shown in figure 1.3.
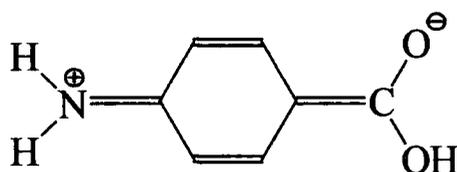
Figure 1.3. Zwitterion formed on irradiation of PABA.

Shaw et al.[25] have studied the photochemistry of this compound and identified the products formed when both aerated and anaerobic aqueous solutions of this compound were exposed to UV radiation. They found that in deoxygenated solutions two photoproducts were formed, 4-(4'-aminophenyl)aminobenzoic acid (I) and 4-(2'-amino-5'-carboxy-phenyl)aminobenzoic acid (II). However in aerated solutions the products formed were 4-amino-3-hydroxybenzoic acid, 4-aminophenol and 4-(4'-hydroxyphenyl)aminobenzoic acid (III). These compounds, however, discoloured rapidly highlighting one of the disadvantages of this compound when it is present in commercially available formulations. They found that (III) was formed from the oxidation of (I) and that 4-(2,5-cyclohexadien-4-one)iminobenzoic acid (IV) is formed as an intermediate in this reaction. They also studied the influence of pH on these photoreactions and found that the quantum yields of formation of compounds (I) and (II) increased from 1×10^{-4} to 1×10^{-3} as the pH increased from 7 to 10.6. The structures of these compounds are shown in figure 1.4.

(I)   (II)   (III)   (IV)
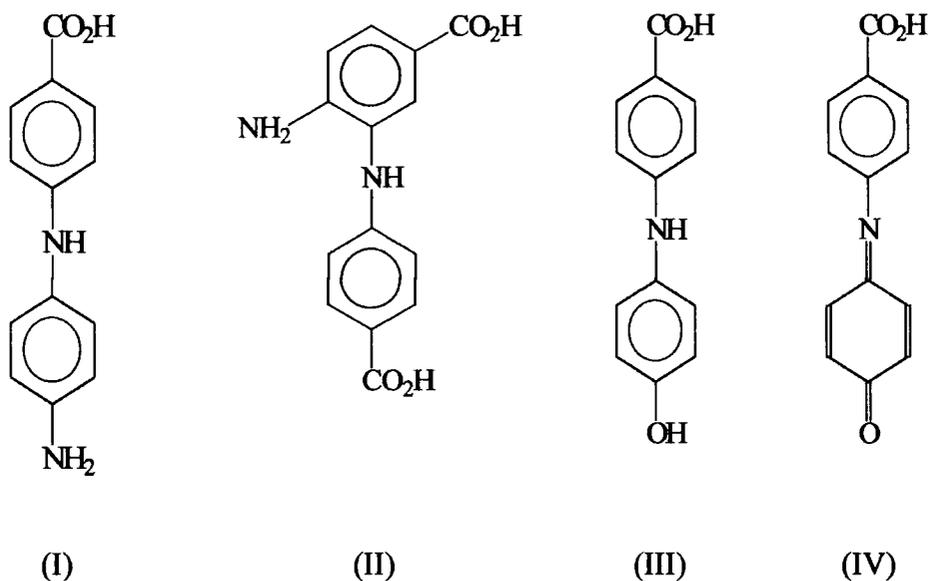
Figure 1.4. Structures of the products formed following irradiation of PABA.

1.3.2. Photochemistry of Salicylates

Salicylates were the first UV filters used in sunscreening preparations[24]. These compounds are *ortho*-disubstituted compounds, with a spatial arrangement that permits intramolecular hydrogen bonding, as shown in figure 1.5. This gives rise to λ_{max} values of ~300 nm. This hydrogen bonding lowers the energy requirements for the promotion of these compounds to their excited states, giving rise to absorption bands at longer wavelengths than the corresponding *para*- or *meta*-substituted derivatives. Unfortunately this '*ortho* relationship' also results in these compounds having much lower molar absorption coefficients than their *para*- or *meta*-substituted counterparts. This is due to the *ortho*-disubstitution pattern between the phenol group and the bulky carboxylic ester group, which results in the formation of the hydrogen bond and great steric strain within the molecule. This strain is reduced by the two groups moving slightly out of the plane of the aromatic ring, which causes a reduction in the symmetry of the molecule and in turn reduces the molar absorption coefficient.

31
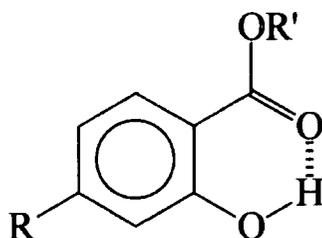
Figure 1.5. A salicylate-based sunscreening compound.

1.3.3. Photochemistry of Cinnamates

The esters of cinnamic acid form the most common family of UV-B absorbers used in modern sunscreen formulations. The absorption bands in the UV-B region and the large absorption coefficients provide skin with an efficient protection against short wavelength radiation[26]. 2-Ethylhexyl p-methoxycinnamate (2-ehmc), also known as Parsol MCX, is the most widely used active ingredient in modern day formulations and has an absorbance maximum at 312 nm and a corresponding molar absorption coefficient of 24200 $dm^3mol^{-1}cm^{-1}$. There are currently 17 cinnamate derivatives approved for use in Europe and four approved by the U.S. FDA for use in America[24].

Shaath has described a mechanism of electron delocalisation throughout the molecule following absorption of radiation of this wavelength as shown in figure 1.6. He commented that energy required for this transition corresponds to a wavelength of ~305 nm and that it has a fairly strong absorption coefficient of ~23000 $dm^3mol^{-1}cm^{-1}$. However, both Morlière[26] and Broadbent[27] have concluded that a *cis-trans* isomerisation results from the absorption, as shown in figure 1.7.
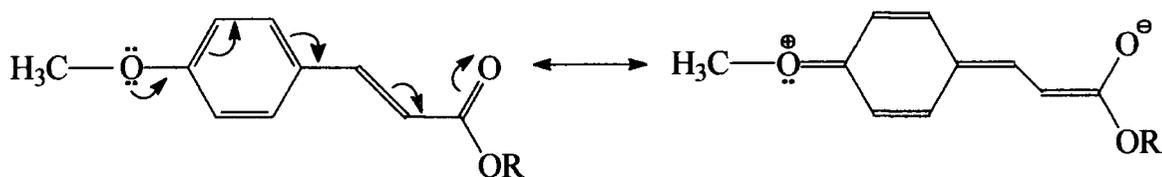
Figure 1.6. The resonance delocalisation of methoxycinnamates.
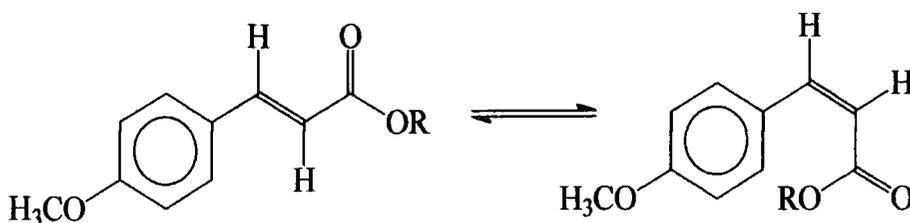
Figure 1.7.   The isomerization of methoxycinnamates.

These compounds have been well documented in the literature. Morlière[26] _et al._ studied the photochemical properties of some cinnamate derivatives, including 2-ehmc (I), 2-ethoxy-hexyl methoxycinnamate (II) and diethanolamine methoxycinnamate (III) using steady state and laser flash photolysis. Steady state photolysis indicated that an _cis→trans_ isomerization took place and that no other species were formed. They determined values of the quantum yields of isomerization, $\Phi_{cis \rightarrow trans}$ and $\Phi_{trans \rightarrow cis}$ in various solvents under both aerobic and anaerobic conditions. The laser flash photolysis studies of the 2-ehmc system demonstrated that the _cis→trans_ photoisomerisation occurs in less than 50 ns without any detectable intermediate. They concluded that the isomerization could proceed through either the singlet excited state or a short-lived triplet state. They also carried out triplet quenching experiments and found that the compound efficiently quenched the triplet states of both 8-methoxypsoralen and 5-methoxypsoralen, resulting in the isomerization of the cinnamate. A summary of the data they obtained is given in Table 1.1.

Compound	Solvent	Irradiation wavelength/ nm	N_2 ϕ_{trans} $\rightarrow cis$	N_2 $\phi_{cis\rightarrow}$ $trans$	O_2 ϕ_{trans} $\rightarrow cis$	O_2 $\phi_{cis\rightarrow}$ $trans$
(I)	Methanol	334	0.9	0.6	0.95	0.55
(I)	Ethanol	334	0.85	0.55	0.80	0.5
(I)	Ethanol	313	0.9	0.6	0.85	0.6
(I)	Ethanol/water	334	0.7	0.4	0.7	0.4
(I)	Cyclohexane	313	0.7	0.95	0.75	0.9
(II)	Water	334	0.60	0.70	0.55	0.7
(III)	Water	313	1	1	1	1

__Table 1.1. Quantum yield data for the photoisomerisation of cinnamate__
__derivatives[26].__

Gonzenbach[28] *et al.* probed the triplet energy level of 2-ehmc to determine whether this compound could sensitise thymine triplets and promote thymine dimerisation in the skin, a potential precursor to the development of skin cancer. They used quenching of donor phosphorescence and oxygen perturbation measurements to determine the lowest triplet energy level. The oxygen perturbation measurements involved recording the absorption spectrum under very high pressures (~2000 psi). In this environment the spin selection rules break down and direct absorption from the ground state to the first excited triplet state can be detected.

Using this technique and the quenching of the acetophenone, benzophenone and benzil triplet states they determined the lowest triplet energy to be 240 kJmol[-1]. As this is much lower than the lowest triplet energy of thymine (315 kJmol[-1]) they concluded that 2-ehmc is unable to sensitise the formation of thymine triplets.

Work by Broadbent *et al.*[27] used capillary supercritical fluid chromatography combined with atmospheric pressure chemical ionisation mass spectrometry to investigate the photoproducts formed on the ultraviolet irradiation of 2-ehmc. They found that the commercially available *trans*-2-ehmc undergoes photoisomerisation on irradiation at wavelengths greater than 300 nm. They separated and identified photodimers, indicating that the species can undergo [2+2] cycloaddition reactions with itself, and

carried out experiments to analyse 2-ehmc in the presence of thymine to determine if it would undergo a photoreaction to form an ehmc-thymine adduct. This could be potentially carcinogenic if formed on the skin since it would block the reading of the genetic code and interfere with the replication process. Their results showed no evidence of such adduct formation.

1.3.4. Photochemistry of Benzophenones

These compounds are used primarily as UV-A absorbers due to their λ_{max} values of ~330 nm. The general structure of these compounds is shown in figure 1.8.
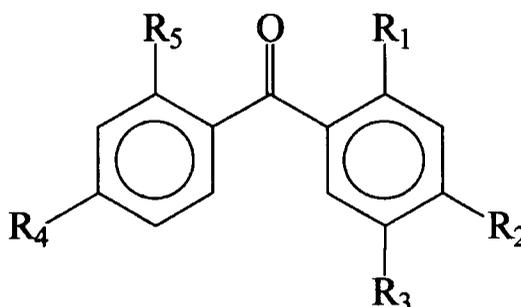
Figure 1.8. The structure of benzophenone-based sunscreens.

When exposed to UV light these compounds undergo electron delocalisation which is aided in many cases by electron withdrawing groups such as hydroxyl groups and methoxy groups *ortho-* and *para-* to the carbonyl group, as is the case in oxybenzone. Oxybenzone (R_1 = OH, R_2 = OCH$_3$, R_3 = R_4 = R_5 = H) has a λ_{max} value of 321 nm in a polar solvent and a corresponding molar absorption coefficient of 9300 dm^{3}mol^{-1}cm^{-1}.[24]

1.3.5. Photochemistry of Anthranilates

The anthranilate esters are also *ortho*-disubstituted compounds like the salicylates described previously. The ease of electron delocalisation between the *ortho* carboxylic ester and amine groups, as shown in figure 1.9, results in these compounds having λ_{max} values in the UV-A region at ~330 nm. As with the salicylates the same '*ortho* effect'

results in relatively low molar absorption coefficients of the order of $5000 \ dm^3mol^{-1}cm^{-1}$.
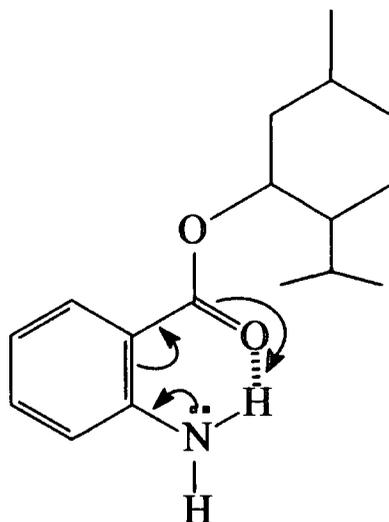
Figure 1.9. Electron delocalisation in menthyl anthranilate.

1.3.6. Photochemistry of Dibenzoylmethanes

The dibenzoylmethanes represent a relatively new class of UV filters that absorb radiation in the UV-A region. Their general structure is shown in figure 1.10, and their absorbance properties arise from a keto-enol tautomerism. The keto-forms of these compounds have λ_{max} values in the region of 260 nm, but the enol forms have λ_{max} values around 345 nm. The compounds also have exceptionally high molar absorption coefficients of the order of $30000 \ dm^3mol^{-1}cm^{-1}$.
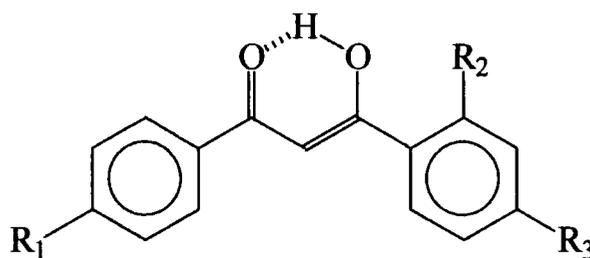
Figure 1.10. A general dibenzoylmethane.

1.3.7. Photochemistry of Camphors

One of the most common ingredients in modern day sunscreen formulations is 4-methylbenzylidene camphor. This is one member of a family of six benzylidene camphor compounds approved by COLIPA for use in the EC countries in sunscreen formulations. These compounds have high molar absorption coefficients (usually above 20000 $dm^3mol^{-1}cm^{-1}$) and most of them absorb in the UV-B range of 290-300 nm. However, new ranges of camphor derivatives, including Mexoryl-SX, absorb in the UV-A range[24].

4-methylbenzylidene camphor, also known as Parsol 5000 has a λ_{max} value of ~300 nm and is used within some formulations as a photochemical filter to stabilise other active ingredients[29].

Shaath[24] has suggested that the photoabsorptivity is due to the resonance delocalisation shown in figure 1.11. Beck *et al.*, however, state that benzylidene camphors, like most α,β-unsaturated ketones, undergo a photo-induced *cis-trans* isomerisation when solutions of such derivatives are exposed to UV light[30]. This is shown in figure 1.12. They claim that in practice it is the mixture of the *cis* and *trans* forms that acts as the UV filter.
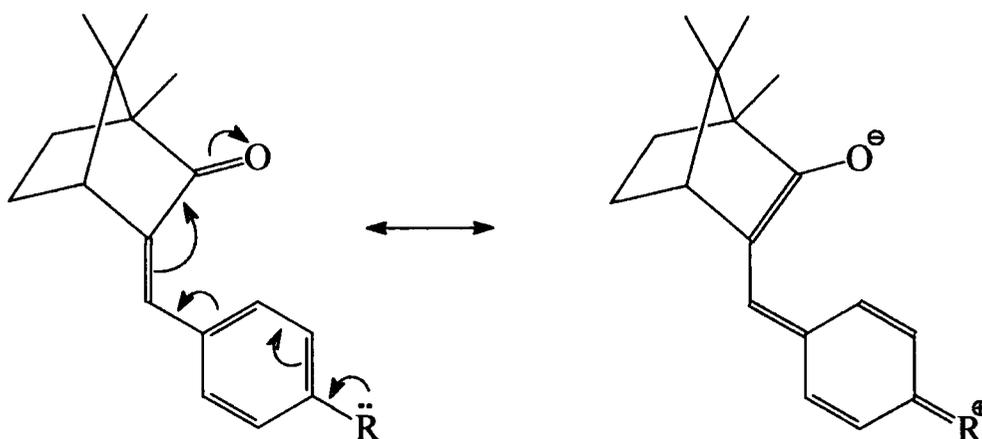
Figure 1.11. The resonance delocalisation of benzylidene camphor derivatives.
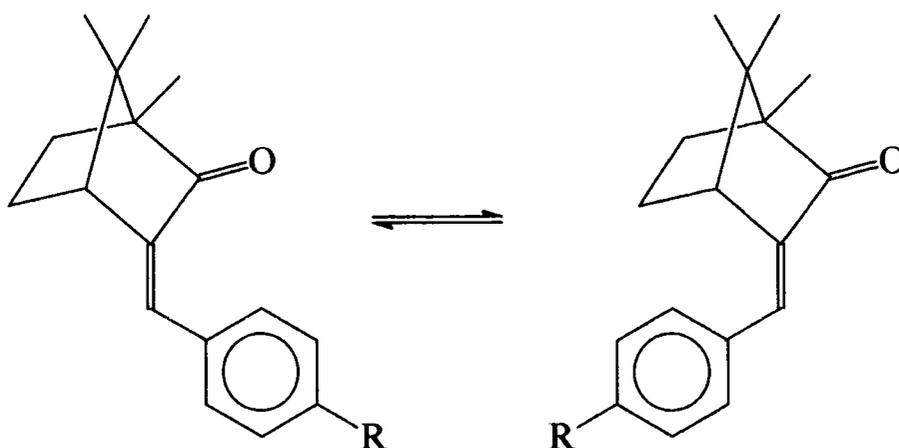
Figure 1.12. The cis-trans isomerization of benzylidene camphor derivatives.

The literature contains many articles[31,32,33,34,35] concerned with this photo-induced isomerization but this will not be dealt with here.

Work has been carried out on the photochemistry of several members of the benzylidene camphor family, but surprisingly no work has been published on 4-methylbenzylidene camphor itself.

Beck and co-workers[30] obtained the absorption spectra of benzylidene camphor (I), p-dimethylaminobenzylidene camphor (II) and p-trimethylaminobenzylidene camphor methylsulfate (III) in a variety of solvents and assigned the bands.   They also determined the initial quantum yields of isomerization for both isomers in several solvents, i.e. $\Phi_{cis \to trans}$ and $\Phi_{trans \to cis}$ and determined the ratio, $\{trans\}_\infty$ / $\{cis\}_\infty$, of the respective concentrations of the 'trans' and 'cis' isomers in the photostationary state obtained under their experimental conditions.   Photodegradation quantum yields of both isomers of the three compounds were also determined.   They found that the isomerization process was totally reversible and, as for α,β-unsaturated ketones in general, the cis isomer absorbs at a longer wavelength than the trans isomer.

They found that the 'trans' isomers possessed two bands, one at shorter wavelength being the π-π^* band and the other being the n-π^*.   In the case of p-dimethylaminobenzylidene camphor these bands overlapped but for the other compounds two distinct bands were detected.

A summary of the data obtained is given in tables 1.2 and 1.3.

	Concentration / moldm^{-3}	Solvent	$\lambda_{\text{irradiation}}$/nm	$\phi_{cis\rightarrow trans}$ or $\phi_{trans\rightarrow cis}$	$\{trans\}_\infty$/ $\{cis\}_\infty$
I$_E$	3.6x10^{-5}	Cyclohexane	290	0.13	0.99
I$_Z$	3.4x10^{-5}	Cyclohexane	370	0.3	3.1
II$_E$	3.53x10^{-4}	Cyclohexane	350	0.27	0.49
II$_Z$	3.53x10^{-4}	Cyclohexane	350	0.26	0.54
III$_E$	2.44x10^{-4}	Water	290	0.11	0.46
III$_Z$	2.44x10^{-4}	Water	290	0.09	0.46

Table 1.2. Summary of the photoisomerisation quantum yields[30].

	Concentration /moldm^{-3}	Solvent	$\lambda_{\text{irradiation}}$/nm	ϕ
I$_E$	1.23 x 10^{-2}	Isopropyl myristate	290	≤ 9 x 10^{-5}
I$_Z$	1.53 x 10^{-2}	Isopropyl myristate	300	≤ 9 x 10^{-5}
II$_E$	1.65 x 10^{-5}	Cyclohexane	350	≤ 1.6 x 10^{-4}
II$_Z$	3.33 x 10^{-5}	Cyclohexane	350	≤ 2 x 10^{-4}
III$_E$	3.35 x 10^{-5}	Water	290	≤ 1.3 x 10^{-5}
III$_Z$	2.55 x 10^{-5}	Water	290	≤ 9 x 10^{-5}

Table 1.3. Summary of the photodegradation quantum yields[30].

Further work by Beck *et al.* studied, quantitatively, the benzophenone- and acetophenone-photosensitised *cis→trans* isomerization of benzylidene camphor and p-trimethylaminobenzylidene camphor methylsulfate[36]. They measured the initial sensitised quantum yields and concentrations of both isomers in the photostationary states for benzophenone and benzylidene camphor and acetophenone and benzylidene

camphor systems, and simultaneously determined the rate constants of the quenching of the phosphorescent triplet states of the sensitizers. They found that the energy transfer between acetophenone and benzylidene camphor was diffusion controlled, whereas that between benzophenone and benzylidene camphor was slower. Similar experiments carried out on trimethylaminobenzylidene camphor methylsulfate found that this derivative was as efficient as benzylidene camphor at quenching the triplet states of these ketones. They also studied the interaction of the triplet state of 8-methoxypsoralen (a well known skin photosensitiser) with the trimethylammonio-derivative and found that this compound quenches the photocycloaddition of the sensitiser to N-methylmaleimide (used as a model of DNA). They concluded that these compounds show useful excited state quenching properties in addition to the usual filtering effects.

Moneyron *et al.*[37] studied the photochemical isomerization of hydroxybenzylidene camphors and some benzylidene tetrahydrofuranone derivatives in various solvents. The quantum yields determined were found to be independent of concentration of the species or the irradiation wavelength and no oxygen or solvent effects were observed. They also determined the kinetic constants of the thermal Z→E isomerization at 30 °C and found that the rate was dependent on the solvent, with the rate increasing with the protolysis constant of the solvent.

Dean and co-workers[38] studied the photomutagenicity potential of three benzylidene camphor derivatives commonly used in sunscreens and found that none of them gave rise to photomutagenic properties following irradiation with UV light.

1.4.   Basic Photophysics

The absorption of radiation by an atom or molecule can lead to the production of a range of electronically excited states that may exhibit chemical and physical properties that are different from the ground state, 'parent' species. The energy absorbed can be

dissipated in many ways, including heat, emission of radiation of longer wavelength, or initiation of chemical reactions.

The modified Jablonski diagram shown in figure 1.13 summarises the excited states formed on absorption of light and some of the deactivation pathways.

In the majority of organic molecules the ground state has no unpaired electrons, and so is a singlet state, S_0. Absorption of light of the correct energy can result in the promotion of an electron, usually with the retention of spin to the S_1 state. Absorption takes place from the lowest vibrational level of the S_0 state, but results in the population of many of the vibrational levels of the S_1 state. However, rapid vibrational relaxation, resulting in heat loss to the solvent, occurs within the S_1 manifold so that all further processes occur from the lowest vibrational level. The lifetime of this excited singlet state is short, typically of the order of ns due to rapid internal conversion to higher vibrational levels of the ground state, and/or by the spin-allowed radiative decay back to the ground state giving rise to fluorescence.

Intersystem crossing from the lowest vibrational level of the S_1 state to the vibrational manifold of the T_1 state can result in a change of spin of the molecule. As with the singlet excited state rapid vibrational relaxation occurs within the T_1 manifold such that all further processes occur from its lowest vibrational state. The excited triplet states tend to be much longer lived that the excited singlet states due to the spin-forbidden nature of S ↔ T transitions. Deactivation mechanisms include back intersystem crossing to a high vibrational level of the S_0 manifold followed by vibrational relaxation back to the lowest vibrational level of the S_0 state and radiative decay back to the S_0 state giving rise to phosphorescence.

Abs – Absorbance   VR – Vibrational relaxation
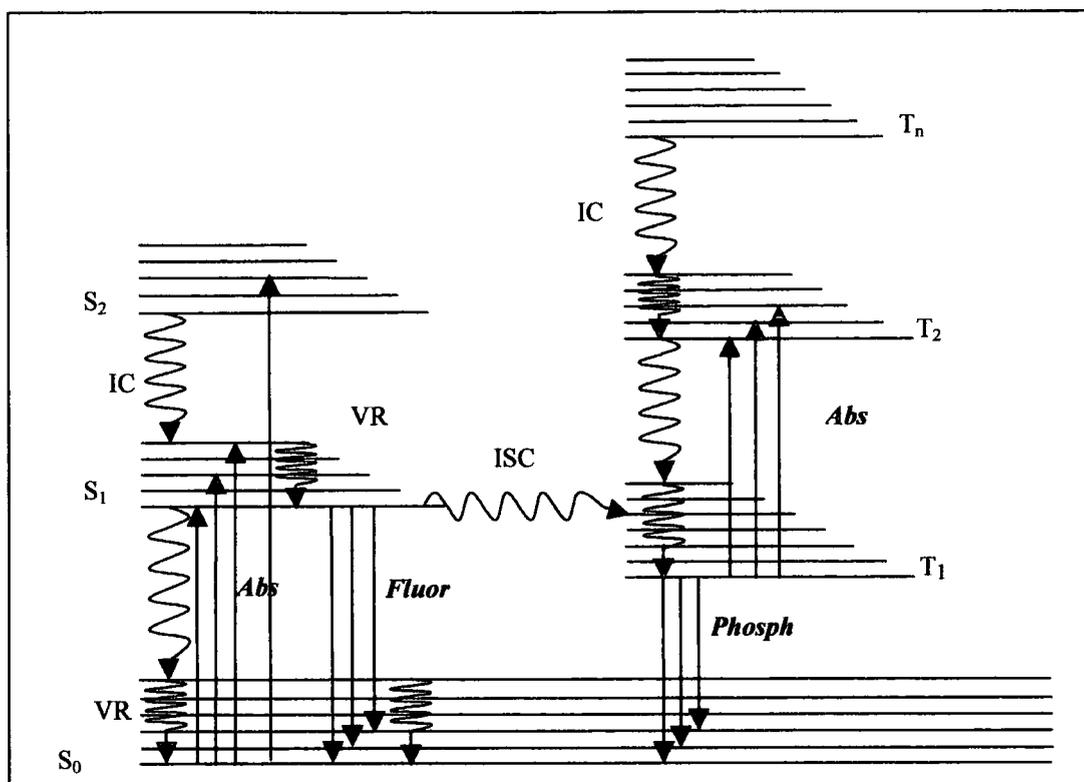
Fluor – Fluorescence emission   IC – Internal conversion

Phosph – Phosphorescence emission   ISC – Intersystem crossing

Figure 1.13. Modified Jablonski Diagram.

The triplet state species can also undergo a process in which two molecules interact to give rise to a S_1 state and a S_0 state. This is known as triplet-triplet annihilation and results in the observation of delayed fluorescence. The elucidation of the mechanism for the production of P-type delayed fluorescence was based on the observation that the intensity the emission is proportional to the square of the intensity of the incident light[39] and is independent of temperature, unlike E-type delayed fluorescence. The accepted mechanism[40] of P-type delayed fluorescence is:

S_0 $\longrightarrow$ S_1 absorption

S_1 $S_0 + h\upsilon'$ prompt fluorescence

S_1 T_1 intersystem crossing

T_1 $S_0 + h\upsilon''$ phosphorescence

$T_1 + T_1$ X

                                                          } Triplet-triplet annihilation
                                                            (spin-allowed)
X $S_1 + S_0$

X $S_0 + S_0$ deactivation

S_1 $S_0 + h\upsilon'$ delayed fluorescence

Application of the steady state approximation shows that under conditions of low exciting light intensity, where $[T_1]$ will be small, and terms involving $[T_1]^2$ can be neglected, the intensity of delayed fluorescence (I_{DF}) is given by:

$$ I_{DF} = \frac{k_{tta}k_x}{k_x + k_d}\left[\frac{k_{isc}I}{k_p(k_f + k_{isc})}\right]^2 \qquad \text{Equation 1.1} $$

Also,

$$ k_{DF} = -\frac{d(\ln I_{DF})}{dt} = -\frac{d(\ln [T_1]^2)}{dt} = -2\frac{d(\ln [T_1])}{dt} \qquad \text{Equation 1.2} $$

so that $k_{DF} = 2k_p$ and $\tau_{DF} = \tfrac{1}{2}\tau_p$

Thus the intensity of the delayed fluorescence should decay with a lifetime equal to one half that of the phosphorescence.

Quenching by both ground state molecules and other extrinsic quenching agents such as molecular oxygen also results in the deactivation of the triplet state.

An understanding of the excited state species formed, and deactivation mechanisms that take place following absorption of radiation is paramount to understanding the properties of the active sunscreen ingredients when exposed to solar UV radiation. As these species are formed on the skin surface the reactions that they undergo with molecules present in the skin is also a matter of grave concern.

1.5. This work

The harmful effects of UV radiation of the skin are now well known and documented and the majority of people now realise the need to use sunscreen formulations when out in the sun.

The active ingredients contained within the formulations are well tested and must be approved by either COLIPA or the FDA, but the photophysical and photochemical properties of them are often poorly understood and documented.
As demands for the 'perfect' sunscreen increase and the use of such products becomes more widespread the amount of safety data required to defend such formulations and the ingredients within them is unlikely to decrease. It is probable that more data will be required, such as the results of investigations predicting the interactions between the chemicals, UV light and skin.

This work has involved the comprehensive photophysical study of two compounds that have been used as active ingredients in commercially available sunscreen formulations. Menthyl anthranilate (chapter 3) is approved for use as an UV-A absorber in the U.S. and Australia. It has been described as 'an ideal sunscreen to add to formulations containing 2-ethylhexyl p-methoxycinnamate [the most commonly used UV-B sunscreen in modern formulations] to both increase the SPF and provide protection in the UV-A region[41].
N-acetyl-menthyl anthranilate (chapter 4) was synthesised and studied as an analogue of N-acetyl-homomenthyl anthranilate, a compound which was approved for use as an active ingredient in the EC until 1989[42].

The formulations that are commercially available are well tested before going onto the market but the techniques used are often invasive and involve exposing the volunteers to UV light. Other *in vitro* techniques used avoid these problems but may not be representative of the interactions that occur between the formulations and the skin.

Infrared spectroscopy has been used to analyse sunscreen formulations with a view to developing a new technique and protocol to study the composition of sunscreen formulations on the skin surface (chapter 5). This has been extended to study the substantivity of the formulations and the water resistance. The work demonstrates how this technique could meet the requirements of a more comprehensive and stringent analysis of sunscreen agents within final formulations. It has the potential to study application techniques, substantivity, water resistance and also possibly the absorption of ingredients through the skin.

The infrared protocol developed was then tested in a collaborative study with Prof. B. Diffey and Dr R. Stokes (Regional Medical Physics Department, Dryburn Hospital, Durham) (chapter 6). The work involved the correlation of infrared absorbance values obtained from thin films of sunscreen to the values of the SPF determined by an *in vitro* transmission spectroscopy technique. The correlation was then used to study the water-resistance of formulations, by virtue of the reductions in SPF value following exposure of the sunscreen film to water. This technique offers an alternative to the current water-resistance testing protocols which is less time consuming, less expensive and avoids exposing volunteers to unnecessary doses of UV radiation.

1.6.   References

1. Wayne C. E. and R.P. Wayne (1996) *Photochemistry,* Oxford University Press.

2. Diffey B.L. (1991) Solar ultraviolet radiation effects on biological systems. *Phys. Med. Biol.,* **36(3),** 299-328.

3. Walters C., A. Keeney, C.T. Wigal, C.R. Johnston and R.D. Cornelius (1997) The spectrophotometric analysis and modelling of sunscreens. *J. Chem. Educ.*, **74**, 99-102.

4. Hall H.I., D.S. May, R.A. Lew, H.K. Koh, M.P.H. Nadel and M. Nadel (1997) Sun protection behaviours of the U.S. white population. *Preventative Medicine*, **26**, 401-407.

5. Diffey B.L. (1997) Stratospheric ozone depletion and the risk of non-melanoma skin cancer in a British population. *Phys. Med. Biol.*, **37**, 2267-2279.

6. Abney J.R. and B.A. Scalettar (1998) Saving your students skin. Undergraduate experiments that probe UV protection by sunscreens and sunglasses. *J. Chem Ed.*, **75**, 757-760.

7. Pathak M.A. *Photoprotection against harmful effects of solar UVB and UVA radiation: An update* in Sunscreens: Development, Evaluation and Regulatory Aspects, eds. Lowe N.J., Shaath N.A. and Pathak M.A., Marcel Dekker, New York, 1997, pp. 59-79.

8. Fitzpatrick, Eisen, Wolff, Freedberg and Austen. *Dermatology in General Medicine* 3rd Ed., Vol.1, McGraw-Hill, New York, 1987.

9. Shea C.R. and J.A. Parrish. *Skin, Effects of Ultraviolet Radiation* in 'Encyclopaedia of Human Biology' Vol. 7. Academic Press, 1991, pp. 65.

10. McGregor J.M. and A.R. Young (1996) Sunscreens, suntans and skin cancer. *Br. Med. J.*, **312**, 1621-1622.

11. Kimbrough D.R. (1997) The photochemistry of sunscreens. *J. Chem. Ed.*, **74(1)**, 51-53.

12. Ferguson J. *European Guidelines (COLIPA) for evaluation of Sun Protection Factors* in 'Sunscreens: Development, Evaluation and Regulatory Aspects', eds. Lowe N.J., Shaath N.A. and Pathak M.A., Marcel Dekker, New York, 1997, pp. 513- 525.

13. Lowe N.J., S.H. Dromgoole, J. Sefton, T. Bourget and D. Weingarten (1987) Indoor and outdoor efficacy testing of a broad-spectrum sunscreen against ultraviolet A radiation on psoralen-sensitized subjects. *J. Am. Acad. Dermatol.*, **17**, 224-230.

14. Cole C. and R. Van Fossen (1992) Measurement of sunscreen UVA protection; an unsensitized human model. *J. Am. Acad. Dermatol.*, **26**, 178-184.

15. Kaidbey K.H. and A. Barnes (1991) Determination of UVA protection factors by means of immediate pigment darkening in normal skin. *J. Am. Acad. Dermatol.*, **25**, 262-266.

16. Diffey B.L. and J.J. Robson (1989) A new substrate to measure sunscreen protection factors throughout the ultraviolet spectrum. *J. Soc. Cosmet. Chem.*, **40**, 127-133.

17. Roelandts R., N. Sohrbvand and M. Garmyn (1989) Evaluating the UVA protection of sunscreens. *J. Am. Acad. Dermatol.*, **21**, 56-62.

18. Sayre R.M. and P.P. Agin (1990) A method for the determination of UVA protection for normal skin. *J. Am. Acad. Dermatol.*, **23**, 429-440.

19. Anslemi C. (1992) Staying on the surface. *Chemtech*, **22**, 99-104.

20. Diffey B.L. and J. Grice (1997) The influence of sunscreen type on photoprotection. *Br. J.Dermatol.*, **137**, 103-105.

21. Rhodes L.E. and B.L. Diffey (1997) Fluorescence spectroscopy: a rapid, non-invasive method for measurement of skin surface thickness of topical agents. *Br. J. Dermatol.*, **136**, 12-17.

22. Rhodes L.E., and B.L. Diffey (1996) Quantitative assessment of sunscreen application technique by *in vivo* fluorescence spectroscopy. *J. Soc. Cosmet. Chem.*, **47**, 109-115.

23. Stokes, R.P. and B.L. Diffey, (1999) The feasibility of using fluorescence spectroscopy as a rapid, non-invasive method for evaluating sunscreen performance. *J. Photochem. Photobiol. B:Biol.*, **50**, 137-143.

24. Shaath N.A., *Evolution of Modern Sunscreen Chemicals* in 'Sunscreens: Development, Evaluation and Regulatory Aspects', eds. Lowe N.J., Shaath N.A. and Pathak M.A., Marcel Dekker, New York, 1997, pp. 3-33.

25. Shaw A.A., L.A. Wainschel and M.D. Sheltar (1992) The photochemistry of p-Aminobenzoic acid. *Photochem. Photobiol.*, **55**, 647-656.

26. Morlière P., O. Avicet, T. Sa E Melo, L. Dubertret, M. Giraud and R. Santus (1982) A study of the photochemical properties of some cinnamate sunscreens by steady state and laser flash photolysis. *Photochem. Photobiol.*, **36**, 395-399.

27. Broadbent J.K., B.S. Martincigh, M.W. Raynor, L.F. Salter, R. Moulder, P. Sjöberg and K.E. Markides (1996) Capillary supercritical fluid chromatography combined with atmospheric pressure chemical ionisation mass spectrometry for the investigation of photoproduct formation in the sunscreen absorber 2-ethylhexyl-p-methoxycinnamate. *J. Chromatog. A.*, **732**, 101-110.

28. Gonzenbach H., T.J. Hill and T.G. Truscott (1992) The triplet energy levels of UVA and UVB sunscreens. *J. Photochem. Photobiol. B:Biol.*, **16**, 377-379.

29. Patent Number 5549886.

30. Beck I., A. Deflandre, G. Lang, R. Arnaud and J. Lemaire (1981) Study of the photochemical behaviour of sunscreens – benzylidene camphor and derivatives. *Int. J. Cosmet. Sci.*, **3**, 139-152.

31. Jorgenson M.J. and N.C. Yang (1963) Novel photochemical reaction. Conversion of α,β-unsaturated ketones to acetonylcyclopropanes. *J. Am. Chem. Soc.*, **85**, 1698-1699.

32. Yang N.C. and M.J. Jorgenson (1964) Photochemical isomerization of simple α,β-unsaturated ketones. *Tet. Letts.*, **19**, 1203-1207.

33. Saltiel J., J. D'Agostino, E.D. Megarity, L. Metts, K.R. Neuberger, M. Wrighton and O.C. Zarifou (1973) *Cis-trans* photoisomerization of olefins. *Org. Photochem.*, **1**, 1-113.

34. Deflandre A., A. L'hereux, A. Rioual and J. Lemaire (1976) Photochemical behaviour of α,β-unsaturated ketones under direct excitation. *Can. J. Chem.*, **54**, 2127-2134.

35. Rioual A., A. Deflandre and J. Lemaire (1977) An example of radical chain isomerization: photoinduction of *cis-trans* isomerization in 3-penten-2-one. *Can. J. Chem.*, **55**, 3915-3925.

36. Beck I., A. Deflandre, G. Lang, R. Arnaud and J. Lemaire (1985) Study of the photochemical behaviour of sunscreens – benzylidene camphor and derivatives II: Photosensitized isomerization by aromatic ketones and deactivation of the 8-methoxypsoralen triplet state. *J. Photochem.*, **30**, 215-227.

37. Moneyron H., R. Arnaud, J. Lemaire, A. Deflandre and H. Goetz (1993) Photochemical E $\leftrightarrow$ Z isomerization of some benzylidene camphor and benzylidene tetrahydrofuranone derivatives. *J. Photochem. Photobiol.A: Chem.*, **75**, 77-82.

38. Dean S.W., R,H, Dunmore S.P. Ruddock, J.C. Dean, C.N. Martin and D.J. Kirkland (1992) Development of assays for the detection of photomutagenicity of chemicals during exposure to UV light. II. Results of testing three sunscreen ingredients. *Mutagenesis*, **7(3)**, 179-182.

39. Parker C.A., (1968) *Photoluminescence of Solutions*. Elsevier Publishing Co., Amsterdam, pp. 99-103.

40. Barltrop J.A. and J.D. Coyle (1978) Principles of Photochemistry. John Wiley&Sons, Chichester. pp 83-84.

41. Klein, K., and H.A. Finkelmeier (1990) Menthyl Anthranilate. The UVA alternative of the 90's. *Cosmetics and Toiletries*. **105**, 75-77.

42. Brown M. Boots plc. *Personal communication*.

Chapter 2

Experimental Techniques

2.1. Infrared Spectroscopy

2.1.1 Introduction to Infrared Spectroscopy

Infrared (IR) spectroscopy has been used as an analytical tool for many years, both qualitatively and quantitatively. It provides a unique 'fingerprint' that can be used to identify a wide variety of chemical species.

Originally, IR spectra were measured using dispersive instruments. Here the radiation from the source passes through the sample and is dispersed by a prism or a diffraction grating. The dispersed radiation is then focussed by a mirror onto an exit slit which allows one wavelength element at a time to pass through and reach the detector[1,2]. Inherent disadvantages in these systems, including slow scanning speeds and low sensitivity, led to the development of Fourier Transform Infrared Spectroscopy (FT-IR). FT-IR spectrometers differ from the old dispersive instruments by allowing the continuous detection of all the transmitted energy simultaneously. This is achieved using a system based on the Michelson interferometer, shown schematically in figure 2.1.
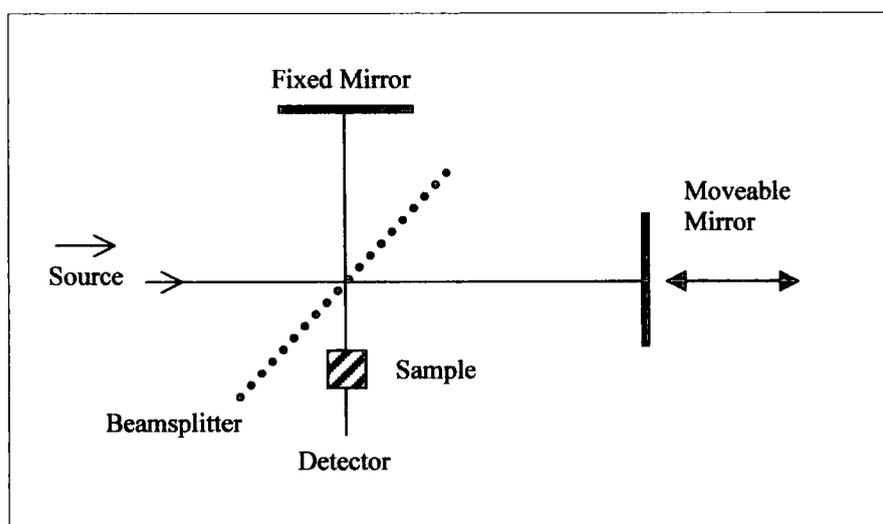
Figure 2.1. Schematic diagram of a Michelson interferometer[3].

The Michelson interferometer, which effectively replaces the monochromator system in dispersive instruments, consists of a beam splitter, a fixed mirror and a moving

mirror. It divides the incident beam of radiation into two and then recombines the two beams after a path difference has been introduced[4]. The radiation from the source is made parallel and strikes the beam splitter at 45°, where half of it is reflected onto the fixed mirror and the other half is transmitted to the moveable mirror. These two beams are then reflected back to the beam splitter where they are again partially reflected and partially transmitted. This creates the conditions under which interference between the beams can occur, and the intensity variations of the beam are measured as a function of the difference in the light path of the two beams. The mirror is moved at a constant velocity and when the path difference is zero or an integral number of wavelengths, (for a given wavelength of radiation) constructive interference occurs and a maximum signal is detected. When the path difference is an odd number of half wavelengths the two beams are exactly $\lambda/2$ out of phase, resulting in destructive interference. For monochromatic radiation this results in a co-sinusoidal variation of signal intensity with path difference – the interferogram. In practice the source is polychromatic, with each wavelength present producing its own co-sinusoidally varying interferogram. The polychromatic interferogram can be considered as a sum of all the cosine waves for the individual wavelength components and is of the form shown in figure 2.2. The signal is largest when the path difference between the two beams is zero since all the wavelengths are in phase. This intense signal is known as the 'centre burst'. Elsewhere the different wavelengths are out of phase, interfere with each other and produce cancellation of the signal. The asymmetry of this centre burst, shown in figure 2.2, is due to a slight dispersion by the beam splitter resulting in the waves being slightly out of phase when the path difference is zero[5].

The spectrum of the sample is then obtained from the interferogram by a Fourier transform procedure.

The main advantages of FT-IR spectrometers over dispersive instruments are the generation of high quality spectra in much shorter periods of time, with increased sensitivity which allows the analysis of much smaller quantities of material. The higher throughput of FT-IR spectrometers results in a better signal-to-noise ratio for a given period of acquisition when compared to the dispersive instruments.
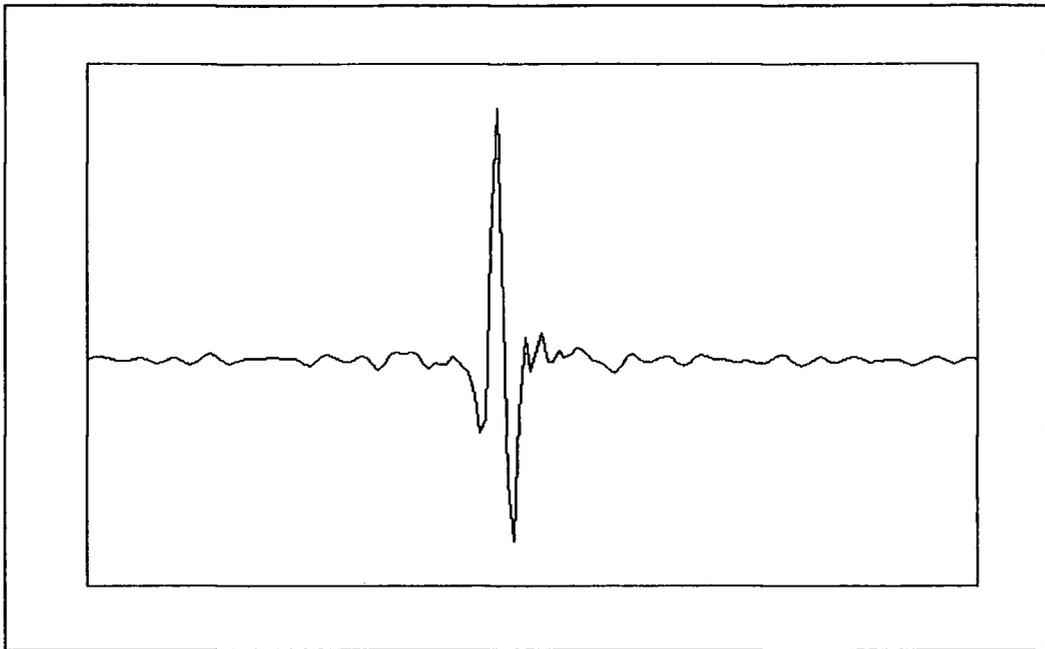
Figure 2.2. An Interferogram.

2.1.2. Attenuated Total Reflectance (ATR)

ATR spectrometry is one of the most popular sampling techniques used by FT-IR spectroscopists[3,4]. It has been used for many years as a means of obtaining spectral data representative of surfaces and interfaces rather than bulk samples. It is based on the phenomenon of total internal reflection, as experienced by light passing from a denser medium (refractive index n_1) to a less dense medium (refractive index n_2) at an angle greater than the critical angle. Figure 2.3 illustrates the physical processes that occur as light passes from one medium into another.

At an angle of incidence of $0°$ (measured from a normal to the interface) the light is mostly transmitted across the boundary and a small amount, ~5%, is reflected back along its original path. For light incident at an angle of incidence (θ_i) between $0°$ and the critical angle (θ_c) the light is refracted according to Snell's Law given in equation

2.1 (where θ_r is the angle of refraction) and reflected such that the angle of reflection, θ_{ref}, equals the angle of incidence, θ_i.
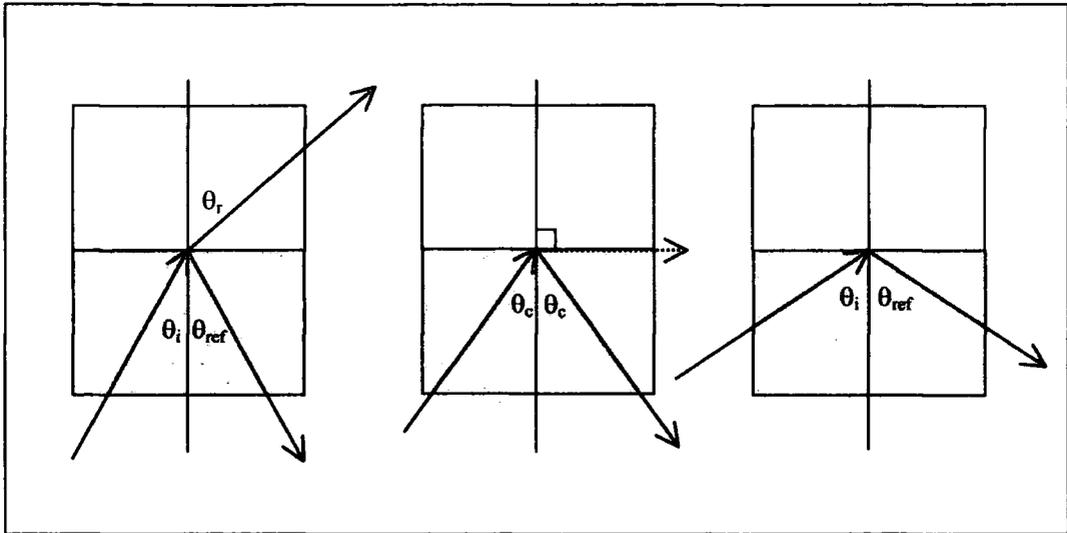
Figure 2.3. The physical processes that occur as light passes from a denser medium into a rarer medium.

$$n_1\sin \theta_i = n_2\sin \theta_r \qquad\qquad \text{Equation 2.1}$$

The critical angle is that special value of θ_i for which $\theta_r = 90°$ and $\theta_i = \theta_{ref} = \theta_c.$[6]

At angles larger that the critical angle, total internal reflection is observed. The critical angle is given by: -

$$\theta_c = \sin^{-1} \frac{n_2}{n_1} \qquad\qquad \text{Equation 2.2}$$

The theoretical treatment of ATR is complex and both Harrick[7] and Fahrenfort[8] give comprehensive accounts. When radiation is reflected, either internally or externally, interference between the incident and reflected waves causes a standing wave to be set up at the interface between the two media. Since the electric field components of the incident beam normal to the interface must be continuous, there must be some sort of transmitted wave, but at the same time there can be no net transfer of energy across the boundary. The resulting wave in the rarer medium is known as the evanescent or

surface wave[7]. It is a non-propagating wave with an electric field amplitude that decays exponentially with distance from the interface according to:

$$E = E_0 \exp\left[\frac{-2\pi}{\lambda_1}(\sin^2\theta - n_{21}^2)^{1/2}Z\right]$$ Equation 2.3

where E_0 is the electric field amplitude at the interface

$\lambda_1 = \lambda/n_1$ and is the wavelength of the radiation in the denser medium

Z is the distance from the surface

θ is the angle of incidence

$n_{21} = n_2/n_1$

The variation of electric field amplitude with distance from the interface is illustrated in figure 2.4.

If the rarer medium is an absorbing species then the evanescent wave will interact with the species resulting in a loss of energy upon total reflection giving rise to 'attenuated total reflection'.
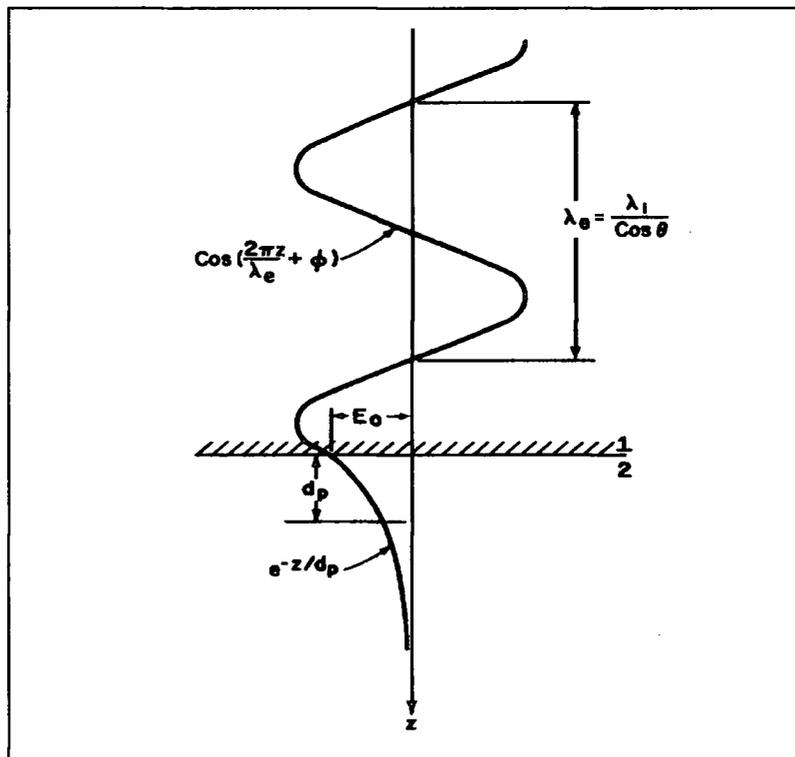
Figure 2.4. Variation of the electric field amplitude with distance from the interface[7].

The theory of ATR centres on the properties of the evanescent wave and its interactions with absorbing media. One important feature of this wave is that it is not transverse and so has vector components in all directions, allowing it to interact with all dipoles. The incident wave is polarised in two directions, one parallel to the plane of incidence (P wave) and the other perpendicular to the plane of incidence (S wave) where the plane of incidence is perpendicular to the plane of the interface between the two media. This gives rise to the electric field amplitudes at the interface in the rarer medium as is illustrated in figure 2.5.
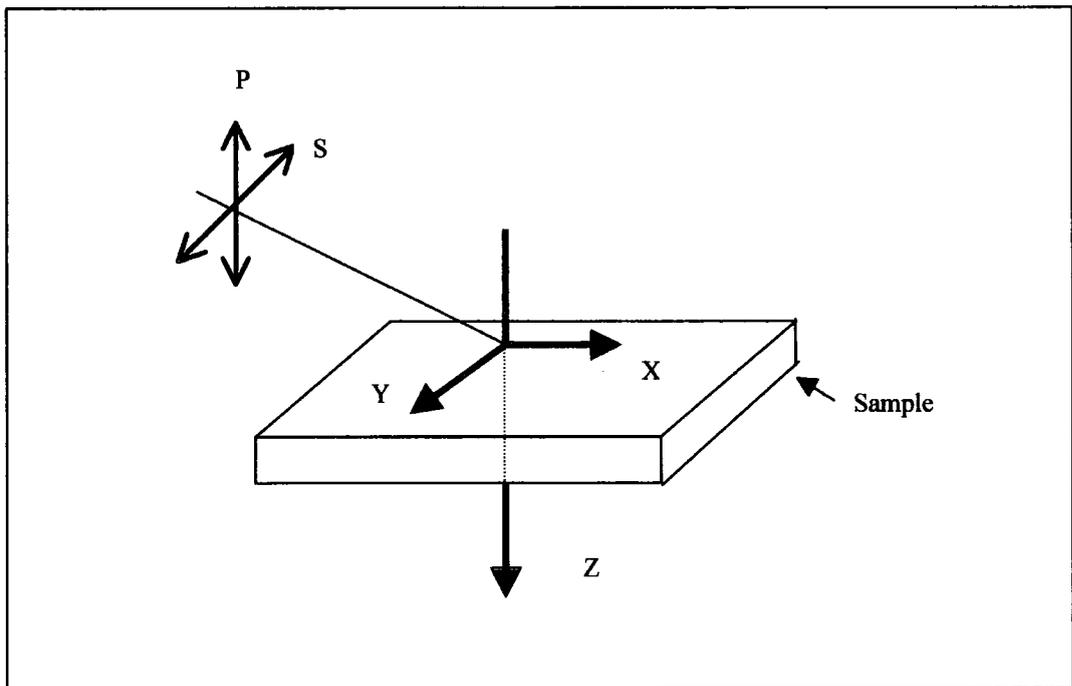
Figure 2.5. Illustration of properties of the waves at the interface.

The S wave has one electric field amplitude associated with it, E_{y0}, which is parallel to the plane of the interface and perpendicular to the plane of incidence. The P waves, however, have two electric field amplitudes associated with them – one parallel to the plane of incidence and perpendicular to the plane of the interface, E_{z0}, while the other is parallel to both the plane of incidence and the plane of the interface, E_{x0}.

For bulk materials these electric field amplitudes are given by:[7]

$$E_{y0} = \frac{2\cos\theta}{(1 - n_{21}^2)^{1/2}}$$

Equation 2.4

$$E_{z0} = \frac{2\sin\theta\cos\theta}{(1-n_{21}^2)^{1/2}[(1+n_{21}^2)\sin^2\theta - n_{21}^2]^{1/2}} \qquad \text{Equation 2.5}$$

$$E_{x0} = \frac{2(\sin^2\theta - n_{21}^2)^{1/2}}{(1-n_{21}^2)^{1/2}[(1+n_{21}^2)\sin^2\theta - n_{21}^2]^{1/2}} \qquad \text{Equation 2.6}$$

These combine to give an electric field amplitude at the interface of E_0. It is important to note that the electric field amplitudes given vary as a function of the angle of incidence (θ).

The electric field intensity at the interface is one of the main factors that control the strength of the coupling between the evanescent wave and the rarer medium.

The reflectivity for bulk materials and thin films can be written as:

$$R = 1 - \alpha d_e \qquad\qquad \text{Equation 2.7}$$

where   R is the reflectivity,

α is the absorption coefficient, and

d_e is the effective thickness, which is related to the absorption parameter a for a single reflection by $d_e = a/\alpha$, and $a = (100-R)\%$

For N multiple reflections, as is usually the case in practical ATR spectroscopy, the reflected power is given by:

$$R^N = (1-\alpha d_e)^N \qquad\qquad \text{Equation 2.8}$$

One of the most important parameters defined by Harrick[7] is the depth of penetration – the distance required for the electric field strength of the evanescent wave to reach 1/e of its initial value at the interface. It is given by:

$$d_p = \frac{\lambda_1}{2\pi(\sin^2\theta - n_{21}^2)^{1/2}} \qquad\qquad \text{Equation 2.9}$$

where $\lambda_1 = \lambda/n_1$ is the wavelength in the denser medium,

θ is the angle of incidence, and

$n_{21} = n_2/n_1$ (where n_2 is the refractive index of the rarer medium and n_1 that of the denser medium).

An important point to note is that the depth of penetration of the evanescent wave is a function of wavelength. Thus, bands appear stronger with decreasing wavenumber, especially when compared to the transmission spectra of the same system. This can be corrected for using the application software with the instrument and knowing the number of reflections, the angle of incidence and the refractive index of the ATR crystal.

Practically ATR involves bringing the samples into contact with an internal reflection element (IRE) that is infrared transparent and of a higher refractive index than the sample. Common IREs include silicon, germanium, zinc selenide and KRS-5 (a mixture of thallium bromide and thallium iodide) [9]. The IREs are usually trapezoid in shape, typically 10 cm^2 in area and a few millimetres thick. An angle of incidence is chosen which allows the radiation to enter the crystal and be reflected off the crystal/sample interface a number of times before it is redirected into the spectrometer. This is illustrated schematically in figure 2.6. As described above, the radiation interacts with the sample at the points of reflection resulting in absorption of some of the radiation and attenuation of the reflected beam. Multiple reflections increase the absorption of the sample by increasing the total pathlength of the radiation through the sample.
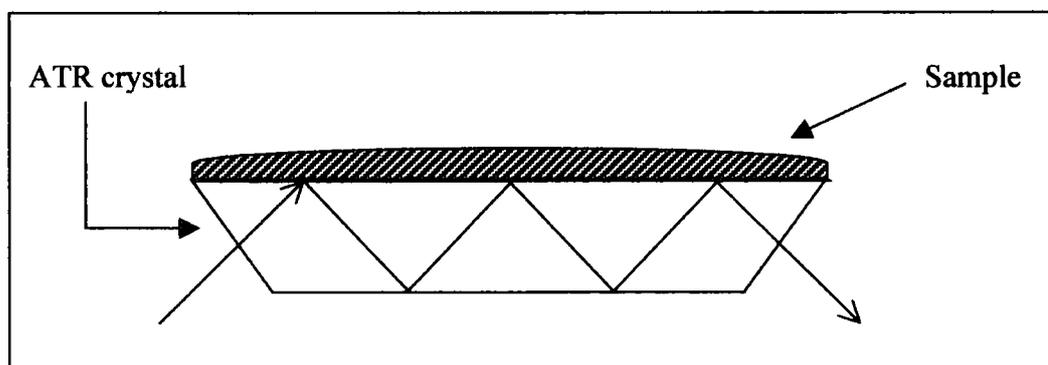
Figure 2.6. Reflections within an ATR element.

2.1.3. Infrared Probe

The FT-IR probe is an accessory recently developed by Graseby Specac Ltd. that works on the basis of ATR[10]. Light is delivered to the probe via a chalcogenide fibre optic. At the tip the radiation enters a zinc selenide prism, which has a 90° angle at its apex. It is this prism which acts as the IRE when brought into contact with the sample. The radiation undergoes two total internal reflections at the tip, returning to the spectrometer via a second fibre.

The zinc selenide tip allows penetration depths of between 0.4 μm at 4000 cm^{-1} and 3.8 μm at 400 cm^{-1} (calculated from eq. 2.6, using n_1=2.403 and n_2=1.333, the refractive index of water). Figure 2.7 shows a schematic diagram of the probe and guides.

Applications of this accessory include quality control, reaction monitoring and skin analysis[10]. The small tip (approximately 1 cm^2 in contact area) allows intimate contact with the surfaces resulting in minimal disruption of the sample.
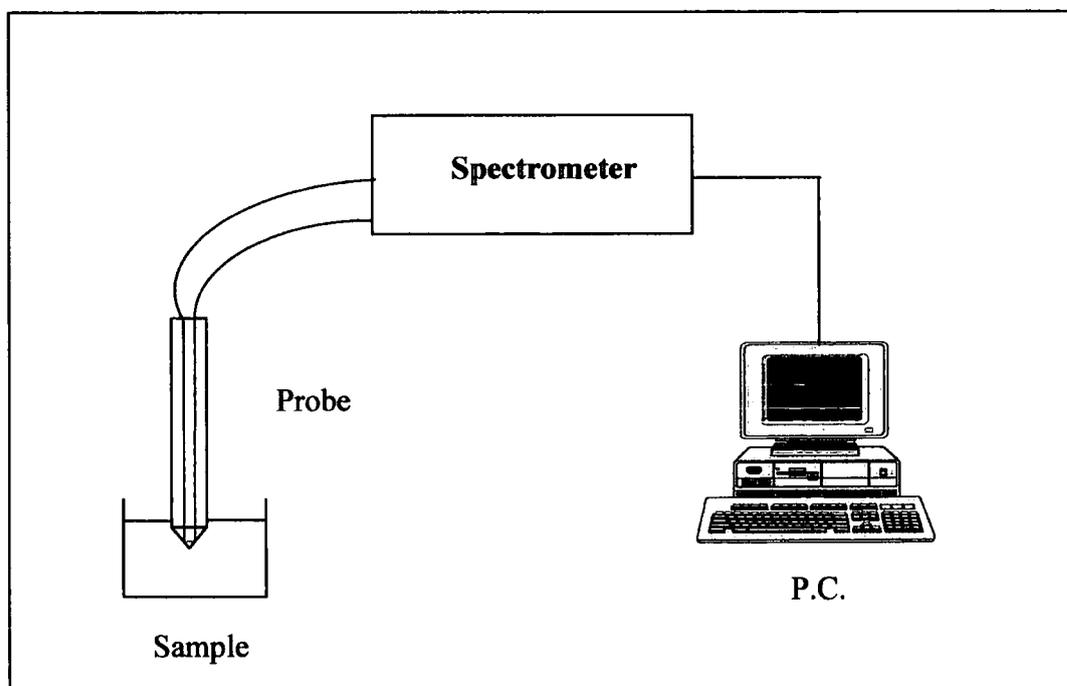
Figure 2.7. Schematic of the infrared probe.

2.1.4. Instrument Parameters

The IR spectra shown in these studies were obtained using a Perkin Elmer Paragon 1000 FT-IR spectrometer, controlled by GRAMS 1000 software, unless otherwise stated. This software was also used for spectral data manipulations and ATR corrections.

The instrument parameters adopted are detailed below unless otherwise stated.

Probe:	Graseby Specac Infrared probe with a 90° Zinc Selenide tip
ATR Plate:	Graseby Specac Benchmark Overhead ATR system fitted with a 45° Zinc Selenide six-reflection crystal
Golden Gate:	Graseby Specac Golden Gate containing a 45° single reflection type IIa diamond
No. scans:	16
Resolution:	4 cm^{-1}
Spectral range:	Probe: - 4000-2200 cm^{-1}, 2100-1000 cm^{-1}[*]
	ATR Plate: - 4000-700 cm^{-1}
	Golden Gate: - 4000-400 cm^{-1}

[*]The discontinuity in the spectral range of the probe is due to the absorption bands of the chalcogenide glass optical fibres.

2.2. Ultraviolet-Visible Absorption Spectroscopy

UV-Visible absorption spectra were obtained using an ATI Unicam UV2-100 spectrometer, controlled using Unicam Vision Software (Version 3.41) running on a PC. The spectrometer is a double beam scanning spectrometer using a combination of tungsten ($\lambda > 325$ nm) and deuterium lamps ($\lambda < 325$ nm) as the source. Light from the source passes through the monochromator and is directed onto a beam splitter to

produce the sample and reference beams. After passing through the sample compartment the beams are recombined and directed onto the detector.

Room temperature spectra were obtained from samples contained in 1 cm pathlength quartz cuvettes, usually over the range 190-600 nm. The instrument baseline was determined with the appropriate solvent prior to running each spectrum.

Low temperature spectra were obtained from samples held in a liquid nitrogen cooled cryostat (Oxford Instruments, DN 1704). The temperature was controlled and monitored using an ITC-601 temperature controller. The layout of the cryostat is shown in figure 2.8. The solvents used for low temperature work were carefully chosen so that they would form good quality, clear glasses upon cooling to 77 K. EPA[11] (a 5:5:2 mixture of diethyl ether: isopentane: ethanol) was used as a polar solvent mixture whilst a 4:1 mixture of methyl cyclohexane: isopentane was employed as a non-polar solvent.

Molar extinction coefficients, ε, were determined using the Beer-Lambert Law (equation 2.10),[12]

$$A = \varepsilon\, c\, l = \log_{10} \frac{I_0}{I_t} \qquad\qquad \text{Equation 2.10}$$

where   A is the absorbance at the wavelength of interest,

ε is the molar extinction coefficient in $dm^3 mol^{-1} cm^{-1}$,

c is the concentration of the solution in $mol\,dm^{-3}$,

l is the pathlength of the cuvette in cm,

I_0 is the intensity of incident radiation, and

I_t is the intensity of the transmitted radiation.
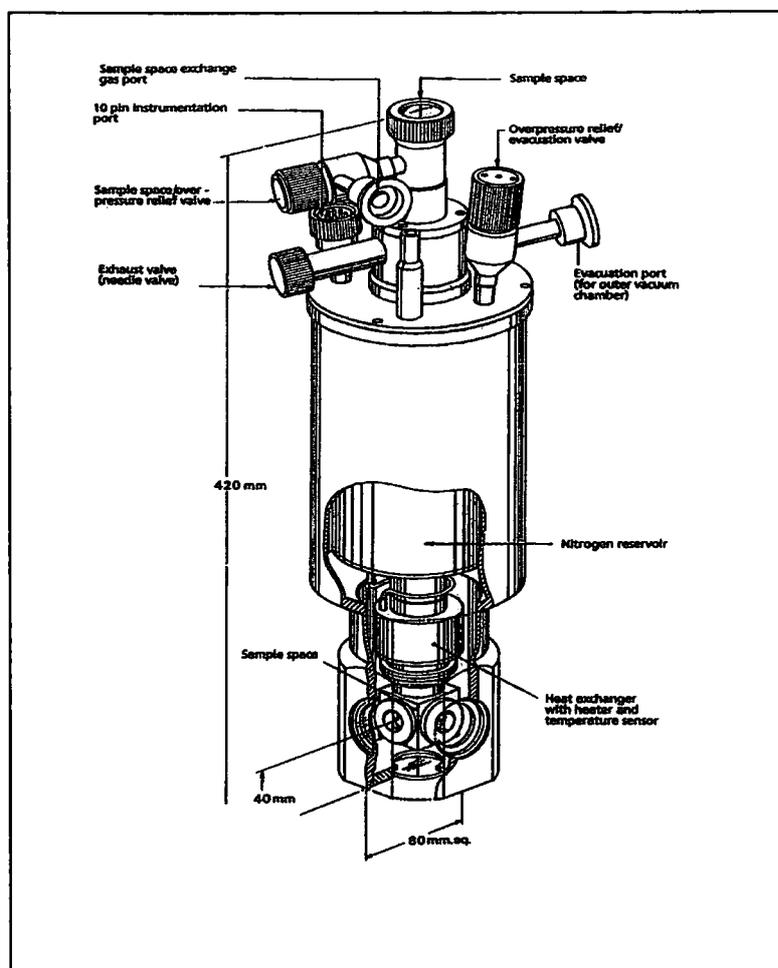
Figure 2.8. Layout of the Oxford Instruments DN 1704 Cryostat[13].

2.3. Luminescence Spectroscopy

2.3.1. Fluorescence Spectroscopy

2.3.1.1. Spectra

Fluorescence emission and excitation spectra were obtained using a Perkin Elmer LS-50B luminescence spectrometer fitted with a Hamamatsu R928 photomultiplier tube (PMT) and controlled using FL-Winlab 3.0 software running on a PC. The layout of the spectrometer is shown in figure 2.9.

A pulsed xenon lamp produces radiation in the range 200-800 nm, with a pulse duration of ~10 µs. The light is then focussed onto the entrance slit of the excitation

monochromator used to select a narrow wavelength band. The majority of the energy is then directed onto the sample using a series of mirrors and filters, but a small amount is diverted onto the reference photomultiplier which corrects for the wavelength dependence of the excitation beam. The emission from the sample is collected and passed through a similar set of optics, focussed onto the entrance slit of the emission monochromator and the intensity is recorded by the sample photomultiplier tube. When the spectrometer is operating in fluorescence mode the signal is integrated over a gate time of 80 μs to collect all the light emitted from the sample at each wavelength. The effect of dark current (i.e. the background signal detected when no light falls on the detector) is subtracted from the 'real' signals at both the reference and sample PMTs, and is measured by integrating the output of the two PMTs just prior to the next pulse.

For the measurements detailed in this work both the excitation and emission slit widths were set to give a bandpass of 5 nm and a scan speed of 120 nmmin^{-1} was employed.
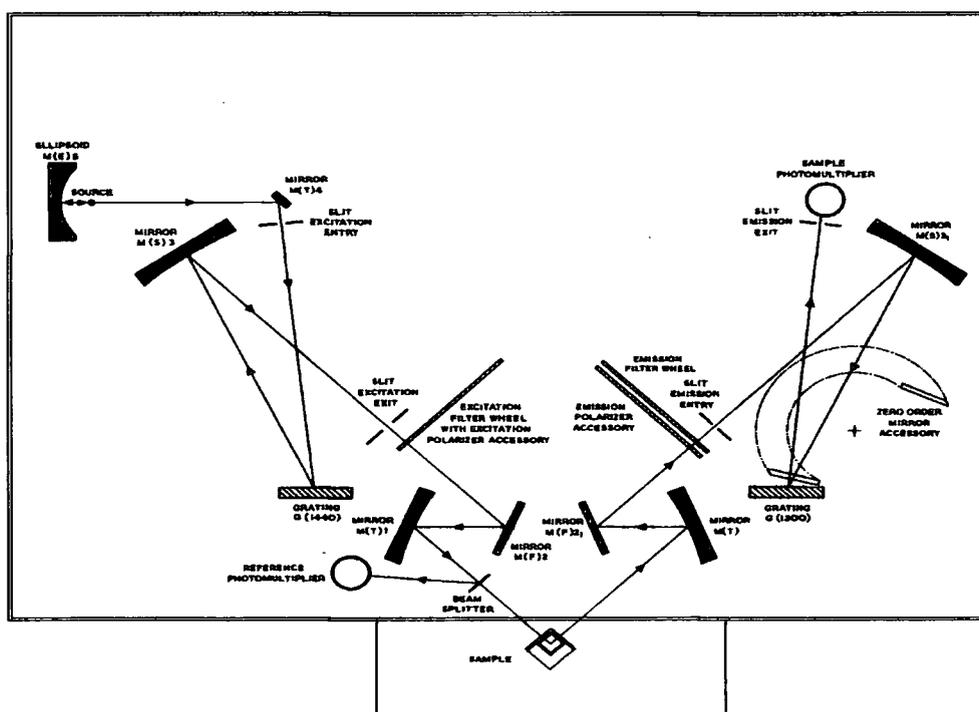
Figure 2.9. Optical diagram of the Perkin Elmer LS-50B Fluorimeter[14].

Emission spectra were usually obtained in the region 330-600 nm following excitation at either 340 nm (anthranilate esters) or 310 nm (N-acetyl-menthyl anthranilate) and excitation spectra were obtained in the region 200-580 nm.

All emission spectra reported in this work have been corrected for the response of the PMT using a correction curve determined for the spectrometer. The excitation spectra are, however, corrected internally for variation in the excitation intensity using a built-in Rhodamine dye quantum counter.   In order to minimise inner filter effects,[15] samples were prepared such that their maximum absorbance at the excitation wavelength was ≤ 0.1 when held in a 1 cm x 1 cm quartz fluorescence cuvette.

2.3.1.2.   Quantum Yields

The fluorescence quantum yield is defined in equation 2.11.

$$\Phi_f = \frac{\text{Number of quanta emitted as fluorescence/ vol/ time}}{\text{Number of photons absorbed/ vol/ time}} \qquad \text{Equation 2.11}$$

This can be expressed in terms of competing decay processes from the first excited state by assuming steady state conditions, i.e. the rate of formation of the first excited singlet state equals the rate of decay.

Process	Equation	Rate
Absorption of light	$S_0 + h\upsilon \rightarrow S_1$	I_a
Radiative Decay	$S_1 \rightarrow S_0 + h\upsilon$	$k_f [S_1]$
Internal conversion	$S_1 \rightarrow S_0 + \text{heat}$	$k_{ic} [S_1]$
Intersystem crossing	$S_1 \rightarrow T_1$	$k_{isc} [S_1]$

Using the steady state approximation for absorption by the S_1 state:

$$I_a = k_f [S_1] + k_{ic} [S_1] + k_{isc} [S_1] \qquad \text{Equation 2.12}$$

and:
$$\Phi_f = \frac{k_f}{k_f + k_{ic} + k_{isc}}$$
Equation 2.13

In practice it is difficult to determine the quantum yield of fluorescence by absolute methods, so the comparative method using reference compounds with known fluorescence quantum yields tends to be more widely used. This has been described by Williams et al.[16]

The reference compounds used in this work were anthracene in ethanol ($\Phi_f = 0.27 \pm 0.03$), 2-aminopyridine in 0.2 M H_2SO_4 ($\Phi_f = 0.60 \pm 0.05$), quinine bisulfate in 2 M H_2SO_4 ($\Phi_f = 0.55$) and 9,10-diphenylanthracene in cyclohexane ($\Phi_f = 0.90 \pm 0.02$)[17,18]. The fluorescence quantum yields were calculated using equation 2.14.

$$\Phi_x = \Phi_r \cdot \frac{A_r}{A_x} \cdot \frac{E_x}{E_r} \cdot \frac{I_r}{I_x} \cdot \frac{n_x^2}{n_r^2}$$
Equation 2.14

where r and x refer to the reference compounds and sample compounds respectively,

Φ is the quantum yield of fluorescence,

A is the absorbance at λ_{ex},

E is the corrected integrated emission intensity,

I is the corrected intensity of excitation (since all of the measurements were made using identical excitation conditions this term can be ignored), and

n is the refractive index of solvent.

Air-equilibrated solutions of the compounds of interest were optically matched (± 0.001 absorbance units) at the excitation wavelength to that of two standard reference solutions. The reference compounds were chosen such that their fluorescence emission spectra overlapped with those of the compounds being studied. Five solutions of the compound and standard, with absorbances between 0.02 and 0.10 (to minimise excitation and emission inner filter effects), were analysed in a 1 cm pathlength quartz fluorescence cuvette and the integrated emission intensity for each

solution was determined. Plots of total integrated emission intensity against absorbance produced straight lines and yielded the ratios of E/A, allowing the unknown quantum yields to be calculated more simply by using equation 2.15.

$$\Phi_x = \Phi_r \cdot \frac{\text{slope}_x}{\text{slope}_r} \cdot \left(\frac{n_x}{n_r}\right)^2 \qquad \text{Equation 2.15}$$

2.3.1.3.   Lifetimes

Fluorescence lifetimes were recorded using the method of time correlated single photon counting (TCSPC). The theory of TCSPC has been described in detail in several texts[19,20] and only a brief summary will be given here. The decay of fluorescence from a fluorophore usually occurs via a first order process and may be represented by a single exponential decay, $I_t = I_0 \exp(-t/\tau)$. A short time after excitation the probability of detecting a photon is larger than at longer time intervals when much of the fluorescence has decayed. The time, t, taken for a single photon to be detected is recorded for each event and a histogram of the number of photons vs. time is produced. The measured decay is a convolution of the time response of the excitation source, the electronics of the apparatus and the true fluorescence decay. The true fluorescence decay is then determined using the technique of 'iterative re-convolution'.

In practice the decays are recorded using a sub-nanosecond pulsed excitation source to excite the sample repeatedly and the time, t, is measured using a time to amplitude converter which is started by the excitation pulse and stopped by the detection of a photon. An instrument response function, obtained from a scattering solution analysed under the same conditions as the sample of interest, is reconvolved with an exponential function using estimates for the values of A and τ. These are then varied until the best fit using non-linear least squares analysis is obtained.

The fluorescence lifetime measurements described in this work were carried out at the Rutherford Appleton Laboratory. The samples were excited using the frequency doubled output from a cavity dumped, mode locked dye laser (Rhodamine 6G)

synchronously pumped by a Nd:YAG laser. The fluorescence was collected at 90° to the incident beam, and the emission wavelength was selected using a monochromator and detected using a microchannel plate photomultiplier tube (Hamamatsu 1564). The data were acquired using a PC-based Picoquant card (SPC-300) and analysed using the F-900 Edinburgh Instruments data analysis package. In all cases, excellent fits were obtained for a single exponential decay as judged by reduced chi-squared, random residuals and an autocorrelation function.

2.3.2. Phosphorescence Spectroscopy

2.3.2.1.   Spectra

Phosphorescence spectra were obtained from samples held in organic glasses at 77 K as described in section 2.2. Spectra were recorded using the Perkin Elmer LS-50B luminescence spectrometer described in section 2.3.2.1 which had been adapted to hold the Oxford Instruments cryostat. Phosphorescence is a much longer lived process than fluorescence and phosphorescence lifetimes can be several seconds long. When the spectrometer is operated in phosphorescence mode a delay time, T_d, between exciting the sample and observing the emission is introduced to remove the contribution of fluorescence from the spectral profile. Also much longer gate times, T_g, are used than for measuring fluorescence spectra since the emission intensity may not be seen to vary in the time interval between the pulses. Typical gate times are in the region 0.01-10 ms. This is shown graphically in figure 2.10.
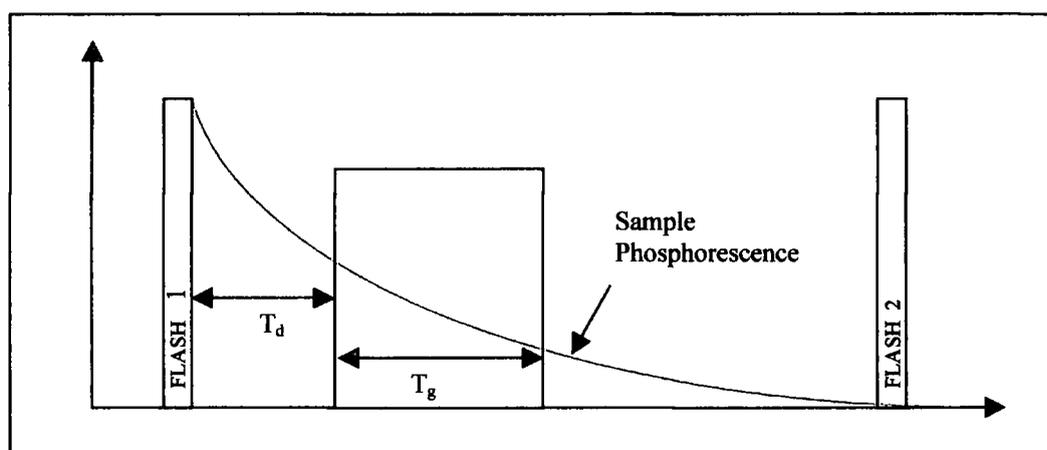
Figure 2.10. Time gating of the LS-50B in phosphorescence mode.

2.3.2.2.   Lifetimes

Phosphorescence lifetimes were measured by fixing the emission and excitation wavelengths and were obtained using the FL-Winlab Time Drive facility. The Time Drive application enables luminescence measurements to be made at fixed wavelengths, with defined intervals over a specified period of time. The sample was excited as described above, the lamp stopped and the phosphorescence intensity recorded as a function of time.

As with fluorescence, the decay of phosphorescence usually occurs via a first order process and so the data obtained were fitted to a single exponential decay of the form $I_t = I_0 \exp(-t/\tau)$. The values of I_0 and τ were varied using non-linear least squares analysis to obtain the best fit.

2.3.2.3.   Triplet State Energies

Triplet state energies were estimated from the phosphorescence emission spectra. The wavelength of the (0,0) transition was taken to be that at which the intensity of the phosphorescence at the blue edge of the emission band was 10% of the maximum. This wavelength value was then converted into kJmol^{-1} using equation 2.16.

$$E = \frac{hc}{\lambda} \cdot N_a$$

Equation 2.16

where   E is the triplet state energy, and

λ is the wavelength.

2.4.   Laser Flash Photolysis

2.4.1.   Introduction to Laser Flash Photolysis

Flash photolysis was first developed in 1950 by Porter, who observed that high intensity light could produce high concentrations of transient species[21,22]. The technique provides a method to study charge-transfer reactions, energy transfer phenomena and short-lived species with lifetimes in the nanosecond to millisecond range[23,24].

On absorbing light the sample is excited to a higher excited singlet state, S_n. This state then decays via several mechanisms such as radiative decay, i.e. fluorescence and non-radiative decay, i.e. internal conversion and intersystem crossing to the triplet state, T_1, (see figure 2.11).
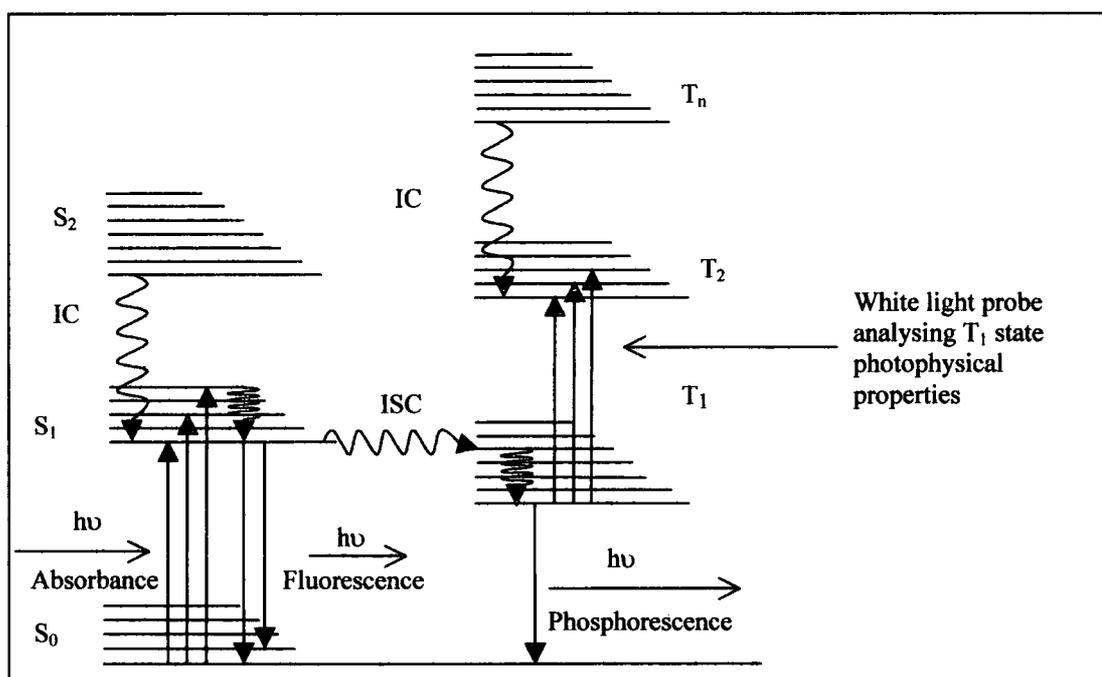
Figure 2.11.   Theory of flash photolysis.

The photophysics of this triplet state (absorption spectrum, lifetime, quantum yield) are then probed by a continuous white light source. This probe light excites the T_1 state to higher triplet states allowing the concentration of the T_1 state to be monitored by following the changes in the intensity of the probe light with time as shown in figure

2.12. I_0 is the incident intensity of the probe beam, I_a is the change in intensity associated with the transient, and I_t is the intensity of light transmitted at time t.
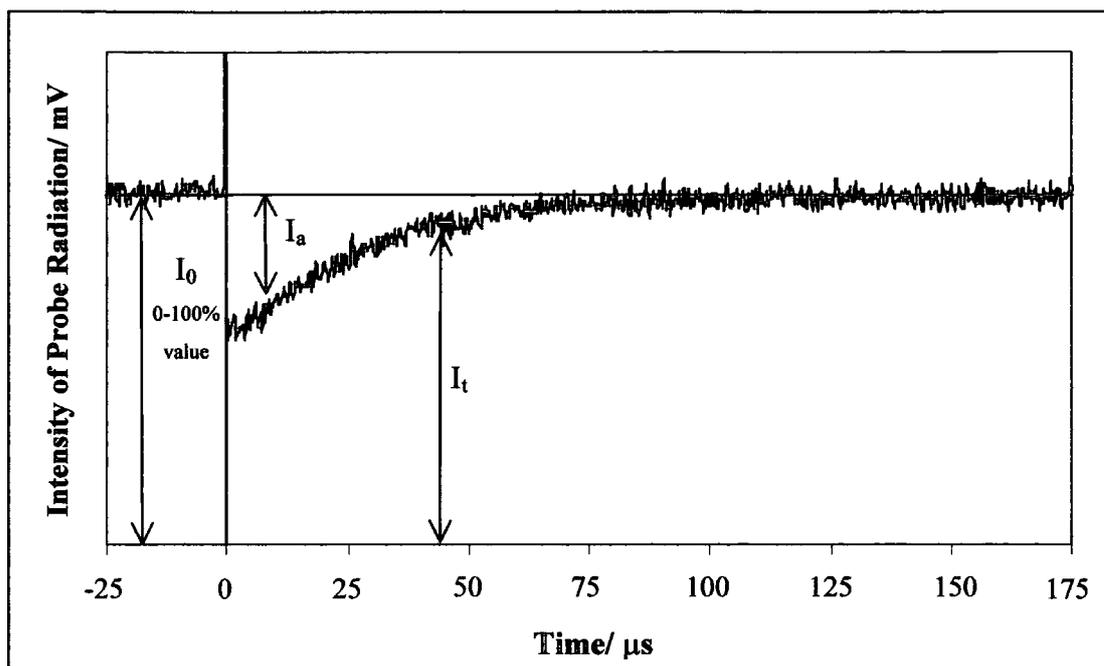
Figure 2.12. A typical transient decay.

At time t < 0, i.e. prior to the excitation of the sample, the absorbance of the system due to the ground state species is given by:

$$\text{Absorbance}(\lambda, t < 0) = \log_{10}\left(\frac{I_0(\lambda)}{I_t(\lambda, t < 0)}\right) \qquad \text{Equation 2.17}$$

At time t after excitation of the sample the absorbance of the system is given by:

$$\text{Absorbance}(\lambda, t) = \log_{10}\left(\frac{I_0(\lambda)}{I_t(\lambda, t)}\right) = \log_{10}\left(\frac{I_0(\lambda)}{I_0(\lambda, t) - I_a(\lambda, t)}\right)$$

$$\text{Equation 2.18}$$

The change in absorbance, ΔA due to the transient can then be obtained by subtraction of the absorbance at time t<0 from that at time t and yields equation 2.19.

$$\Delta A\left(\lambda, t\right) = \log_{10}\left(\frac{I_t(\lambda, t < 0)}{I_t(\lambda, t)}\right) \qquad \text{Equation 2.19}$$

Figure 2.13 shows a typical ΔA vs. time trace.
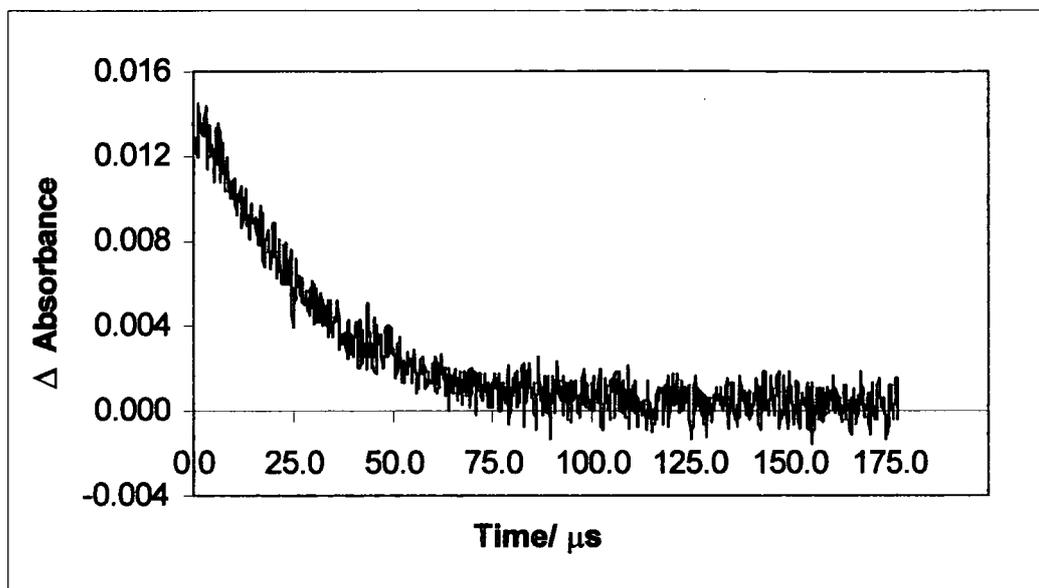
Figure 2.13. Transient absorbance trace.

By varying the wavelength at which the measurements are made a difference absorption spectrum can be built up by plotting the transient height at any given time delay against the wavelength, as shown in figure 2.14.

The treatment described so far examines the absorbance of the transient species, however at wavelengths where only the ground state species absorbs, an inverted trace is seen, i.e. I_a is negative, corresponding to the bleach and recovery of the ground state species.
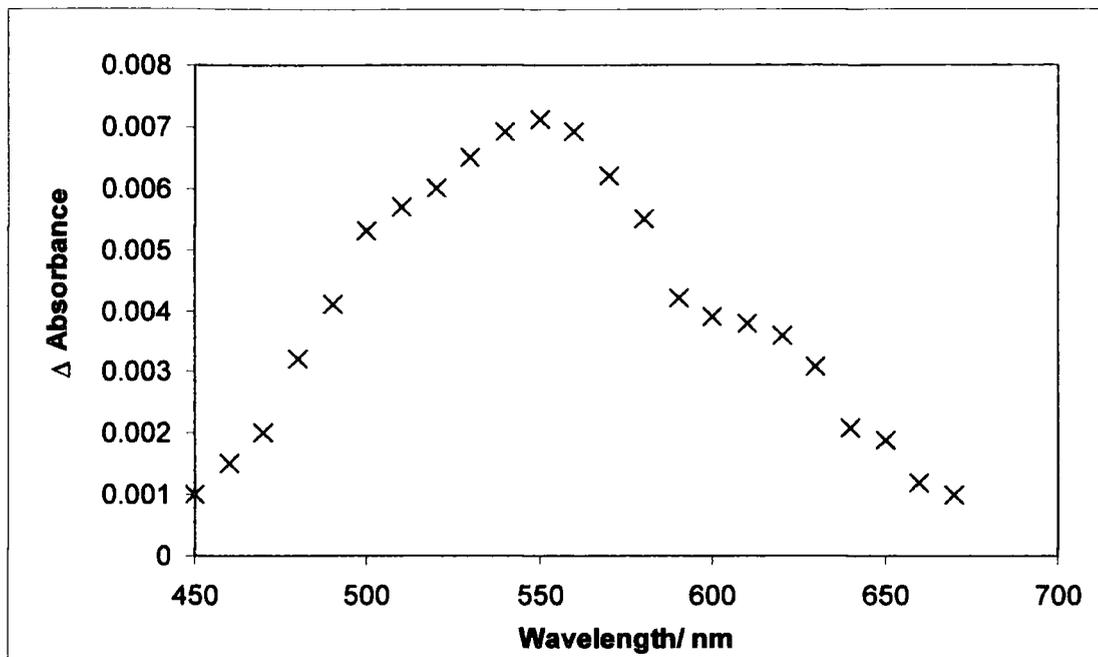
Figure 2.14. Transient absorbance spectrum.

2.4.2. Experimental Set-up

In nanosecond laser flash photolysis, the output from a pulsed laser is directed onto a sample cuvette at right angles to, or co-linear with, a continuous polychromatic analysing beam.

The studies described here were performed using the experimental set-up shown in figure 2.15. The excitation sources employed were either the third (λ_{ex} = 355 nm) or fourth (λ_{ex} = 266 nm) harmonic of a Q-switched Nd:YAG laser (Spectra Physics Quanta-Ray GCR-150-10). The laser produces a 10 Hz train of pulses with a FWHM of ~5 ns. The pulse energy of ~200 mJ was highly attenuated to give an energy at the sample of ~1 mJ.

In the studies carried out on the anthranilate esters described in chapters 3 and 4 it was found that in a 90° geometry delayed fluorescence was so intense that it obscured the transient absorption signal. In order to be able study more dilute solutions in long pathlength cells a co-linear pump and probe set-up was adopted.

In the case of 355 nm excitation a 5 mm liquid light guide was used to direct the laser light onto a 355 nm dichroic mirror, through a $CoSO_4$ filter and then onto the sample

($A_{355} \sim 0.5$). The $CoSO_4$ filter was used to remove residual 532 nm and 1064 nm in the laser beam. However the light guide was unsuitable for use with 266 nm light, so in this case the laser light was delivered to the sample using a series of dichroic mirrors and prisms.

The transient produced upon excitation was probed using a tungsten-halogen lamp (12 V, 100 W) co-linear with the excitation beam which was focussed so that the two beams passed through the same region of the sample. After passing through the sample the probe beam was then focussed into the monochromator (Instruments SA Triax 320) and the intensity at the selected wavelength was measured using a Hamamatsu R928 photomultiplier tube (PMT). The signal from the PMT was then split and fed into the two channels of a Tektronix TDS-320 digital oscilloscope. Channel one of the oscilloscope was AC coupled allowing the small and rapidly changing signal due to the transient decay to be detected, whilst channel two was DC coupled to allow the relatively large I_0 value to be measured. The data from the oscilloscope were then transferred to a PC for storage and analysis using Microsoft Excel.
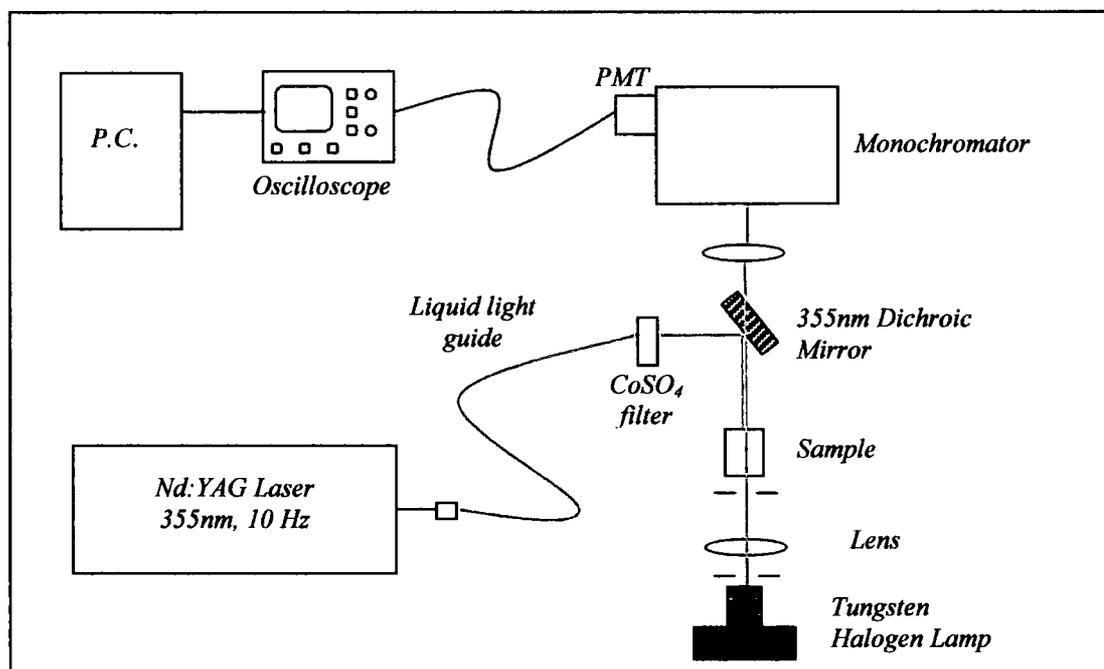
Figure 2.15. Experimental arrangement of the flash photolysis set-up.

2.4.3. Triplet Lifetime Measurements

Equation 2.20 gives the rate of decay of a triplet species in solution:

$$k_T = k_p + k_0 + k_{TT}[T_1] + k_s[S] + \sum_i k_Q[Q_i] \qquad \text{Equation 2.20}$$

where k_T is the rate constant for triplet state decay,

k_p is the rate constant for phosphorescence emission,

k_0 is the intrinsic rate constant for non-radiative decay of the triplet species,

$k_{TT}[T_1]$ is the triplet-triplet annihilation rate term,

$k_s[S]$ is the self-quenching rate term, and

$k_Q[Q_i]$ is the bimolecular quenching rate term.

In aerated solutions at room temperature phosphorescence is negligible due to quenching by oxygen, and radiationless pathways dominate the decay. The use of dilute solutions and low laser powers reduces the probability of triplet-triplet annihilation and degassing of the samples removes oxygen, the main extrinsic quenching agent. Therefore by careful control of the experimental conditions equation 2.20 can be reduced to the Stern-Volmer equation:

$$k_T = k_0 + k_s[S] \qquad \text{Equation 2.21}$$

At any given sample concentration the decay of the triplet state will follow first order kinetics and so the rate constant can be determined from a mono-exponential fit to the absorbance vs. time traces obtained. This yields the observed lifetime τ_T since, $\tau_T = 1/k_T$.

2.4.4. Self-Quenching Rate Constants

From equation 2.20 it can be seen that there are many factors that affect the measured lifetime of a transient species. At high sample concentrations, τ_T may be reduced due to self-quenching or by triplet-triplet annihilation which leads to non-exponential

decays at high triplet state concentrations. The self-quenching rate constant can be easily determined using equation 2.21 by measuring the lifetime, τ_T, at various sample concentrations. In the work described here five samples of varying concentrations were degassed and the τ_T values determined. Plots of $1/\tau_T$ vs concentration of the ground state species yielded straight lines of intercept, $1/\tau_0$, and gradient k_s.

2.4.5.   Oxygen-Quenching Rate Constants

Potentially the most important quenching mechanism for excited state species is that which involves molecular oxygen, the major quenching impurity. Samples were thoroughly degassed using the freeze-pump-thaw technique[25] and the lifetime measured. The samples were then exposed to a controlled air pressure measured using a MKS Baratron pressure gauge and the lifetime re-measured. Corrections were then made for the contribution to the total pressure by the solvent vapour,[26] and the pressure converted into oxygen concentration in $moldm^{-3}$.[11] As described above plots of $1/\tau_T$ against oxygen concentration yielded straight lines of intercept $1/\tau_0$ and gradient k_{O_2}, where τ_T is the observed lifetime, τ_0 is the intrinsic lifetime in the absence of quencher and k_{O_2} is the oxygen quenching rate constant.

2.5.   Singlet Oxygen Detection

2.5.1.   Introduction to Singlet Oxygen

Singlet oxygen, $^1O_2$, is usually generated following the quenching of a triplet state molecule by ground state molecular oxygen $(^3\Sigma_g^-)O_2$, and proceeds via an encounter complex[27]. There are two states of singlet oxygen, $^1\Delta_g$ and $^1\Sigma_g^+$, however, the $^1\Delta_g$ state is assumed to be the only reactive state since it is far more stable than the $^1\Sigma_g^+$ state and may have a lifetime in gaseous media of several minutes. This is due to the spin forbidden nature of the $^1\Delta_g \rightarrow {}^3\Sigma_g^-$ transition[28].

Equation 2.22 gives the expression for the quantum yield of singlet oxygen formation, Φ_Δ:

$$\Phi_\Delta = \Phi_T \frac{k_{\Delta O_2}[O_2]}{(k_{\Delta O_2} + k_{\Sigma O_2})[O_2] + k_{nr} + k_r} \qquad \text{Equation 2.22}$$

where Φ_T is the quantum yield of triplet state formation,

$k_{\Delta O_2}$ is the rate constant for quenching by ground state oxygen to give $(^1\Delta_g)O_2$,
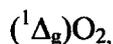
$k_{\Sigma O_2}$ is the rate constant for quenching by ground state oxygen to give $(^1\Sigma_g^-)O_2$,
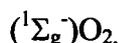
k_{nr} is the rate constant for non-radiative deactivation of the triplet state, and

k_r is the rate constant for radiative deactivation of the triplet state.

In most systems oxygen quenching occurs at a much faster rate than the other deactivation processes and so k_{nr} and k_r can be ignored, allowing simplification of equation 2.22 to give:

$$\Phi_\Delta = \Phi_T \left(\frac{k_{\Delta O_2}}{k_{\Delta O_2} + k_{\Sigma O_2}} \right) \qquad \text{Equation 2.23}$$

The collection of rate terms is effectively the fraction of triplet state molecules quenched by oxygen to yield $^1\Delta_g$ singlet oxygen and can be represented by S_Δ. Equation 2.23 then simplifies further to:

$$\Phi_\Delta = \Phi_T S_\Delta \qquad \text{Equation 2.24}$$

Deactivation of the excited state singlet oxygen in solution occurs via several mechanisms. These include non-radiative decay by transfer of vibrational energy to surrounding solvent molecules, physical or chemical quenching by added species and radiative decay giving rise to a phosphorescent emission at 1269 nm, allowing easy detection of singlet oxygen in solution. The predominant mechanism has been shown to be non-radiative[29]. Both the radiative decay rate, k_r, and the non-radiative decay rate, k_{nr}, have been shown to be solvent dependent. The non-radiative mechanism is

controlled by the ability of the solvent to act as an energy sink by absorbing vibrational energy from the excited state molecules.

Singlet oxygen may also be detected using chemical traps or quenchers such as cholesterol[30], diphenylisobenzofuran[31] and p-nitrosoaniline[32].

Complications with such methods include lack of solubility in the system being considered or side reactions between the added species and the sensitiser molecules.

2.5.2. Experimental Set-up
2.5.2.1. Chemical trapping

The methods of chemical trapping described by Gorman et al.[31] and Kraljic et al.[32] were adopted in an attempt to detect the formation of singlet oxygen by sensitisers in final sunscreen formulations. The method by Gorman involved monitoring the bleach of the 1,3-diphenylisobenzofuran (DPBF) absorption peak at 415 nm on irradiation with ultraviolet light.

The method of Kraljic monitors the bleach of p-nitrosodimethylaniline (RNO) (λ_{max} = 440 nm) caused by its reaction with the transannular peroxide (AO$_2$) formed by the reaction of imidazole (A) with singlet oxygen.

2.5.2.2. Phosphorescence

The experimental set-up adopted to determine singlet oxygen lifetimes and quantum yields is shown in figure 2.16.

Samples were held in 1 cm pathlength quartz cuvettes and were excited using either the third or fourth harmonic of a Nd:YAG laser. The phosphorescence was collected at 90°, passed through an interference filter centred at 1270 nm (Infra Red Engineering Ltd.) and then focussed onto the active area of a liquid nitrogen cooled germanium photodiode (North Coast E0-817P) by an elliptical mirror.
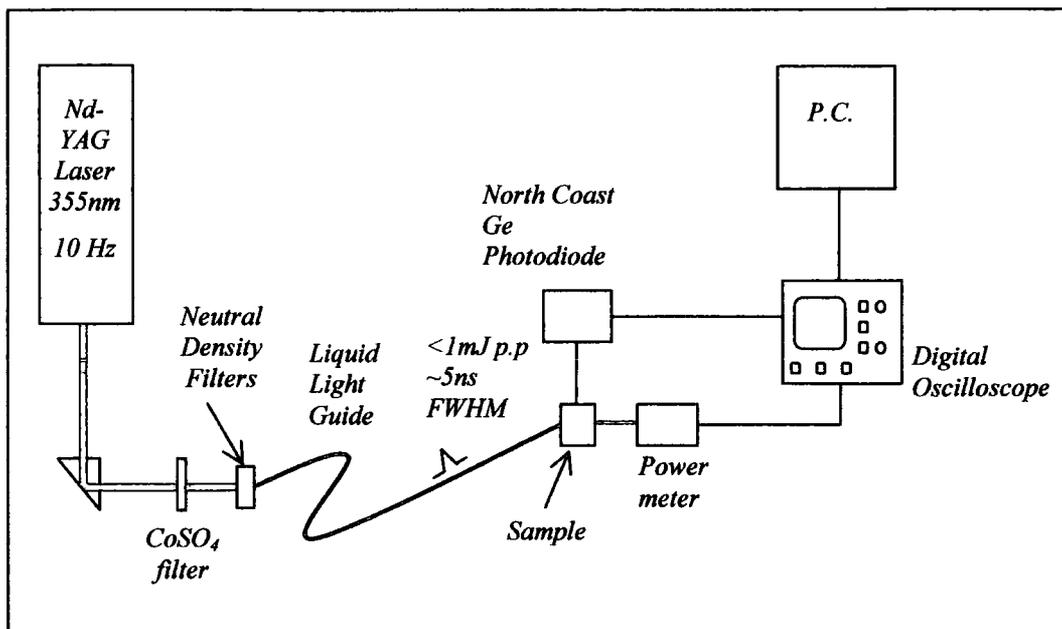
Figure 2.16. Experimental set-up for singlet oxygen detection following 355 nm

excitation.

The output from this device was then amplified and AC coupled to a digital oscilloscope which digitized and averaged the transients. Typically 20 laser shots were used for each sample. The averaged data were then transferred to a PC where they were stored and analysed. A typical signal is shown in figure 2.17.
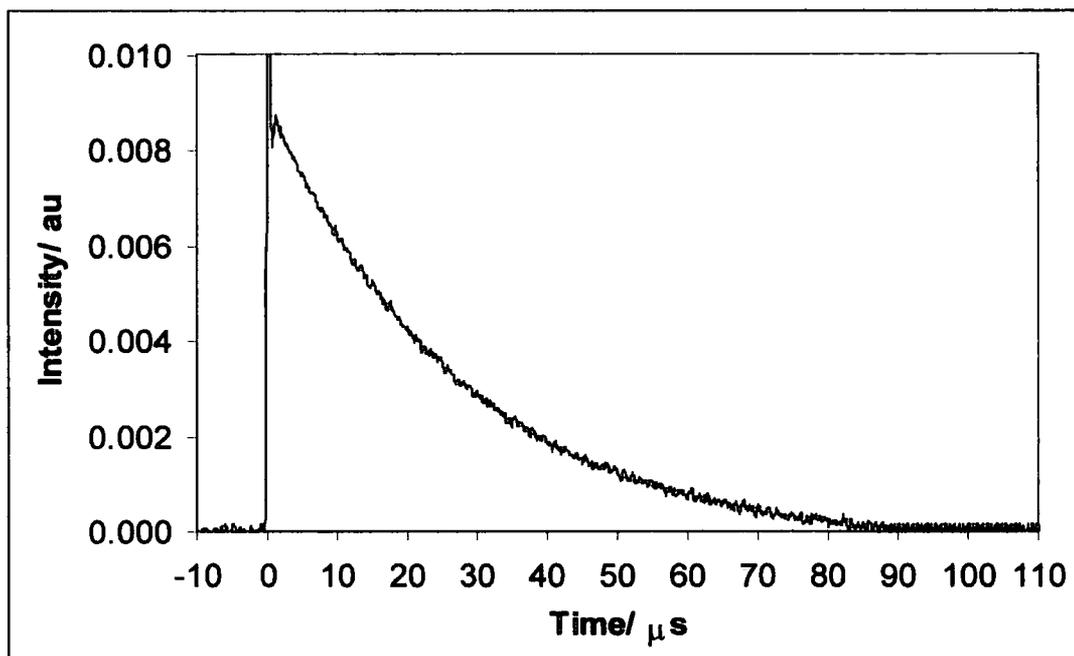
Figure 2.17. Typical singlet oxygen phosphorescence decay.

2.5.3. Quantum Yields of Singlet Oxygen Formation

Quantum yields of singlet oxygen formation, Φ_Δ, were determined relative to *meso*-tetraphenylporphyrin, TPP, in toluene ($\Phi_\Delta = 0.58$) or cyclohexane ($\Phi_\Delta = 0.67$), acridine in acetonitrile ($\Phi_\Delta = 0.82$) and perinaphthenone in ethanol ($\Phi_\Delta = 0.97$)[33] using the method recently described by Nonell[34]. The method exploits the relationship between Φ_Δ and the "zero-time" phosphorescence intensity $S(0)$, according to equation 2.25.

$$S(0) = \frac{\kappa}{n_r^2} k_R \, \Phi_\Delta \frac{E_l \left(1 - 10^{-A}\right)}{N_A \, h \, v \, V} \qquad \text{Equation 2.25}$$

where κ is a proportionality constant, including geometrical and electronic factors,

n_r is the solvent refractive index,

k_R is the radiative decay constant,

Φ_Δ is the quantum yield of singlet oxygen production,

E_l is the energy of the laser flash,

A is the sensitizer absorbance at the excitation wavelength,

v is the laser frequency, and

V is the irradiated volume.

The singlet oxygen emission decay was recorded for each sample using five laser energies and the data from each measurement were fitted to an exponential decay of the form $S(t) = S(0)\exp(-t/\tau)$ using a fitting function which optimised both $S(0)$ and τ. A plot of $S(0)$ against laser energy was drawn for each sample and the slope, $S(0)_{EA}$, determined. This was repeated for a range of solutions of different absorbances and a plot of the slopes obtained above against $1\text{-}10^{-A}$ was drawn. The slope of this plot is then proportional to the quantum yield which was calculated using equation 2.26.

$$\Phi_{\Delta, \text{sample}} = \Phi_{\Delta, \text{reference}} \frac{S(0)_{EA, \text{sample}}}{S(0)_{EA, \text{reference}}} \qquad \text{Equation 2.26}$$

Due to the large dependence of k_{nr} and k_r on solvent, the sample and reference compounds were analysed in the same solvent.

2.5.4. Singlet Oxygen Quenching Measurements

Singlet oxygen quenching rate constants were determined using the Stern-Volmer equation given below:

$$k = \frac{1}{\tau} = \frac{1}{\tau_0} + k_q[Q] \qquad\qquad \text{Equation 2.27}$$

where   k is the first order rate constant for the phosphorescence decay,

k_q is the bimolecular rate constant for the quenching of singlet oxygen by quencher Q,

τ_0 is the lifetime of singlet oxygen phosphorescence in the absence of quencher,

τ is the singlet oxygen lifetime in the presence of quencher, and

[Q] is the concentration of quencher in $moldm^{-3}$.

Singlet oxygen was generated by the 532 nm irradiation of solutions containing the quencher in question and the photosensitizer TPP in toluene or cyclohexane. Use of this wavelength ensured that only the TPP was excited and quenched by oxygen to produce singlet oxygen. Five solutions with varying quencher concentrations were prepared and the lifetime of singlet oxygen produced in each was monitored. A plot of $1/\tau$ vs quencher concentration yielded a straight line of gradient k_q allowing the combined physical and chemical quenching rate constant for the following reaction to be determined.

$$\text{Quencher} + {}^1O_2 \xrightarrow{\;k_q\;} \text{Products}$$
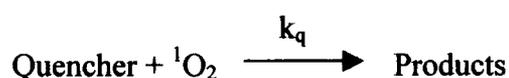
2.6.   NMR

NMR spectra were recorded on a Varian Unity 300 (299.91 MHz) spectrometer. All chemical shifts are reported in ppm.

2.7.   Synthesis of N-acetyl-menthyl anthranilate

Figure 2.18 shows the reaction undertaken in the preparation of the above compound.
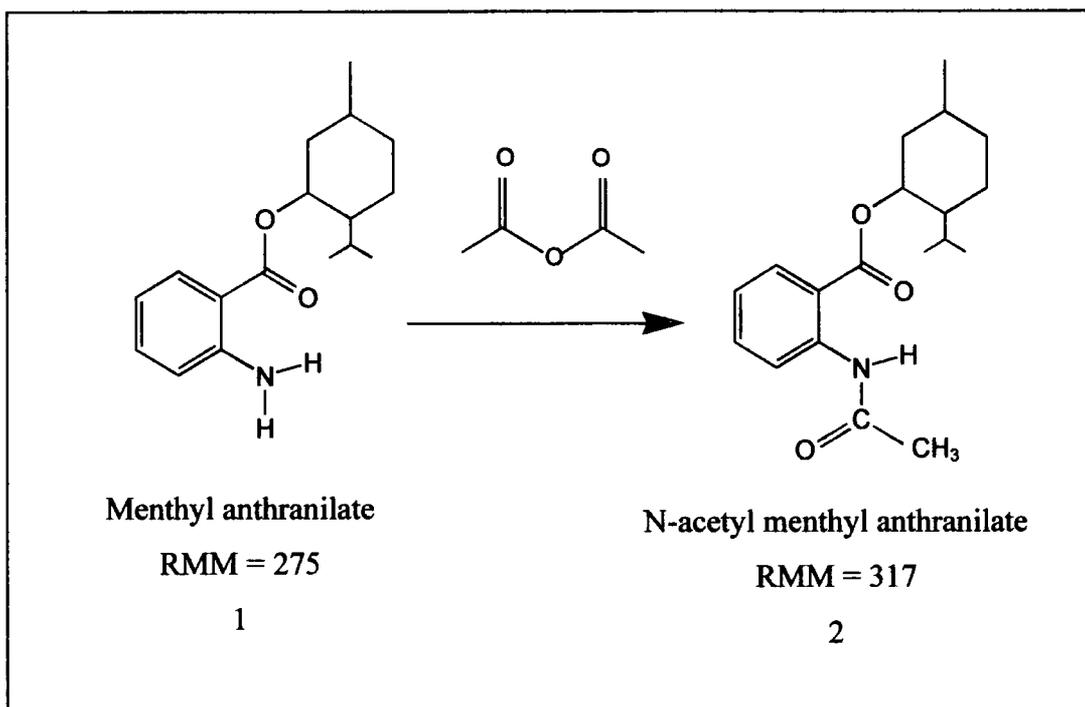
Figure 2.18. Synthetic scheme for the production of N-acetyl-menthyl anthranilate.

Menthyl anthranilate, 1, (Aldrich, 5.75 g, 20 mmol) and acetic anhydride (Aldrich, 4.08 g, 40 mmol) were placed in a round bottom flask with a magnetic stirrer bar. The mixture was heated to 60 °C and stirred for two hours. On cooling, water and NaHCO$_3$ were added to remove excess acetic anhydride and the crude product mixture was extracted into dichloromethane and dried over Na$_2$SO$_4$.

Purification was achieved by chromatography using a silica column with dichloromethane (CH$_2$Cl$_2$, Fisher Chemicals, Analar Grade) as eluent, to remove the

highly fluorescent traces of menthyl anthranilate. The product was obtained as a white solid after drying under vacuum.

Yield: 56%. (3.90 g)

δ_H (CDCl₃):   2.23 (s, 3H, -COC$\underline{H}$₃), 4.82 (m, 1H, -O-C$\underline{H}$-), 7.01-8.78 (m, 4H, Ar-H), 11.19 (m, 1H, N-$\underline{H}$).

$\delta_C\{^1H\}$ (CDCl₃): 16.7 (-CH₃), 21.0, 22.3, 23.8, 25.8, 26.7, 31.8, 34.3, 41.1, 47.4, 75.8 (C-O), 115.5, 120.5, 122.6, 130.9, 134.7, 141.9, 168.1 (C=O), 169.3 (C=O).

IR ($\bar{\upsilon}_{max}$/ cm⁻¹): 3317m (N-H), 1694s (OC=O), 1672s (NC=O), 1522m (HC-N), 1367m (OC-CH₃), 1256s (C-O-C).

Elemental Analysis: Found %:   C, 71.76; H, 8.55; N, 4.41.
                                    Calculated %:   C, 71.89; H, 8.57; N, 4.41

MS (EI):   m/z 317 (Calculated 317)

Melting pt: 67-69 °C

UV-Vis (CH₃OH), λ_{max}/ nm, (log ε)):   222 (4.46), 252 (4.14), 307 (3.73)

2.8. References

1. Colthup N.B., L.H. Daly and S.E. Wiberley (1990) *Introduction to Infrared and Raman Spectroscopy*, Academic Press, New York.

2. Nicolet Analytical Instruments, (1986) *Theory of FT-IR*.

3. Banwell C.N. and E.M. McCash (1994) *Fundamentals of Molecular Spectroscopy*, McGraw-Hill, London.

4. Griffiths P.R. and J.A. deHaseth (1986) *Fourier Transform Infrared Spectrometry*, Wiley, New York.

5. Hecht E. (1987) *Optics*, Addion-Wesley Publishing Company Inc., USA.

6. Hollas J.M. (1997) *Modern Spectroscopy*, John Wiley & Sons, Chichester.

7. Harrick N.J., (1967) *Internal Reflection Spectroscopy*, Interscience Publishers, New York.

8. Fahrenfort J. (1961) Attenuated total reflection. *Spectrochimica Acta* **17**, 698-709.

9. *Advances in Applied Fourier Transform Infrared Spectroscopy*, (1980) (Edited by M.W. Mackenzie). John Wiley & Sons, Chichester.

10. Graseby Specac Ltd. *Sampling Techniques for Infrared Analysis*, Kent, UK.

11. Murov, S.L., I. Carmichael and G.L. Hug (1995) *Handbook of Photochemistry*, 2nd ed., Marcel Dekker Inc., New York, pp. 283-297.

12. Jaffé H.H. and M. Orchin (1962) *Theory and Applications of Ultraviolet Spectroscopy*, John Wiley & Sons Inc., New York.

13. Variable Temperature liquid nitrogen Cryostat DN 1704 Operator's Handbook, Oxford Instruments.

14. Perkin Elmer LS-50 B User's Manual.

15. Parker C.A., (1968) *Photoluminescence of Solutions*, Elsevier Publishing Co., Amsterdam, pp. 220-234.

16. Williams A.T.R., S.A. Winfield and J.N. Miller (1983) Relative fluorescence quantum yields using a computer controlled luminescence spectrometer. *Analyst*, **108**, 1067-1071.

17. Eaton David F., (1989) Luminescence Spectroscopy. In *Handbook of Organic Photochemistry*, Vol 1 (Edited by J.C. Scaiano), CRC Press, Florida, pp. 231-239.

18. Parker C.A., (1968) *Photoluminescence of Solutions*. Elsevier Publishing Co., Amsterdam, pp. 266-267.

19. O'Connor D.V., and D. Phillips (1984) *Time Correlated Single Photon Counting*, Academic Press, London.

20. Birch D.J.S., and R.E. Imhof (1991) in *Topics in Fluorescence Spectroscopy*, Vol. 1: Techniques, (Edited by Lakozwicz J.R), Plenum Press, New York, pp. 1-95.

21. Porter G. and R.G.W. Norrish (1949) Chemical reactions produced by very high light intensities. *Nature*, **154**, 658.

22. Porter G. (1950) Flash photolysis and spectroscopy. A new method for the study of free radical reactions. *Proc. Roy. Soc.*, **200**, 284-300

23. Patterson L. and G. Porter (1970) Lasers in photochemical kinetics. *Chem Br.*, **6**, 246-250.

24. Hadel, L.M. (1989) Laser Flash Photolysis in *Handbook of Organic Photochemistry*, Vol 1 (Edited by J.C. Scaiano), CRC Press, Florida, pp. 279-292.

25. Luyckx G., and J. Ceulemans (1987) Deoxygenation, deaeration and degassing : a survey and evaluation of methods., *Bull. Soc. Chim. Belges.*, **96(2)**, 151-163.

26. *Handbook of Chemistry and Physics*, 61st ed., (1980) (edited by R.C. Weist). CRC Press, Florida.

27. Turro N.J. (1991) *Modern Molecular Photochemistry*, University Science Press, California, pp. 583-614.

28. Badger R.M., A.C. Wright and R.F. Whitlock (1965) Absolute intensities of the discrete and continuous absorption bands of oxygen gas at 1.26 and 1.065μ and the radiative lifetime of the $^1\Delta_g$ state of oxygen. *J. Chem. Phys.*, **43**, 4345-4350 .

29. Krasnovsky A.A. (1981) Quantum yield of photosensitised luminescence and radiative lifetime of single ($^1\Delta_g$) molecular oxygen in solution. *Chem. Phys. Lett.*, **81**, 443-445.

30. Bensasson R.V., E.J.Land and T.G. Truscott. (1993) *Excited States and Free Radicals in Biology and Medicine*. Oxford University Press, New York, pp.118.

31. Gorman, A.A., G. Lovering and M.A.J. Rodgers (1978) A pulse radiolysis study of the triplet sensitized production of singlet oxygen: determination of energy transfer efficiencies, *J. Am. Chem. Soc.*, **100**, 4527-32.

32. Kraljic I., and S. El Moshni (1978) A new method for detection of singlet oxygen in aqueous solutions. *Photochem. Photobiol.*, **28**, 577-81.

33. Wilkinson F., W.P. Helman, and A.B. Ross (1993) Quantum Yields for the Photosensitized Formation of the Lowest Excited Singlet State of Molecular Oxygen in Solution. *J. Phys. Chem. Ref. Data.* **22(1)**, 113-262.

34. Nonell S., and S.L. Braslavsky (2000) Time Resolved Singlet Oxygen Detection. In *Singlet Oxygen, UV-A and Ozone, Methods in Enzymology*, Volume 319, (Edited by L. Packer and H. Sies), Academic Press.

Chapter 3

The Photophysical Properties

of

Menthyl and Methyl Anthranilate

3.1. Introduction

3.1.1. Menthyl Anthranilate as a sunscreen

The deleterious effects of solar UV radiation on human skin are now widely known[1], and this has led to an increase in the use of topical sunscreen formulations designed to offer 'photoprotection'. Originally, sunscreens were designed to let through the 'tanning' UV-A (320-400 nm) rays whilst blocking the 'burning' UV-B (290-320 nm) radiation. As our awareness of the contribution of UV-A exposure to photoageing and other dermatological conditions[2] has increased, the commercially available sunscreen products have been changed to offer broadband protection across the entire UV range.

The first compound incorporated into sunscreen formulations to offer UV-A protection was oxybenzone (2-hydroxy-4-methoxybenzophenone). However, this material has certain disadvantages, specifically it is solid at room temperature, has a yellow colouration which imparts undesirable colour to the final product and has limited solubility. Furthermore its absorption bands are solvent dependent and have relatively low absorption coefficients[3]. As a consequence high concentrations are needed in formulations which often leads to crystallization. More recently concerns about this product causing photoallergic responses in some individuals[4,5] and its safety following irradiation by UV light have made the use of this product even less desirable[6, 7, 8, 9].

Menthyl anthranilate (figure 3.1) was highlighted by Klein and Finkelmeier as an alternative to oxybenzone. This material was approved by the U.S. FDA in 1978 at usage levels of 3.5-5%, but has received little attention until relatively recently[10]. The advantages this compound has over oxybenzone include its physical state; it is the only liquid FDA approved UV-A sunscreen agent. It is soluble in all commonly used cosmetic oils, is easily emulsified within aqueous formulations, is colourless and can be obtained 'odour-free'. As an *ortho*-disubstituted aromatic compound, there is believed to be intramolecular hydrogen bonding, resulting in minimal shifts in its λ_{max} value when placed in various solvents unlike oxybenzone and *para*-substituted sunscreens such as Padimate O. Klein and Finkelmeier concluded by describing

menthyl anthranilate as 'an ideal sunscreen to add to formulations containing octyl p-methoxy cinnamate [the most commonly used UV-B sunscreen in modern formulations] to both increase the SPF and provide protection in the UV-A region...'

Menthyl Anthranilate   Methyl Anthranilate
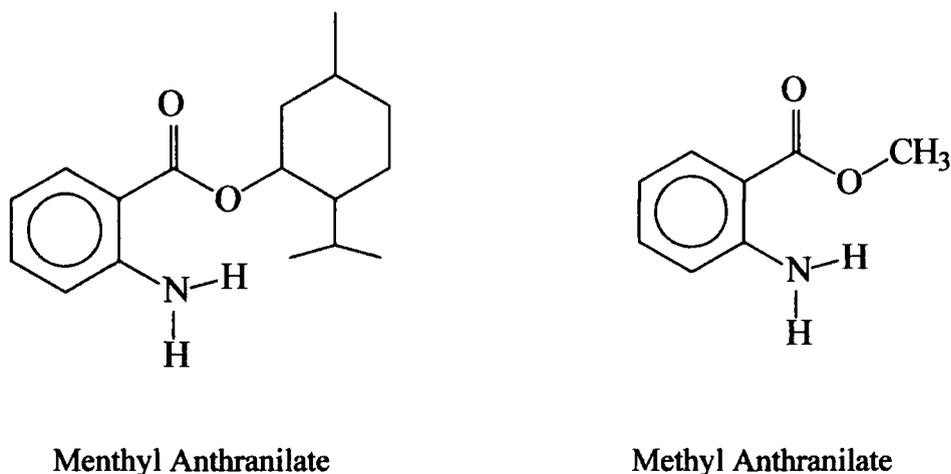
Figure 3.1 The molecular structures of menthyl anthranilate and methyl anthranilate.

3.1.2. Photophysical properties of anthranilate esters

There is surprisingly little information on menthyl and methyl anthranilate to be found in the scientific literature, although clearly their photophysical and photochemical properties should be of great interest, especially as menthyl anthranilate is used in commercial sunscreen formulations in the USA.

Diffey and Stokes[11] used a menthyl anthranilate containing sunscreen to study the feasibility of using fluorescence spectroscopy as a method for evaluating *in vivo* sunscreen performance. They also added pure menthyl anthranilate as a fluorescent marker to non-fluorescent formulations in an attempt to assess this method. Sunscreens that contained menthyl anthranilate as the only UV-A filter showed strong fluorescence. However they found that they were unable to detect fluorescence from those sunscreens which contained other UV-A filters such as 4-butyl-4'-methoxydibenzoylmethane. The origins of this observation were not fully explored but

it was suggested that it was due to either a simple inner filter effect or to the excited singlet state of menthyl anthranilate being quenched by other agents in the formulations.

There have been many studies of the parent acid of this ester, anthranilic acid, (2-aminobenzoic acid). The UV-visible absorption spectrum of this acid has been determined in several solvents and at different pHs[12] and has been explained in terms of ring substitutions in benzene and benzoic acid[13, 14, 15]. These data have been used to investigate the hydrogen bonding present in this, and related molecules, and any possibility of tautomerism[16, 17, 18]. Anthranilic acid is fluorescent in a variety of solvent environments[19, 20]. Berlmann[17] has used its fluorescent properties to provide insights into hydrogen bonding whilst Sokoloa et al. have studied the interactions between this and other compounds in solution[21]. Melhuish has published absolute quantum efficiencies of fluorescence, Φ_f, and rate constants for self-quenching and oxygen quenching of the S_1 singlet state, k_s and k_{O_2} respectively, for this compound and the methyl ester. He reported values of Φ_f for the acid to be 0.55-0.59[22, 23] in benzene and 0.56 in ethanol[22], whilst Φ_f for the methyl ester was determined to be 0.57 in benzene and 0.68 in ethanol[22]. The phosphorescence of this acid has also been studied, both in solution at low temperatures, and at room and lower temperatures when held in solid matrices. Solution state phosphorescence emission[24], triplet-triplet absorption spectra[25,26], and self-[27,28] and temperature-quenching[29,30] rate constants have been determined by various authors. Dikun et al. determined the phosphorescence lifetime of anthranilic acid in a frozen alcohol solution at −183 °C to be 1.6 s[31]. Lysenko et al. conducted several studies on anthranilic acid held in solid matrices such as CaO, $Mg(OCl)_2$ cement, sucrose, and gelatin. They studied the excitation wavelength[32] and temperature dependence[33] of the phosphorescence as well the rate of self-quenching[34].

Despite these studies on the parent acid, little work has been carried out on the esters, apart from the determination of the fluorescence quantum yield of methyl anthranilate, even though they have several commercial applications, e.g. the methyl ester is used as a food flavouring and a non-lethal bird repellent[35, 36].

In this chapter the results of a solution state photophysical study of menthyl and methyl anthranilate in a range of solvent systems are presented. These include the

measurement of fluorescence and phosphorescence emission spectra and lifetimes, quantum yields of fluorescence, triplet-triplet absorption spectra and oxygen, and self-quenching rate constants of the triplet states. Significantly we have shown that these anthranilate esters produce singlet oxygen by oxygen quenching of the T_1 state with quantum yields of ~0.10 ± 0.01 in all solvents. This is of particular significance since singlet oxygen is known to be harmful to biological systems[37].

3.2. Solution State Results

3.2.1. Absorption Spectra

The UV absorption spectra of both menthyl and methyl anthranilate in ethanol exhibit three peaks at ~ 220 nm, 249 nm and 340 nm with molar absorption coefficients of ~ 4900 $dm^3mol^{-1}cm^{-1}$ at 340 nm, see figure 3.2.
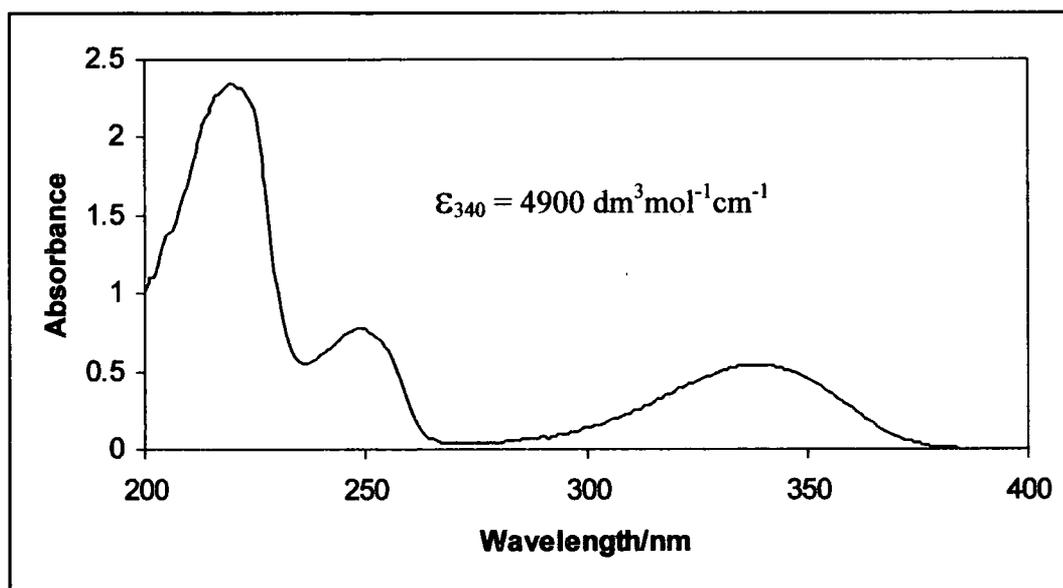
Figure 3.2. The UV-Visible absorption spectrum of menthyl anthranilate in ethanol at a concentration of ~1x10^{-4} moldm^{-3}.

The absorption maxima and extinction coefficients were found to vary only slightly with changing solvent, and data obtained for menthyl anthranilate are shown in table 3.1.

Solvent	Solvent Polarity*	λ_{max} (1)/ nm	λ_{max} (2)/ nm	λ_{max} (3)/ nm	ε at λ_{max} (3)/ $dm^3mol^{-1}cm^{-1}$
Cyclohexane	31.2	212	248	330	4900 ± 200
Chloroform	32.5	-	-	335	3000 ± 200
Dichloromethane	41.1	-	248	332	6100 ± 100
Acetonitrile	46.0	218	250	336	6400 ± 100
Ethanol	51.9	220	249	340	6300 ± 100
Methanol	55.5	218	248	338	5800 ± 100
EPA	-	224	250	338	5800 ± 200

* Solvent polarity scale based on solvatochromic band shifts in 4-(2,4,6-triphenylpyridium)-2-6-diphenylphenoxide and its trimethyl derivative[38].

Table 3.1.   UV-Visible spectroscopic data for menthyl anthranilate.

3.2.2.   Fluorescence

Both anthranilate esters studied were highly fluorescent with emission maxima at ~ 400 nm. This emission was found to be slightly solvent dependent and varied between 390 nm in non-polar solvents and 405 nm in polar solvents. This red shift of the emission maximum with increasing solvent polarity is indicative of increased polarity of the ester in its excited state relative to that in the ground state. Figure 3.3 shows the fluorescence emission and excitation spectra for methyl anthranilate in ethanol. Fluorescence lifetimes and quantum yields for the two compounds are shown in table 3.2. The fluorescence lifetimes were determined to fall in the range 5-7 ns,

with a small solvent dependence. Figure 3.4 shows the decay of fluorescence from menthyl anthranilate in ethanol and the fit obtained. The values determined for Φ_f are comparable to those reported in the literature for anthranilic acid and methyl anthranilate[22] and reveal that following excitation radiative decay from the S_1 state is the dominant decay pathway.
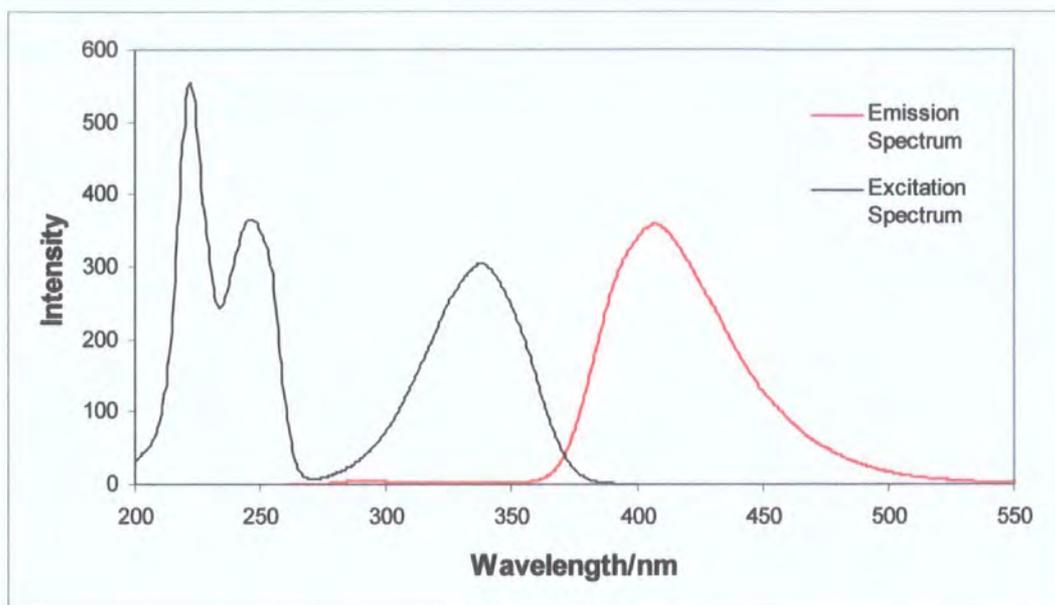
Figure 3.3. The fluorescence emission and excitation spectra of methyl anthranilate in ethanol. $\lambda_{ex} = 340$ nm, $\lambda_{em} = 405$ nm.
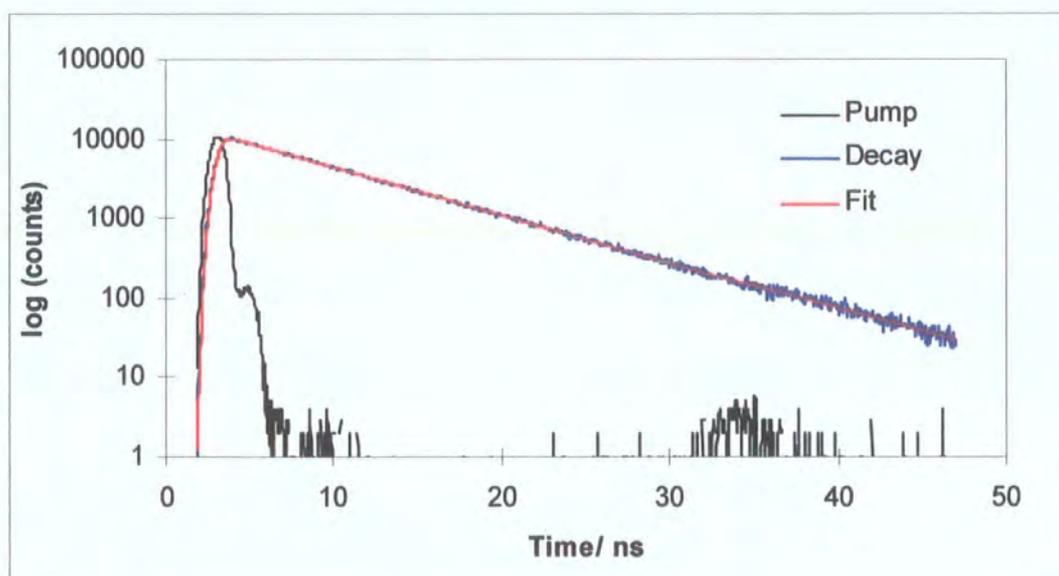
Figure 3.4. The fluorescence decay and fit obtained from menthyl anthranilate in ethanol. $\lambda_{ex} = 340$ nm, $\lambda_{em} = 405$ nm.

	Menthyl Anthranilate			Methyl Anthranilate		
	λ_{max}^{*}/ nm	$\Phi_f^{\dagger}$	$\tau_f^{\ddagger}$/ ns	λ_{max}^{*}/ nm	$\Phi_f^{\dagger}$	$\tau_f^{\ddagger}$/ ns
Toluene	390	0.54 ± 0.05	5.7 ± 0.1	390	0.54 ± 0.05	5.5 ± 0.1
Acetonitrile	400	0.57 ± 0.06	6.7 ± 0.1	399	0.51 ± 0.05	6.4 ± 0.1
Ethanol	405	0.64 ± 0.06	7.3 ± 0.1	407	0.60 ± 0.06	7.7 ± 0.1

* Fluorescence Emission Maxima following 330 nm excitation.

† Fluorescence Quantum Yield.

‡ Fluorescence Lifetime.

Table 3.2. Fluorescence data for menthyl and methyl anthranilate.

3.2.3. Phosphorescence

Low temperature phosphorescence spectra of the two esters show structureless emission ($\lambda_{max} \sim 445$ nm) with lifetimes of ~ 2.5 s, see table 3.3. From the phosphorescence spectra the energy of the triplet states are determined to be 287 ± 1 kJmol^{-1}. The phosphorescence spectrum of menthyl anthranilate in EPA at 77 K is shown in figure 3.5. No attempt was made to determine Φ_p, although by comparison of the total emission spectrum with the fluorescence spectrum its yield can be estimated to be ~ 0.30, representing a significant fraction of the S_1 state undergoing intersystem crossing to the triplet state.
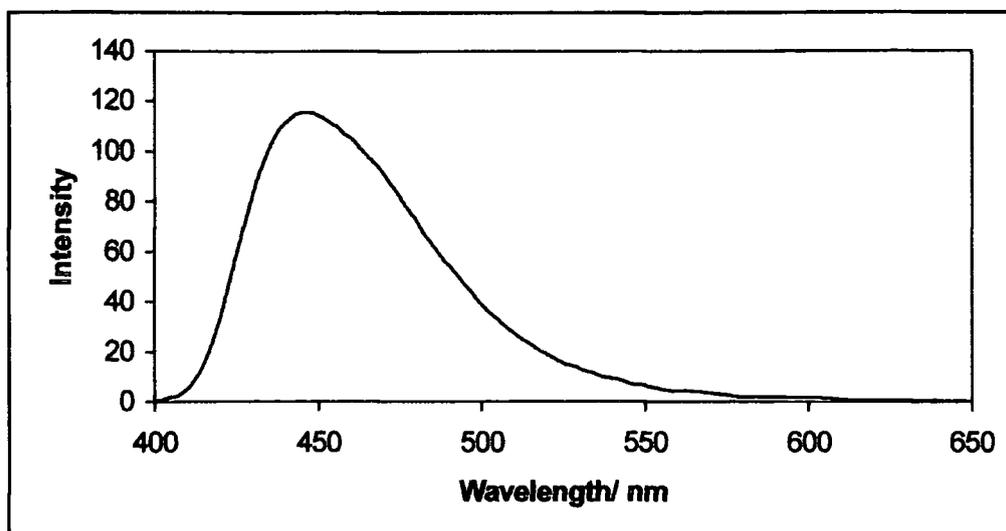
Figure 3.5. _**Phosphorescence spectrum of menthyl anthranilate in EPA following**_
**340 nm excitation.**

	Menthyl Anthranilate		Methyl Anthranilate	
	λ_{max}^*/ nm	$\tau_p^\dagger$/ s	λ_{max}^*/ nm	$\tau_p^\dagger$/ s
EPA	446	2.4 ± 0.1	447	2.5 ± 0.1
4:1 MCH:i-P	444	2.3 ± 0.1	442	2.6 ± 0.1

* Phosphorescence Emission Maxima following 340 nm excitation.

‡ Phosphorescence Lifetime.

Table 3.3. _**Phosphorescence data for menthyl and methyl anthranilate.**_

3.2.4.   Kinetic Absorption Measurements

3.2.4.1.Transient Absorption

Kinetic absorption measurements in degassed solutions revealed a short-lived transient absorption centered around 480 nm with a solvent dependent lifetime in the range 20-120 μs. The transient absorption spectrum following excitation of a 20 μM solution of menthyl anthranilate in degassed toluene at 355 nm is shown in figure 3.6, and the

corresponding kinetic absorption profile and fit is shown in figure 3.7. Due to interference from delayed fluorescence and the limitations of probe wavelengths available using this equipment, it was not possible to record a bleaching of the ground state, and hence no attempt was made to determine ε_{TT} or Φ_T. The lifetimes of the transient species are shown in table 3.4.
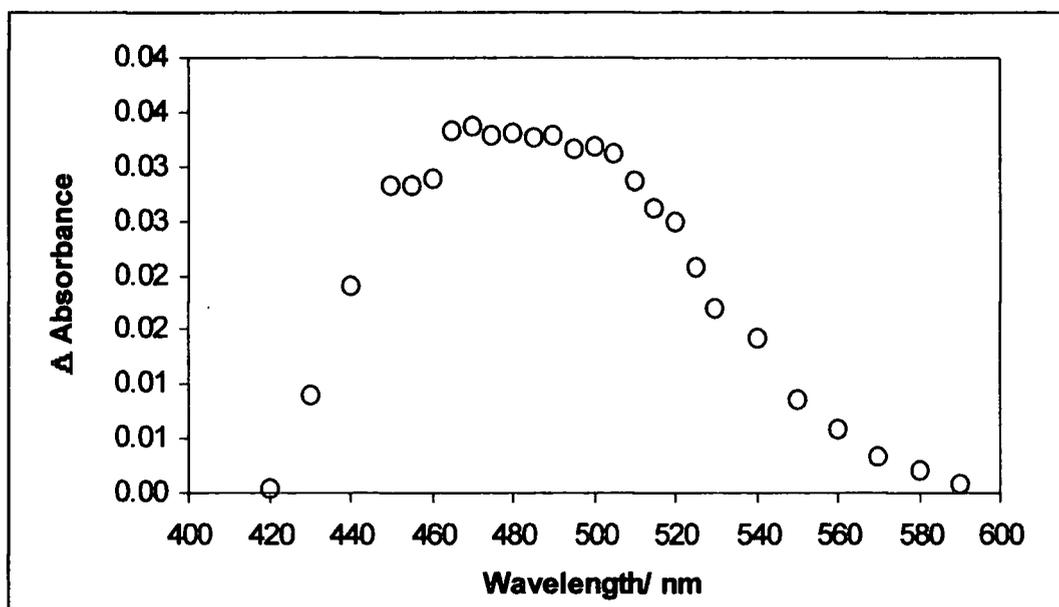
Figure 3.6. Transient absorption spectrum of menthyl anthranilate in toluene.

	τ_T/ μs	
	Menthyl Anthranilate	Methyl Anthranilate
Toluene	25 ± 5	20 ± 5
Acetonitrile	100 ± 10	80 ± 5
Ethanol	30 ± 5	120 ± 5

Table 3.4. Transient lifetimes of menthyl and methyl anthranilate.
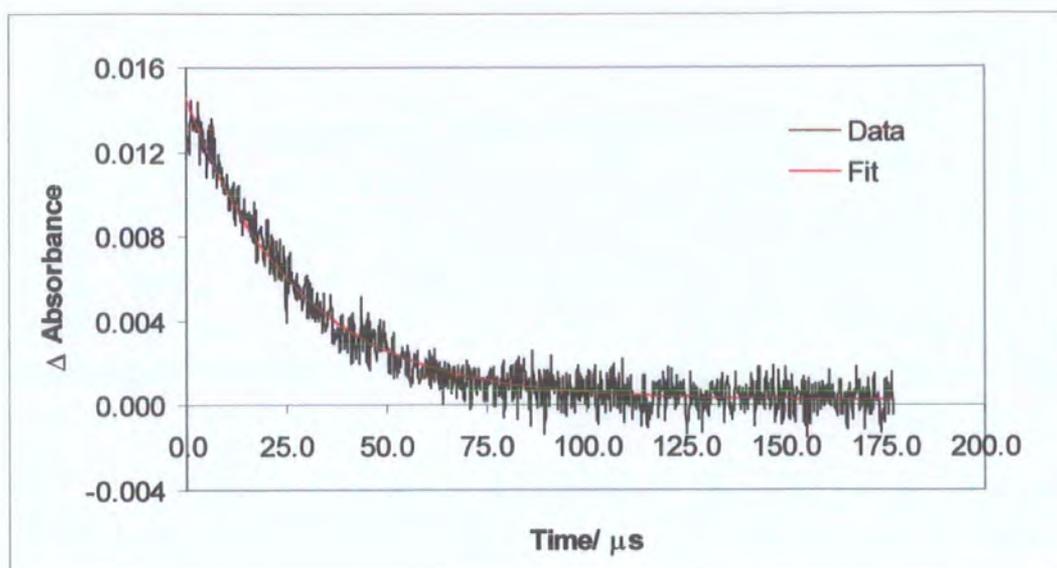
Figure 3.7. The kinetic absorption profile of menthyl anthranilate in toluene at 540 nm, $\lambda_{ex} = 355$ nm.

3.2.4.2. Delayed Fluorescence

During the course of these experiments a long-lived emission was also observed, the intensity of which was found to increase exponentially with laser power. The spectral profile of this emission was found to be identical to the fluorescence spectrum as shown in figure 3.8.
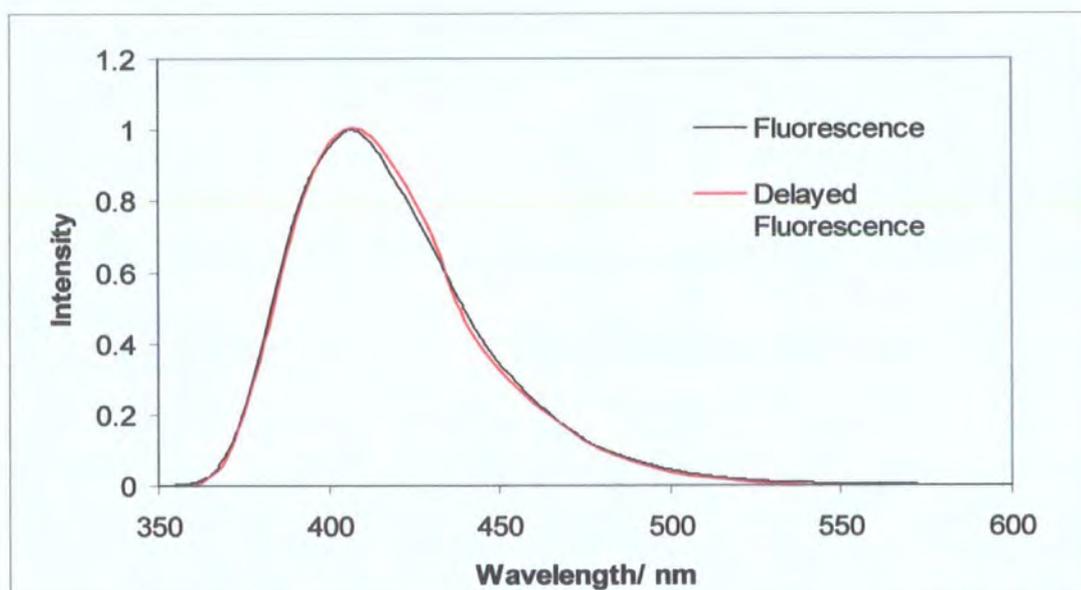
Figure 3.8. Normalised fluorescence and delayed fluorescence spectra of menthyl anthranilate in ethanol.

Aeration of the solutions resulted in loss of both the transient absorption and the long lived emission indicating that the long lived emission is P-type delayed fluorescence, the result of a triplet-triplet annihilation process as illustrated in figure 3.9.

$$MA^* (T_1) + MA^* (T_1) \longrightarrow MA^*(S_1) + MA (S_0)$$

$$\downarrow$$

$$MA (S_0) + h\upsilon \text{ (fluorescence)}$$
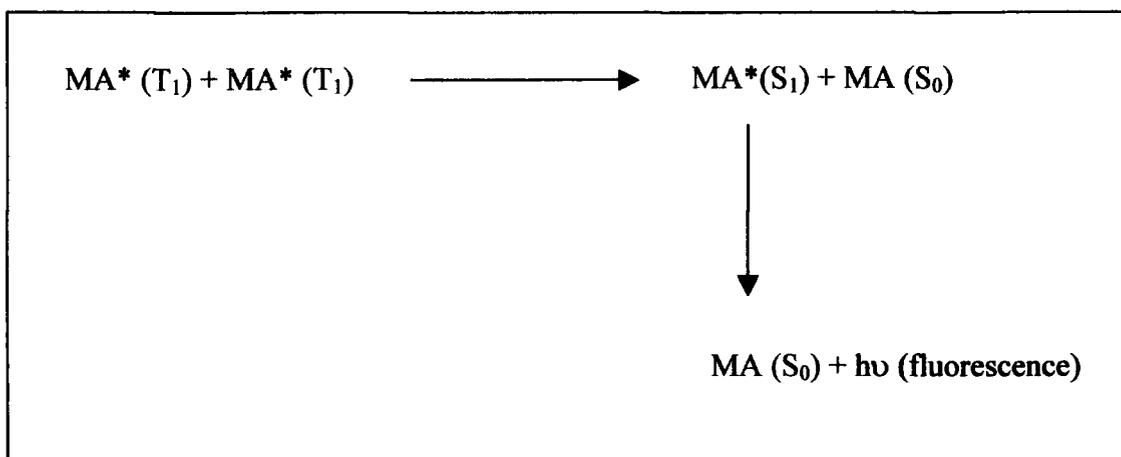
Figure 3.9. Schematic of triplet-triplet annihilation leading to delayed fluorescence.

3.2.4.3. Quenching
3.2.4.3.a. Self-quenching

Self-quenching of the transient species by ground state molecules was found to occur in acetonitrile but was undetectable in toluene and ethanol. The rate constant was determined by recording the transient lifetime, τ, as a function of the ground state concentration. The rate constants are shown in table 3.5.

3.2.4.3.b. Oxygen-quenching

The transient species was efficiently quenched by oxygen, with rate constants in the range of $1\text{-}5 \times 10^8$ $dm^3mol^{-1}s^{-1}$, see table 3.5. Figure 3.10 shows the Stern-Volmer plot for the oxygen-quenching of the transient formed following pulsed 355 nm excitation of methyl anthranilate in acetonitrile.

	Menthyl Anthranilate		Methyl Anthranilate	
	k_{self}[*]/ $10^6 dm^3 mol^{-1}s^{-1}$	k_{O_2}[†]/ $10^8 dm^3 mol^{-1}s^{-1}$	k_{self}[*]/ $10^6 dm^3 mol^{-1}s^{-1}$	k_{O_2}[†]/ $10^8 dm^3 mol^{-1}s^{-1}$
Toluene	-	2.78 ± 0.09	-	4.35 ± 0.17
Acetonitrile	9.10 ± 0.63	9.97 ± 1.40	2.98 ± 0.53	3.46 ± 0.16
Ethanol	-	1.19 ± 0.15	-	4.69 ± 0.02

[*] Self-quenching rate constant.

[†] Oxygen-quenching rate constant.

Table 3.5. Quenching rate constants for the transient species.
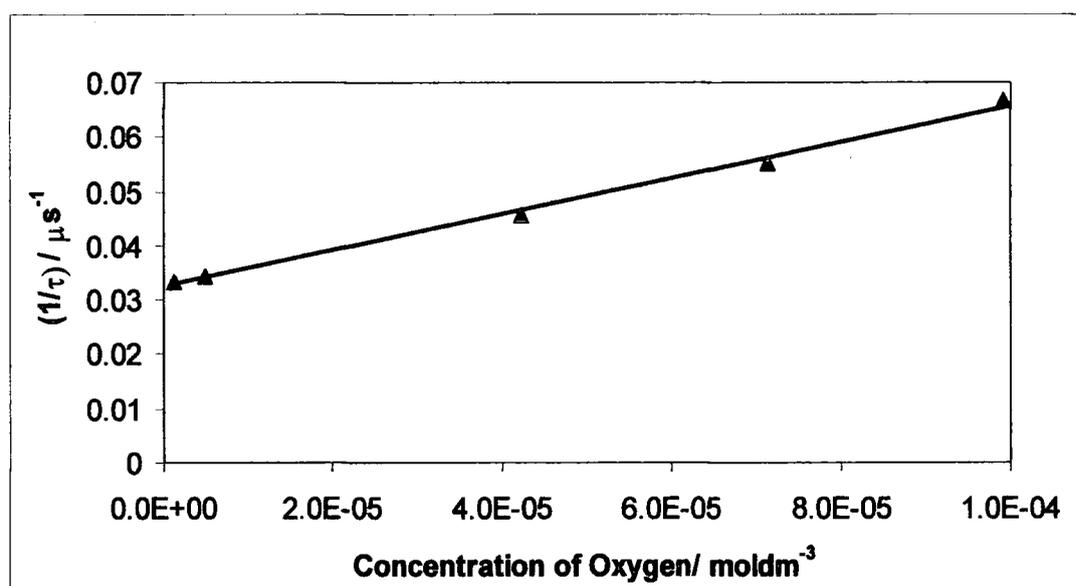
Figure 3.10. Stern-Volmer plot for the oxygen quenching of methyl anthranilate in acetonitrile.

3.2.5. Singlet Oxygen Measurements

3.2.5.1. Production of Singlet Oxygen

Quenching of the transient species by oxygen leads to the formation of singlet oxygen, detected by its characteristic luminescence at 1270 nm. Figure 3.11 shows a typical phosphorescence decay trace and the data fit obtained. The lifetimes of singlet oxygen determined during these experiments were consistent with literature values, 29 µs in

toluene, 70 μs in acetonitrile and 15 μs in ethanol[39]. The quantum yields of singlet oxygen formation are shown in table 3.6 and a plot of $S(0)_{EA}$ against $1\text{-}10^{-A}$ for methyl anthranilate and the reference compound, *meso*-tetraphenylporphyrin, is shown in figure 3.12.

	Menthyl Anthranilate		Methyl Anthranilate	
	Φ_Δ^{*}	$k_\Delta^{\dagger}/$ $10^4\text{dm}^3\text{mol}^{-1}\text{s}^{-1}$	Φ_Δ^{*}	$k_\Delta^{\dagger}/$ $10^4\text{dm}^3\text{mol}^{-1}\text{s}^{-1}$
Toluene	0.12 ± 0.01	10.5 ± 1.0	0.11 ± 0.01	11.0 ± 1.1
Acetonitrile	0.09 ± 0.01	-	0.09 ± 0.01	-
Ethanol	0.09 ± 0.01	-	0.09 ± 0.01	-

* Quantum Yield of Singlet Oxygen Formation

† Singlet Oxygen Quenching Rate Constant

Table 3.6. Singlet oxygen data for menthyl and methyl anthranilate.
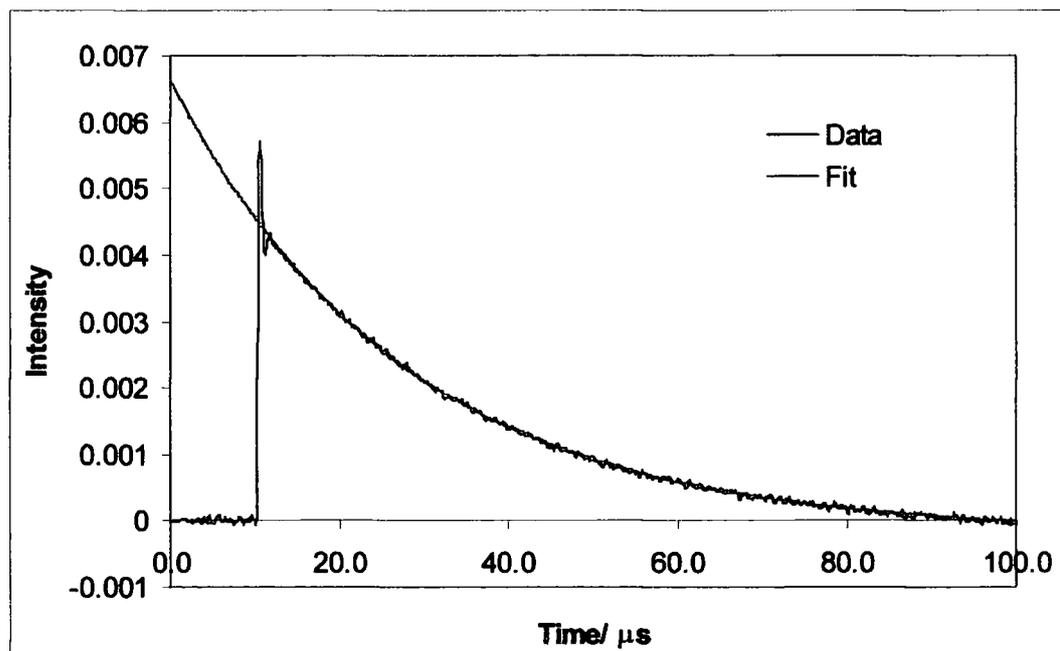
Figure 3.11. Kinetic singlet oxygen luminescence (1270 nm) decay trace following pulsed 355 nm laser excitation of methyl anthranilate in toluene, $\lambda_{ex} = 355$ nm.
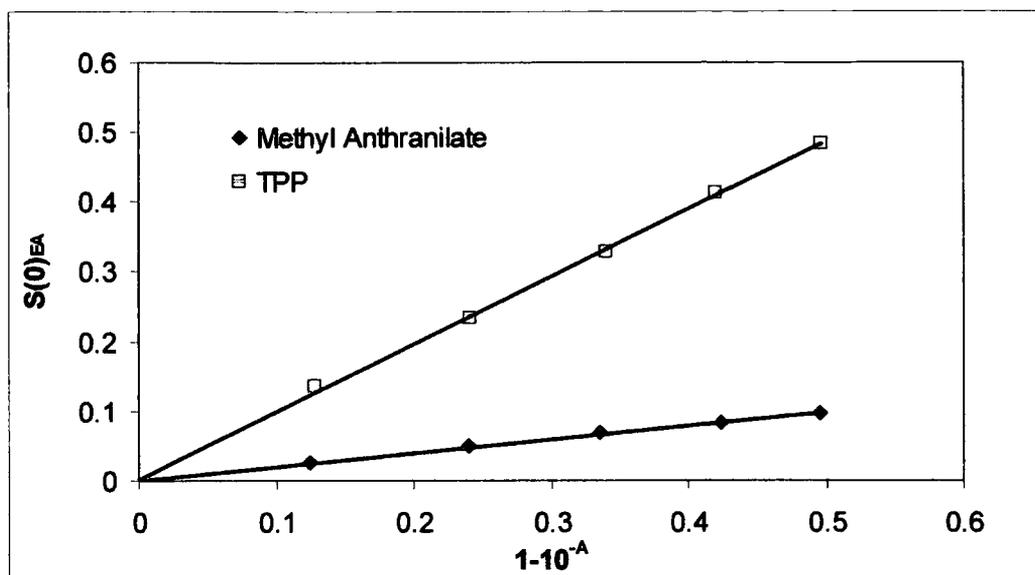
Figure 3.12. Plots of S(0)$_{EA}$ vs 1-10^{-A} for the determination of the singlet oxygen generation quantum yield of methyl anthranilate in toluene.

3.2.5.2. Quenching of Singlet Oxygen

Study of the quenching of singlet oxygen phosphorescence by these materials yielded a relatively small rate constant of $1.05\pm0.1 \times 10^4$ dm^{3}mol^{-1}s^{-1} for menthyl anthranilate and a similar value of $1.10\pm0.1 \times 10^4$ dm^{3}mol^{-1}s^{-1} for the methyl derivative. Figure 3.13 shows the Stern-Volmer plot obtained from methyl anthranilate in toluene.
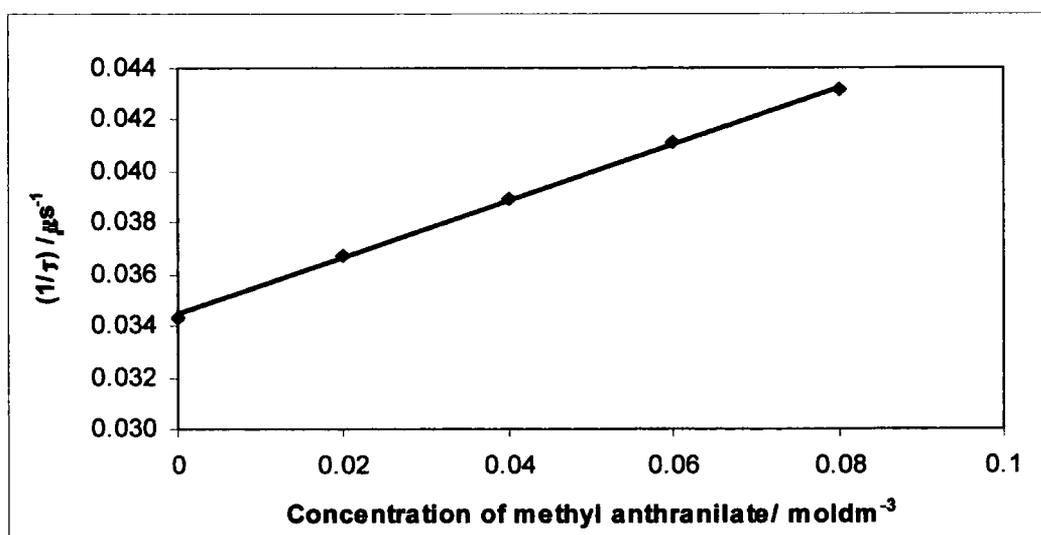
Figure 3.13. Stern-Volmer plot for the quenching of singlet oxygen by methyl anthranilate in toluene.

3.3.   Formulation Results

Studies were carried out on Neutrogena® Sunblock Spray (SPF 20) which contained menthyl anthranilate as one of its active ingredients along with homomenthyl salicylate, octyl methoxycinnamate and octyl salicylate.

3.3.1. Absorption Spectrum

The absorption spectrum of a 2 mgcm^{-2} film of the sunscreen formulation on a quartz slide was recorded.   However, the absorbance in the UV range was too strong to provide a meaningful spectrum.   This demonstrates the broad band protection provided by the formulation across the entire UV range.

3.3.2. Fluorescence

The fluorescence spectrum of a 2 mgcm^{-2} film of the sunscreen was measured and compared with that obtained in the solution state studies.   Figure 3.14 shows that the spectrum of the formulation is very similar to that obtained for menthyl anthranilate in solution.
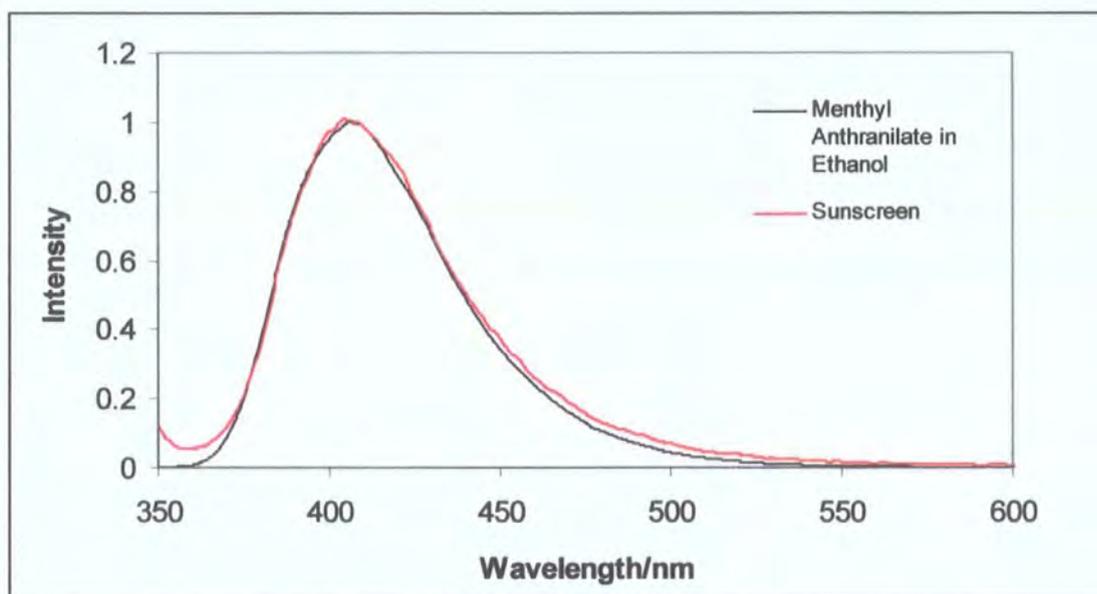
Figure 3.14. Normalised fluorescence spectra of menthyl anthranilate in ethanol and a film of a sunscreen formulation containing menthyl anthranilate.

The fluorescence lifetime of the system was determined and found to be 5.0 ns, a value which is also not significantly different to that obtained in solution.

3.3.3. Singlet Oxygen Measurements

Attempts to study singlet oxygen formation by menthyl anthranilate by the detection of 1270 nm phosphorescence from a 2 $mgcm^{-2}$ film of sunscreen placed at 45° to the incoming laser beam were unsuccessful due to the highly scattering nature of the medium.

Further attempts were made to detect singlet oxygen formation in a thin film of sunscreen on a quartz slide illuminated using a Bentham IL6 Illuminator xenon lamp filtered with a copper (II) sulphate filter. The method by Gorman[40] involving monitoring the bleach of the 1,3-diphenylisobenzofuran (DPBF) absorption peak at 415 nm on irradiation was adapted so that the DPBF had an absorption at 415 nm of ~0.5 in the thin film. However the method was unsuccessful due to 'self-sensitization' and a bleach even in the absence of sensitizer.

The method described by Kraljic[41] employs the bleach of p-nitrosodimethylaniline (RNO) ($\lambda_{max} = 440$ nm) caused by its reaction with the transannular peroxide (AO_2) formed by the reaction of imidazole (A) with singlet oxygen. Solution state studies in methanol proved successful with a bleach at 440 nm but when a 1:200 mixture of RNO:imidazole was mixed with the sunscreen formulation the initial absorbance in a 2 $mgcm^{-2}$ film at 440 nm was too small to detect any change.

3.4. Discussion

Anthranilate esters are amongst the few organic sunscreens that absorb in the UV-A range[42]. Although menthyl anthranilate is an *ortho*-disubstituted compound, and as such has a much lower molar extinction coefficient compared to its *para*-disubstituted counterparts, it has a higher extinction coefficient than other *ortho*-disubstituted aromatic compounds used as sunscreens such as the salicylate esters. This work has highlighted another advantage of menthyl anthranilate as a sunscreening agent, namely
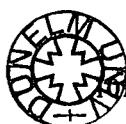
that it has a relatively low triplet energy (287 kJmol^{-1}), and as such does not have the potential to cause skin damage via the sensitization of thymine ($E_T \sim 315$ kJmol^{-1}) and the production of thymine dimers[43]. However this work highlights other more disturbing photophysical properties of this material.

The measurements reported above reveal that following excitation radiative decay from the relatively long lived S_1 state is the dominant decay pathway, but that intersystem crossing to the triplet state also occurs to a significant extent. Importantly, the triplet state has a significant lifetime in degassed solution and is efficiently quenched by molecular oxygen producing singlet oxygen in aerated solutions.

Both compounds were found to be highly fluorescent in all solvent systems studied, with fluorescent lifetimes of 5-7 ns. The values determined for Φ_f are comparable to those reported in the literature for anthranilic acid and methyl anthranilate[22].

The high fluorescent quantum yields observed in our solution state studies and the small Stokes shift observed for the fluorescence spectrum means that a significant fraction of the emitted radiation falls in the UV-A spectral region, i.e. $\lambda < 400$ nm.

From both this work and that reported by Stokes et al.[11] it is known that commercial sunscreen preparations containing menthyl anthranilate are highly fluorescent when deposited on the skin, although no quantum yields of luminescence have been reported. In this work the fluorescence spectrum and lifetime of menthyl anthranilate when present in a commercially available sunscreen formulation has been determined. It was found that both the fluorescence spectrum and lifetime of menthyl anthranilate in this environment were similar to those obtained in solution state experiments ($\lambda_{max} = 400$ nm, $\tau_f = 5.0$ ns). This indicates that there is no significant quenching of the excited singlet state in such formulations. A thin film of sunscreen spread onto the skin surface has two interfaces. At the sunscreen-air interface there is a large refractive index difference, hence much of the light emitted from within the film will not escape, but rather will undergo total internal reflection at the interface. Conversely, the refractive index difference between the film and the skin will be less and hence more light will pass through this interface. Thus it is likely that a significant fraction of the luminescence is transmitted onto the skin, increasing the intensity of radiation at the skin surface in the 370 – 400 nm range.

The transient species produced following 355 nm excitation of these compounds in various solvents are assigned to the triplet states by virtue of their quenching by oxygen and the resulting generation of singlet oxygen and also by the emission of P-type delayed fluorescence. The similarities of the transient absorption spectra for each compound in all solvents suggest that the same species is produced in each case, although the different lifetimes may indicate the role of the solvent in stabilising, or destabilising the triplet states formed. Attempts were not made to measure ε_{TT} or Φ_T, however, based on the values of Φ_f and Φ_Δ measured here we can determine that $0.1 < \Phi_T < 0.4$.

Deactivation of the triplet states has been shown to occur in at least three ways. Firstly, in low temperature glasses, radiative decay results in long-lived phosphorescence ($\tau \sim 2.5$ s), with an emission maximum of ~ 445 nm. Secondly the triplet states are rapidly quenched by oxygen, which results in the generation of singlet oxygen with quantum yields of formation of 0.09 - 0.12 for both compounds in all the solvents systems studied. Finally, under 355 nm pulsed laser excitation, P-type delayed fluorescence has been observed arising from triplet-triplet annihilation.

Quenching of the triplet states by ground state molecules has been observed to be rather slow and could not be detected in toluene or ethanol under the conditions used.

The results of the luminescence studies reported here show that the use of menthyl anthranilate within a formulation is likely to result in a fluorescent product, which, at the least, will appear slightly blue under normal lighting conditions. This is confirmed by the study conducted by Stokes et al.[11] who reported the use of fluorescence intensity to monitor the performance of sunscreens on skin.

More significantly, however, the results from the laser flash photolysis experiments clearly demonstrate the formation of the long lived triplet state of menthyl anthranilate under various solvent conditions. Furthermore oxygen quenching of this triplet state was shown to generate singlet oxygen in solution.

3.5. Conclusions

Conventional room temperature and low temperature luminescence spectroscopy, laser flash photolysis, and near infrared luminescence measurements have been used to conduct a thorough study of the photophysical properties of the sunscreen ingredient menthyl anthranilate and the food flavouring methyl anthranilate.

Luminescence studies indicate that following excitation the dominant deactivation process is fluorescence ($\Phi_f \sim 0.60\pm0.06$), but a significant proportion of the excited molecules undergo intersystem crossing to the triplet state. This has been observed to have a long lifetime in solution (20-200 µs) and a very long lived phosphorescence lifetime in low temperature glasses of ~ 2.5 s. From these data it has been established that $E_T \sim 287$ kJmol^{-1}.

Kinetic absorption measurements reveal triplet-triplet absorption bands with maxima at ~ 480 nm, that are readily quenched by oxygen. Under high intensity illumination delayed fluorescence can be observed from degassed solutions, attributed to triplet-triplet annihilation.

Finally, in aerated solution these anthranilate esters have been shown to have a significant quantum yield of production of singlet oxygen ($\Phi_\Delta = 0.09 - 0.12$).

Menthyl anthranilate is currently used in a number of commerical sunscreen formulations available in the USA, including Neutrogena$^{®}$ Sunblock Spray (SPF 20) and Hawaiian Tropic$^{®}$ Protective Tanning Oil (SPF 6). Both these sunscreen formulations are highly fluorescent. Our study of both these formulations has shown that the singlet state lifetime of menthyl anthranilate contained in the sunscreen film is not significantly reduced. It seems reasonable to deduce that these sunscreens will generate the triplet state of menthyl anthranilate which may subsequently form singlet oxygen close to the skin surface. Although our experiments to detect singlet oxygen in the film have been unsuccessful this has been due to 'self-sensitisation' in the case of the Gorman[40] method, too weak an absorbance in the case on the Kraljic[41] method and due to scattering when trying to detect the 1270 nm phosphorescence directly.

3.6. References

1. Gasparro, F.P., M. Mitchnick, and J.F. Nash (1998) A review of sunscreen safety and efficacy. *Photochem. Photobiol.* **68**, 243-256.

2. Kligman, L.H., F.J. Akin, and A.M. Kligman (1985) The contributions of UVA and UVB to connective tissue damage in hairless mice. *J. Invest. Derm.* **84**, 272-276.

3. Klein, K. (1997) Sunscreen Products: Formulation and Regulatory Considerations. In *Sunscreens. Development, Evaluation, and Regulatory Aspects*, 2nd ed., (Edited by Nicholas J. Lowe, Nadim A. Shaath and Madhu A. Pathak), Marcel Dekker, Inc., New York, pp. 285-311.

4. Knobler, E., L. Almeida, A.M. Ruzkowski, J. Held, L. Harber and V. DeLeo (1989) Photoallergy to Benzophenone. *Arch. Dermatol.* **125**, 801-804.

5. Collins, P., and J. Ferguson (1994) Photoallergic contact dermatitis to Oxybenzone. *Br. J. Dermatol.* **131**, 124-129.

6. Schallreuter, K.U., J.M. Wood, D.W. Farwell, J. Moore, and H.G.M. Edwards (1996) Oxybenzone oxidation following solar irradiation of skin: Photoprotection versus antioxidant inactivation. *J. Invest, Dermatol,* **106(3)**, 583-586.

7. Roscher, N.M., M.K.O. Lindemann, S.B. Kong, C.G. Cho, and P.Jiang (1994) Photodecomposition of several compounds commonly used as sunscreen agents. *J. Photochem. Photobiol. A:Chem.* **80**, 417-421.

8. Allen, J.M., C.J. Gosset, and S.K. Allen (1996) Photochemical formation of singlet molecular oxygen in illuminated aqueous solutions of several commercially available sunscreen active ingredients. *Chem. Res. Toxicol.* **9**, 605-609.

9. Schallreuter, K.U., J.Moore, and J.M. Wood (1998) On Photostability of Oxybenzone. *J. Invest. Dermatol.* **110(1)**, 95-98.

10. Klein, K., and H.A. Finkelmeier (1990) Menthyl Anthranilate. The UVA alternative of the 90's. *Cosmetics and Toiletries.* **105**, 75-77.

11. Stokes, R.P. and B.L. Diffey, (1999) The feasibility of using fluorescence spectroscopy as a rapid, non-invasive method for evaluating sunscreen performance. *J. Photochem. Photobiol. B:Biol.* **50**, 137-143.

12. Jain, D.V.S., F.S. Nandel, P. Singla, and D.J. Kaur, (1986) Experimental and Theoretical Studies on electronic spectra of o-, m- and p-aminobenzoic acids and their protonated and deprotonated species. *Indian J. Chem., Sect. A.* **25A(1)**, 15-19.

13. Shüler, V.H. (1948) The molecular field mechanisms in disubstituted benzenes. *Z. Naturforsch Teil A.* **3a**, 313-320.

14. Doub, L. and J.M. Vandenbelt (1949) The Ultraviolet Absorption Spectra of Simple Unsaturated Compounds II. m- and o-disubstituted benzene derivatives. *J. Am. Chem. Soc.* **71**, 2414-2420.

15. Dannenberg, H. (1949) Classification of ultraviolet absorption. I. Substituted acetophenones, benzoic acids and cinnamic acid. *Z. Naturforsch Teil B.* **4b**, 327-344.

16. Dearden J.C., and W.F. Forbes (1960) The study of hydrogen bonding and related phenomena by ultraviolet light absorption. *Can. J. Chem.* **38**, 1837-1851.

17. Berlmann I.B. (1969) Evidence of intramolecular hydrogen bonding from spectroscopic data. *Chem. Phys. Lett.* **3(2)**, 61-63.

18. Tramer, A. (1969) Role of nonradiative transitions in quenching of the tautomeric forms of o-aminobenzoic acid. *Transitions Non-Radiat. Mol., Reunion Soc. Chim. Phys. 20th.* 239-242.

19. Mataga, N. (1963) Solvent effects on the absorption and fluorescence spectra of naphthylamines and isomeric benzoic acids. *Bull. Chem. Soc. Japan.* **36**, 654-662.

20. Kavanagh, F. and R.M. Goodwin (1949) Relation between pH and fluorescence of several organic compounds. *Arch. Biochem.* **20**, 315-324.

21. Sokoloa, L.K., T.N. Pegova, and R.M. Fofnova (1973) Intermolecular interactions and radiationless transitions. *Izv. Vyssh. Ucheb. Zaved., Fiz.* **16(2)**, 15-19.

22. Melhuish, W.H (1961) Quantum Efficiencies of Fluorescence of Organic Substances: Effect of solvent and concentration on the fluorescent solute. *J. Phys. Chem.* **65**, 229-235.

23. Melhuish, W.H. (1955) Measurement of absolute quantum efficiencies of fluorescence. *New Zealand J. Sci. Technol.* **37B**, 142-149.

24. Teplyakov, P.A. (1959) Phosphorescence spectra of alcoholic solutions of aminobenzoic acid, sulfobenzoic acid and bromobenzoic acid at low temperature. *Izv. Vyssh. Ucheb. Zaved., Fiz.* **2**, 135-139.

25. Zhmyreva, I.A., V.P. Kolobkov, and S.V. Volkov (1966) Triplet-triplet absorption spectra of solid solutions of some organic compounds. *Optika i Spektroskopiya*, **20(2)**, 303-307.

26. Carmichael, I., and G.L Hug (1986) Triplet-triplet absorption spectra of organic molecules in condensed phases. *J. Phys. Chem. Ref. Data.* **15(1)**, 1-250.

27. Teplyakov, P.A. (1962) Concentration quenching of phosphorescence of aromatic compounds in acetone at low temperatures. *Uch. Zap. Gorkovsk. Gos. Ped. Inst.* **40**, 81-88.

28. Teplyakov, P.A and B.A. Pyatnitskii (1956) The effect of concentration and the solvent on the phosphorescence of aromatic compounds at low temperatures. *Bull. Acad. Sci. U.S.S.R., Phys. Ser.* **20**, 476-478.

29. Fadeeva, M.S. (1962) Temperature quenching of phosphorescence of aromatic compounds. *Uch. Zap. Gorkovsk. Gos. Ped. Inst.* **40**, 62-69.

30. Pyatnitskii, B.A., and M.S. Fadeeva (1956) Temperature quenching of the phosphorescence of some aromatic compounds. *Bull. Acad. Sci. U.S.S.R., Phys. Ser.* **20**, 479-482.

31. Dikun, P.P., A.A. Petrov, and B. Ya. Sveshnikov (1951) Duration of the phosphorescence of benzene and its derivatives. *Zhur. Eksptl. Teoret. Fiz.* **21**, 150-163.

32. Kisylak, G.M., G.M. Lysenko and V.I. Ponochovnyi (1969) Anti-Stokes phosphorescence of organic substances. *Ukr. Fiz.Zh. (Russ. Ed.).* **14(2)**, 338-340.

33. Kisylak, G.M, and G.M. Lysenko (1963) Effect of temperature quenching on the phosphorescence of organic materials. *Izv. Akad. Nauk. SSSR Ser. Fiz.* **27(6)**, 717-719.

34. Lysenko, G.M, G.M. Kisylak, and V.I. Ponochovnyi (1970) Effect of the concentration of an activator on the law of phosphorescence decay for organic substances. *Zh. Prikl. Spektorsk.* **13(2)**, 266-270.

35. U.S. Patent No. 4 329 372/1980

36. Aronov, E.V., and L. Clark, (1996) Degradation studies of the non-lethal bird repellent, methyl anthranilate. *Pesticide Science*, **47(4)**, 355-362.

37. Bensasson R.V., E.J. Land and T.G.Truscott, (1993) *Excited States and Free Radicals in Biology and Medicine*. Oxford University Press Inc., New York.

38. Kamlet, M.J., J.L.M. Abboud and R.W. Taft (1984). In *Progress in Physical Organic Chemisty* Vol. 13, (Edited by R.W. Taft), Wiley&Sons, New York, pp. 485-630.

39. Gorman, A.A. and M.A.J. Rodgers (1989) Singlet Oxygen. In *Handbook of Organic Photochemistry*, Vol. II (edited by J.C. Scaiano), CRC Press, Florida, pp. 229-247.

40. Gorman, A.A., G. Lovering and M.A.J. Rodgers (1978) A pulse radiolysis study of the triplet sensitized production of singlet oxygen: determination of energy transfer efficiencies, *J. Am. Chem. Soc.*, **100**, 4527-32.

41. Kraljic I., and S. El Moshni (1978) A new method for detection of singlet oxygen in aqueous solutions. *Photochem. Photobiol.*, **28**, 577-81.

42. Shaath, Nadim A. (1997) Evolution of Modern Sunscreen Chemicals. In *Sunscreens. Development, Evaluation, and Regulatory Aspects* (Edited by Nicholas J. Lowe, Nadim A. Shaath and Madhu A. Pathak), Marcel Dekker, Inc., New York, pp. 3-33.

43. Gonzenbach, H., Hill, T.J., and Truscott, T.G. (1992) The triplet energy levels of UVA and UVB sunscreens. *J. Photochem. Photobiol. B: Biol.* **16**, 377-379.

Chapter 4

The Photophysical Properties

of

N-acetyl-menthyl Anthranilate

4.1. Introduction

4.1.1. N-acetyl-menthyl anthranilate in sunscreen formulations

Over the past decade an increase in the use of sunscreen formulations has resulted from an increased awareness of the damaging effects of solar UV radiation on human skin[1]. The recent association of UV-A exposure with skin-ageing and other dermatological conditions[2] has furthered this increase.

Shaath[3] describes the anthranilates as an 'interesting' class of UV filters and describes in detail the two derivatives approved for commercial use, menthyl anthranilate in the USA and N-acetyl-homomenthyl anthranilate in the EC, see figure 4.1. He comments on the 'ortho-effect' that is evident in these compounds, namely the red-shift of the absorption maxima and low molar absorption coefficients when compared to their para-disubstituted counterparts. This shift is attributed to the ease of electron delocalisation in the ortho-compounds as opposed to the para-compounds. However, steric crowding due to the ortho-disubstitution in these compounds causes deviations from coplanarity of the molecules resulting in a reduction of the intensity of the absorption and lower molar absorption coefficients.
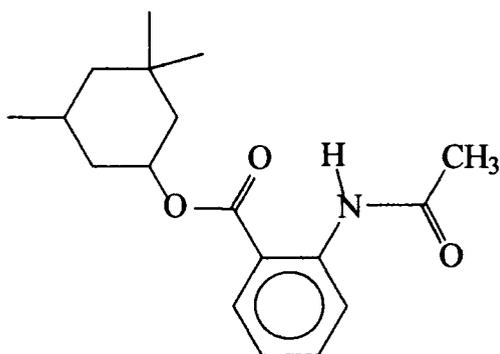
Figure 4.1. N-acetyl-homomenthyl anthranilate.

Agrapidis-Paloymis et al.[4] have commented that the anthranilates, like the salicylates, are stable and safe compounds to use, owing to this ortho-disubstituted relationship, and do not exhibit significant solvent effects in cosmetic formulations. Fisher[5] has also described the anthranilates as extremely rare sensitisers in his review on sunscreen dermatitis.

Despite the apparent advantages of these compounds Brown of the Boots Company plc has recently reported[6] that the N-acetyl-homomenthyl anthranilate derivative was removed from the list of approved sunscreens in the EC in 1989, although the reasons for this withdrawal have not been published.

4.1.2. Photophysical properties of N-acetyl-anthranilate esters

Despite the approval for the use of N-acetyl-homomenthyl anthranilate in commercially available sunscreens there is surprisingly little information on the compound in the scientific and medical literature. The photophysical and photochemical properties of this compound should have been of great interest at the time of its admission onto the list of approved sunscreens. Also, unlike the anthranilate esters studied in chapter 3, there is little information on the photophysics and photochemistry of the parent acid of this ester.

Several UV-visible spectroscopy studies have been carried out on N-acetyl anthranilic acids. Dannenberg[7] determined the absorption spectra of benzoic acid and its hydroxy, methoxy, amino and acetamino derivatives, amongst others, to compare and quantify the shifts in absorption bands caused by the different ring substitutions.

Ungnade[8] has studied the ultraviolet absorption spectra of 36 acetanilides and related compounds. The intensities and λ_{max} values have been interpreted in terms of the electronic and steric effects of the substituents. The spectrum of N-acetyl anthranilic acid has been reported to have bands at 221 nm, 252 nm and 305 nm, and the molar absorption coefficient at 305 nm has been determined to be 4650 $dm^3mol^{-1}cm^{-1}$. The red shift and increased intensity of the 252 nm band, and the blue shift and reduction in the intensity of the 305 nm band relative to the spectrum of anthranilic acid have been discussed. The changes have been attributed to the increase in conjugation of the system following acetylation of the amine group and the associated reduction in the tendency of the nitrogen electrons to migrate into the aromatic ring, due to the loss of planarity of the molecule.

Grammaticakis[9] recorded the UV spectra of a range of N-substituted o-nitro and o-carboxy anilines including N-acetyl anthranilic acid. The peak shifts and intensity changes of the absorption bands of o-alkylanilines and their N-arylidene and

N,N-dimethyl derivatives following substitution of the alkyl in the *ortho* position by -NO$_2$, -COOH and -COCH$_3$ were studied. It was found that substitution had little or no effect on the absorption bands. Further work by Grammaticakis[10] studied the near-ultraviolet and visible absorption of some isomeric arylamines and their nitrogen substituted derivatives. The absorption spectra of 60 arylamines of the form XC$_6$H$_4$NY have been determined, where X = -CH$_3$, -OCH$_3$, -COOH, -COOCH$_3$ or -NO$_2$ and NY = -NH$_2$, -N(CH$_3$)$_2$, -NHCOCH$_3$, -NHCOC$_6$H$_5$ or -NO$_2$. In compounds of the form XC$_6$H$_5$NHCOCH$_3$, acetylation of the amine group was found to cause a red shift in the middle band ($\sim$ 250 nm) and a blue shift in the band at longer wavelength ($\sim$ 300 nm), in agreement with the work by Ungnade.

Lee and Ahn have described the preparation of several aminobenzoic acids by the oxidation of N-acetyl-toluidines with potassium permanganate[11]. The products formed were characterised using IR, NMR and UV spectroscopy. They found that N-acetyl anthranilic acid was formed with a yield of 95% from the corresponding toluidine. The UV-visible spectrum of the acid had two bands in ethanol at 251 nm and 303 nm. The molar absorption coefficient at 303 nm was determined to be 4570 dm^{3}mol^{-1}cm^{-1}. These values are consistent with those of Ungnade and Grammaticakis.

The photolysis of N-acetyl anthranilic acid has been carried out by Staudemayer and Roberts[12], in order to study the neighbouring group participation in the cyclization rearrangements known to occur in acetanilides under UV light. They irradiated 0.01M solutions of N-acetyl anthranilic acid in acetonitrile at 254 nm for 100 hours and the changes were monitored using UV spectroscopy. After 100 hours irradiation the solution was found to be a mixture containing starting material, anthranilic acid, 3-aceto-2-aminobenzoic acid, and 5-aceto-2-aminobenzoic acid, all products of photo-Fries-like cleavage and rearrangements. Since photo-Fries and similar reactions have been postulated to occur from singlet excited states[13] further experiments were conducted to probe the reactions of the triplet state of the acid species. They found that in benzene solutions energy transfer from the triplet state of the benzene molecules to the acid molecules occurred to yield the triplet state of the acid. The product formed following the irradiation of the acid in benzene for 200 hours was found to be benzoxazinone (figure 4.2). They concluded that N-acetyl anthranilic acid forms

photo-Fries-like cleavage and rearrangement products via the excited singlet state, and
that it cyclizes to benzoxazinone via the triplet state.
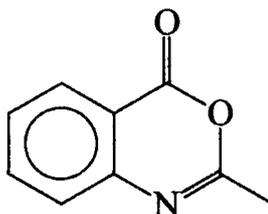
__Figure 4.2. Benzoxazinone.__

Several workers have probed the luminescence properties of N-acetyl anthranilic acid,
although there is surprisingly little quantitative data in the literature. Staudemayer *et
al.* determined the luminescence spectra of N-acetyl anthranilic acid as part of the work
described above in order to determine a suitable triplet state sensitiser. They found that
in acetonitrile fluorescence emission occurred with a maximum at 367 nm and
phosphorescence emission occurred with a maximum at 428 nm.

Hardy *et al.*[14] have studied the triboluminescence of several aromatic compounds. In
their work on N-acetyl anthranilic acid they found that the room temperature
triboluminescence (TL) and photoluminescence (PL) spectra were similar with maxima
at ~420 nm and a shoulder at ~470 nm. However, the band at ~470 nm was more
intense in the TL spectrum than in the PL spectrum. This difference has been
attributed to changes in the Frank-Condon factors (and thus to changes in the vibronic
intensities of the emission) caused by the application of mechanical energy or stress to
the crystals. The PL spectrum has also been assigned to phosphorescence on the basis
of its lifetime of 515 ms at 77 K.

The absorption, fluorescence emission and fluorescence excitation spectra of methyl
anthranilate and N-acetyl anthranilate have been used to identify the fluorophores in
diterpenoid alkaloids[15]. Ostakhov *et al.* compared the above spectra with the
analogous spectra of lappaconitine and N-deacetyllappaconitine. On the basis of the
coincidence of the spectra they concluded that the $-OOC-C_6H_4-NRH$ groups formed
the fluorophore in the alkaloids studied. The high quantum yield of fluorescence and
bathochromic   shift   in   the   luminescence   and   absorption   spectra   of   the

N-deacetyllappaconitine as compared to those of lappaconitine were explained by an increase in the electron releasing ability of the –NRH group following the deacetylation. This is in agreement with the work by Ungnade and Grammaticakis.

Despite these studies on N-acetyl anthranilic acid, little work has been carried out on the photophysics and photochemistry of the esters, even though the use of one such compound as a sunscreen ingredient has been approved until relatively recently.

In this chapter the results of a solution state study of N-acetyl-menthyl anthranilate (figure 4.3) in a range of solvent systems are discussed. The N-acetyl-menthyl anthranilate was synthesised (see chapter 2) as an analogue to the N-acetyl-homomenthyl anthranilate ester, since the latter compound is not commercially available. Acetylation of commercially available menthyl anthranilate was achieved using acetic anhydride, and purification to remove all traces of the highly fluorescent starting material was achieved using column chromatography. It is expected that the photophysical properties of N-acetyl-menthyl anthranilate will closely resemble those of the homomenthyl derivative based upon the earlier work comparing the methyl and menthyl esters of anthranilic acid.
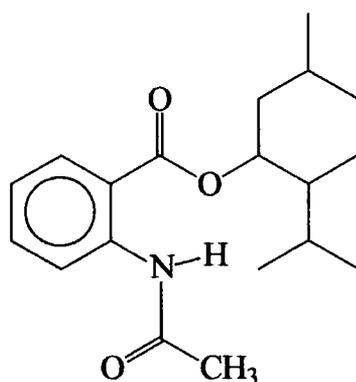
Figure 4.3. N-acetyl-menthyl anthranilate.

The work presented here includes measurement of fluorescence and phosphorescence emission spectra and lifetimes, quantum yields of fluorescence, triplet-triplet absorption spectra and the determination of oxygen- and self-quenching rate constants. Significantly we have shown that this N-acetyl anthranilate ester produces singlet

oxygen, a species known to be harmful to biological systems[16], by the oxygen quenching of the T_1 state. The quantum yields of singlet oxygen formation have been determined to be ~ 0.20±0.02 in all solvent systems studied.

4.2. Results

4.2.1. Absorption Spectra

The UV-Visible absorption spectrum of N-acetyl-menthyl anthranilate in ethanol is shown in figure 4.4. It exhibits three bands at ~224 nm, 253 nm and 315 nm and has molar absorption coefficients at 315 nm in the range 5400 – 7000 $dm^3mol^{-1}cm^{-1}$ for all solvent systems studied.
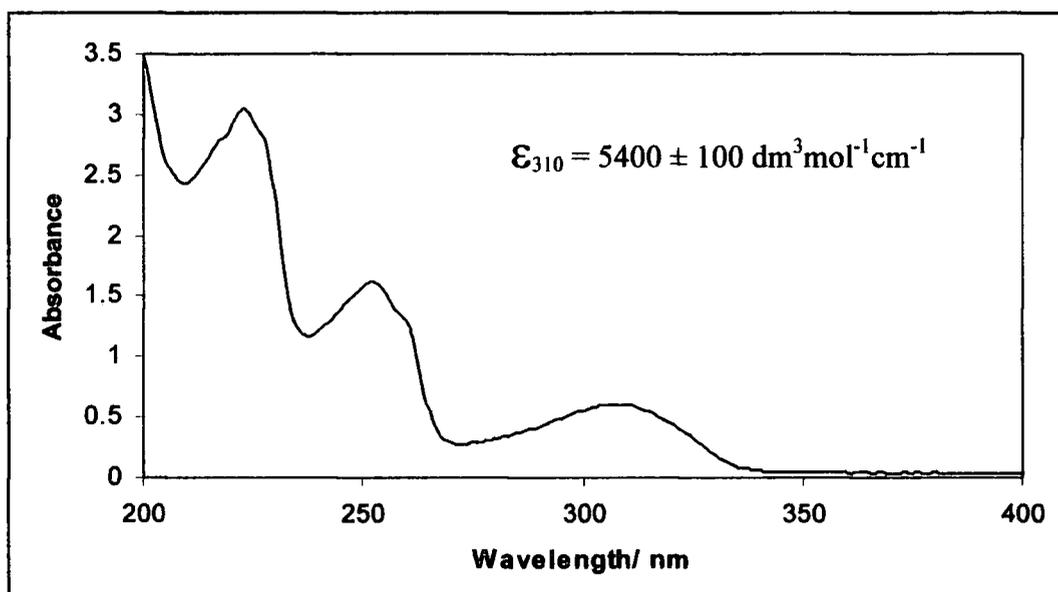
Figure 4.4. The UV absorption spectrum of N-acetyl-menthyl anthranilate in ethanol at a concentration of ~ $1.2x10^{-4}$ moldm^{-3} in a 1cm pathlength cuvette.

The data obtained from N-acetyl-menthyl anthranilate in a variety of solvents are shown in table 4.1. It can be seen that both the absorption maxima and the molar absorption coefficients only vary slightly with solvent. The peak at ~310 nm is, however, shown to vary to a higher degree than the shorter wavelength bands.

115

Solvent	Solvent Polarity*	λ_{max} 1/ nm	λ_{max} 2/ nm	λ_{max} 3/ nm	ε at λ_{max} 3/ $dm^3mol^{-1}cm^{-1}$
Toluene	33.9	-	-	313	7000 ± 100
Cyclohexane	31.2	224	253	315	6800 ± 100
Ethanol	51.9	224	252	310	5400 ± 100
Acetonitrile	46.0	223	252	310	5700 ± 100
Methanol	55.5	222	252	307	5400 ± 100
Dichloromethane	41.1	-	253	310	6300 ± 100
Chloroform	39.1	-	253	312	5900 ± 100
EPA	-	226	254	315	-
MCH:i-P	-	226	254	317	-

Table 4.1. UV-Visible data for N-acetyl-menthyl anthranilate.

* Solvent polarity scale based on solvatochromic band shifts in 4-(2,4,6-triphenylpyridium)-2-6-diphenylphenoxide and its trimethyl derivative[17].

4.2.2. Fluorescence

The fluorescence properties of this compound were studied and quantified in a range of solvents. The emission and excitation spectra of a 20 μM solution of N-acetyl-menthyl anthranilate in ethanol are shown in figure 4.5 and the quantum yields and lifetimes are given in table 4.2.

The fluorescence emission maxima is slightly solvent dependent showing a red shift of 7 nm from non-polar to polar solvents. As with menthyl anthranilate and methyl anthranilate this indicates that the excited state species is more polar than the ground state species. From table 4.2 it can be seen that the fluorescence is short lived in the range 3-4 ns and that the quantum yields lie in the range 0.13-0.16 in all solvent systems studied.
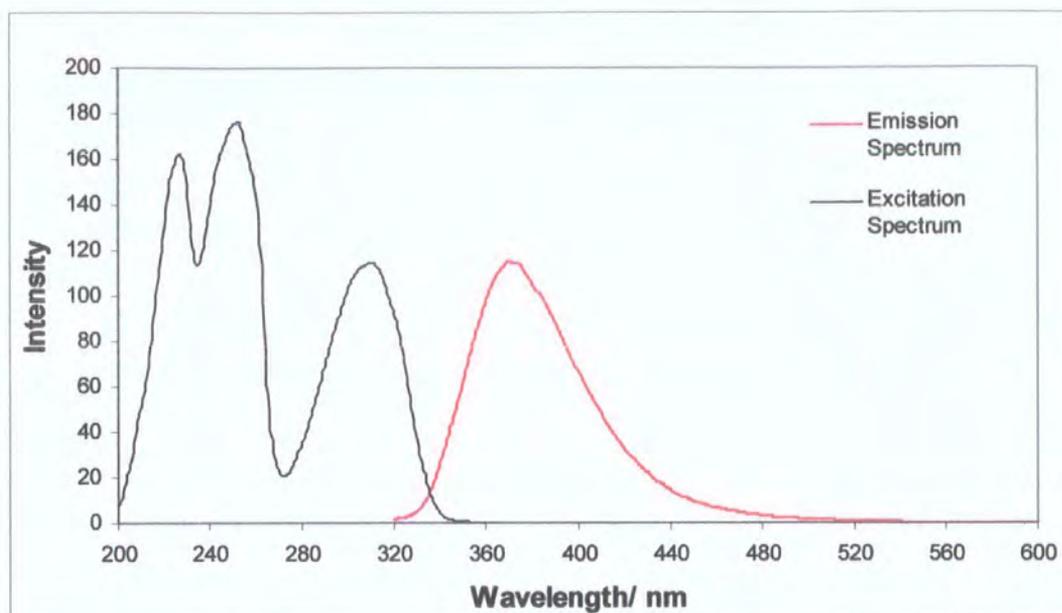
**Figure 4.5. The fluorescence emission and excitation spectra of N-acetyl-menthyl anthranilate in ethanol. λ_{ex} = 310 nm, λ_{em} = 370 nm.**

Solvent	Photophysical Parameter		
	$\lambda_{max}{}^{*}$ / nm	$\tau_f{}^{\dagger}$/ ns	$\Phi_f{}^{\ddagger}$
Toluene	368	3.9 ± 0.1	0.16 ± 0.01
Cyclohexane	363	4.0 ± 0.1	0.13 ± 0.01
Ethanol	370	3.6 ± 0.1	0.13 ± 0.01
Acetonitrile	369	3.4 ± 0.1	0.14 ± 0.01

*   Fluorescence Emission Maximum, following 310 nm excitation.

†   Fluorescence Lifetime.

‡   Fluorescence Quantum Yield relative to 2-aminopyridine in 0.2 M H_2SO_4 and quinine bisulphate in 2 M H_2SO_4.

**Table 4.2. Fluorescence data for N-acetyl-menthyl anthranilate in a range of solvents.**

4.2.3. Phosphorescence

Low temperature phosphorescence spectra of N-acetyl-menthyl anthranilate show a structureless emission centred at ~420 nm. The spectrum obtained from a solution in 4:1 methylcyclohexane: isopentane (4:1 MCH:i-P) is shown in figure 4.6. From this spectrum we estimated the energy of the triplet state to be 307 kJmol^{-1}. The phosphorescent emission was found to be long lived, with a lifetime of ~1.3 s. The phosphorescence data are summarised in table 4.3.
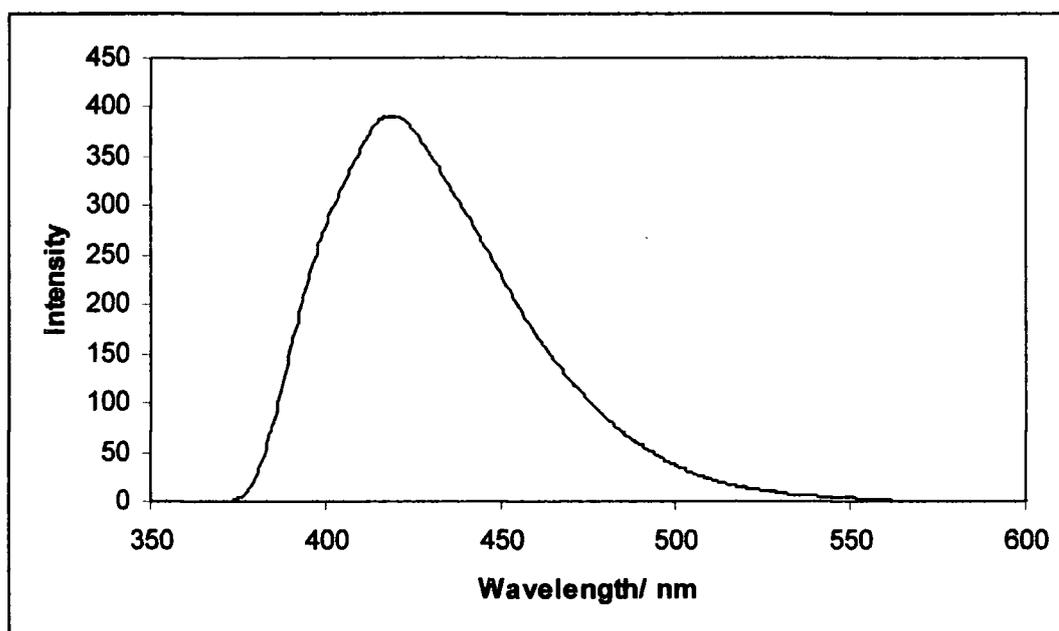
Figure 4.6. Low temperature phosphorescence of N-acetyl-menthyl anthranilate in 4:1 MCH:i-P.

Solvent	Photophysical parameter		
	λ_{max}*/ nm	τ_p†/ s	E_T‡/ kJmol^{-1}
EPA	420	1.3	311
4:1 MCH:i-P	425	1.3	307

*   Phosphorescence Emission Maximum, following 310 nm excitation.

† Phosphorescence Lifetime.

‡ Triplet State Energy

Table 4.3. Phosphorescence data for N-acetyl-menthyl anthranilate.

4.2.4. Kinetic Absorption Measurements

4.2.4.1.Transient Absorption

Kinetic absorption measurements on N-acetyl-menthyl anthranilate in dilute degassed solutions revealed a transient with an absorption centred around 450 nm. The transient absorption spectrum in degassed ethanol is shown in figure 4.7 and the corresponding kinetic absorption trace and first order fit is shown in figure 4.8. The lifetime of this transient was found to be solvent dependent in the range 120-240 μs, as shown in table 4.4.

Solvent	$\tau_T/$ μs
Cyclohexane	120 ± 10
Acetonitrile	240 ± 25
Ethanol	180 ± 15

***Table 4.4. Lifetimes of the transient formed following 266 nm excitation of
N-acetyl-menthyl anthranilate in a range of solvents.***
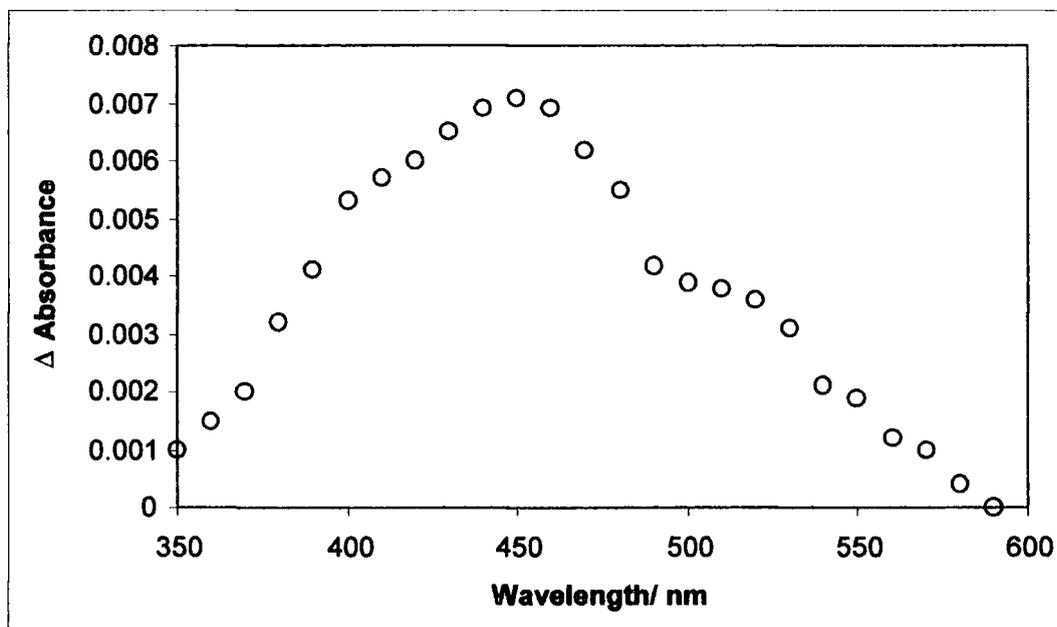
***Figure 4.7. Transient absorption spectrum obtained following 266 nm excitation of
N-acetyl-menthyl anthranilate in degassed ethanol at 295 K.***

119
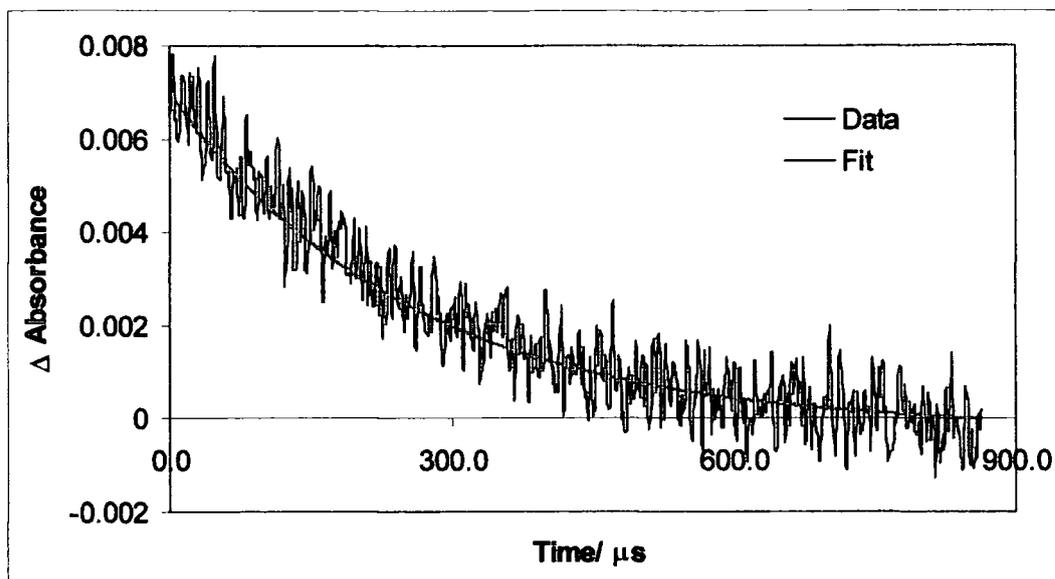
Figure 4.8.   The kinetic absorption trace and fit obtained from N-acetyl-menthyl ***anthranilate in degassed ethanol. λ_{pump} = 266 nm, λ_{probe} = 450 nm.***

As with the work carried out on the anthranilate esters, a combination of interference from sample fluorescence and limitations in our probe wavelengths meant it was not possible to record a bleach of the ground state or to determine ε_{TT} or Φ_T. Aeration of the solutions resulted in the loss of the transient signal.

4.2.4.2 Delayed Fluorescence

A long-lived emission was observed during the course of these kinetic absorption experiments. The intensity of the emission was found to increase exponentially with laser power and the spectral profile was recorded and found to be identical to the fluorescence spectrum as shown in figure 4.9. The fluorescence spectrum was obtained using a solution with an absorbance of ~0.1 and an irradiation wavelength of 310 nm. The delayed fluorescence spectrum was obtained following 266 nm laser excitation of a degassed solution. The absorbance of the solution was ~0.5 in a 1 cm pathlength cuvette and the laser energy was ~1 mJ pp. Aeration of the solution resulted in the loss of the emission, indicative of P-type delayed fluorescence resulting from a triplet-triplet annihilation process. The processes involved in P-type delayed fluorescence are shown schematically in chapter 3, figure 3.9.
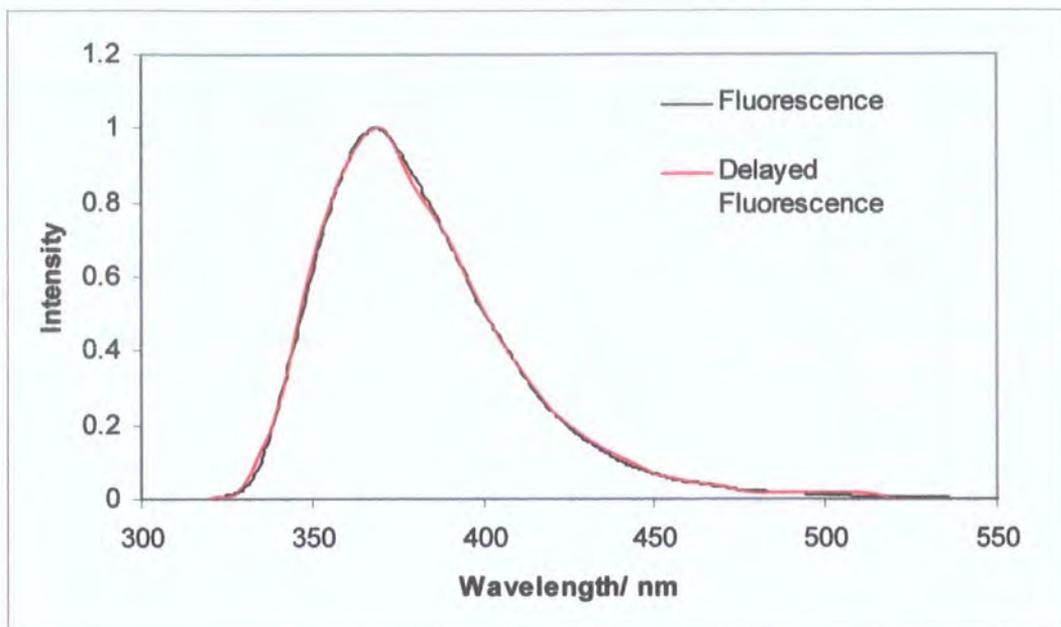
Figure 4.9. Normalised fluorescence and delayed fluorescence spectra of N-acetyl-menthyl anthranilate in acetonitrile.

4.2.4.3. Quenching

4.2.4.3.a. Self-quenching

The quenching of the transient species formed by ground state molecules was studied in a range of solvent systems. The rate constants for self-quenching were found to lie in the range $2.0 \times 10^6 - 3.2 \times 10^7$ $dm^3 mol^{-1} s^{-1}$ as shown in table 4.5. The Stern-Volmer plot for self-quenching in acetonitrile is shown in figure 4.10.

	$k_{self}^{*} / 10^6 dm^3 mol^{-1} s^{-1}$	$k_{O_2}^{\dagger} / 10^8 dm^3 mol^{-1} s^{-1}$
Cyclohexane	32.0 ± 7.0	4.0 ± 0.1
Acetonitrile	5.2 ± 0.8	4.6 ± 0.2
Ethanol	2.0 ± 0.1	5.0 ± 0.1

* Self-quenching rate constant.

† Oxygen-quenching rate constant.

Table 4.5. Quenching rate constants for the transient species formed following 266 nm excitation of N-acetyl-menthyl anthranilate.
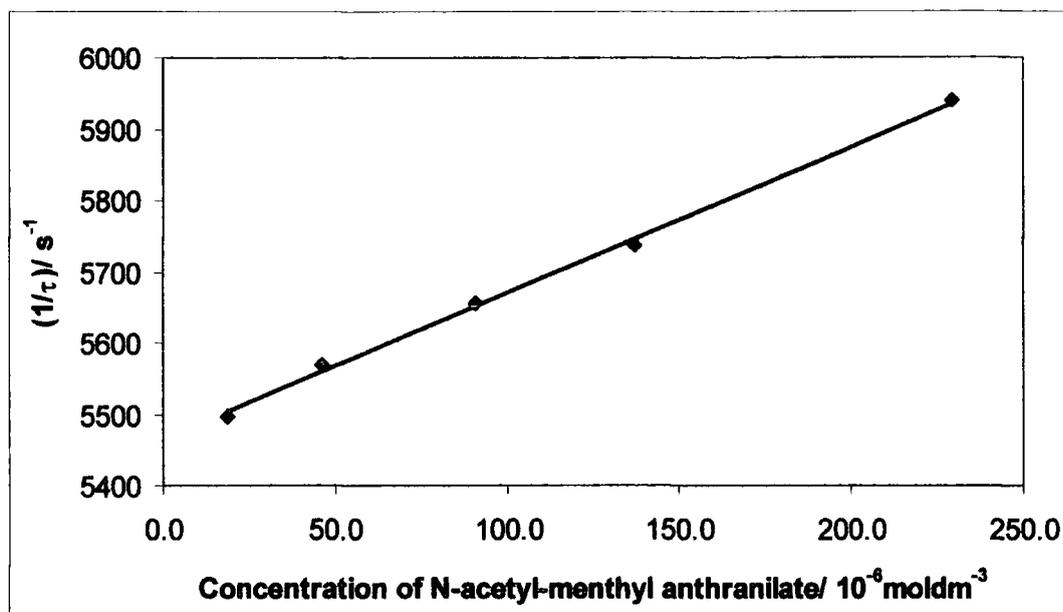
**Figure 4.10. Stern-Volmer plot for the self-quenching of N-acetyl-menthyl**
**anthranilate in acetonitrile.**

4.2.4.3.b.   Oxygen-quenching

The total loss of the transient signal on aeration of the solution demonstrates that the species formed is efficiently quenched by oxygen, indicating that the species is probably a triplet state. This phenomenon was studied and quantified to determine the oxygen quenching rate constants. For the three solvent systems studied they were found to be in the range 4.0-5.0 x $10^8 \, dm^3 mol^{-1} s^{-1}$, as shown in table 4.5. Figure 4.11 shows the Stern-Volmer plot for oxygen quenching in cyclohexane.
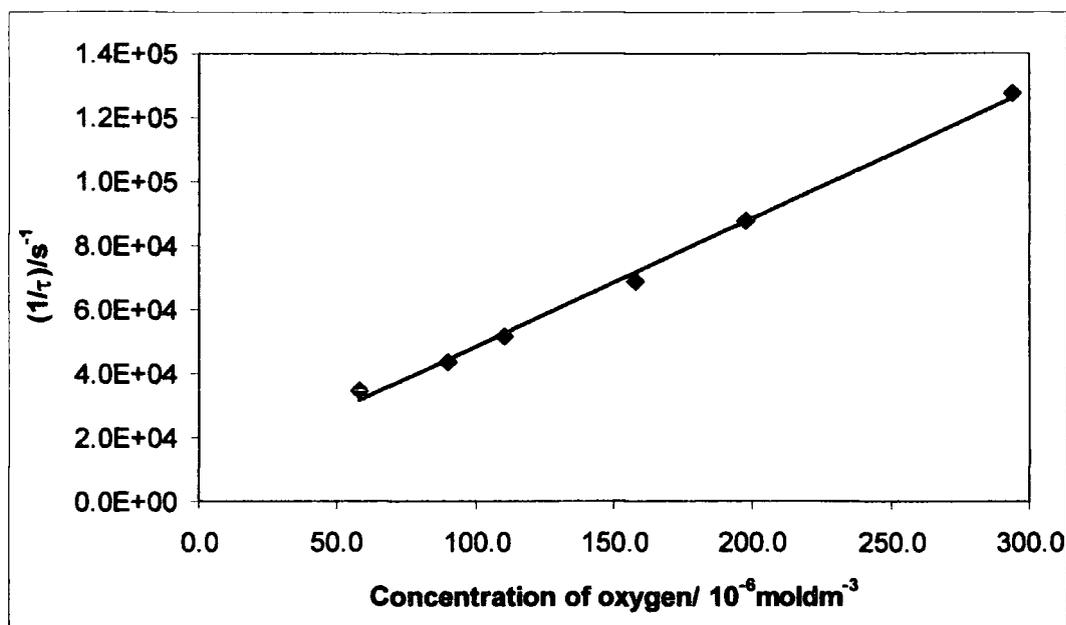
Figure 4.11. Stern-Volmer plot for the oxygen-quenching of N-acetyl-menthyl anthranilate in cyclohexane.

4.2.5. Singlet Oxygen Measurements

4.2.5.1. Production of Singlet Oxygen

The efficient oxygen-quenching of the transient species formed results in the formation of singlet oxygen, detected by its characteristic luminescence at 1270 nm. A typical singlet oxygen phosphorescence decay trace and the first order fit are shown in figure 4.12.

Solvent	Φ_Δ*	k_Δ[†]/ 10^4dm^{3}mol^{-1}s^{-1}
Cyclohexane	0.19 ± 0.02	2.4 ± 0.3
Acetonitrile	0.21 ± 0.02	not recorded
Ethanol	0.20 ± 0.02	not recorded

* Quantum yield of singlet oxygen formation relative to *meso*-tetraphenylporphyrin in cyclohexane, acridine in acetonitrile and perinaphthenone in ethanol.

[†] Singlet oxygen quenching rate constant

Table 4.6. Singlet oxygen data for N-acetyl-menthyl anthranilate.
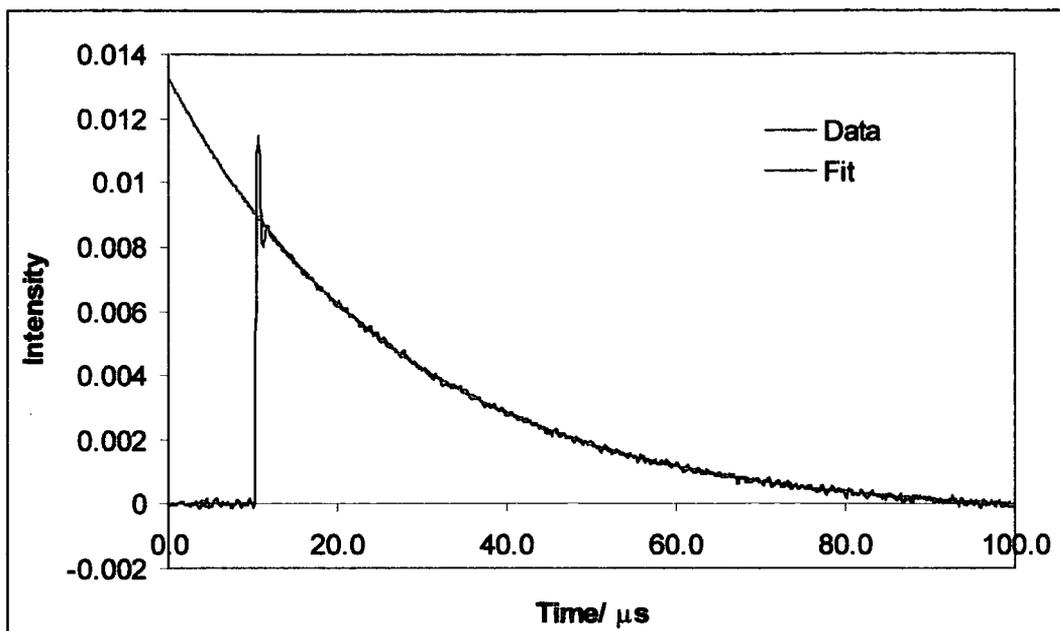
Figure 4.12. Kinetic singlet oxygen phosphorescence decay trace following 266 nm laser excitation and the first order fit obtained.

The lifetimes of singlet oxygen were determined to be 22 μs in cyclohexane, 68 μs in acetonitrile and 17 μs in ethanol, all of which are consistent with literature values[18]. Table 4.6 contains the quantum yields of singlet oxygen formation and the plot of $S(0)_{EA}$ against $1-10^{-A}$ for the solution of N-acetyl-menthyl anthranilate in cyclohexane is shown in figure 4.13.
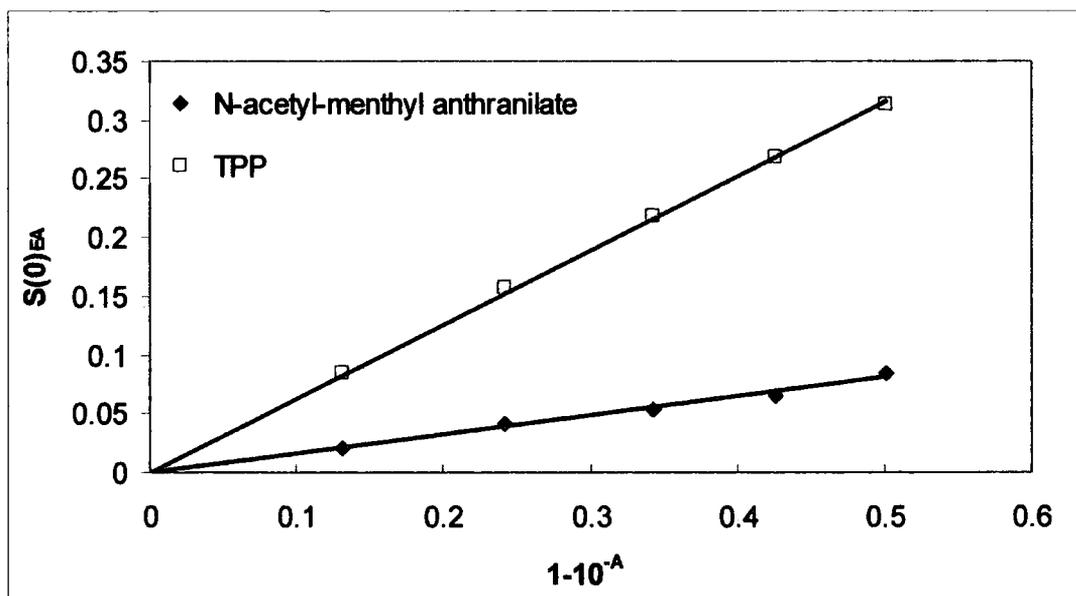
Figure 4.13. Plots of $S(0)_{EA}$ vs $1-10^{-A}$ for singlet oxygen quantum yield determination.

4.2.5.2. Quenching of Singlet Oxygen

The quenching of the characteristic singlet oxygen phosphorescence by N-acetyl-menthyl anthranilate was studied in cyclohexane following excitation of a solution containing TPP at 532 nm. Use of this excitation wavelength ensured that the production of singlet oxygen was only due to sensitization by the TPP. The rate constant in cyclohexane was determined to be $2.43 \pm 0.03 \times 10^4$ $dm^3 mol^{-1} s^{-1}$. Figure 4.14 shows the Stern-Volmer plot obtained.
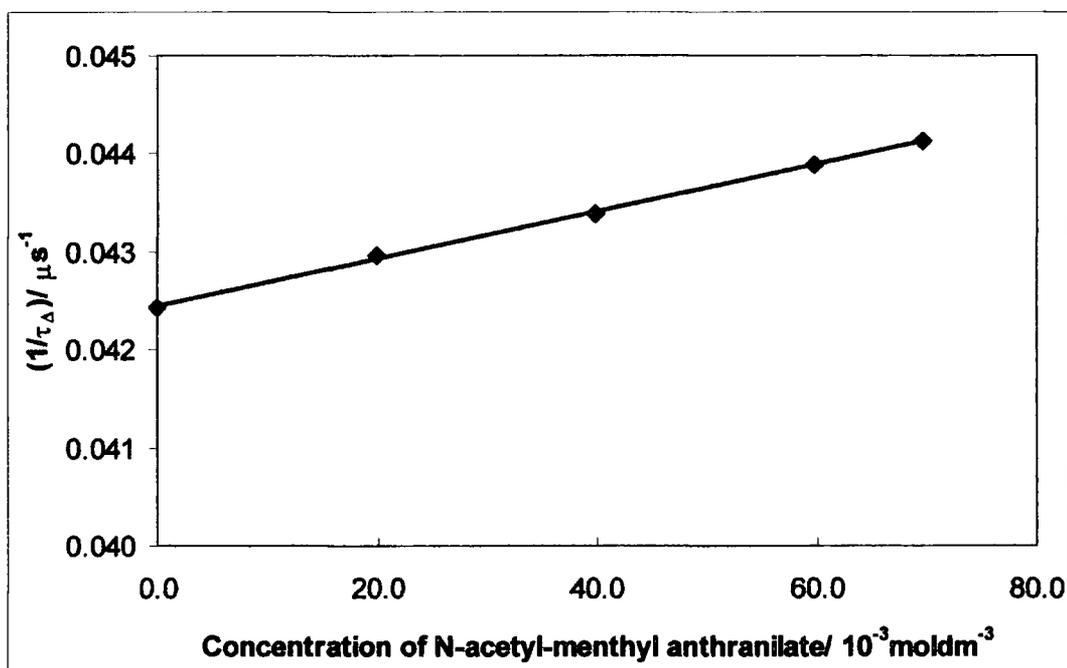
Figure 4.14. Stern-Volmer plot for the quenching of singlet oxygen by N-acetyl-menthyl anthranilate in cyclohexane.

4.3.   Discussion

N-acetyl-menthyl anthranilate has been synthesised as an analogue to N-acetyl homomenthyl anthranilate, a compound which, until relatively recently, was approved for use in sunscreen formulations in the EC. Given the similarities of the photophysical and photochemical properties of menthyl anthranilate and methyl

anthranilate (chapter 3), we expect that the properties of N-acetyl-menthyl anthranilate will be similar to those of the homomenthyl ester and so will provide a good indication of the photophysics and photochemistry of the sunscreen agent.

Anthranilate esters have been described as being among the few chemical sunscreens that absorb in the UV-A region[3], whilst providing minimal protection in the UV-B region[5]. However, the absorption spectrum of N-acetyl-menthyl anthranilate shows that this compound offers protection in both the UV-B and UV-A ranges. The absorption maximum at ~310 nm is situated in the UV-B region, but it also offers some protection in the UV-A range as the absorption band stretches from 270 nm (UV-B) – 340 nm (UV-A). Unfortunately the protection provided in the UV-A range does not extend to 400 nm so in order for a formulation to offer broad band protection across the UV range it would need to contain another UV-A absorber, potentially increasing the manufacturing costs. Another disadvantage of this compound is the low molar absorption coefficient, arising from the *ortho*-disubstitution pattern of the compound. As with menthyl anthranilate the absorption coefficient is higher than in other *ortho*-disubstituted sunscreens such as the salicylates, but considerably lower than *para*-disubstituted counterparts such as the para-aminobenzoic acid derivatives. This work, however, highlights other more disturbing photophysical properties of this material.

From the measurements reported above we have revealed that following excitation intersystem crossing from the S_1 state to the triplet state is the dominant deactivation pathway but that radiative decay also occurs to a significant extent. We have found that the triplet state is relatively long-lived in degassed solution, while in aerated solutions it is efficiently quenched by oxygen to produce singlet oxygen.

The absorption spectra of this compound in ethanol shows three bands at 224 nm, 252 nm and 310 nm. When these bands are compared to those in the analogous spectra of menthyl anthranilate several differences can be noted resulting from acetylation of the amine group. Firstly, there is a red shift in the shortest wavelength band from 220 nm to 224 nm. Secondly, there is a slight red shift in the 249 nm band to 252 nm and an increase in relative intensity when compared to the shorter wavelength bands.

Finally, the longest wavelength band has been blue shifted from 340 nm to 310 nm and shows a reduction in relative intensity. These findings are consistent with those of Ungnade[8] and Grammaticakis[10] who have explained them in terms of an increase in conjugation and the loss of molecular planarity following acetylation. The latter results in the reduction in the tendency of the lone pair of electrons on the nitrogen to migrate into the aromatic ring.

Luminescence studies have determined that this compound is both fluorescent and phosphorescent. The fluorescence was determined to be short lived ($\tau_f \sim 4$ ns) with a solvent dependent emission maximum in the range 362-370 nm. This value is in agreement with the findings of Staudemayer et al.[12] Comparison of the fluorescence spectra and quantum yields with those obtained for menthyl anthranilate shows a blue shift of the emission maxima and a reduction in the quantum yields. This is consistent with the work of Ostakhov[15] who attributed this to a reduction in the electron releasing ability of the -NRH group following acetylation. The fluorescence quantum yields observed in these solution state studies and the small Stokes shift observed for the fluorescence spectrum means that a high proportion of the emitted radiation falls in the UV-A range, i.e. 320-400 nm.

The phosphorescence was determined to be long-lived with a lifetime of ~ 1.3 s at 77 K and an emission maximum at ~ 420 nm. As with the fluorescence data this is in agreement with Staudemayer's work. Attempts were not made to measure ε_{TT} or Φ_T, however, based on the values of Φ_f and Φ_Δ measured here we can determine that $0.2 < \Phi_T < 0.85$. The triplet energy of this compound has been estimated from the phosphorescence spectrum to be ~ 310 kJmol^{-1}. This highlights a further disadvantage of this compound, namely its ability to act as a photosensitiser and photopotentiate harmful reactions in the skin such as the dimerization of thymine. The lowest triplet energy of thymine has been estimated from phosphorescence measurements to be 315 kJmol^{-1}.[19] It has also been established that triplet-triplet energy transfer will occur quite efficiently from donors whose triplet energies are either above, equal to, or 8-12 kJmol^{-1} below that of the acceptor[20]. This implies that there is at least the possibility that this compound could sensitise the formation of thymine triplets resulting in the

generation of thymine dimers, which are known to be potential precursors to skin cancer[21].

The transient species formed following excitation of this compound at 266 nm may be assigned to the triplet states by virtue of their quenching by oxygen to produce singlet oxygen. The absorption spectra of the transient species in all solvent systems were similar, with an absorption maximum at ~450 nm, suggesting that the same species is formed in each case. The decrease in triplet state lifetime as we go from ethanol through acetonitrile to cyclohexane indicates that the species formed is more stable in polar environments.

Deactivation of the triplet states has been shown to occur by four pathways. At 77 K in organic glasses, radiative decay results in long lived phosphorescent emission. At room temperature in aerated solutions the triplet states are efficiently quenched by oxygen resulting in the formation of singlet oxygen with quantum yields of formation of ~ 0.20 in all the solvent systems studied. P-type delayed fluorescence has also been observed from degassed solutions of this compound at room temperature following 266 nm pulsed excitation, resulting from triplet-triplet annihilation. Finally, quenching of the triplet states by ground state molecules has been shown to occur in degassed solutions of higher concentrations.

By comparison of the results reported here with work involving sunscreen formulations containing menthyl anthranilate,[22,23,24,25] it is likely that the use of N-acetyl-menthyl anthranilate within a sunscreen formulation is likely to result in a fluorescent product. Most of the fluorescent emission will be in the UV-A range and, as discussed in chapter 3, a significant amount will be transmitted to the skin. This indicates that incorporation of this ingredient into a formulation could result in a product that may, in fact, increase the intensity of radiation at the skin surface in this range.

More significantly, however, the results of laser flash photolysis and near infrared luminescence measurements clearly demonstrate the formation of a long-lived triplet state which is efficiently quenched by oxygen to generate singlet oxygen with a significant quantum yield.

4.4. Conclusions

A thorough study of the photophysical properties of N-acetyl-menthyl anthranilate has been conducted using conventional room temperature and low temperature luminescence spectroscopy, laser flash photolysis, and near infrared luminescence measurements. This compound was synthesised as an analogue of N-acetyl-homomenthyl anthranilate, a compound that, until relatively recently, was approved for use as a sunscreen in the EC.

The luminescence studies indicate that, following excitation, radiative decay from the S_1 state resulting in fluorescence occurs to a significant extent ($\Phi_f \sim 0.15\pm0.02$), but that intersystem crossing to the triplet state is the dominant deactivation pathway (e.g. $\Phi_\Delta \sim 0.20\pm0.02$).

The triplet state has been shown to have a long lifetime in degassed solution (120 - 240 μs) and a long lived phosphorescence lifetime of ~ 1.3 s when held in low temperature organic glasses. From the phosphorescence emission spectrum the triplet state energy, E_T, has been estimated to be ~ 310 kJmol^{-1}. This relatively high value indicates that this compound has the potential to sensitise the formation of thymine triplets in skin resulting in the generation of thymine dimers, species which are known to be potential precursors to skin cancer.

Kinetic absorption measurements on degassed solutions have revealed a triplet-triplet absorption band at ~ 420 nm that is independent of solvent and that is readily quenched by oxygen on aeration. Also under high intensity pulsed illumination delayed fluorescence has been observed. The intensity of this emission increased exponentially with the laser power and was quenched by oxygen indicating P-type delayed fluorescence resulting from triplet-triplet annihilation.

Finally, in aerated solutions this N-acetyl anthranilate ester has been shown to produce singlet oxygen, with a quantum yield of 0.20 ± 0.02 in all solvents studied.

From a comparison of the results reported here with the work on formulations containing menthyl anthranilate it seems reasonable to deduce that the triplet state of N-acetyl-menthyl anthranilate will be generated in sunscreen formulations, and that it may subsequently generate singlet oxygen close to the skin surface.

4.5. References

1. Gasparro, F.P., M. Mitchnick, and J.F. Nash (1998) A review of sunscreen safety and efficacy. *Photochem. Photobiol.* **68**, 243-256.

2. Kligman, L.H., F.J. Akin, and A.M. Kligman (1985) The contributions of UVA and UVB to connective tissue damage in hairless mice. *J. Invest. Derm.* **84**, 272-276.

3. Shaath, Nadim A. (1997) Evolution of Modern Sunscreen Chemicals. In *Sunscreens. Development, Evaluation, and Regulatory Aspects* (Edited by Nicholas J. Lowe, Nadim A. Shaath and Madhu A. Pathak), Marcel Dekker Inc., New York, pp. 3-33.

4. Agrapidis-Paloymis L.E., R.A. Nash and N.A. Shaath (1987) The effect of solvents on the ultraviolet absorbance of sunscreens. *J. Soc. Cosmet. Chem.*, **38**, 209-221.

5. Fisher A.A. (1992) Sunscreen Dermatitis: Part IV – The Salicylates, the Anthranilates, and Physical Agents. *Cutis*, **50**, 397-398.

6. Brown M. Boots plc. *Personal communication.*

7. Dannenberg H. (1949) Classification of ultraviolet absorption. I. Substituted acetophenones, benzoic acids and cinnamic acid. *Z. Naturforsch*, **4b**, 327-344.

8. Ungnade H.E. (1954) Ultraviolet absorption spectra of acetanilides. *J. Am. Chem. Soc.*, **76**, 5133-5135.

9. Grammaticakis P. (1950) The ultraviolet absoprtion of o-substituted anilines. III. N-substituted o-nitro- and o-carboxyanilines. *Bull. Soc. Chim. France.* 158-166.

10. Grammaticakis P. (1951) Near ultraviolet and visible absorption of some isomeric arylamines and their nitrogen substituted derivatives. I. *Bull. Soc. Chim. France.* 220-226.

11. Lee C.K. and Y.M. Ahn (1989) Reactions of amides with potassium permanganate in neutral aqueous solution. *J. Org. Chem.* **54(14)**, 3744-3747.

12. Staudemayer R. and T.D. Roberts (1974) Neighbouring group participation in photolysis of o-substituted aryls. *Tet. Letts.* **13**, 1141-1144.

13. Stenberg V.I., In *Organic Photochemistry,* Vol. I. (edited by O.L. Chapman), Marcel Dekker, New York, pp. 127.

14. Hardy G.E., J.C. Baldwin, J.I. Zink, W.C. Kaska, P.H. Liu and L. Dubois (1977) Triboluminescence spectroscopy of aromatic compounds. *J. Am. Chem. Soc.* **99(11)**, 3552-3558.

15. Ostakhov S.S., E.M. Tsyrlina, S.G. Yunusova, M.S. Yunusov and V.P. Kasakov (1997) Fluorescence of the diterpenoid alkaloids lappaconitine and N-deacetyllappaconitine in acetonitrile. *Russ. Chem. Bull.*, **46(4)**, 705-707.

16. Bensasson R.V., E.J. Land and T.G.Truscott, (1993) *Excited States and Free Radicals in Biology and Medicine.* Oxford University Press Inc., New York.

17. Kamlet, M.J., J.L.M. Abboud and R.W. Taft (1984). In *Progress in Physical Organic Chemisty* Vol. 13, (Edited by R.W. Taft), Wiley&Sons, New York, pp. 485-630.

18. Gorman, Anthony A. and Michael A.J. Rodgers (1989) Singlet Oxygen. In *Handbook of Organic Photochemistry*, Vol. II (edited by J.C. Scaiano), CRC Press, Florida, pp. 229-247.

19. Lamola A.A. (1968) Applications of electronic energy transfer in solution. *Photochem. Photobiol.*, **8**, 601-616.

20. Evans D.F. (1957) Perturbation of singlet-triplet transitions of aromatic molecules by oxygen under pressure. *J. Chem. Soc.* 1351-1537.

21. Gonzenbach, H., Hill, T.J., and Truscott, T.G. (1992) The triplet energy levels of UVA and UVB sunscreens. *J. Photochem. Photobiol. B: Biol.* **16**, 377-379.

22. Rhodes L.E., and B.L. Diffey (1996) Quantitative assessment of sunscreen application technique by *in vivo* fluorescence spectroscopy. *J. Soc. Cosmet. Chem.*, **47**, 109-115

23. Rhodes L.E. and B.L. Diffey (1997) Fluorescence spectroscopy: a rapid, non-invasive method for measurement of skin surface thickness of topical agents. *Br. J. Dermatol.*, **136**, 12-17.

24. Azurdia R.M., J.A. Pagliaro, B.L. Diffey and L.E. Rhodes (1999) Sunscreen application by photosensitive patients is inadequate for protection. *Br. J. Dermatol.*, **140**, 255-258.

25. Stokes, R.P. and B.L. Diffey, (1999) The feasibility of using fluorescence spectroscopy as a rapid, non-invasive method for evaluating sunscreen performance. *J. Photochem. Photobiol. B:Biol.* **50**, 137-143.

Chapter 5

Detection and Analysis of Sunscreens using Infrared Spectroscopy

5.1 Introduction

5.1.1 Sunscreen Formulations

The growing awareness that exposure to sunlight can cause skin cancer and degenerative skin changes such as ageing has resulted in a sharp increase in the sales of sun-protective and accessory products in recent years.

As cosmetics manufacturers are also now using UV-A and UV-B filters in many of their products, not just those specifically designed to prevent sunburn, such chemical UV filters will become even more important in reducing the risk of premature ageing and skin cancer. Such filters are subjected to stringent testing prior to their acceptance by bodies such as COLIPA (EC) and the U.S. FDA for use in commercially available products. As demands increase and the use of such products becomes more widespread the amount of safety data required to defend these chemicals is unlikely to decrease. It is probable that more data will be required, such as the results of investigations studying the interactions between the sunscreening chemicals, UV light and skin. These interactions contribute to factors such as the substantivity or adhesion of the final sunscreen products to the skin and are thought to involve mechanisms which are not well defined such as absorption, ion exchange and other chemical interactions[1]. This highlights the need for more accurate and universal testing methods that are quick, easy and inexpensive.

5.1.2. Properties of sunscreen formulations

The effectiveness of any sunscreen formulation depends on a number of factors, all of which need to be determined before a product can be marketed. The most important property is the ability of the formulation to offer photoprotection in the UV range, usually expressed numerically as the sun protection factor (SPF) for protection in the UV-B range. Other properties include the resistance of the product to sweat and abrasion or rub off, known as the substantivity of the formulation, the water resistance of the formulation and the absorption of the formulation, or individual components through the skin.

5.1.3.   Techniques used to analyse sunscreen formulations

The majority of preliminary sunscreen research has been performed *in vivo* on animal models, but the physiology of most animal skin is very different from human skin. Animals are also expensive to maintain, and the use of animals in the testing of cosmetic products is becoming socially less acceptable[2]. The development of a simple method for testing the protection afforded by sunscreens, and other properties, is of fundamental importance.

5.1.3.1. Spectrophotometric Methods

Both Cumpelik[3] and Vogelman *et al.*[4] have developed spectrophotometric techniques for evaluating the properties of sunscreen formulations. Cumpelik measured the absorption spectra of thin films of final formulations pressed between two optically matched quartz cuvettes and compared the "as is" absorption spectrum with that obtained from alcoholic solutions of the active ingredients. The results demonstrate the solvent induced distortion of the absorption bands of the active ingredients in polar solvents when compared to the bands detected from thin films of the final formulations. Vogelman *et al.* measured the SPF of formulations by comparing their absorption spectra with that of a standard 8% homosalate preparation of known SPF. The formulations were dissolved in isopropanol and their absorption spectra run. The areas under the plots were then compared to that of the standard homosalate formulations (SPF = 2) and the SPFs calculated. Although this method has the advantage of not exposing human volunteers to unnecessary irradiation the results may not correlate well with SPF values found *in vivo* due to absorption shifts induced by the solvent as highlighted by Cumpelik.

5.1.3.2. *In vivo* assays

The only country in the European Union (EU) to have published an official SPF testing protocol for assessing the photoprotection of final sunscreen formulations is Germany[5]. However, this method, known as the DIN method, was not widely accepted by the other members of the EU mainly because of the inadequacy of the recommended UV source. Work by COLIPA in 1990 resulted in the establishment of a test protocol[6] for the

determination of sunscreen SPF factors. This protocol has since been officially adopted by all of the EU except Germany, which continues to use its DIN testing method. The COLIPA method has all the main elements of SPF tests used world-wide. In summary it is a human volunteer test requiring a minimum of 10 volunteers, performed in a laboratory with a standard solar simulator UV source. It tests a sunscreen application thickness of 2 mgcm^{-2} spread over an area of at least 35 cm^2 on the back of each volunteer, and involves the simultaneous irradiation of the site of sunscreen application and a test 'sunscreen-free' site with the standard UV source. Each test site is split into 1 cm^2 areas and irradiated for increasing time intervals with each interval being incremented by a factor of 1.25. This is carried out for a minimum of 5 sites. The minimal erythemal dose, (MED), the time needed for the first area to show a perceivable redness is assessed for both the sunscreen covered site and the test sunscreen-free site after 20 hours. The SPF is then calculated from the ratio of the times correlating to the MED for the two sites.

Work by Kaidbey and Kligman[7] has used a similar *in vivo* assay to develop laboratory methods for appraising the efficacy of sunscreens. Their comprehensive study included the measurement of SPF factors for several commercially available formulations as well as dose response and wash-off studies and they also compared results obtained using a solar simulator in the laboratory with those obtained using natural sunlight. They found that there was a good correlation between results obtained in sunlight and in the laboratory and concluded that the protection offered by a sunscreen layer increased with the dose applied. They also determined that the physical sunscreens tested were less water and sweat resistant than their chemical counterparts.

Agin and Levine[8] have used an *in vivo* assay to study the substantivity of sunscreens and claim that, when on skin, sunscreens retain their protective capability for up to eight hours after application. They investigated the time dependence of sunscreen effectiveness for a range of time intervals between application and exposure to ultraviolet radiation. Their results indicate that sunscreen formulations can maintain their efficacy for several hours post-application. They concluded that one application of a sunscreen product may provide several hours of high level protection as long as the product is not rubbed off. Clearly this situation does not give a realistic model, since in their normal

application the sunscreen user will be pursuing activities in the sun where a substantial amount of 'rub-off' may be caused due to contact with clothing, or other articles.

In contrast Urbach[9] has stated that the rapid loss of sunscreen from a substrate over time, due to rub-off and penetration, may result in a drop in SPF of 50% within two hours of application contradicting the long term protection predicted by Agin *et al*.

The *in vivo* assays described above have two major disadvantages. The first is the need to expose human volunteers to potentially large doses of UV radiation, especially when testing high SPF formulations. The second disadvantage is that the techniques are very time consuming, requiring the volunteers to attend the testing centre for at least two days. Many techniques have since been developed to study sunscreen formulations on a variety of substrates in an attempt to determine their properties using methods that are quicker and easier and that avoid exposing volunteers to unnecessary doses of UV radiation.

5.1.3.3. Transmission Measurements

Brown and Diffey[10] used both *in vitro* transmission measurements and an *in vivo* assay to probe the effect of applied thickness of a formulation on the protection it offers. They found that the protection increased with applied thickness although the increase was not logarithmic as predicted by Beer's law for a uniform layer of sunscreen on the skin surface. They also found that the results obtained from both techniques were in agreement demonstrating that the transmission technique provides a reliable method for the evaluation of sunscreen performance *in vitro*.

Work by Stokes and Diffey[11] used *in vitro* spectral transmission measurements using excised human epidermis to quantify the photoprotection provided by physical and chemical sunscreens. The technique involved measuring the transmission of UV radiation through the substrate and then through the substrate covered with the sunscreen. A wide variety of substrates have been used for such assays including wool, pigskin, lyophilised pig epidermis, hairless mouse epidermis, human epidermis, human stratum corneum, synthetic skin casts, textured collagen sheets (e.g. VitroSkin™), surgical tape (e.g. Transpore™)[12], and three-dimensional dermal and skin equivalents[13]. In this case the substrate of choice was excised human epidermis because this was thought to

produce results closest to *in vivo* assays. Their study encompassed a wide range of SPF values, and they found that their measured values were in strong agreement with the quoted values of the products (determined by the usual *in vivo* assay). They concluded that this *in vitro* technique could prove reliable for the evaluation of the SPF of high-protection sunscreens. The only drawback to the technique is the need for excised human epidermis, limiting the wide spread application of this technique for use by the cosmetic industry as a whole.

Following on from this work Stokes *et al.*[14] have also shown that the application thickness of the formulation has significant effects on the SPF achieved and that under normal conditions most users only achieve 20-50% of the SPF stated on the product label.

Recently Stokes and Diffey[15,16] have extended the application of their transmission spectroscopy technique to study the water resistance of sunscreens on human epidermis *in vitro*. The advantage offered by this substrate is that the physicochemical changes in the sunscreen binding that result from water immersion can be expected to mimic the *in vivo* situation more closely than artificial substrates. They found that this technique provides a method which is cheaper, and less time consuming than existing *in vivo* water resistance testing. It offers the possibility to study the effect that water immersion may have on the absorption spectrum of products, something which cannot be determined *in vivo* and from this can provide valuable information on which, if any, of the active ingredients present in the formulations are being preferentially removed. The technique also lends itself to study the effects of other factors such as water temperature, salinity and turbulence on sunscreen substantivity.

5.1.3.4. Fluorescence Spectroscopy

Stenberg and Larkö[17] used fluorescence spectroscopy as a method of assessing sunscreen application techniques and their effect on the SPF achieved. The work involved monitoring the application of five different sunscreen formulations by 50 volunteers. The sunscreens contained 10% dihydroxyacetone to make them fluoresce. The fluorescence from the sunscreen was easily detected following irradiation with a Wood's light source and the area of application readily determined. Knowing the area covered and the amount of sunscreen used the application thickness was found to be ~1 mgcm^{-2},

half that used in testing procedures as recommended by the FDA and COLIPA. Studies were then carried out to determine the effect on the SPF of this reduced application thickness when compared to that determined at 2 mgcm^{-2}. It was found that the SPF value achieved was approximately half that expected.

A similar qualitative study by Loesch and Kaplan[18] used fluorescence spectroscopy to study the differences in application techniques between men and women. Fifty volunteers were asked to apply sunscreen to their faces and the areas of application were determined. They noted that there were several areas of incomplete coverage, particularly the ears and around the eyes, but that the only statistical difference between men and women was for application to the ears, with women being prone to miss this area.

Rhodes and Diffey investigated *in vivo* fluorescence spectroscopy as a means of quantifying the skin surface thickness of topically applied agents and demonstrated the potential of this technique to assess application techniques and the substantivity of sunscreens[19, 20]. They used formulations that possessed an intrinsic fluorescence and established a dose-response relationship for a series of five doses in the range 0.5-8.0 μlcm^{-2}. They examined the influence of application technique (by comparing light application of the cream to firm rubbing), the substantivity of the creams and their water resistance. They found a strong correlation between the fluorescence intensity and the logarithm of the surface density. This work has potential applications to determine the recommended interval for re-application of topical agents, make assessments of application techniques, study the substantivity of creams on both wet and dry skin and the water resistance properties. The main drawback is the need for the formulation to be auto-fluorescent. The use of fluorescent markers within the formulations was not considered to be appropriate due to the potential differences in solubility and substantivity of the markers compared to the formulations.

Stokes and Diffey[21] used a sunscreen containing menthyl anthranilate to study the feasibility of using fluorescence spectroscopy as a method for evaluating *in vivo* sunscreen performance. This compound was also added as a fluorescent marker to other non-fluorescent sunscreen formulations in an attempt to assess this method. Sunscreens

that contained menthyl anthranilate as the only UV-A filter showed strong fluorescence, in accordance with the work presented in chapter 3. However, they found that they were unable to detect fluorescence from those sunscreens which contained other UV-A filters and concluded that the feasibility of the method remained unproved.

Azurdia et al.[22] have recently used fluorescence spectroscopy to quantitatively assess the sunscreen application techniques of photosensitive patients who complained that such products seemed to be of little benefit. They used the same menthyl anthranilate containing sunscreen as Stokes et al.[21] and their results agreed with those of Stenberg[17] in that the average application thickness was approximately half that used for testing, resulting in an SPF of only half that predicted by the manufacturer.

5.1.3.5. Cytotoxicity Studies

Episkin has been used by Roguet et al. to assess the irritancy of topically applied products[23] and also determine an in vitro model to evaluate phototoxicity and sunscreen photoprotective properties[24]. It is a reconstituted organotype culture of keratinocytes which form a multi-layer differentiated epidermis on a collagen matrix. The material has been described as being comparable to human epidermis due to its layers of proliferating basal cells, layers of differentiated cells, and that UV-A and UV-B radiation penetrate Episkin and human skin to a similar extent. In this work the cytotoxic effects of UV-A and UV-B irradiation on the Episkin system were studied. The experiments were then repeated with different concentrations of the sunscreen Mexoryl SO on the substrate. They found an increase in the protection provided with increasing concentration of sunscreen which was determined by a reduction in the cytotoxic effects of the radiation. A similar study by Bell et al.[25] used a living skin equivalent, developed to resemble human skin, to carry out similar studies on the photoprotection provided by topically applied formulations.

5.1.3.6. Percutaneous Penetration Measurements

An issue of ongoing concern is that of systemic absorption of sunscreen ingredients after topical application. This results in loss of the protection provided by the formulation and

may also result in toxicity. Work by Hagedorn-Leweke and Lippold[26] studied the absorption of sunscreens, including oxybenzone, 4-methylbenzylidene camphor and 4-isopropyl dibenzoylmethane, through human skin *in vivo*. Saturated solutions of the above compounds in a propylene glycol/water mixture were fixed to the upper arms of volunteers in glass chambers. The maximum fluxes were calculated from the concentration decreases in the vehicle and were found to be in the range 0.5-130 $\mu gcm^{-2}h^{-1}$. From their results they also derived a method to predict maximum fluxes of penetrants through the skin.

Hayden *et al.*[27] studied the absorption of oxybenzone through the skin from a formulation containing 6% oxybenzone, 7.5% octyl methoxycinnamate, 5% octyl salicylate and 7% octocrylene. HPLC analysis of urine collected from volunteers 48 hours after application of the formulation showed the presence of significant amounts of oxybenzone and its metabolites. They estimated that over a 10 hour period 1-2% of the applied amount of oxybenzone had been absorbed through the skin. Although this would result in little change to the sunscreen content of the topical product, and oxybenzone has low acute toxicity in animals, little is known about its chronic toxicity in humans.

The skin penetration and sun protection factors of UV filters in two different vehicles, an oil-in-water emulsion-gel and petroleum jelly, were studied by Treffel *et al.*[28]. The UV filters used were oxybenzone, (2-ethylhexyl)-4'-methoxycinnamate and (2-ethylhexyl)salicylate and both *in vitro* and *in vivo* studies were carried out. The penetration of the UV filters from the two vehicles were found to be significantly different, but the resulting reductions in SPF were found to be the same. They concluded that penetration of UV filters through skin or conversely retention of them on the skin surface, as well as the expected SPF, depended on the formulation vehicle and so could be optimised simply by changing this property.

5.1.3.7. Infrared Spectroscopy

Despite the wide range of analytical techniques, described above, that have been used to probe the properties of sunscreen formulations infrared spectroscopy has received relatively little attention for such studies. ATR spectroscopy has been used

successfully in the study of the absorption of drugs through the skin[29], for the qualitative and quantitative analysis of cosmetics and household products[30, 31] and for the analysis of skin[32]. Tajima has recently used ATR to investigate the differences between cosmetically treated and untreated living human skin[33].

The only work in the literature regarding the use of ATR to study sunscreens is that of Gabriel *et al.*[34]. They used this technique to analyse (2-ethylhexyl)-4'-methoxycinnamate (1) and octyl-PABA (2) in ethanol, a test sunscreen containing (1) in a vehicle and three commercial sunscreens containing (1), (2) and oxybenzone. They compared spectra of the individual ingredients with those of the formulations and were able to identify (1) in the test sunscreen and in formulations containing other sunscreens. They also conducted substantivity studies by the tape stripping method and water substantivity tests following immersion in water. Although they appear to have carried out a comprehensive study of sunscreens using this technique the work was not carried out using the guidelines set down by the FDA and COLIPA regarding application thickness and water resistance testing. Furthermore, the ATR crystal they used was a KRS-5 internal reflection element constructed of thallium bromide, a compound known to be highly toxic[35]. This would effectively prevent the industry-wide application of their technique. Finally, their spectra were only recorded in the 1500-1050 cm^{-1} range which excludes important information from the carbonyl stretching bands commonly found in sunscreen agents. This work has not been cited since its publication.

5.1.4. The *in vivo* and *in vitro* detection and analysis of sunscreens

The work described here using infrared spectroscopy demonstrates how this technique could meet the requirements of a more comprehensive and stringent analysis of sunscreen agents within final formulations. Studies have been carried out on individual active ingredients and these have been identified in the spectra obtained from commercially available sunscreen formulations on skin. Preliminary substantivity studies with sunscreens on skin using an ATR probe, and on a model surface using ATR methodology have been carried out along with dose-response studies. Finally, changes in the spectra of the formulations were studied following the UV irradiation of a film of sunscreen on an ATR internal reflection element.

The technique has been shown to have the potential to study application techniques, substantivity and water resistance of sunscreen formulations on skin and also changes in the ingredients or formulations following exposure to UV light. It could also be extended to study the penetration of sunscreen ingredients through the skin.

5.2.   Results

5.2.1. Identification of active ingredients within formulations
5.2.1.1. Active Ingredients

Reference spectra of the pure active ingredients were obtained using either the Golden Gate or an ATR internal reflection element. The compounds analysed are given in the table below.

Sunscreen	Common name	UV absorption region
(2-ethylhexyl)-4'-methoxycinnamate	Parsol MCX	UV-B
4-butyl-4'-methoxydibenzoylmethane	Parsol 1789	UV-A
4-methylbenzylidene camphor	Parsol 5000	UV-B
2-hydroxy-4-methoxybenzophenone	Oxybenzone	UV-A
Menthyl anthranilate	-	UV-A
(2-ethylhexyl)-2'-cyano-3',3'-diphenylacrylate	Octocrylene	UV-B

Table 5.1. The active ingredients studied.

The structures of these materials, their IR spectra and assignments of the bands to the molecular vibrations are given below.

142
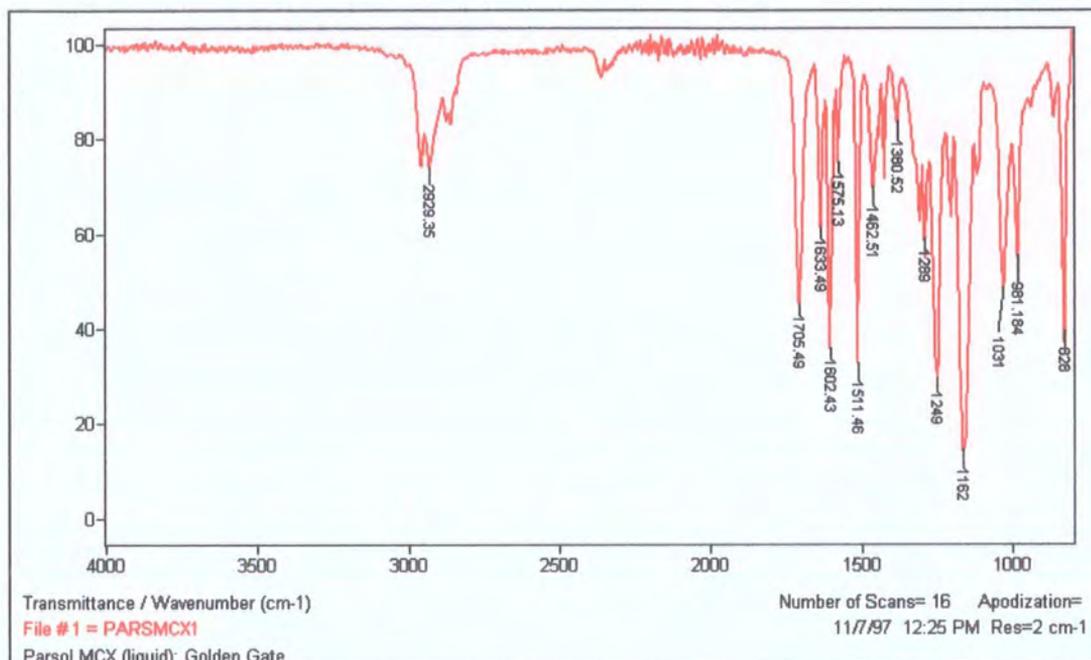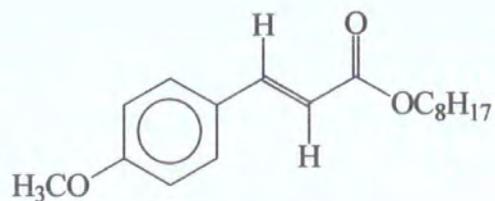
Parsol MCX

Figure 5.1. The structure and IR spectrum of Parsol MCX.

Band Wavenumber/cm^{-1}	Assignment
1705	-C=O stretch
1633	-C=C- stretch
1602, 1511	Aromatic C-C stretches
1463	O-CH$_3$ stretches
1249	-O-Ø stretch or C-O-C$_8$H$_{17}$ stretch
1162	O=C-O stretch
1031	Ø-O-CH$_3$ stretch

Table 5.2. The band assignments for Parsol MCX.

143
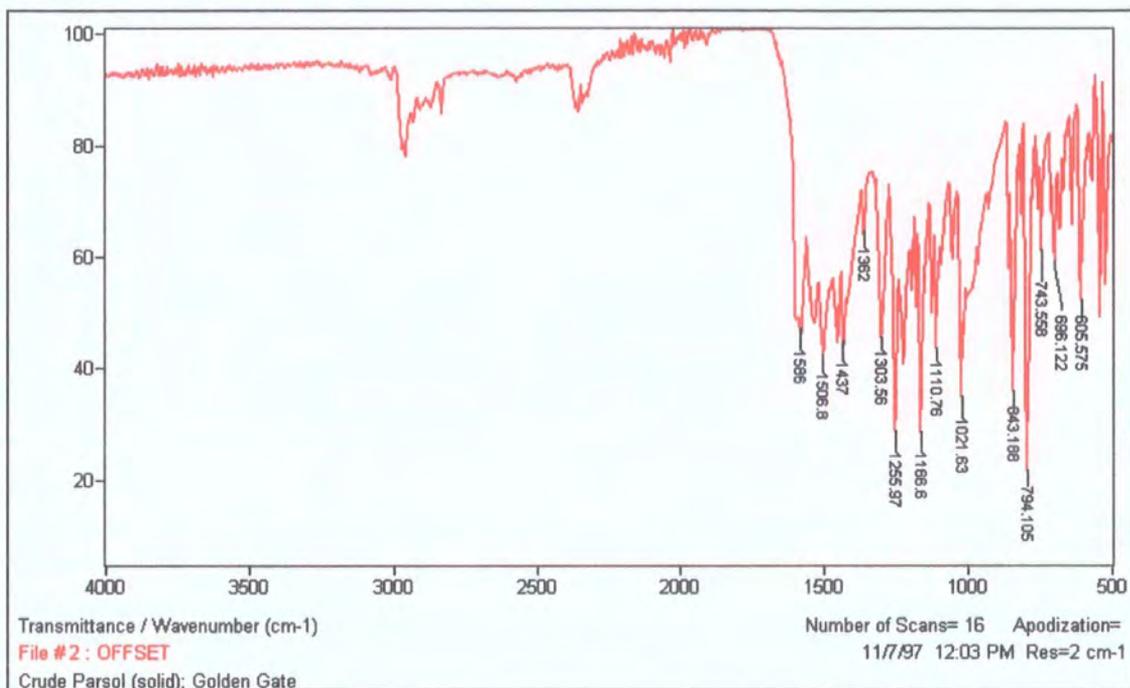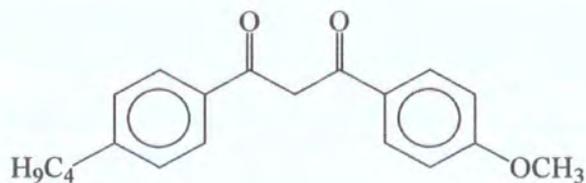
Parsol 1789

Figure 5.2. The structure and IR spectrum of Parsol 1789.

Band Wavenumber/cm^{-1}	Assignment
1588	O-C-C stretch of H-bonded enol
1507, 1111, 843	Aromatic C-C stretches
1362	-C-(CH$_3$)$_3$ stretch
1304, 1256	-O-Ø stretches
1167	O-C-C-C-O enol nulceus stretch
1022	Ø-O-CH$_3$ stretch

Table 5.3. The band assignments for Parsol 1789.

Parsol 5000
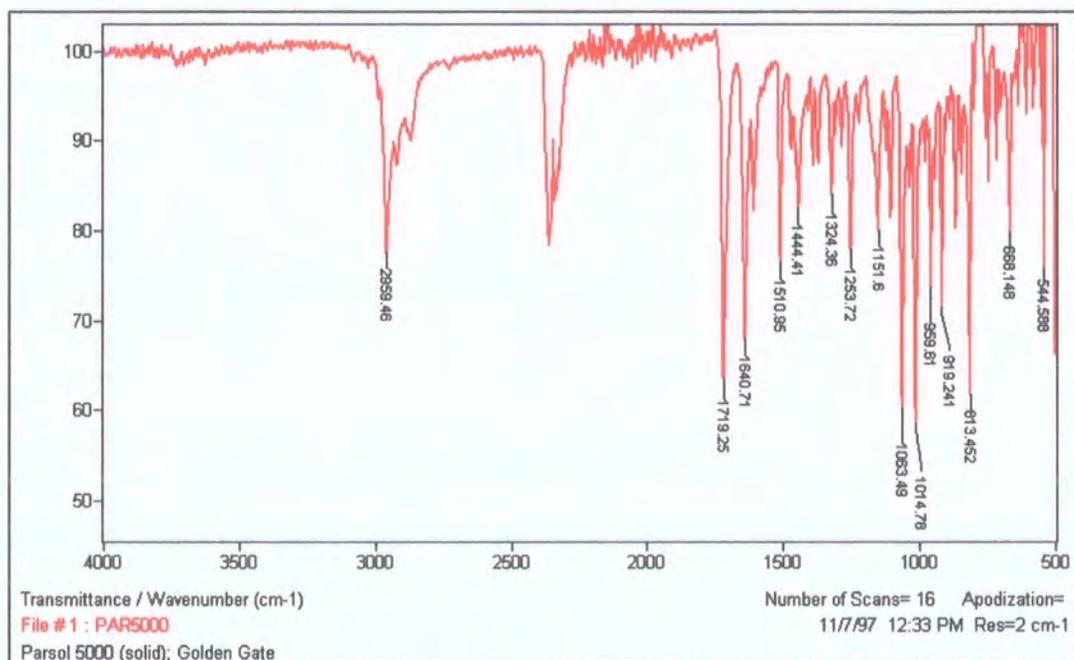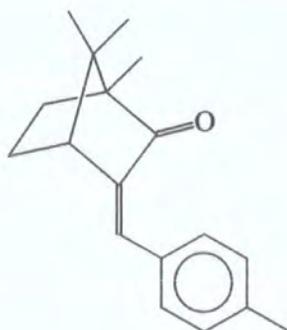
Figure 5.3. The structure and IR spectrum of Parsol 5000.

Band Wavenumber/cm^{-1}	Assignment
1719	-C=O stretch
1641	-C=C- stretch
1511, 1152, 1015, 813	Aromatic C-C stretches
1444, 1324	Ø -CH$_3$ stretches
1253	α,β-unsaturated C=O stretch
1063	p-disubstituted benzene ring stretch
668, 545	C-C ring deformations

Table 5.4. The band assignments for Parsol 5000.

Oxybenzone
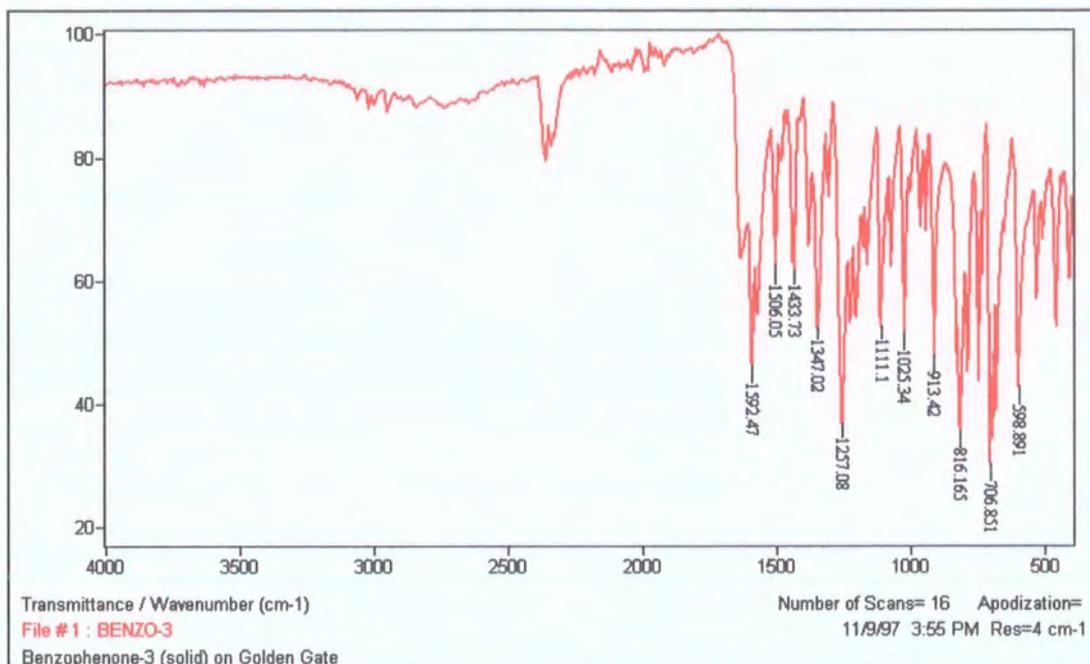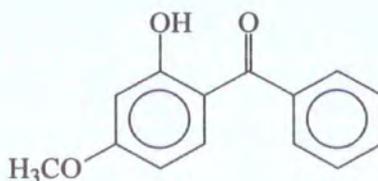
Figure 5.4. The structure and IR spectrum of Oxybenzone.

Band Wavenumber/cm^{-1}	Assignment
2157, 1347, 1380	Aryl C-OH stretch
1632	-C=O stretch
1592	m-disubstituted benzene ring stretch
1443	Ø -CH$_3$ stretches
1304	Aryl C-OMe stretch
1075, 789-681	Aromatic C-H stretches
1025	-O-CH$_3$ stretches

Table 5.5. The band assignments for Oxybenzone.

Menthyl anthranilate
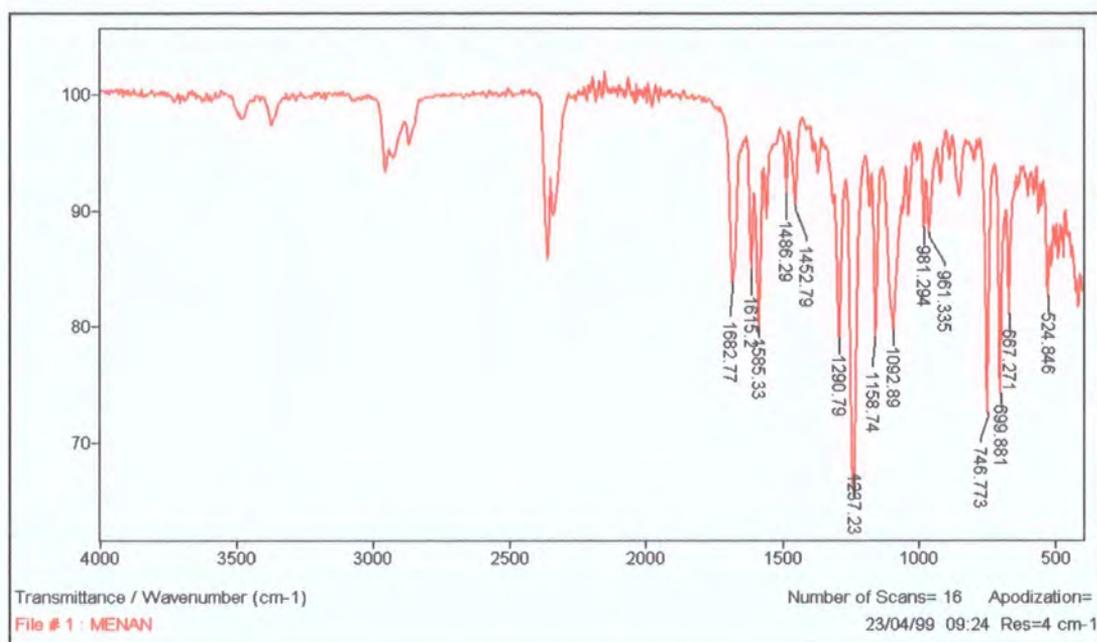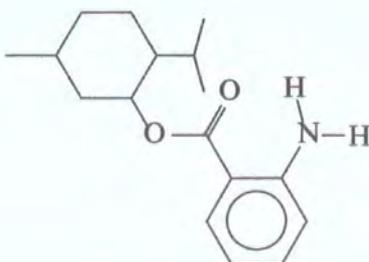
Figure 5.5. The structure and IR spectrum of Menthyl anthranilate.

Band Wavenumber/cm⁻¹	Assignment
3447, 3374	N-H stretches
1683	C=O stretch
1615	NH₂ deformation
1585, 1486, 1450	o-disubstituted benzene ring stretches
1291	Ø-N stretch
1237	C-N or C-O stretch
1158	O=C-O stretch
1092, 746	Aromatic C-C stretches

Table 5.6. The band assignments for Menthyl anthranilate.

Octocrylene

The structure of octocrylene showing CN, OC$_8$H$_{17}$ and C=O groups.

Transmittance / Wavenumber (cm-1)   Number of Scans= 16   Apodization=
File # 1 : OCTOCRYL   13/04/99 16:51 Res=4 cm-1
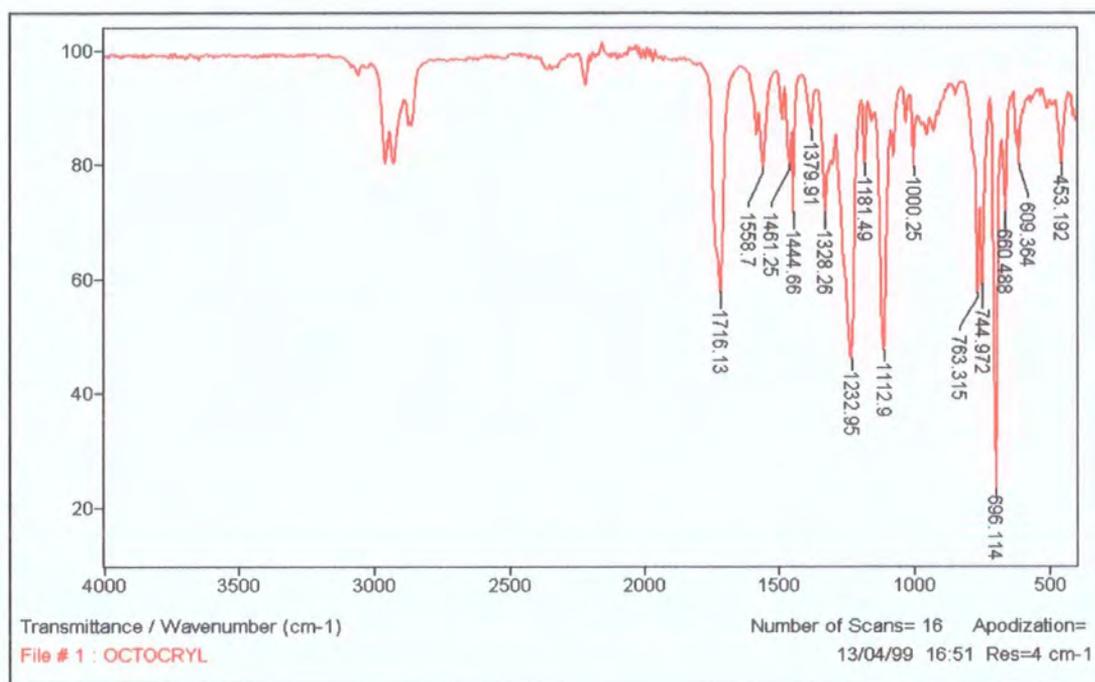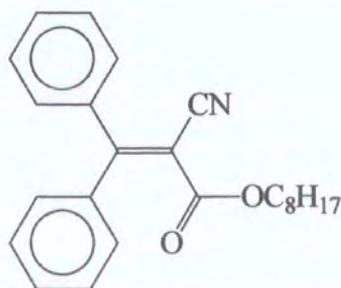
Figure 5.6. The structure and IR spectrum of Octocrylene.

Band Wavenumber/cm^{-1}	Assignment
2351-2220	-C≡N stretch
1716	-C=O stretch
1559, 1461	Aromatic ring stretches
1232, 1181	C-O stretch
1162	O=C-O stretch
763, 744, 696	Aromatic C-C stretches

Table 5.7. The band assignments for Octocrylene.

148

5.2.1.2. Sunscreen Formulations

Infrared spectroscopy using the probe accessory was used to detect sunscreens *in vivo* on skin or on a balloon surface. A series of commercially available sunscreen formulations, containing one or more of the above compounds, were spread onto an area of clean forearm skin, or the surface of a balloon, and allowed to dry for 20 minutes. IR spectra were then obtained using either the probe or a flat top ATR internal reflection element, which were placed gently against the surface of the substrate. The sunscreens analysed were Nivea Sun® Sport&Sun Lotion (SPF 25), Almay (SPF 20), Ambre Solaire Moisturising Tanning Cream (SPF 4), Banana Boat® Maximum Sunblock (SPF 50) and Neutrogena® Sunblock Spray (SPF 20). The active ingredients contained within each of these formulations are shown in table 5.8. The spectra obtained for each of the above sunscreens and the assignment of the bands to the individual active components are shown in figures 5.7-5.11 and tables 5.9-5.13.

Sunscreen Formulation	Active Ingredients
Nivea Sun® Sport&Sun Lotion	Parsol MCX, Parsol 1789, Parsol 5000
Almay	Parsol MCX, Oxybenzone, Parsol 1789
Ambre Solaire Moisturising Tanning Cream	Octocrylene, Octyl Palmitate, Mexoryl SX, Parsol 1789
Banana Boat® Maximum Sunblock	Octocrylene, Parsol MCX, Oxybenzone, Octyl salicylate
Neutrogena® Sunblock Spray	Homosalate, Parsol MCX, Octyl salicylate, Menthyl anthranilate

Table 5.8. The active ingredients contained in the sunscreens analysed.

Nivea Sun® Sport&Sun Lotion
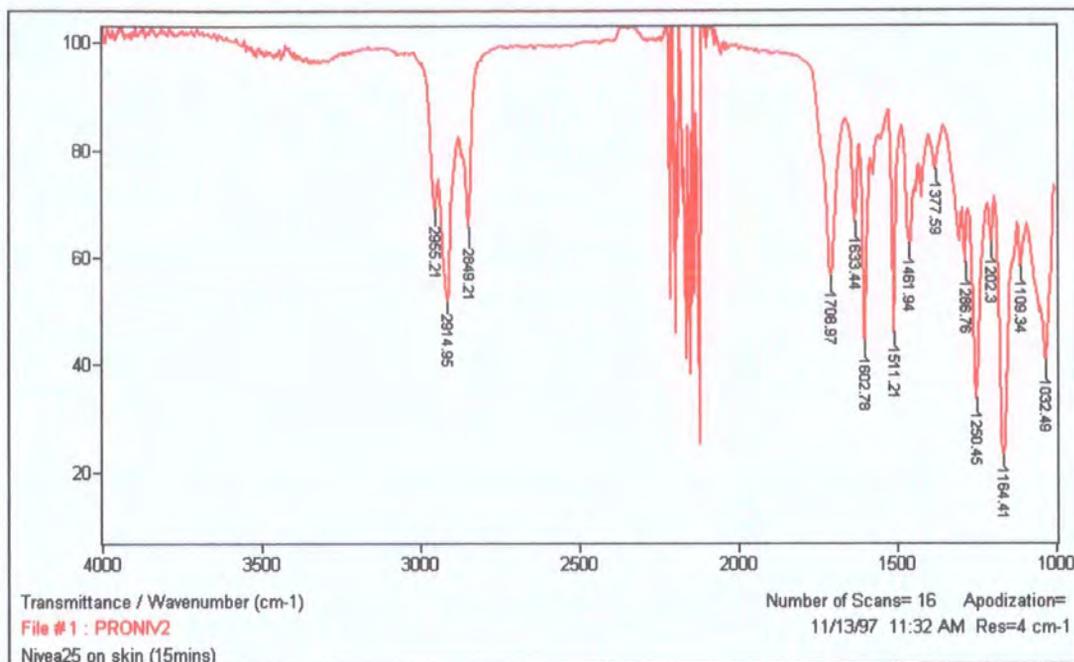
Figure 5.7. The infrared spectrum of Nivea Sun® Sport&Sun Lotion

on skin.

Band Wavenumber/cm⁻¹	Assignment
1709	Parsol MCX
1633	Parsol 5000
1603	Parsol MCX
1511	Parsol MCX or Parsol 5000
1462	Parsol MCX
1377	Parsol MCX
1287	Parsol MCX or Parsol 5000
1250	Parsol MCX, Parsol 5000 or Parsol 1789
1202	Parsol MCX
1164	Parsol 1789
1109	Parsol 1789 or Parsol MCX
1032	Parsol MCX

Table 5.9. The band assignments for the bands in the spectrum of Nivea Sun®

Sport&Sun Lotion .

Almay
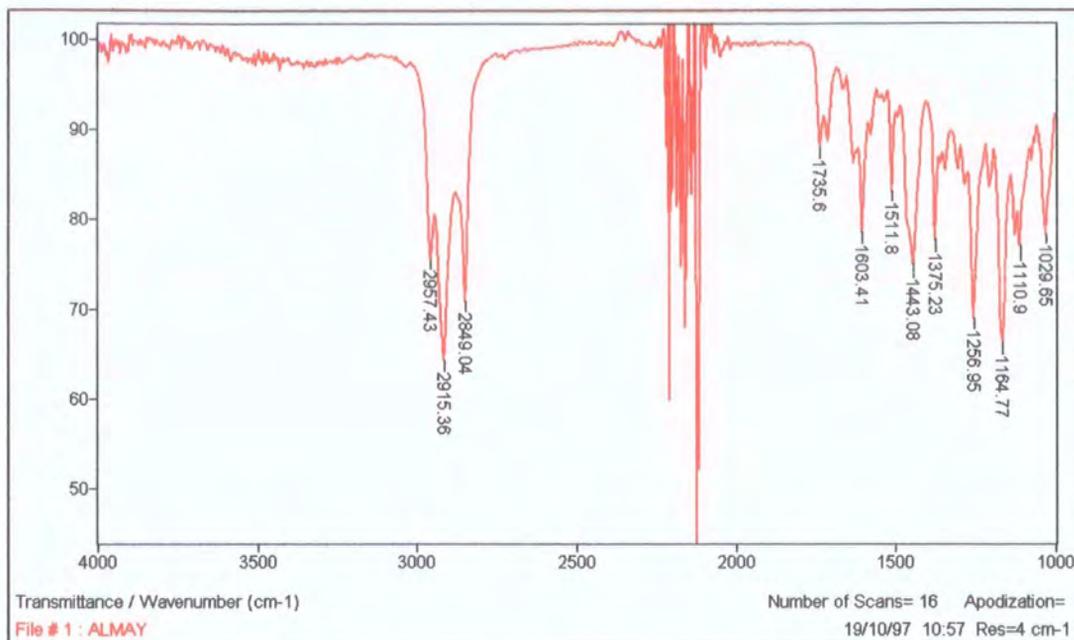
Figure 5.8. The infrared spectrum of Almay on skin.

Band Wavenumber/cm^{-1}	Assignment
1736	Parsol MCX
1603	Parsol 1789
1512	Parsol 1789 or Parsol MCX
1443	Parsol MCX or Oxybenzone
1375	Parsol 1789
1257	Parsol MCX
1164	Parsol MCX
1111	Parsol 1789
1030	Oxybenzone or Parsol MCX

Table 5.10. The band assignments for the bands in the spectrum of Almay.

Ambre Solaire Moisturising Tanning Cream
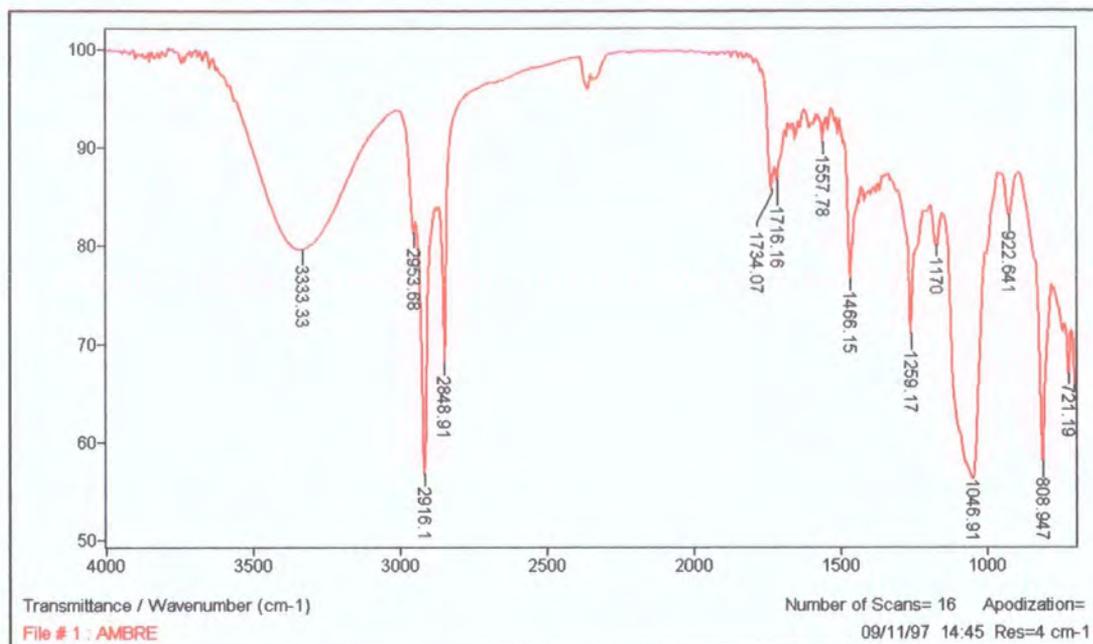
Figure 5.9. The infrared spectrum of Ambre Solaire Moisturising Tanning Cream on skin.

Band Wavenumber/cm⁻¹	Assignment
3333	Water
1734	Octocrylene
1716	Octocrylene
1558	Parsol 1789
1466	Octocrylene
1259	Parsol 1789
1170	Parsol 1789
1047	Parsol 1789
808	Parsol 1789

Table 5.11. The band assignments for the bands in the spectrum of Ambre Solaire Moisturising Tanning Cream.

Banana Boat® Maximum Sunblock
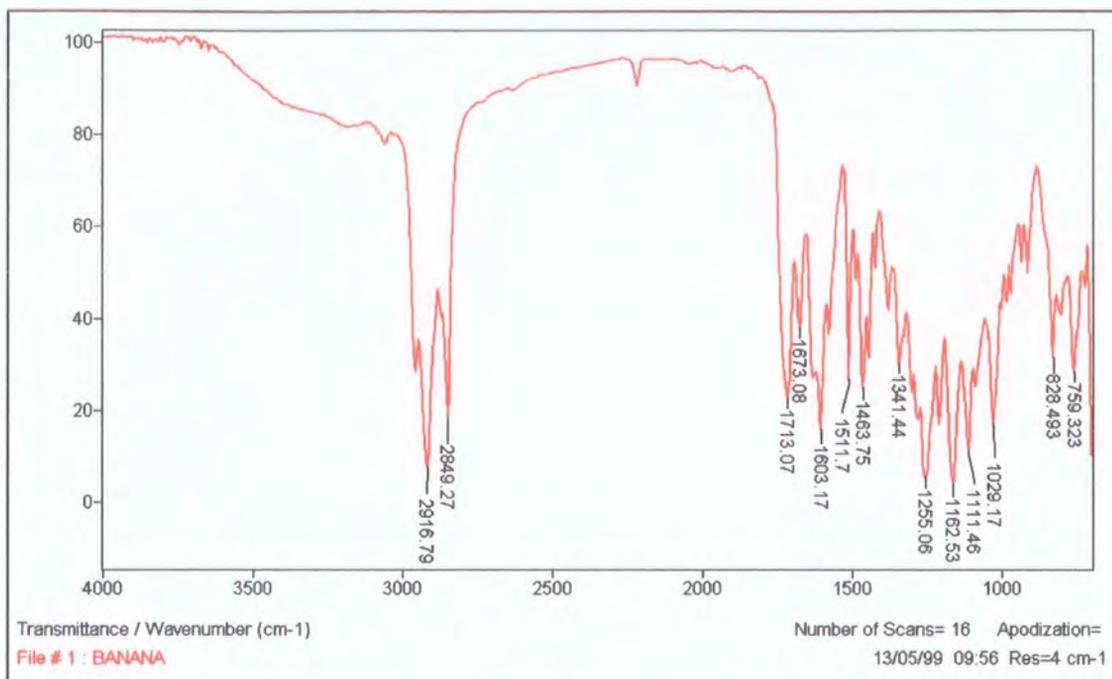
Figure 5.10. The infrared spectrum of Banana Boat® Maximum Sunblock on skin.

Band Wavenumber/cm⁻¹	Assignment
1713	Octocrylene or Parsol MCX
1603	Oxybenzone
1512	Parsol MCX
1464	Parsol MCX
1341	Oxybenzone
1255	Oxybenzone or Parsol MCX
1163	Parsol MCX
1111	Octocrylene or Oxybenzone
1029	Oxybenzone or Parsol MCX
828	Parsol MCX
759	Octocrylene

Table 5.12. The band assignments for the bands in the spectrum of Banana Boat® Maximum Sunblock.

Neutrogena® Sunblock Spray
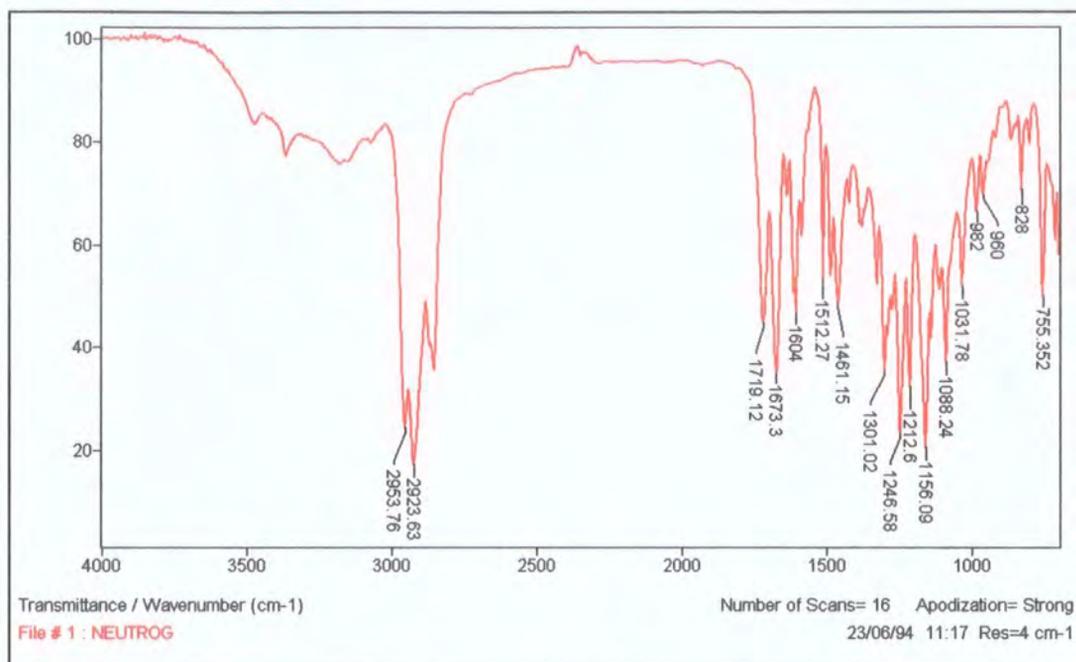
**Figure 5.11. The infrared spectrum of Neutrogena® Sunblock Spray on skin.**

Band Wavenumber/cm⁻¹	Assignment
1719	Parsol MCX
1673	Menthyl anthranilate
1604	Parsol MCX
1512	Menthyl anthranilate
1461	Menthyl anthranilate or Parsol MCX
1307	Menthyl anthranilate
1247	Menthyl anthranilate or Parsol MCX
1156	Menthyl anthranilate or Parsol MCX
1088	Menthyl anthranilate
1032	Parsol MCX

**Table 5.13. The band assignments for the bands in the spectrum of Neutrogena®**

**Sunblock Spray.**

5.2.2.   Preliminary Substantivity and Wash-Off Studies

Infrared spectroscopy using the probe accessory as outlined above, was used to investigate the water-resistance claims of some commercially available sunscreen formulations and to determine if it was possible to detect the selective removal of certain ingredients.

A layer of the sunscreen to be examined was placed on an area of clean forearm skin (approximately 5 x 5 cm^2) and allowed to air dry before the spectrum was obtained as outlined above. Washing experiments were carried out by placing the area of sunscreen coated skin under running water for 20 minutes in such a way that the water did not impact directly on the area of interest. This was done in an attempt to simulate the interactions between the sunscreen on the skin surface and water during swimming. The area containing the sunscreen was allowed to air dry for 10 minutes before a second spectrum was obtained. The washing procedure was then repeated for a further 20 minutes and the surface allowed to air-dry before a third spectrum was obtained. The spectra obtained were ratioed against a spectrum of clean skin obtained prior to the application of the sunscreen in order to obtain spectral data pertaining to the formulation alone.

Similar experiments were carried out by applying the sunscreen to an area of a balloon surface and then floating the balloon in a sink of water. The water was agitated by a continuous flow of water to simulate the interaction during swimming. As above the formulation on the surface was allowed to air dry for 10 minutes prior to the initial spectrum being recorded, immersed for 20 minutes and dried for 10 minutes before the second spectrum was recorded. This was then repeated for a second immersion cycle.

For each of the sunscreens studied the spectra of the dry formulation and those obtained after 20 and 40 minutes immersion in water were compared. Figure 5.12 shows the spectra obtained from a sample of Nivea Sun® Sport&Sun Lotion (SPF 25) spread onto the surface of a balloon. The loss of the sunscreen components as the sample is exposed to water is clearly visible over this time period. It can also be seen that in this case wash-off of the product occurs for the formulation as a whole and not for any active ingredient preferentially.

155
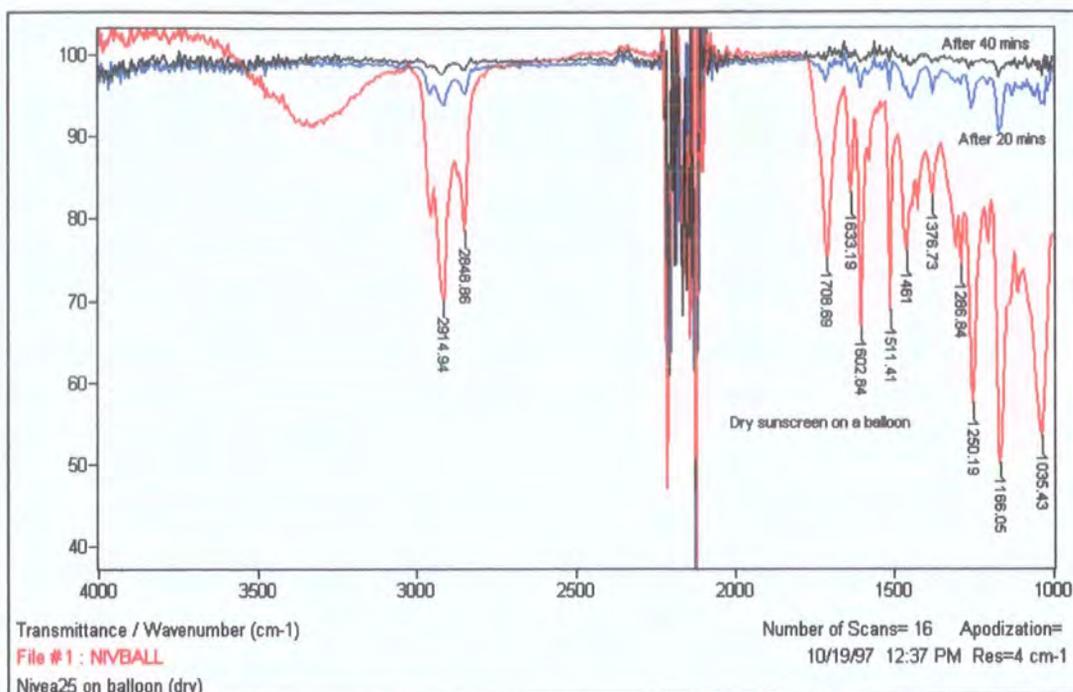
Figure 5.12. Infrared Spectra of Nivea Sun® Sport&Sun Lotion (SPF 25) on a balloon surface before and after exposure to water.

5.2.3. Quantitative Studies

The work described above was carried out on a purely qualitative basis simply with a view to determining the feasibility of using infrared spectroscopy for such *in vivo* analyses. In order to compare this technique with those already established such as UV transmission spectroscopy[2,15,16] and fluorescence spectroscopy[19,20] quantitative dose-response studies were carried out.

The standard coverage used by industry to determine the SPF value of any sunscreen formulation is 2 mgcm[-2]. The U.S. FDA, COLIPA, the Standards Association of Australia and the International Commission on Illumination all recommend this surface loading of sunscreen, while the German standards organisation (Deutches Institut für Normung) recommends the slightly lower surface density of 1.5 mgcm[-2].[19] In this work a micropipette was use to dispense the required volume of the sunscreen formulation under investigation onto the crystal of an ATR plate. The sunscreen was spotted at regular intervals over the crystal and spread using a gloved finger with a

light circular rubbing motion to give as uniform a layer as possible. This methodology was taken from the method approved by COLIPA for *in vivo* SPF testing. The sunscreen was allowed to dry for 20 minutes and the IR spectrum (in absorbance mode) was obtained. This was conducted with coverages of 0.5, 1.0, 1.5, 2.0, 2.5 and 3.0 mgcm^{-2}, and a plot of sunscreen surface density vs. absorbance was obtained.

Figure 5.13 shows the spectra obtained for the different surface densities of the Nivea Sun® Sport&Sun Lotion formulation while figure 5.14 shows the dose-response plots obtained.
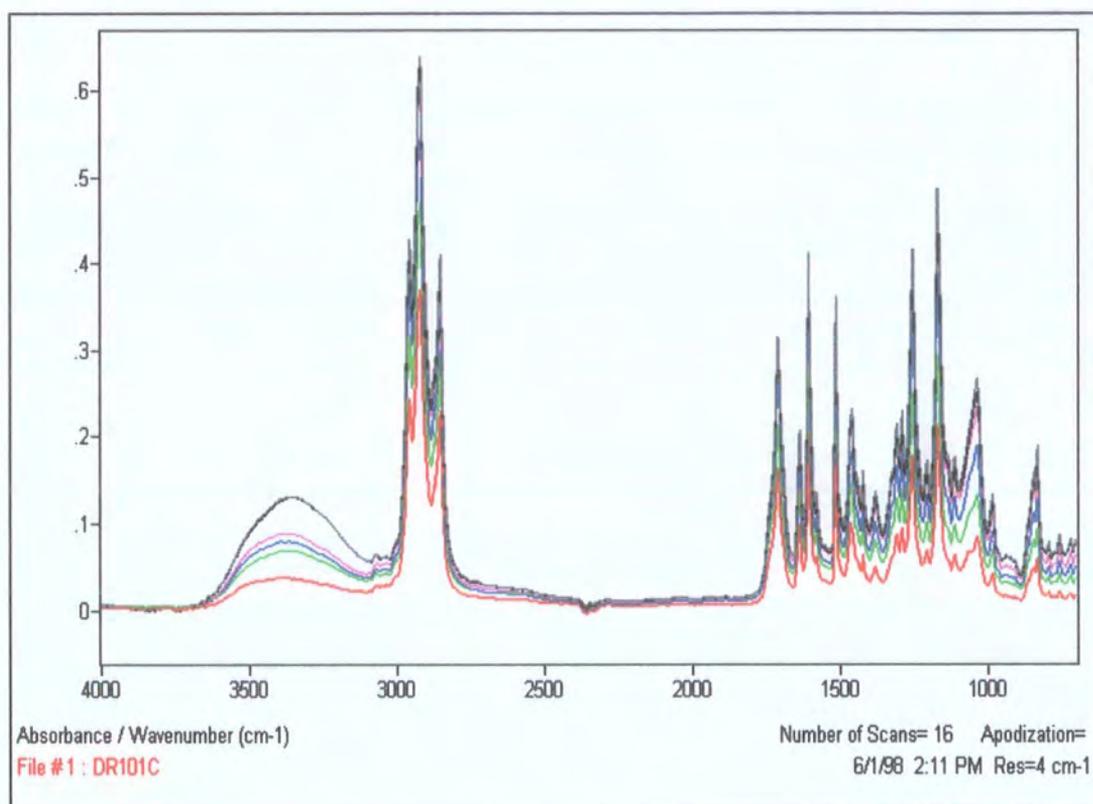
Figure 5.13. Infrared spectra of Nivea Sun® Sport&Sun Lotion (SPF 25) with increasing surface loading.
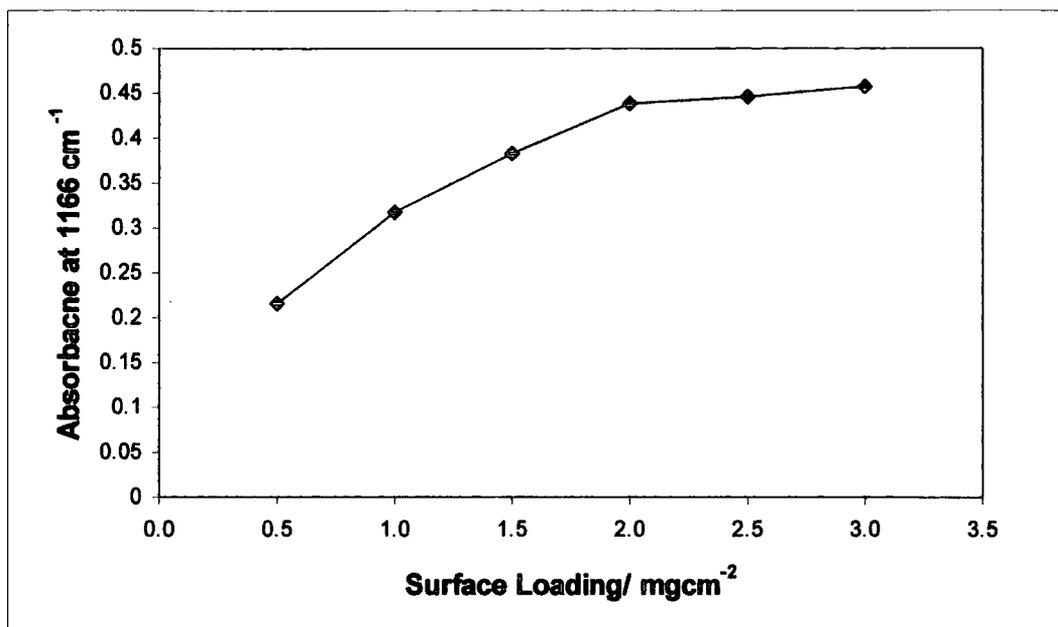
Figure 5.14.   Dose-response plot of Nivea Sun[®] **_Sport&Sun Lotion (SPF 25) on a_**
balloon surface.

These plots clearly demonstrate a relationship between the absorbance of the infrared
radiation and the surface loading of the formulation.

5.2.4.   Irradiation Studies

One of the fundamental gaps in the knowledge of sunscreens is the processes that
occur on the absorption of radiation, in particular the products that are formed and their
potential toxicity.

The work described here involved using IR spectroscopy to detect any changes that
occur in the individual active ingredients when exposed to UV light. This method was
extended to study any changes that occur in thin films of final formulations when
irradiated on an ATR crystal.

The infrared spectra of 0.5 M solutions of the sunscreen ingredients Parsol MCX,
Parsol 5000 and menthyl anthranilate in cyclohexane were recorded using a trough
ZnSe ATR plate. Each solution in turn was irradiated in a quartz fluorescence cuvette
for 10 minutes and the new spectrum recorded and compared to the initial spectrum.
This method was repeated for a total irradiation time of 30 minutes. A background

spectrum of cyclohexane was pre-recorded and removed from each spectrum. It was found that no differences could be detected between the irradiated and unirradiated solutions of each compound using this method.

The work on the final formulations was carried out using a surface loading of 2 mgcm^{-2} on a flat ATR crystal. The thin film was spread onto the crystal and a spectrum recorded. The plate was then irradiated for 120 minutes with a spectrum recorded every 10 minutes. After this time the film was left overnight to see if any changes were reversible.

The sunscreens analysed using this method were Nivea Sun® Sport&Sun Lotion (SPF 25), Johnsons Suncare (SPF 8), Nivea Sun® Sport&Sun Lotion (SPF 15), Nivea Sun® Moisturising Sun Lotion (SPF 16), Aquasun Sports Gel (SPF 18), Banana Boat® Maximum Sunblock (SPF 50) and Oil of Ulay Anti-UV Daily Moisture Fluid. The active ingredients in the Nivea Sun® SPF 25 and Banana Boat® formulations are as given in table 5.8, and the active ingredients in the remaining formulations are given below.

Sunscreen Formulation	Active Ingredients
Nivea Sun® Sport&Sun Lotion (SPF 15)	Parsol 5000, Parsol 1789, Parsol MCX,
Johnsons Suncare	Parsol MCX, Parsol 1789
Nivea Sun® Moisturising Sun Lotion	Parsol 5000, Parsol 1789
Aquasun Sports Gel	Parsol MCX, Oxybenzone, Parsol 1789
Oil of Ulay Anti-UV Daily Moisture Fluid	Parsol MCX

Table 5.14. The active ingredients contained in the sunscreens irradiated.

In all the formulations listed above it was found that changes could be detected following irradiation. In each case there was a slight loss of absorption across the entire IR range over time, but more profound changes with respect to the shifting of peaks, the total loss of peaks, and the formation of new peaks were also observed. All changes were found to be non-reversible when the films were left overnight.

Figures 5.15 and 5.16 show that changes detected in the Nivea Sun® Sport&Sun Lotion (SPF 25) formulation and the Nivea Sun® Moisturising Sun Lotion (SPF 16).
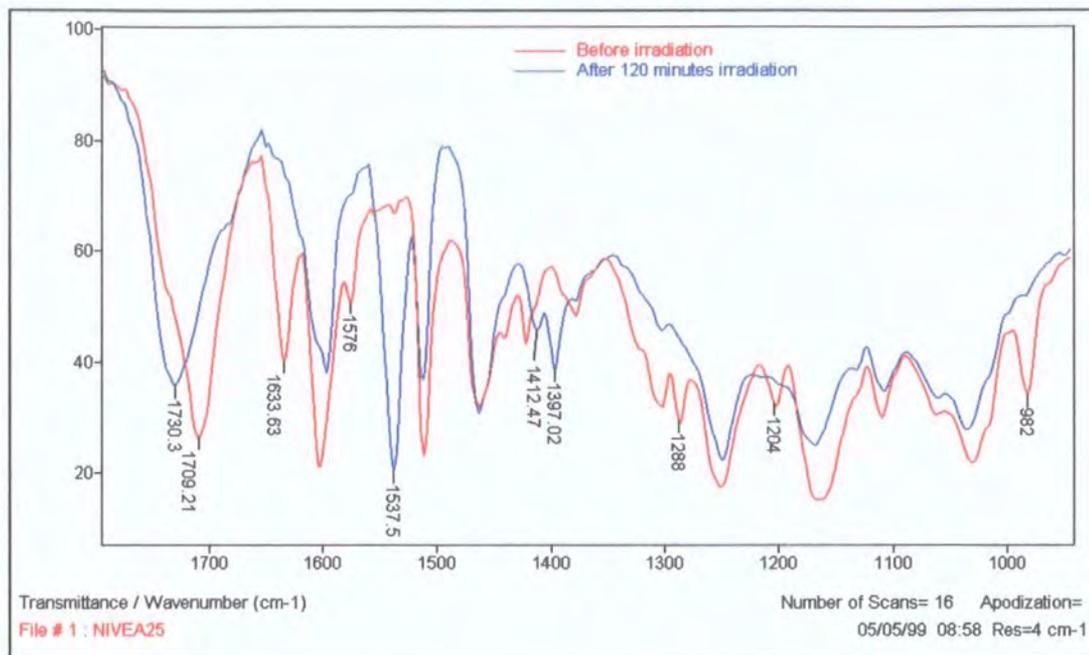
Figure 5.15. Changes in the IR spectrum of Nivea Sun® Sport&Sun Lotion (SPF 25) following irradiation.
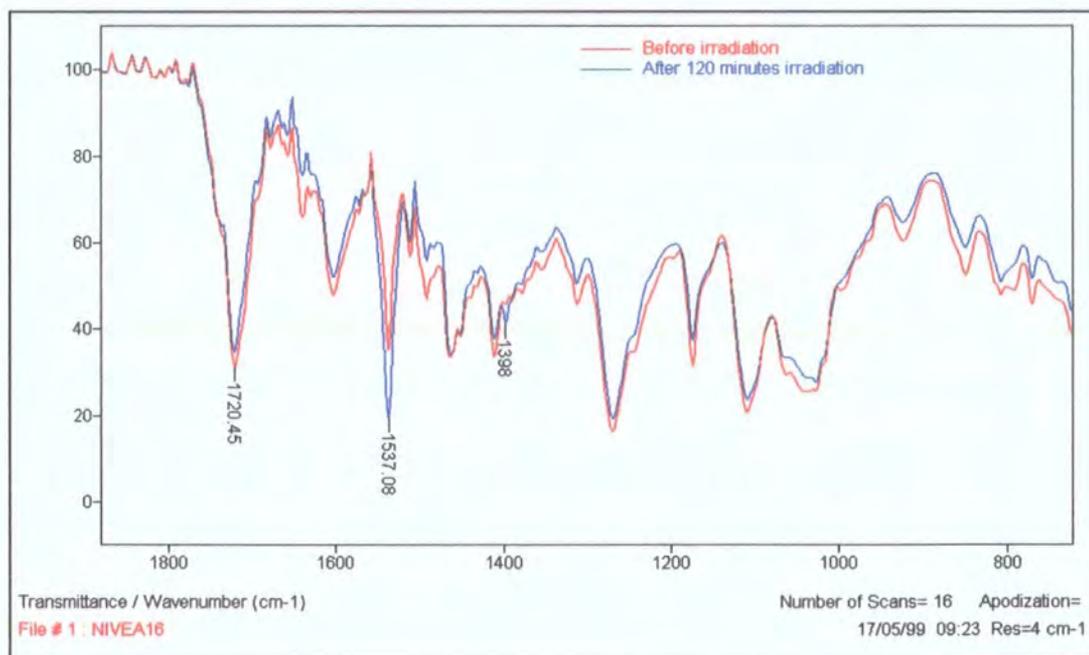
Figure 5.16. Changes in the IR spectrum of Nivea Sun® Moisturising Sun Lotion (SPF 16) following irradiation.

The most noticeable change in figure 5.15 is the shift of the peak at 1709 cm^{-1} to higher wavenumber. This shift also occurs in the spectra of the Aquasun Sports Gel and the Oil of Ulay lotion to approximately the same degree and to a lesser extent in the Banana Boat® formulation. The spectra of the Johnsons Suncare formulation show the loss of a peak at 1714 cm^{-1}, whilst no noticeable shift occurs in the Nivea Sun® Moisturising Sun Lotion (SPF 16) or the Nivea Sun® Sport&Sun Lotion (SPF 15).

Other noticeable changes include the loss of the peaks at 1634 cm^{-1}, 1576 cm^{-1}, 1422 cm^{-1}, 1288 cm$^{-1,}$ 1204 cm^{-1}, 982 cm^{-1} and 790 cm^{-1} and the appearance of peaks at 1538 cm^{-1}, 1412 cm^{-1} and 1397 cm^{-1}. As with the peak shift at ~1709 cm^{-1} these changes also occur to a greater or lesser extent in the spectra of the Aquasun Sports Gel, the Johnsons Suncare lotion and the Oil of Ulay lotion.

The spectra of the Nivea Sun® Moisturising Sun Lotion (SPF 16) following irradiation are shown in figure 5.16. The only changes in both this formulation and the Nivea Sun® Sport&Sun Lotion (SPF 15) are the increase in intensity of the peak at 1538 cm^{-1} and the appearance of a peak at 1398 cm^{-1}. The grow-in of peaks here also occurs in the Banana Boat® spectra.

5.3. Discussion

A thorough understanding of the behaviour of sunscreen formulations when in contact with the skin is vital. Many techniques have been developed to study the properties of sunscreens, both *in vitro* using a wide variety of substrates to simulate the skin surface and *in vivo*. However, *in vivo* studies are made difficult due to restrictions in the sampling methods for currently used spectroscopic techniques such as UV and fluorescence spectroscopy.

The work described above demonstrates that infrared spectroscopy, utilising a recently developed ATR probe, or an ATR flat top crystal, can be used to detect sunscreen formulations when they are present on the skin surface at normal usage coverages and probe their properties.

The results in section 5.2.1 show how the technique can be used to identify the individual active components within the formulations even in the presence of other active ingredients. We have demonstrated that it is possible to identify Parsol 1789, Parsol MCX, Parsol 5000, octocrylene, oxybenzone and menthyl anthranilate in formulations that contain at least one other of the above ingredients. This technique can easily be extended to identify other active ingredients not studied here.

Following on from this, the work in section 5.2.2 shows how this technique has been used to study the water resistance claims of the manufacturers of several commercially available sunscreen formulations. Many people take part in activities such as swimming, bathing and water-sports whilst wearing sunscreens and this has led to the development of highly substantive products which resist wash-off. Most sunscreens on the market today make claims about their substantivity and water-resistant properties. According to the U.S. FDA, a sunscreen is declared 'water-resistant' if it can maintain its original SPF value after two 20 minute immersions in water and 'very water-resistant' if it retains its protective integrity after four such immersions[36, 37]. COLIPA has proposed that a product may be claimed 'water resistant' if it retains 50% or more of its sun protection factor (SPF) after two 20 minute immersions in water, and 'very water-resistant' or 'waterproof' if it retains 80% or more of its SPF after two 20 minute immersions[15]. Our work demonstrates that infrared spectroscopy utilising such probe and ATR accessories is capable of monitoring the loss of sunscreen lotions and creams from the skin surface and from a balloon surface used as a model substrate. The sunscreens analysed have been shown to be washed-off as a complete formulation rather than with the preferential removal of individual ingredients.

Studies by Diffey and co-workers found that the application thickness had a significant effect on the sun protection factor and that most users achieve a SPF of only 20-50% of that expected from the product label[14]. A number of studies have also shown that the typical thicknesses applied in practice are much less than the 2 mgcm^{-2} used by industry for the evaluation of the products[17,18]. For these reasons dose-response relationships were obtained for thin films of sunscreen on skin in the range 0.5-3.0 mgcm^{-2}. The work in section 5.2.3 has demonstrated that there is a relationship between the surface loading and the absorption of the infrared radiation. This

relationship is neither linear, nor exponential as would be expected from Beer's law. These findings, however, are in agreement with work by Brown and Diffey[10] who used both an *in vitro* transmission spectroscopy method and a variation on the *in vivo* assay described above to study the dose-response relationships for the protection at different application thicknesses.

One final application of this technique is for the detection of changes that may occur within a sunscreen formulation following irradiation with UV light. The work detailed in section 5.2.4 describes the changes in the infrared spectra of final formulations that have been detected following irradiation of a thin film on an ATR crystal. The most notable change that occurs is the shift of a carbonyl peak from ~1710 cm^{-1} to ~1730 cm^{-1}. In section 5.2.1.2 this band has been attributed largely to Parsol MCX. Formulations that contain this ingredient on its own or as the major sunscreening component show a very pronounced shift. However the formulations that do not contain this ingredient or where it is a secondary or tertiary active component show a highly reduced shift if one occurs. Other changes include the loss of a peak at ~1634 cm^{-1} which has often been assigned to the alkene double bond of Parsol MCX. Both the shift in carbonyl frequency and the loss of this peak could be indicative of a *trans→cis* isomerisation. Colthup[38] has noted that the C=O and C=C bands are further apart in s-*cis*-α,β-unsaturated ketones than in the s-*trans*-ketones with typical values shown in table 5.15. This is in agreement with other work on Parsol MCX following irradiation[37, 39, 40] which demonstrates the occurrence of a *cis-trans* isomerisation about the double bond. Although this change can be readily detected using UV-spectroscopy we were unable to detect it in the IR spectra of pure Parsol MCX upon irradiation. This may be as a consequence of the inner filter effect, i.e. insufficient incident radiation reaching the bulk of the sample due to the high concentrations of the solutions being irradiated.

	C=O band/ cm^{-1}	C=C band/ cm^{-1}
s-*trans* α,β-unsaturated ketone	1690 – 1675	1644 – 1618
s-*cis* α,β-unsaturated ketone	1700 – 1687	1624 – 1617

Table 5.15. Typical carbonyl and ketone group frequencies for cis and trans α,β-unsaturated ketones[38].

5.4. Conclusions

Attenuated total reflection fourier transform infrared spectroscopy (ATR-FTIR) has been used to probe the properties of sunscreen formulations *in vivo* on skin and on other substrates used as a model for the skin surface.

We have shown that this technique, employing either a probe or a crystal ATR internal reflection element, can be used to successfully identify the individual active components within a sunscreen formulation when it is spread on skin, a balloon or directly onto the ATR crystal. Identification is still possible in complex formulations that contain more than one active ingredient.

The suitability of this technique for monitoring the loss of sunscreen formulations from the skin surface has also been demonstrated. The technique, which is easy to use, reproducible and non-invasive provides a less dangerous and time consuming alternative to established *in vivo* phototesting methods. It also offers the possibility of studying the effect that water immersion has on the infrared spectra of the formulations providing information on which, if any, of the active ingredients are preferentially removed by water. The method described can also be easily adapted to study the effects of external influences, such as water temperature, salinity, chlorination and turbulence, on the substantivity. This could potentially provide a more reliable method for monitoring the water resistance of sunscreen formulations, *in vivo*, which avoids the unnecessary exposure of volunteers to ultraviolet radiation.

Dose-response studies carried out have shown a relationship between the IR absorbance of a film of sunscreen and the surface loading. This demonstrates the

feasibility of this technique for the quantitative analyses of sunscreen formulations on skin. Applications of this method could allow the quantification of the loss of sunscreen with exposure to water or over time, a measurement that cosmecutical companies and regulatory bodies are keen to make. The collaboration of this work with work carried out using transmission spectroscopy (see chapter 6) to determine the relationship between absorbance and SPF could provide a quantitative technique for the evaluation of the water resistance properties of sunscreens formulations.

Finally we have demonstrated that this technique can detect changes in thin films of sunscreen formulations following irradiation with visible and ultraviolet light. The changes in some of the formulations have been attributed to a *cis-trans* isomerisation of the active ingredient (2-ethylhexyl)-4'-methoxycinnamate (Parsol MCX). However, other changes may result in the formation of species that are harmful and potentially damaging to the skin.

In summary, the *in vivo* protocols developed are quick to carry out, non-invasive, use relatively inexpensive equipment and allow the determination of many important properties of sunscreens without exposing volunteers to unnecessary doses of ultraviolet radiation, making them ideal for adoption by the industry as a whole.

5.5. References

1. Anselmi C. (1992) Staying on the surface. *Chemtech*, **22(2)**, 99-104.

2. Davenport V., J.F. Morris, and A.C. Chu (1997) Immunologic protection afforded by sunscreens *in vitro*. *J. Invest. Dermatol.*, **108**, 859-863.

3. Cumpelik B.M. (1980) Sunscreens at skin application levels: direct spectrophotometric evaluation. *J. Soc. Cosmet. Chem.*, **31**, 316-366.

4. Vogelman J.H., E. Nieves, J.L. Brind, R.A. Nash and N. Orentreich (1985) A Spectrometric Method for Determining Relative SPF Values of Sunscreen Preparations. *J. Appl. Cosmetol.*, **3**, 1-11.

5. Deutches Institut für Normung: Expermentelle dermatologische Bewertung des Erythemschutzes von externer Sonnenschutzmittlen für die menschliche Hauf (1984) DIN 65701.

6. COLIPA Sun Protection Factor Test Method published by the European Cosmetic, Toiletry and Perfumery Association (COLIPA) (October 1994), Brussels, Belgium.

7. Kaibdey K.H., and A.M. Kligman (1978) Laboratory methods for appraising the efficacy of sunscreens. *J. Soc. Cosmet. Chem.*, **29**, 525-536.

8. Agin P.P. and D.J. Levine (1992) Sunscreens retain their efficacy on human skin for up to 8 h after application. *J. Photochem. Photobiol. B:Biol.*, 1992, **15(4)**, 371-374.

9. Urbach F. (1995) The efficacy of sunscreens. *Photochem. Photobiol.*, **61**, 50S.

10. Brown S. and B.L. Diffey (1986) The effect of applied thickness on sunscreen protection: *In vivo* and *in vitro* studies. *Photochem. Photobiol.*, **44(4)**, 509-513.

11. Stokes R.P. and B.L. Diffey (1997) *In vitro* assay of high SPF sunscreens. *J. Soc. Cosmet. Chem.*, **48**, 289-295.

12. Diffey B.L., (1997) *Indices of protection from in vitro assays of sunscreens* in 'Sunscreens: Development, Evaluation and Regulatory Aspects', eds. Lowe N.J., Shaath N.A. and Pathak M.A., Marcel Dekker, New York, pp. 589-600.

13. Augustin C., C. Collombel and O. Darmour (1997) Measurements of the Protective Effect of Topically Applied Sunscreens using *in vitro* Three-dimensional Dermal and Skin Equivalents. *Photochem. Photobiol.*, **66**, 853-859.

14. Stokes R. and B. Diffey B (1997) How well are sunscreen users protected? *Photodermat. Photoimmunol. Photomed.*, **13**, 186-188.

15. Stokes R.P., L.C. Dawson, S.P. Barton and B.L. Diffey (1998) A novel *in vitro* technique for measuring the water resistance of sunscreens. *Int. J. Cosmet. Sci.*, **20**, 235-240.

16. Stokes R. and B. Diffey (1999) Water substantivity of sunscreen and day-care products. *Br. J. Dermatol.*, **140(2)**, 259-263.

17. Stenberg C. and O. Larkö (1985) Sunscreen application and its importance for the sun protection factor. *Arch. Dermatol.*, **121**, 1400-1402.

18. Loesch H. and D.L. Kaplan (1994) Pitfalls in sunscreen application. *Arch. Dermatol.*, **130**, 665-666.

19. Rhodes L.E. and B.L. Diffey (1997) Fluorescence spectroscopy: a rapid, non-invasive method for measurement of skin surface thickness of topical agents. *Br. J. Dermatol.*, **136**, 12-17.

20. Rhodes L.E., and B.L. Diffey (1996) Quantitative assessment of sunscreen application technique by *in vivo* fluorescence spectroscopy. *J. Soc. Cosmet. Chem.*, **47**, 109-115.

21. Stokes, R.P. and B.L. Diffey, (1999) The feasibility of using fluorescence spectroscopy as a rapid, non-invasive method for evaluating sunscreen performance. *J. Photochem. Photobiol. B:Biol.*, **50**, 137-143.

22. Azurdia R.M., J.A. Pagliaro, B.L. Diffey and L.E. Rhodes (1999) Sunscreen application by photosensitive patients is inadequate for protection. *Br. J. Dermatol.*, **140**, 255-258.

23. Roguet R., C. Cohen, K.G. Dossou and A. Rougier (1994) Episkin, A reconstituted human epidermis for assessing *in vitro* the irritancy of topically applied compounds. *Toxic. In Vitro*, **8(2)**, 283-291.

24. Cohen C., K.G. Dossou, A. Rougier and R. Rouguet (1994) Episkin: An *in vitro* model for the evaluation of phototoxicity and sunscreen photoprotective properties. *Toxic. In Vitro*, **8(4)**, 669-671.

25. Bell E., N. Parenteau, R. Gay, C. Nolte, P. Kemp, P. Bilbo, B. Ekstein and E. Johnson (1991) The Living Skin Equivalent: Its manufacture, its organotypic properties and its responses to irritants. *Toxic. In Vitro*, **5(5/6)**, 591-596.

26. Hagedorn-Leweke U. and B.C. Lippold (1995) Absorption of sunscreens and other compounds through human skin *in vivo*: Derivation of a method to determine maximum fluxes. *Pharm. Res.*, **12**, 1354-1360.

27. Hayden C.G.J., M.S. Roberts and H.A.E Benson (1997) Systemic absorption of sunscreen after topical application. *Lancet*, **350**, 863-864.

28. Treffel P. and Gabard B. (1996) Skin penetration and sun protection factor of ultra-violet filters from two vehicles. *Pharm Res.*, **13(5)**, 770-774.

29. Yozomizo Y. (1996) Effect of phosphatidylcholine on the percutaneous penetration of drugs through the dorsal skin of guinea pigs *in vitro*; and analysis of the molecular mechanism, using attenuated total reflectance-Fourier transform infrared (ATR-FTIR) spectroscopy. *J. Control. Release*, **42(3)**, 249-262.

30. Puttman N.A., S. Lee and B.H. Baxter (1965) Application of attenuated total reflectance IR spectroscopy to toilet articles and household products, 1. Qualitative Analysis. *J. Soc. Cosmet. Chem.*, **16**, 607-615.

31. Puttman N.A., B.H. Baxter, S. Lee and P.L. Stott (1967) Application of attenuated total reflectance IR spectroscopy to toilet articles and household products, 2. Quantitative Analysis. *J. Soc. Cosmet. Chem.*, **17**, 9-16.

32. Puttman N.A., (1972) Attenuated total reflectance studies of the skin. *J. Soc. Cosmet. Chem.*, **23**, 209-226.

33. Tajima T. (1998) Infrared spectroscopy of human skin. *Shimadzu NEWS*, **1**, 2-4.

34. Gabriel K.L., R. Mark, S, Manning, T. Stoudmayer and P.T. Pugliese (1989) Use of attenuated total reflectance Fourier transform infrared spectroscopy to study sunscreen products. *J. Toxicol. – Cut. & Ocular Toxicol.*, **8(4)**, 469-480.

35. Tromme I., D. Van Neste, F. Dobbelaere, B. Bouffioux, C. Courtin, T. Dugernier, P. Pierre and M. Dupuis (1998) Skin signs in the diagnosis of thallium poisoning. *Br. J. Dermatol.*, **138**, 321-325.

36. Griffin M.E., Bourget T.D. and Lowe N.J., *Sun Protection Factor Determination in the United States* in 'Sunscreens: Development, Evaluation and Regulatory Aspects', eds. Lowe N.J., Shaath N.A. and Pathak M.A., Marcel Dekker, New York, 1997, pp. 499-512.

37. Colthup N.B., L.H. Daly and S.E. Wiberley (1990) *Introduction to Infrared and Raman Spectroscopy*, Academic Press, New York.

38. Shaath N.A., *Evolution of Modern Sunscreen Chemicals* in 'Sunscreens: Development, Evaluation and Regulatory Aspects', eds. Lowe N.J., Shaath N.A. and Pathak M.A., Marcel Dekker, New York, 1997, p. 3-33.

39. Morlière P., O. Avicet, T. Sa E Melo, L. Dubertret, M. Giraud and R. Santus (1982) A study of the photochemical properties of some cinnamate sunscreens by steady state and laser flash photolysis. *Photochem. Photobiol.*, **36**, 395-399.

40. Broadbent J.K., B.S Martincigh, M.W. Raynor, L.F. Salter, R. Moulder., P. Sjöberg and K.E. Markides (1996) Capillary supercritical fluid chromatography combined with atmospheric pressure chemical ionisation mass spectrometry for the investigation of photoproduct formation in the sunscreen absorber 2-ethylhexyl-p-methoxycinnamate. *J. Chromatogr. A.*, **732**, 101-110.

Chapter 6

Water Resistance Testing of Sunscreens using Infrared Spectroscopy

6.1.   Introduction

As described in chapter 5, the growing public awareness of the harmful effects of sunlight has resulted in a continually expanding sunscreen market. With increasing leisure time and longer life expectancy, there is a great need for sunscreens that can protect the skin of all sorts of people under all sorts of conditions, be they outdoors workers or sun-worshippers.

Most sunscreens are used on the beach or in areas where contact with water, or loss due to sweating, is highly probable. For this reason the sunscreen formulations must be water resistant if they are to offer the long term protection that is highly desirable.

As explained in chapter 5, in North America a sunscreen product can claim to be 'water resistant' if it remains in the same product category designation (PCD) after two 20 minute immersions in water, and 'very water resistant' if it remains in the same PCD after four 20 minute immersions[1,2,3]. In Europe COLIPA has proposed that a product may be claimed 'water resistant' if it retains 50% or more of its sun protection factor (SPF) after two 20 minute immersions in water, and 'very water-resistant' or 'waterproof' if it retains 80% or more of its SPF after two such immersions.

In vivo water resistance testing of topical sunscreens is time consuming, expensive and the test procedure is subject to sources of considerable variation that cast serious doubts on the reliability of the results[4,5]. The analysis of sunscreens using *in vitro* techniques that correlate with *in vivo* data has been proposed for many years[6], and many different methods have been tried. Pines[7] developed a photoacoustical analysis method to probe the properties of sunscreen formulations when spread as thin films on the skin of hairless mice. Morasso *et al.* measured the amount of sunscreen solution retained by human keratin powder after exposure to water[8], whilst Greiter *et al.* used both wool and pig skin to monitor the amount of sunscreen retained by the substrate after exposure to water[9]. However, these methods suffer from a major limitation, namely that they only assess the water resistance of the sunscreens in terms of the concentration retained by the substrate in question rather than in terms of the SPF values. Sayre *et al.*[10,11] used mouse epidermis substrate to assess the water resistance of sunscreens using the forward transmission of ultraviolet radiation before and after

exposure to water, and interpreted the results in terms of changes in the SPF values. Stokes and Diffey[12,13,14] have extended this work by using human epidermis as the substrate, in an attempt to simulate the *in vivo* conditions more closely. They found close agreement between the results obtained using their *in vitro* method and those obtained using the traditional *in vivo* assay. They described their technique as '*ex vivo*' and concluded that it provides a less expensive and less time consuming alternative to *in vivo* assays and also offers the possibility to study the effect that water immersion may have on the absorption spectra of the products which cannot be determined *in vivo*. This can give information on which, if any, of the active ingredients present in sunscreen formulations are preferentially removed by water. They also commented that the method could easily be adapted to study the effects of the turbulence, salinity and water temperature on the substantivity of formulations

Gupta and Zatz have also developed an *in vitro* method for modelling the water resistance of sunscreen formulations[15]. They used micro-Yucatan pig skin as the substrate to probe the water resistant properties of oxybenzone and octyl methoxycinnamate in hydroalcoholic, diisopropyl adipate oil prototype formulations and oil-in-water and water-in-oil emulsions. The formulations also contained various polymers at a concentration of 5% w/w in an attempt to assess their effect on the retention of the sunscreens by the stratum corneum. They found that in the presence of tricontanyl PVP copolymer there was a statistically significant increase in the retention of oxybenzone. They concluded that their *in vitro* procedure provided a useful method for assessing formulations for water resistance.

6.2. Experimental Protocol

The work described below was carried out as part of a collaborative study with Prof. B. Diffey and Dr. R Stokes of the Regional Medical Physics Department, Dryburn Hospital, Durham. The aim of the work was to correlate the infrared absorbance values obtained from thin films of sunscreen on skin, or another substrate, to the values of the SPF determined by an *in vitro* transmission spectroscopy technique. Once this correlation was established the work was extended to study the water-resistance claims

made by the manufacturers of the formulations studied.   For these reasons a very rigorous experimental protocol was drawn up to ensure that the two studies were carried out under the same conditions and exchange visits were made to ensure the protocols were implemented.

The transmission spectroscopy method used was as described in previous work by Stokes *et al.*[12,13,14] The infrared spectroscopy method used is outlined below.

Dose-response studies

Infrared spectra of each sunscreen were recorded for application thicknesses of 0.5, 1.0, 1.5, 2.0 and 3.0 mgcm^{-2}. Five measurements were taken for each combination of sunscreen and application thickness. The experimental protocol is as follows:

1.   The required amount of sunscreen was applied to a region on the inner forearm of a volunteer, or directly onto the surface of an ATR crystal. The sunscreen was spotted over the whole region using a pipette and rubbed gently with a gloved finger to obtain as uniform a layer as possible.
2.   The sunscreen was allowed to dry for 20 minutes.
3.   The infrared spectrum was recorded.

Wash-Off Studies

The wash-off of each of the sunscreens was assessed six times. The experimental protocol followed was:

1.   A 2 mgcm^{-2} layer of sunscreen was applied to skin of the inner forearm of a volunteer, or to the ATR crystal. The required amount of sunscreen was spotted over the whole region of skin using a pipette and then gently rubbed with a gloved finger to obtain as uniform a layer as possible.
2.   The sunscreen was allowed to dry naturally for 20 minutes.
3.   The infrared spectrum was recorded.
4.   The volunteer's forearm, or the ATR crystal, was immersed in a water bath, in which the water was maintained at 25 °C and agitated at a constant rate for 20 minutes.

5.   The forearm or the crystal was removed from the water bath and allowed to dry naturally for 10 minutes.

6.   The infrared spectrum was recorded.

7.   Steps 4-6 were repeated once.

6.3. Results

Infrared spectroscopy using a probe accessory was used to detect sunscreens *in vivo* on skin as described in chapter 5. A series of commercially available sunscreen formulations were chosen to be studied here to determine infrared absorbance data and to be analysed using the transmission spectroscopy technique at the hospital to determine the SPF values. The sunscreens studied and the active ingredients contained within them are shown in table 6.1.

Sunscreen Formulation	Active Ingredients
Nivea Sun® Sport&Sun Lotion (SPF 15)	Parsol 5000, Parsol MCX and Parsol 1789
Nivea Sun® Lotion (SPF 16)	Parsol 5000, Parsol MCX and Parsol 1789
Oil of Ulay Daily Moisture Fluid (SPF 15)	Parsol MCX

Table 6.1. The sunscreens analysed and the active ingredients contained within them.

The Nivea formulations both make claims about their water-resistant properties. The Sport&Sun Lotion (SPF 15) claims to be 'extra-water-resistant', whilst the Lotion (SPF 16) claims to be 'water-resistant'. The Oil of Ulay Daily Moisture Fluid makes no water-resistance claims.

The IR spectra obtained for each of the above sunscreens are shown in figures 6.1-6.3.
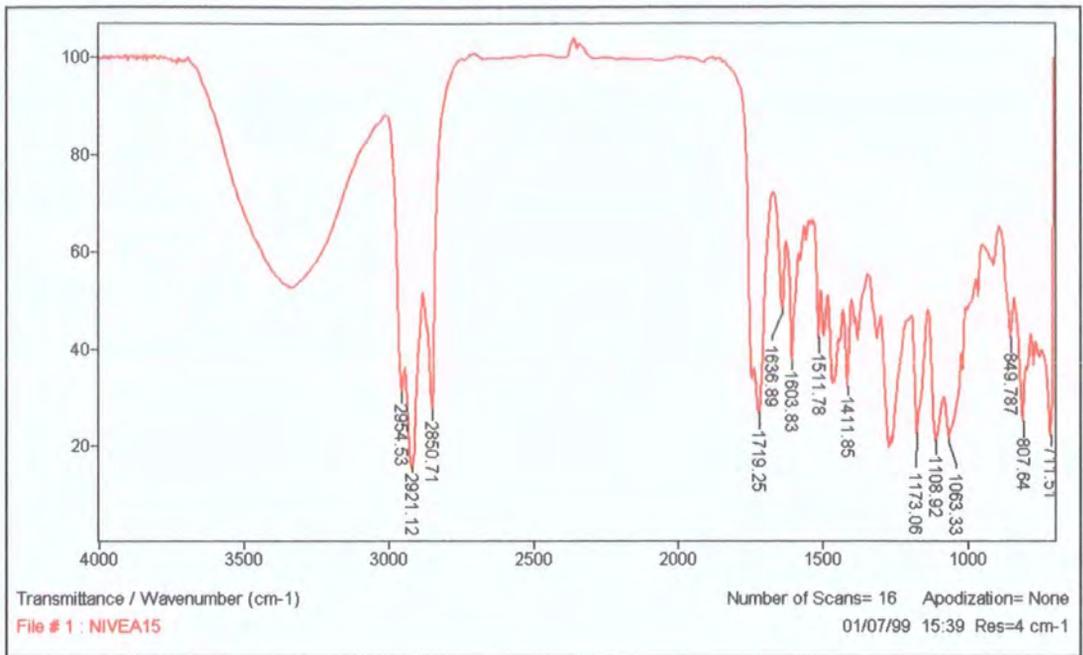
Figure 6.1. Infrared spectrum of Nivea Sun® Sport&Sun Lotion (SPF 15).
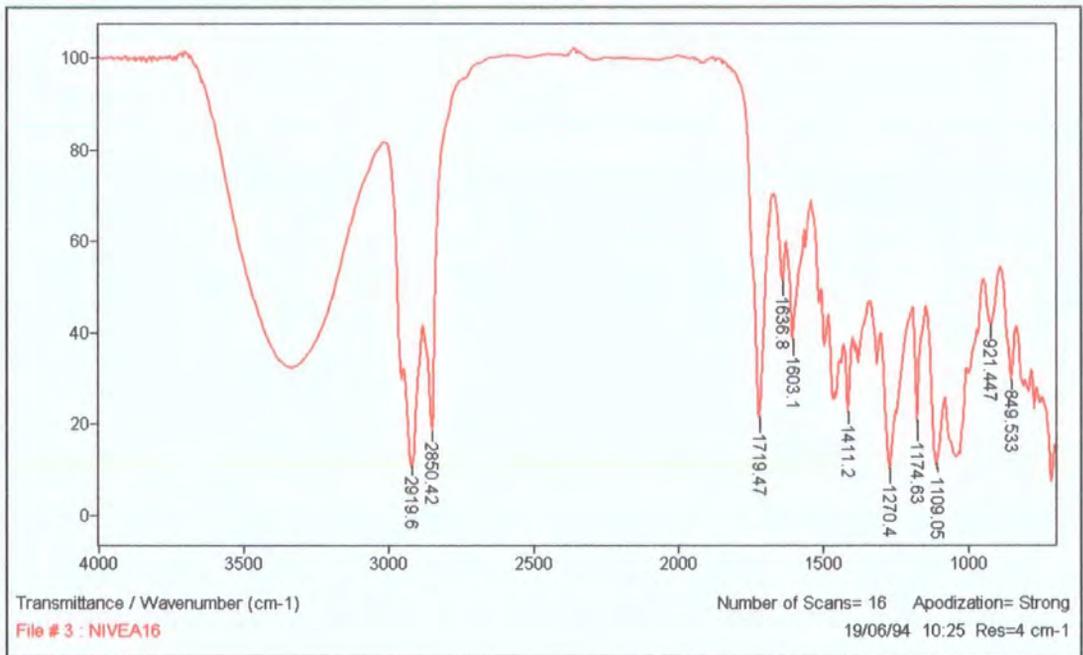
Figure 6.2. Infrared spectrum of Nivea Sun® Lotion (SPF 16).
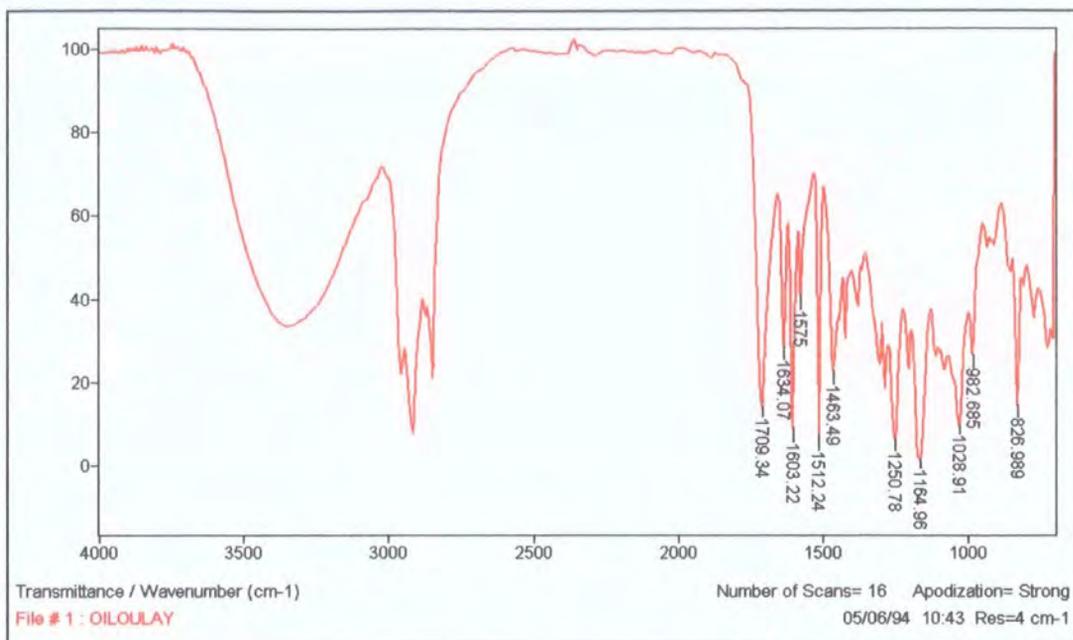
Figure 6.3. Infrared spectrum of Oil of Ulay Daily Moisture Fluid.

6.3.1.   On skin studies

Work was carried out using the infrared probe described in chapters 2 and 5 to analyse sunscreens on skin.   Dose-response curves were obtained for surface application thicknesses in the range 0.5-3.0 $mgcm^{-2}$. Five measurements were taken for each surface loading and the average determined.

6.3.1.1. Nivea Sun® Sport&Sun Lotion (SPF 15)

The dose-response curve obtained from the Nivea Sun® Sport&Sun Lotion is shown in figure 6.4. The band at 1270 cm^{-1} was chosen to monitor the absorbance change due to both its strength and the fact that it has previously been attributed to either Parsol 5000 or Parsol MCX (see chapter 5).
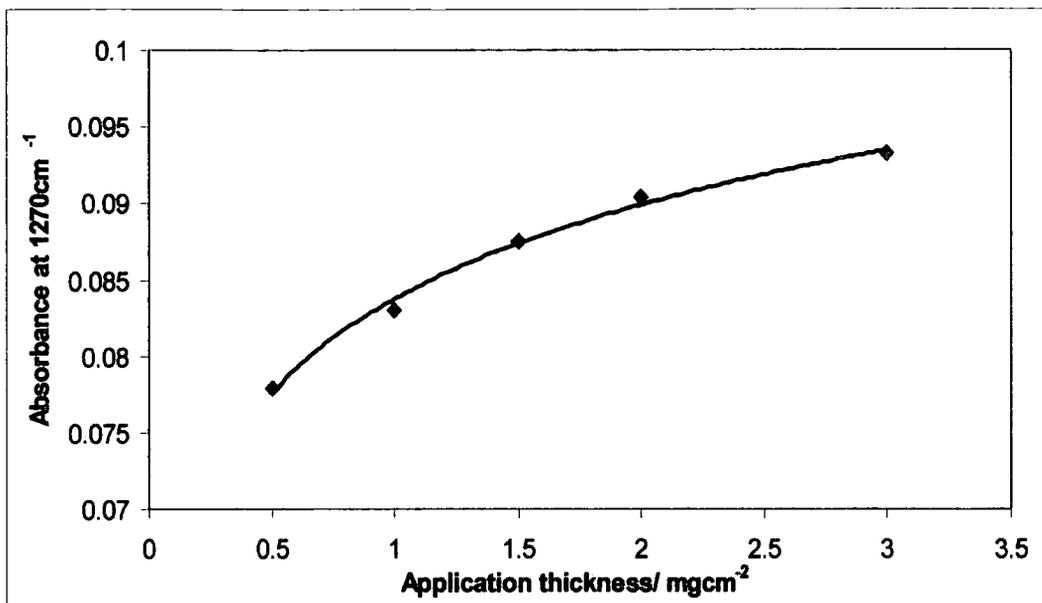
Figure 6.4. Dose-response curve for Nivea Sun[®] Sport&Sun on skin.

By comparison of these data with those provided by Dr Stokes it was possible to correlate the infrared absorbance values to SPF values. The data are shown in table 6.2 and the correlation curve is shown in figure 6.5.

Application thickness/ mgcm^{-2}	Infrared absorbance	SPF
0.5	0.078 ± 0.008	3.2 ± 0.4
1.0	0.083 ± 0.009	8.4 ± 1.5
1.5	0.087 ± 0.009	12.6 ± 1.6
2.0	0.090 ± 0.010	19.8 ± 2.4
3.0	0.094 ± 0.010	39.2 ± 6.0

Table 6.2. Correlation of infrared absorbance data to SPF values for Nivea Sun[®] Sport&Sun Lotion.

45
40
35
30
SPF 25
20
15
10
5
0

0.07   0.075   0.08   0.085   0.09   0.095   0.1

Absorbance at 1270 cm^{-1}
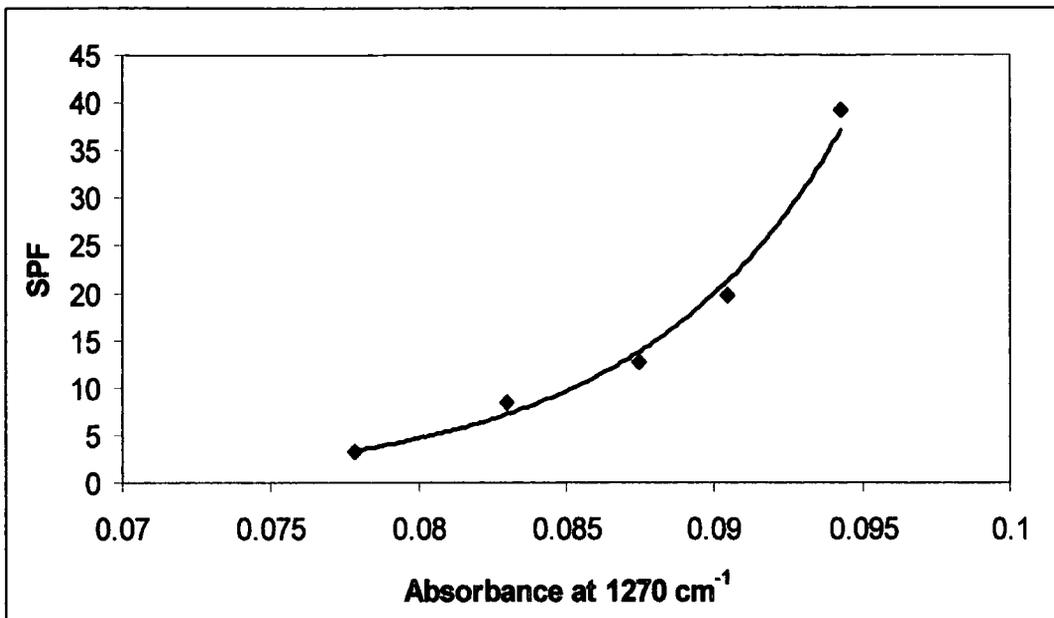
__Figure 6.5. Infrared absorbance and SPF value correlation curve for Nivea Sun__[®]
__Sport&Sun on skin.__

From the correlation curve, the relationship between SPF and infrared absorbance was found to be:

$$SPF = 4 \times 10^{-5} e^{150A}$$

where SPF is the measured SPF of the formulation, and

A is the infrared absorption value at the wavenumber stated.

6.3.1.2. Oil of Ulay Daily Moisture Fluid

The increase in infrared absorbance with application thickness of the Oil of Ulay Daily Moisture Fluid is shown in figure 6.6. Here the band at 1166 cm^{-1} was chosen to monitor the absorbance change since it was the strongest band in the spectrum and has previously been assigned to the O=C-O stretch of Parsol MCX, see chapter 5. This is the only active ingredient in the formulation and so changes in this band will give a direct indication of the changes in the protection offered by the formulation.
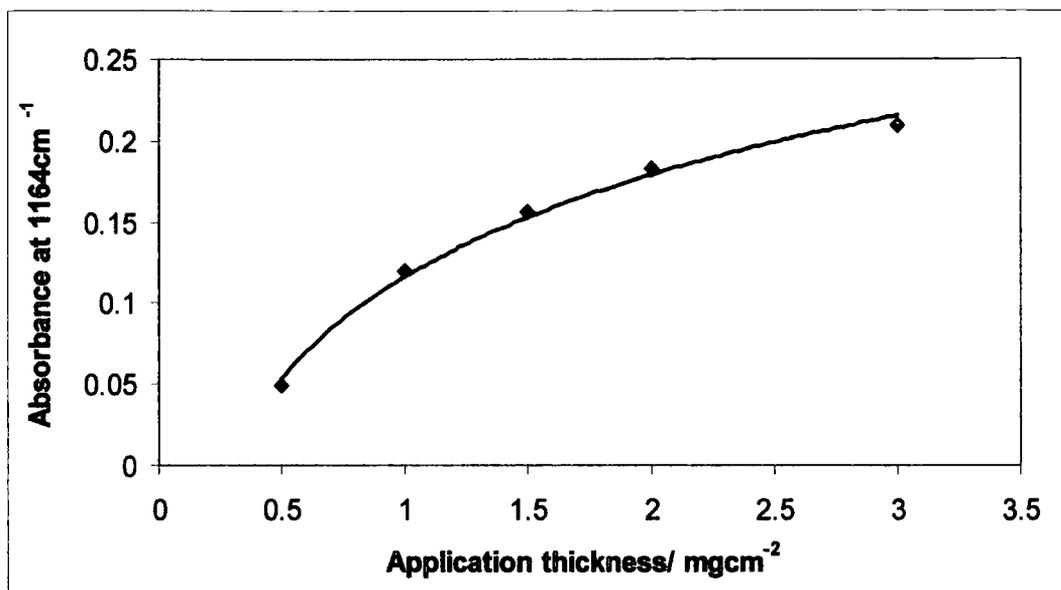
Figure 6.6. Dose-response curve for Oil of Ulay Daily Moisture Fluid on skin.

Comparison of this data set with that provided by Dr Stokes, shown in table 6.3, allowed the correlation of our infrared absorbance values to SPF values.

Application thickness/ mgcm^{-2}	Infrared absorbance	SPF
0.5	0.049 ± 0.010	3.8 ± 0.6
1.0	0.110 ± 0.019	7.0 ± 0.9
1.5	0.156 ± 0.013	12.3 ± 1.8
2.0	0.180 ± 0.023	15.9 ± 1.7
3.0	0.209 ± 0.034	23.0 ± 3.3

Table 6.3. Correlation of infrared absorbance data to SPF values for Oil of Ulay Daily Moisture Fluid.

Figure 6.7 shows the correlation curve obtained, which yields the following relationship:

$$SPF = 2.12\ e^{11A}$$
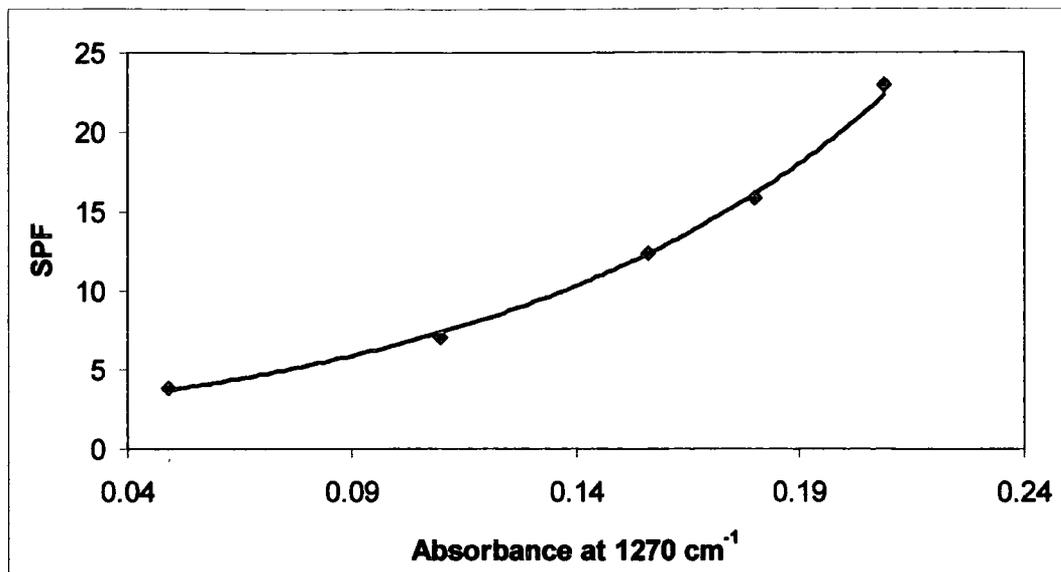
**Figure 6.7. Infrared absorbance and SPF value correlation curve for Oil of Ulay**
**Daily Moisture Fluid on skin.**

Unfortunately, due to the lack of availability of the probe, it was not possible to carry out further work using the SPF and infrared absorbance relationships to determine the water resistance properties of these formulations on skin.

6.3.2.   ATR Studies

Similar studies to those carried out using the probe were carried out using thin films of sunscreen formulation spread directly onto a flat ATR crystal.

6.3.2.1. Nivea Sun[®] Sport&Sun Lotion (SPF 15)

The dose-response plot of the infrared absorbance at different application thicknesses for the Nivea Sun[®] Sport&Sun Lotion is shown in figure 6.8.
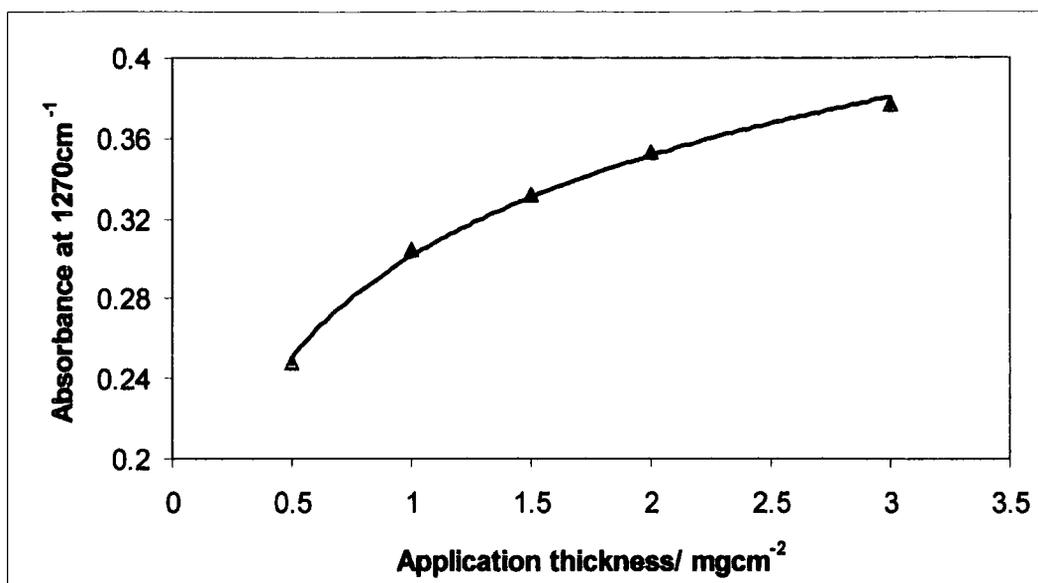
Figure 6.8.   Dose-response curve for Nivea Sun® Sport&Sun Lotion on a flat ATR crystal.

The infrared absorbance data and the SPF values obtained from the two studies are shown in table 6.4, and the corresponding correlation curve is shown in figure 6.9.

Application thickness/ mgcm^{-2}	Infrared absorbance	SPF
0.5	0.244 ± 0.019	3.2 ± 0.6
1.0	0.303 ± 0.019	8.4 ± 1.5
1.5	0.322 ± 0.029	12.6 ± 1.6
2.0	0.344 ± 0.026	19.8 ± 2.4
3.0	0.370 ± 0.032	39.2 ± 6.0

***Table 6.4.   Correlation of infrared absorbance data to SPF values for Nivea Sun®
Sport&Sun Lotion.***

From the correlation curve the relationship between the infrared absorbance at 1270 cm^{-1} and the SPF has been found to be:

$$SPF = 0.03 \ e^{20A}$$
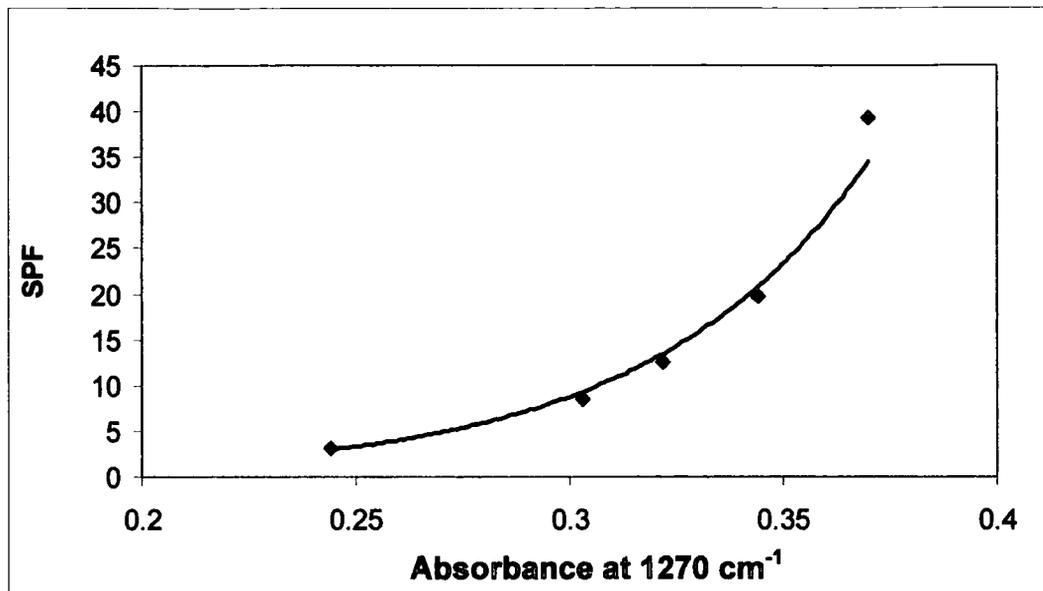
Figure 6.9. Infrared absorbance and SPF value correlation curve for Nivea Sun[®]
Sport&Sun.

Following on from the SPF correlation studies, water-resistance studies were carried out. The reductions in infrared absorption and associated SPF following two 20 minute immersions are given in table 6.5. The values for the reduction in SPF determined using the transmission technique at the hospital are also shown for comparison.

Immersion Time/ mins	IR absorbance value	SPF value determined by IR protocol	SPF value determined by transmission protocol
0	0.361 ± 0.014	24.8 ± 3.2	18.6 ± 3.2
20	0.358 ± 0.009	23.5 ± 2.8	12.6 ± 1.8
40	0.340 ± 0.017	16.9 ± 1.9	12.9 ± 1.9

Table 6.5. Reduction in infrared absorbance and SPF values following immersion
of the Nivea Sun[®] Sport&Sun Lotion.

6.3.2.2. Nivea Sun® Lotion (SPF 16)

A similar dose-response plot to that obtained for the Nivea Sun® Sport&Sun Lotion was obtained for this Nivea product, see figure 6.10.
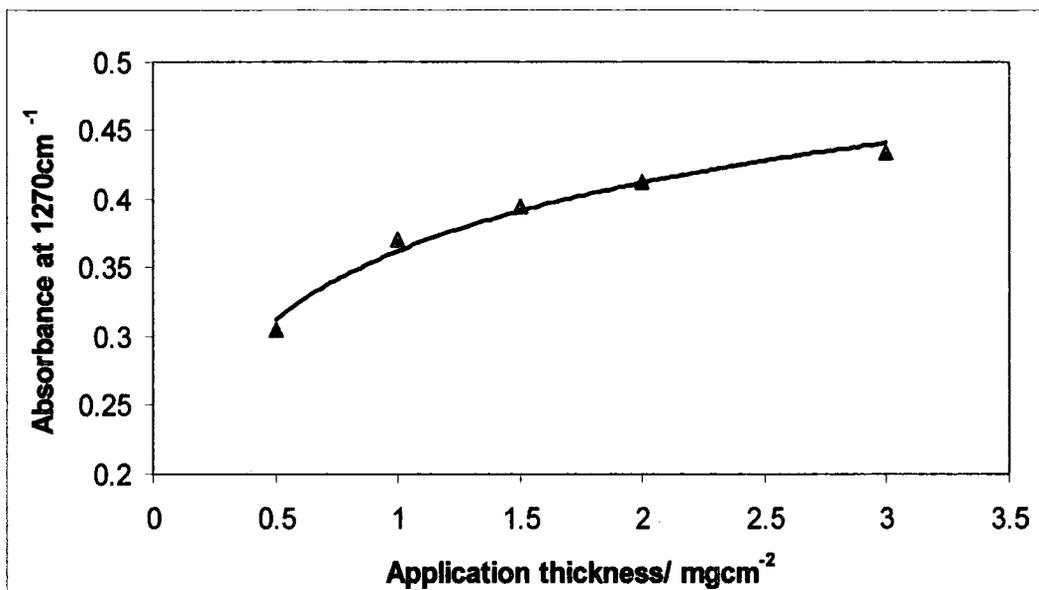
Figure 6.10. Dose-response curve for Nivea Sun® Lotion on a flat ATR crystal.

Correlation of these values with the SPF values determined by Dr Stokes showed that the following relationship exists:

$$SPF = 0.01 \, e^{19A}$$

The infrared absorbance and corresponding SPF values are shown in table 6.6, and the correlation curve is given in figure 6.11.

Application thickness/ mgcm^{-2}	Infrared absorbance	SPF
0.5	0.244 ± 0.013	3.4 ± 0.7
1.0	0.303 ± 0.028	9.5 ± 1.2
1.5	0.322 ± 0.039	16.8 ± 2.2
2.0	0.344 ± 0.027	23.5 ± 2.4
3.0	0.37 ± 0.026	39.2 ± 8.8

__Table 6.6.   Correlation of infrared absorbance data to SPF values for Nivea Sun__[®]
__Lotion.__
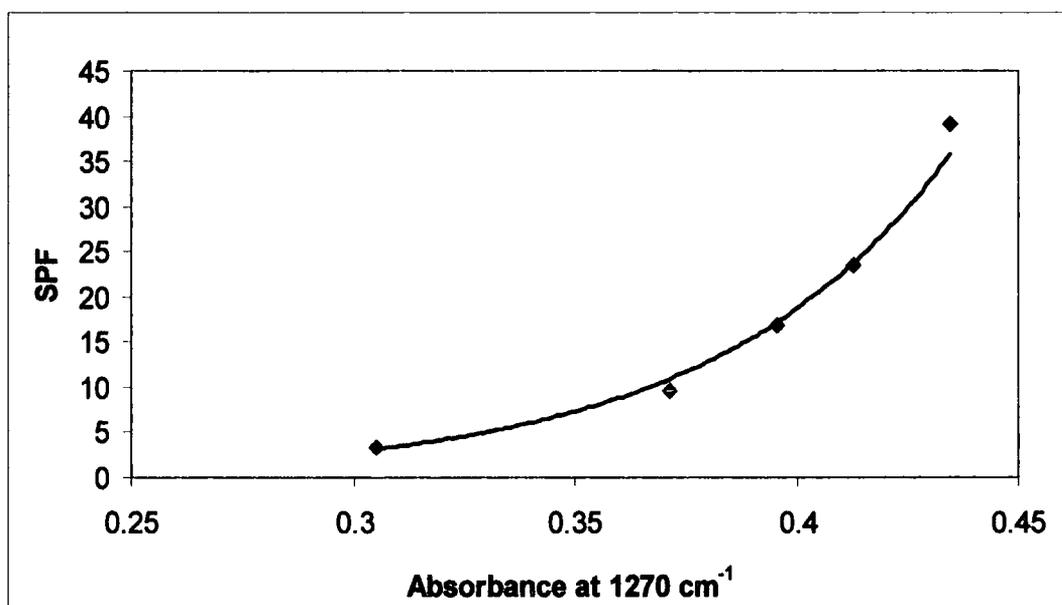
__Figure 6.11.   Infrared absorbance and SPF value correlation curve for Nivea Sun__[®]
__Lotion.__

Table 6.7 shows the values of infrared absorbance and SPF obtained from the water-resistance measurements. As above, the values of SPF obtained by Dr Stokes are shown for comparison.

Immersion Time/ mins	IR absorbance value	SPF value determined by IR protocol	SPF value determined by transmission protocol
0	0.407 ± 0.036	25.5 ± 3.2	21.3 ± 2.6
20	0.308 ± 0.042	8.4 ± 1.2	11.2 ± 3.8
40	0.303 ± 0.033	8.0 ± 1.6	10.0 ± 2.6

Table 6.7. Reduction in infrared absorbance and SPF values following immersion of the Nivea Sun® Lotion.

6.3.2.3. Oil of Ulay Daily Moisture Fluid (SPF 15)

The dose-response plot for the infrared absorbance at different application thicknesses is shown in figure 6.12.
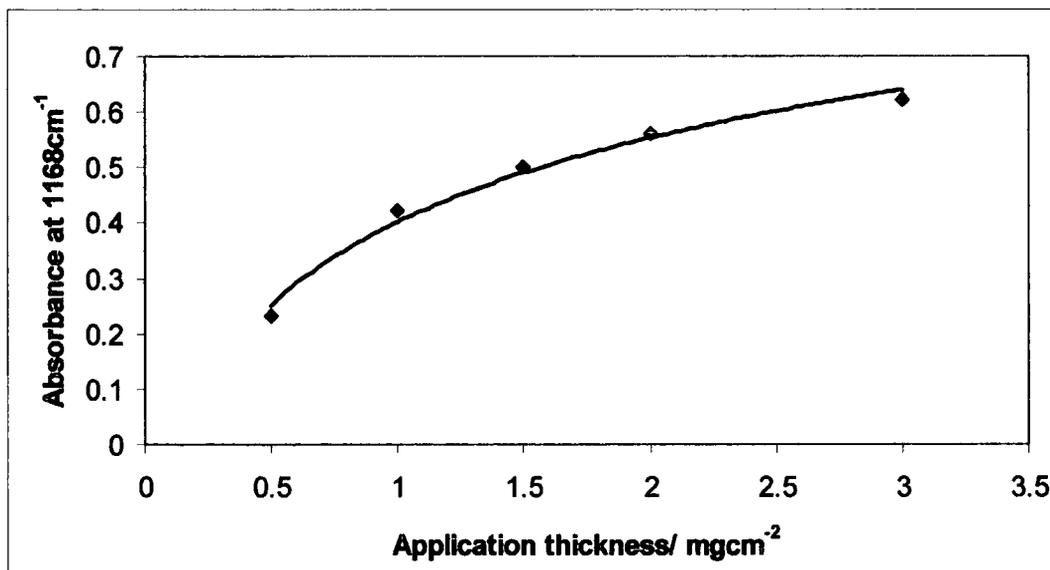
Figure 6.12. Dose-response curve for Oil of Ulay Daily Moisture Fluid on a flat ATR crystal.

The SPF and infrared absorption data obtained for each application thickness are shown in table figure 6.8 and the correlation curve relating these two quantities is shown in figure 6.13.

Application thickness/ $mgcm^{-2}$	Infrared absorbance	SPF
0.5	0.234 ± 0.026	3.8 ± 0.6
1.0	0.392 ± 0.043	7.0 ± 0.9
1.5	0.501 ± 0.064	12.3 ± 1.8
2.0	0.556 ± 0.051	15.9 ± 1.7
3.0	0.621 ± 0.068	23.0 ± 3.3

Table 6.8. Correlation of infrared absorbance data to SPF values for Oil of Ulay Daily Moisture Fluid.
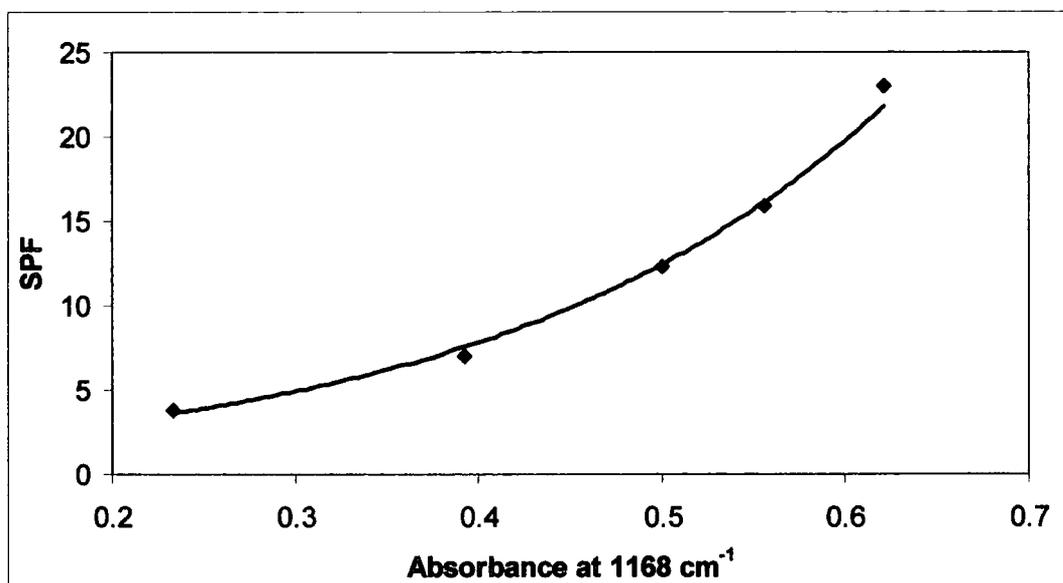
Figure 6.13. Infrared absorbance and SPF value correlation curve for Oil of Ulay Daily Moisture Fluid.

The relationship between SPF and infrared absorbance at 1168 cm^{-1} has been determined to be:

$$SPF = 1.2 \; e^{4.6A}$$

Exposure of a 2 mgcm^{-2} film of this formulation to water resulted in a decrease in infrared absorbance at 1168 cm^{-1}. The associated decreases in SPF calculated from the infrared absorbance data are shown in table 6.9, with the decreases in SPF determined by transmission spectroscopy included for comparison.

Immersion Time/ mins	IR absorbance value	SPF value determined by IR protocol	SPF value determined by transmission protocol
0	0.579 ± 0.050	16.7 ± 1.7	15.6 ± 1.6
20	0.475 ± 0.038	10.4 ± 1.2	6.7 ± 1.1
40	0.469 ± 0.052	10.2 ± 1.4	6.5 ± 1.2

Table 6.9. Reduction in infrared absorbance and SPF values following immersion of the Oil of Ulay Daily Moisture Fluid.

6.4.   Discussion

The current methodology used for *in vivo* water resistance testing of sunscreens has many problems, namely it is time-consuming, expensive, experimentally problematic and involves exposing volunteers to potentially large doses of UV radiation. The determination of the properties of sunscreens using *in vitro* techniques that correlate to *in vivo* measurements would be the ideal solution to the above-mentioned problems.

The work described above demonstrates that infrared spectroscopy, utilising either a probe or flat crystal ATR accessory, can be used to study the properties of sunscreens when spread on the skin surface, or directly onto the ATR crystal. We have also shown that the results obtained can be correlated to those obtained using an *in vitro* transmission spectroscopy technique. The transmission spectroscopy technique has been shown to produce results that correlate well with those determined using the traditional *in vivo* assay[16].

The on skin results clearly show that a correlation exists between the infrared absorbance, at a given wavenumber, and the SPF of the formulation at application thicknesses in the range 0.5-3.0 mgcm^{-2}.

Stockdale[17] and Petro[18] give comprehensive reviews of the theory behind relating spectrophotometric data to sun protection factors, and both give a logarithmic relationship between the SPF and the absorbance at any given wavelength in the form:

$$SPF = 10^A$$

where SPF is the sun protection factor offered at a particular wavelength

A is the absorbance at that wavelength.

In these studies we have related SPF and absorbance exponentially to give relationships of the form:

$$SPF = x \exp(yA)$$

where x and y are arbitrary constants.

In the case of the 'on skin' studies the data do not fit exactly to the theoretical logarithmic relationship given. This can be attributed to any of a series of reasons why such expressions based on Beer-Lambert's law will not hold true. These include the lack of linearity at high concentrations. The concentration of sunscreen in a thin film on the skin will certainly be very high. Also there is unlikely to be an even distribution of the sunscreen agent in the applied film. This may be due to crystal formation or droplet formation in oil in water emulsions, and can result in gaps in areas of application where there is effectively no protection offered by the sunscreen. Following on from this there is also the problem of applying a uniform film of sunscreen. Even in a laboratory environment it is difficult to achieve a uniform coverage, especially given the uneven skin surface. As the absorbance at any wavelength is proportional to the film thickness and this is present in the exponential part of the equation then any small variation in the film thickness will have a large

effect on the SPF achieved. The penetration depths of the infrared beam into sample will also influence this.

Despite these problems the fits obtained can clearly be seen to follow a logarithmic trend, unlike the results of Brown and Diffey[16] and Kaidbey and Kligman[19]. Brown and Diffey have stated that the relationship they found was not logarithmic whereas Kaidbey and Kligman found a dose-dependant increase showing that the SPFs increased with larger amounts of sunscreen, though not in any fixed way.

The work using the flat ATR crystal as the substrate yielded data that followed the logarithmic relationship more closely. This is to be expected since the surface of the substrate is almost perfectly smooth enabling a much more uniform surface coverage. It can be seen that the relationships between SPF and absorbance obtained from the two different substrates for the Nivea Sun® Sport&Sun Lotion and the Oil of Ulay Daily Moisture Fluid are not the same. This may be due to the problems mentioned above regarding the non-uniformity of the sunscreen agent within the film, and the non-unformity of the film thickness.

From the results shown in tables 6.5, 6.7 and 6.9 it can be seen that the reductions in SPF determined using this technique show the same trends as those determined using the transmission technique alone. From both the transmission spectroscopy results and the infrared spectroscopy results it would appear that the Nivea Sun® Sport&Sun Lotion could claim to be 'water-resistant' according to COLIPA guidelines. However, according to the U.S. FDA guidelines and these results the manufacturers should not be making this claim about the product.

Similarly the Nivea Sun® Lotion cannot make any claims about its water-resistant properties according to the U.S. FDA guidelines, but using the COLIPA guidelines and the infrared spectroscopy technique it can claim to be 'water-resistant'. The transmission spectroscopy measurements, however, dispute this claim.

The Oil of Ulay Daily Moisture Fluid can however claim to be 'water-resistant' according to COLIPA, but can make no claims, as it does, according to the U.S. FDA.

The work described above demonstrates the ability of this technique to monitor the water resistance of sunscreen formulations, in a way that can be correlated to SPF values and so comply with the guidelines set down by the U.S. FDA and COLIPA.

6.5.   Conclusions

Attenuated total reflectance Fourier transform infrared spectroscopy has been used to study the dose-response relationship between application thickness and the infrared absorbance of a thin film of a sunscreen formulation. These data have been correlated with SPF data obtained for the same sunscreens under the same conditions using an *in vitro* transmission spectroscopy technique. We have shown that an exponential relationship exists, as predicted by theory[17,18], in the range 0.5-3.0 mgcm^{-2}.

These relationships have then been used to study the water resistance properties of the sunscreen products using infrared spectroscopy. This technique has been used to determine the reductions in SPF following exposure of the sunscreen film to water, and can therefore be used to test the claims made by manufacturers concerning water resistance, and determine the claims that can be made.

This technique offers an alternative to the current water-resistance testing protocols which is less time consuming, less expensive and avoids exposing volunteers to unnecessary UV radiation. It also offers the possibility to study the effect that water immersion may have on formulations *in vivo* on the skin surface.

6.6.   References

1. Griffin M.E., Bourget T.D. and Lowe N.J., *Sun Protection Factor Determination in the United States* in 'Sunscreens: Development, Evaluation and Regulatory Aspects', eds. Lowe N.J., Shaath N.A. and Pathak M.A., Marcel Dekker, New York, 1997, pp. 499-512.

2. Shaath N.A., *Evolution of Modern Sunscreen Chemicals* in 'Sunscreens: Development, Evaluation and Regulatory Aspects', eds. Lowe N.J., Shaath N.A. and Pathak M.A., Marcel Dekker, New York, 1997, pp. 3-33.

3. Sunscreen drug products for over-the-counter human use: tentative final monograph (1993) *Federal Register*, **58**, 28194-28302.

4. Azizi E., M. Modan, A.P. Kushelevsky and M. Schewch-Miller (1987) A more reliable index of sunscreen protection, based on life table analysis of individual sun protection factors. *Br. J. Dermatol.*, **116**, 693-702.

5. Farr P.M. and B.L. Diffey (1985) How reliable are sunscreen protection factors? *Br. J. Dermatol.*, **112**, 113-118.

6. Springsteen A., R. Yurek, M. Frazier and K.F. Carr (1999) *In vitro* measurement of sun protection factors of sunscreens by diffuse transmittance. *Anal. Chim. Acta* **380**, 155-164.

7. Pines E. (1978)   A new technique to assess sunscreen effectiveness. *J. Soc. Cosmet. Chem.,* **29**, 559-564.

8. Morasso M.I., A.M. Thielemann, C. Pinto, M. Figueroa and A. Arancibia (1985) *In vitro* and *in vivo* study of the substantivity of p-aminobenzoic acid and two of its esters. *J. Soc. Cosmet. Chem.*, **36**, 355-362.

9. Greiter F., P. Bilek, S. Doskoczil, J. Washüttl and F. Wurst (1979) Methods for the water resistance testing of sun protection products. *Int. J. Cosmet. Sci.*, **1**, 146-157.

10. Sayre R.M., P.P. Agin, D.L. Desrochers and E. Marlowe (1980) Sunscreen testing methods: *In vitro* predictions of effectiveness.   *J. Soc. Cosmet. Chem.*, **31**, 133-143.

11. Sayre R.M., E. Marlowe, P. PohAgin, G.J. LeVee and W. Rosenberg (1979) Performance of six sunscreen formulations on human skin. *Arch. Dermatol.*, **115**, 46-54.

12. Stokes R.P. and B.L. Diffey (1997) *In vitro* assay of high-SPF sunscreens. *J. Soc. Cosmet. Chem.,* **48**, 289-295.

13. Stokes R.P. and B.L. Diffey (1999) The water resistance of sunscreen and day-care products. *Br. J. Dermatol.*, **140**, 259-63.

14. Stokes R.P., B.L. Diffey, L.C. Dawson and S.P. Barton (1998) A novel *in vitro* technique for measuring the water resistance of sunscreens. *Int. J. Cosmet. Sci.*, **20**, 235-240.

15. Gupta V.K. and J.L. Zazt (1999) In vitro method for modelling the water resistance of sunscreen formulations. *J. Cosmet. Sci.*, **50**, 79-90.

16. Brown S. and B.L. Diffey (1986) The effect of applied thickness on sunscreen protection: *In vivo* and *in vitro* studies. *Photochem. Photobiol.*, **44(4)**, 509-513.

17. Petro A.J. (1981) Correlation of spectrophotometric data with sunscreen protection factors. *Int. J. Cosmet. Sci.*, **3**, 185-596.

18. Stockdale M. (1985) Sun protection factors *Int. J. Cosmet. Sci.*, **7**, 235-246.

19. Kaidbey K.H. and A.M. Kligman (1978) Laboratory methods for appraising the efficacy of sunscreens. *J. Soc. Cosmet. Chem.*, **29**, 525-536.

SUMMARY

* A comprehensive photophysical study has been carried out on two anthranilate ester compounds used as active sunscreen ingredients and has highlighted disturbing properties of these compounds following absorption of light.

    - The compounds are fluorescent, emitting in the UV-A region of the spectrum. Menthyl anthranilate has a fluorescence quantum yield of ~ 0.60.

    - Population of the triplet state in both compounds produces long lived species which are readily quenched by oxygen to produce singlet oxygen. Singlet oxygen quantum yields have been determined to be ≥ 0.10.

    - The triplet energy of N-acetyl-menthyl anthranilate has been shown to be high enough, $E_T \sim 315$ kJmol^{-1} to sensitise the formation of thymine triplets in skin, which are known to combine to form thymine dimers, and result in DNA damage.

* Studies of sunscreen formulations containing menthyl anthranilate have been shown to fluoresce with the same lifetime as solution state menthyl anthranilate. As other ingredients in the formulation do not appear to quench the fluorescence it is likely that the triplet state will be formed and quenched in the formulation leading to the production of singlet oxygen close to the skin.

* Studies have been carried out on commercially available sunscreen formulations using infrared spectroscopy. The analysis and detection of sunscreen formulations present on skin at normal usage levels using this technique has been demonstrated.

    - Individual active components have been identified.

    - Wash-off of the formulation after exposure to water has been studied

    - Changes in thin films of the formulation following irradiation have been monitored.

    - A relationship between IR absorbance and SPF values has been determined and used to test the water resistance claims of manufacturers.

Appendix A

Photochemistry of the π-Extended 9,10-Bis(1,3-dithiol-2-ylidene)-9,10-dihydroanthracene System: Generation and Characterisation of the Radical Cation, Dication and Derived Products

Allison E. Jones, Christian A. Christensen,
Dmitrii F. Perepichka, Andrei S. Bastanov, Andrew Beeby,
Paul Low, Martin R. Bryce and Anthony W. Parker.

A.1. Introduction

Tetrathiafulvalene (TTF) is a well-known π-electron donor molecule which undergoes two one-electron oxidation waves to afford the radical cation and dication species. These oxidation waves have been shown to be reversible[1,2,3] and formation of the 1,3-dithiolium cation results in a gain in heteroaromaticity[4].

A considerable amount of attention has been given to related bis(1,3-dithiole) systems where π-conjugation is extended between the dithiole rings by the insertion of vinylogous[5,6,7,8,9] and quinonoid[10,11] spacer units. This insertion results in reduced intramolecular Coulombic repulsion in the oxidised states. Derivatives of the 9,10-bis(1,3-dithiol-2-ylidene)-9,10-dihydroanthracene system[12], e.g. TTFAQ, as shown in figure A.1, are particularly interesting in this context, as they undergo a single, quasi-reversible, two electron oxidation wave to yield a thermodynamically stable dication at $E^{ox} \sim$ +0.3-0.4 V in the cyclic voltammogram[13,14] (in acetonitrile vs Ag/AgCl). Hünig et al. give a comprehensive review of multi-stage redox systems[15].

TTFAQ   TTFAQ[+•]   TTFAQ[2+]
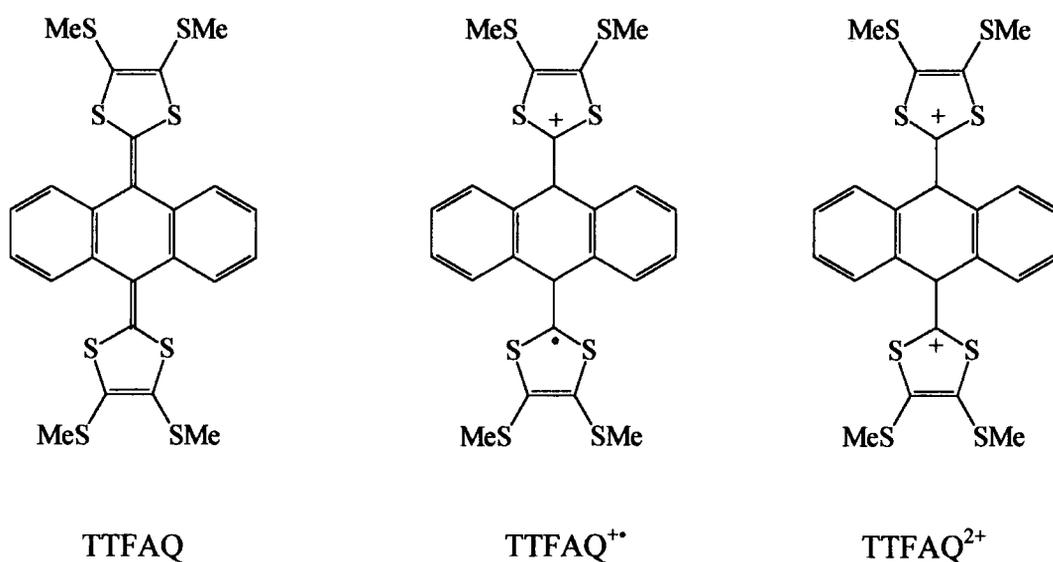
Figure A.1. Structures of the neutral, radical cation and dication TTFAQ species.

The X-ray crystal structures of TTFAQ[12] and several derivatives[16,17] show that following oxidation to the dication a conformational change takes place. The neutral molecules are saddle-shaped with the central ring of the anthracenediylidene moiety adopting a boat conformation. However, following oxidation the dications formed have a planar anthracene system with the 1,3-dithiolium cations almost orthogonal to the plane of the anthracene unit[14,18,19]. Theoretical calculations support these crystallographic data[20]. Steric hindrance between the sulfur atoms and the peri hydrogen atoms in the neural species dictates the conformation adopted. However, in the dication there is aromatisation of the dithiolium rings and the anthracene core. Calculations also suggest that the radical cation largely retains the saddle conformation of the neutral species, restricting any potential gain in aromaticity at this redox stage. This is in agreement with the electrochemical data[20]. The strong electron donating ability of such compounds has led to their use as components in intermolecular[14,18,19] and intramolecular[21,22,23,24] charge-transfer systems.

The aim of the work described was to explore the photolytic generation of the elusive π-radical cation species, TTFAQ[+•]. The characterisation of TTFAQ[+•] has been achieved by UV-visible and Raman spectroscopy, and the decomposition products have also been isolated and identified, and found to be the dication, TTFAQ[2+] and a ketone, see figure A.2.
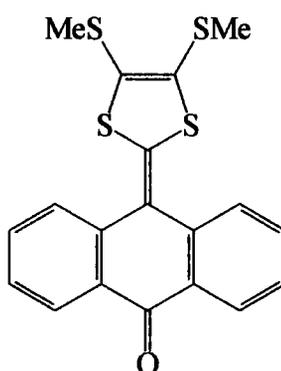
Figure A.2. Structure of the ketone decomposition product formed following irradiation of TTFAQ in aerated solution.

The spectroelectrochemistry of TTFAQ has also been probed and the X-ray crystal structure has been obtained of $TTFAQ^{2+}(ClO_4^-)_2$, produced electrochemically during this work. During the course of these experiments, Guldi *et al.*[25] have reported that $TTFAQ^{+\bullet}$ can be generated by the pulse radiolysis of TTFAQ in oxygenated dichloromethane solution. The species formed was characterised and found to have an absorption maximum at ~ 675 nm[24]. The species was found to be stable over several hundred microseconds and showed no significant decay on the pulse radiolytic time scale.

A.2. Experimental Methods

A.2.1. Spectroelectrochemistry

Spectroelectrochemical data were recorded for TTFAQ (0.35 mM) in dichloromethane solutions containing 0.1 M NBu_4PF_6 as the supporting electrolyte with a platinum gauze working electrode and platinum wire counter and reference electrodes. Spectra were recorded at room temperature using a Varian Cary 5 spectrophotometer in the range 300-1000 nm. All spectra were corrected for the background absorption due to the cell, electrolyte and working electrode. The optically transparent thin-layer electrode, OTTLE, cell employed has been described elsewhere[26] and was driven by a home-built potentiostat.

A.2.2. Steady State Photolysis and Isolation

Steady state photolysis was carried out on both aerated and degassed chloroform solutions of TTFAQ using the output of a Bentham IL6 Illuminator xenon lamp filtered with a copper (II) sulfate filter to remove any infrared radiation ($\lambda_{ex} = 320$-600 nm). Isolation of the products obtained from both the degassed and aerated solutions was achieved by column chromatography (silica gel, eluent chloroform) and characterised by UV-Visible and fluorescence spectroscopy, melting point, TLC and mass-spectrometry. UV-Visible spectra were obtained using an ATI Unicam UV2-100

spectrometer, controlled using Unicam Vision Software (Version 3.41) running on a PC. Fluorescence spectra were measured on an ISA Fluoromax 2 spectrophotometer.

A.2.3. Singlet Oxygen Measurements

The experimental set-up for the time resolved near-infrared luminescence experiments have been described elsewhere[27]. Solutions of TTFAQ and the ketone decomposition product in aerated chloroform were studied with absorbances at the excitation wavelength (266 nm) of ~ 0.1. A solution of the dication TTFAQ^{2+} in acetonitrile was also studied using 355 nm excitation.

The rate constant for the quenching of singlet oxygen production was determined using solutions containing TTFAQ and the photosensitiser, tetraphenylporphyrin, TPP. Irradiation was carried out at 532 nm to ensure that only the TPP was excited and quenched by oxygen to produce singlet oxygen in the solutions. The lifetime of singlet oxygen based luminescence was monitored as a function of TTFAQ concentration, allowing the rate constant for singlet oxygen quenching to be determined using the Stern-Volmer relationship. The solutions were made up in the dark to avoid the room light sensitisation of the TPP.

A.2.4. Time Resolved Measurements

The experimental set-up used for the laser flash photolysis experiments has been described in detail elsewhere[27]. The radical cation, TTFAQ$^{+\bullet}$, lifetime and absorbance spectrum were obtained from 250 μM solutions of TTFAQ in chloroform. The solutions were flowed through a 1 mm pathlength cuvette, such that fresh solution was excited by each laser shot. This was to due to the rapid photodecomposition of the TTFAQ solutions following excitation at either 266 nm or 355 nm.

A.2.5. Raman Spectroscopy

For time resolved resonance Raman spectroscopy the pump laser (266 nm, 5 ns pulsewidth) was produced from the quadrupled output of a Spectra-Physics GCR-11. The probe pulse was generated from a Lumonics Pulsemaster PM-800 excimer (XeCl,

308 nm, 15 ns pulsewidth) pumping a Lambda-Physik FL3002 dye laser using Rhodamine 101 dye to produce 630 nm light. Synchronisation of the two lasers was better than ± 5 ns. Pulse energies were obtained using a 90° collection geometry with the liquid sample passed through a capillary (2 mm ID) held perpendicular to the spectrograph collection optics and entrance slit. The spectrograph was an Acton Research Corporation Spectra-Pro 500. Rayleigh scattered light was prevented from entering the spectrograph by using a holographic notch filter (Kaiser). Light was detected using a thinned, back illuminated liquid nitrogen CCD camera (Princeton Instruments LN/CCD-1024 TKB) which was controlled via a PC and manufacturer's supplied software. Typical accumulation times were 200 seconds. Raman spectra are accurate to 5 cm^{-1} and were calibrated using the toluene values given by Schrader[28].

A.2.6. Preparation of TTFAQ^{2+}(ClO$_4^-$)$_2$

A solution of TTFAQ in dry degassed dichloromethane (6 mg in 17 mL) was placed in the anodic chamber of a glass electrocrystallisation cell in which the two chambers were separated by a glass frit. 7 ml of dry degassed dichloromethane were placed in the cathodic chamber. 50 mg of dry tetrabutylammonium perchlorate were added to each chamber and the cell was flushed with argon. The platinum electrodes were mounted to seal the solutions from the atmosphere. A potential of 1.0 V was applied, which provided an initial current of 2.0 μA. The cell was stored in the dark for two days at 20°C, during which time the current dropped to 0.5 μA and red blade-shaped crystals of TTFAQ^{2+}(ClO$_4^-$)$_2$ (up to 5 mm in length) grew on the anode. The crystals were harvested and washed with dry dichloromethane.

A.2.7. X-ray Crystallography

The X-ray diffraction experiment was carried out on a SMART 3-circle diffractometer with a 1 K CCD area detector, using graphite mounted Mo-K_α radiation ($\lambda = 0.71073$ Å) and a Cryostream (Oxford Cryosystems) open flow N$_2$ gas cryostat. Full sphere of the reciprocal space was covered by a combination of five sets of ω scans; each set at different φ and/or 2θ angles. Reflection intensities were integrated

using the SAINT program[29] and corrected for absorption by a semi-empirical method (comparison of Laue equivalents), using the SADABS program[30]. The structures were solved by direct methods and refined by full-matrix least squares against F^2 of all the data, using the SHELXTL software[31].

Crystal data: $C_{24}H_{20}S_8{}^{2+}(ClO_4^-)_2$, f.w. 763.78, T = 103 K, monoclinic, space group $P2_{1/c}$ (No. 14), a = 16.206(1), b = 7.798(1), c = 12.819(1) Å, β = 112.09(1), U = 1501.1(2) Å^3, Z = 2, μ = 0.82mm^{-1}, 15578 reflections ($2\theta \leq 55°$), 3450 unique, R_{int} = 0.039, 196 refined parameters, R = 0.031 [2888 data with $F^2 \geq \sigma(F^2)$], $wR(F^2)$ = 0.076.

A.3. Results and Discussion

A.3.1. Spectroelectrochemistry of TTFAQ

In order to obtain a reference spectrum of the TTFAQ^{2+} dication a spectroelectrochemical study covering the UV, visible and near-IR regions of the spectrum was undertaken. Previous electrochemical studies[13,14] have demonstrated that on the cyclic voltammetry time scale derivatives of TTFAQ undergo a two-electron oxidation to yield the corresponding dication TTFAQ^{2+}. Electrolysis of TTFAQ in dichloromethane was performed in an OTTLE cell and the solution analysed in situ. The working electrode was held at a potential at which no electrochemical work was being done in the cell and a spectrum of the neutral TTFAQ was recorded. The potential was then increased in 50-100 mV increments and held until equilibrium had been obtained, as detected by a sharp drop in cell current. Complete electrolysis of the sample within the thin-layer region was achieved, as indicated by the vanishingly small currents which flowed through the cell and observation of identical absorption profiles at applied potentials of 0.65, 0.75 and 0.85 V. Reduction in situ and the recovery of the initial spectrum confirmed the full reversibility of the redox system under these conditions. The compiled spectra, shown in figure A.3, contain clean isosbestic points marking the clean conversion of the neutral species to the dication.

The spectrum of the neutral TTFAQ species consists of two strong bands with maxima at 366 nm (ε = 5460 $dm^3mol^{-1}cm^{-1}$) and 435 nm (ε = 9650 $dm^3mol^{-1}cm^{-1}$). During electrolysis these bands collapse and new bands appear at 377 nm (ε = 3250 $dm^3mol^{-1}cm^{-1}$), 392 nm (ε = 3620 $dm^3mol^{-1}cm^{-1}$), 419 nm (ε = 4850 $dm^3mol^{-1}cm^{-1}$) and 479 nm (ε = 3580 $dm^3mol^{-1}cm^{-1}$) which is a broad band that tails into the visible portion of the spectrum. These new bands have been ascribed to the $TTFAQ^{2+}$ dication species. Neither neutral TTFAQ nor the dication $TTFAQ^{2+}$ give rise to any significant absorption in the range 650-1000 nm. The spectrum of $TTFAQ^{2+}$ obtained by this in situ electrochemical method was identical to that obtained by dissolution in dichloromethane of an authentic sample of the $TTFAQ^{2+}(ClO_4^-)^2$ obtained by electrocrystallisation.
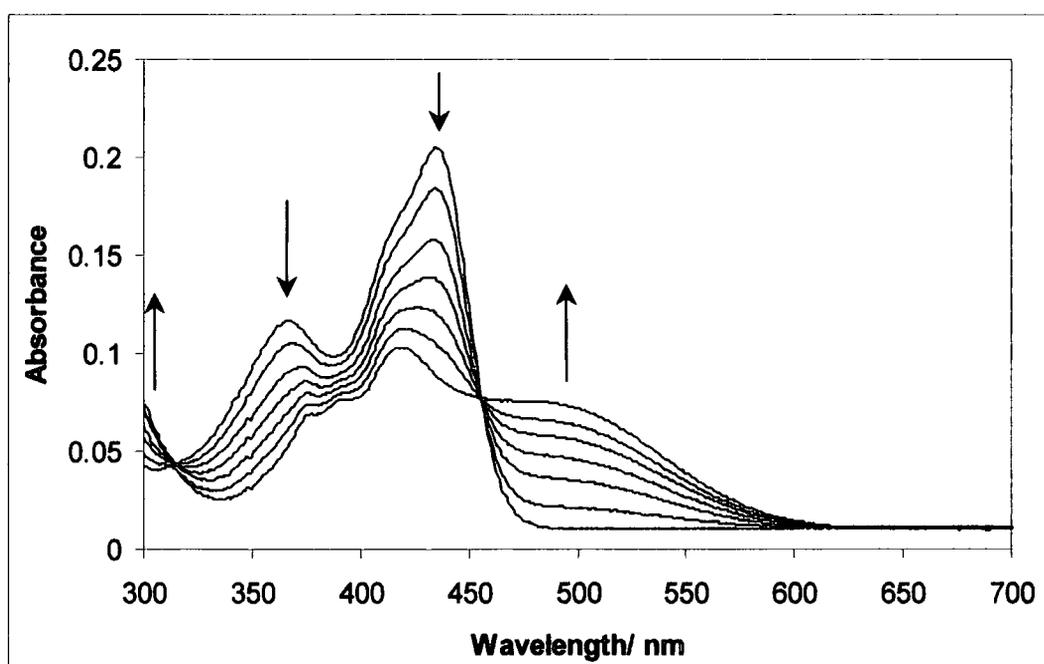
Figure A.3. Spectroelectrochemistry of TTFAQ in dichloromethane.

A.3.2. Steady State Photolysis of TTFAQ

Irradiation of TTFAQ in aerated chloroform solution using the output of a xenon lamp filtered through aqueous copper (II) sulfate (λ_{ex} = 320-600 nm) brought about a marked change in the UV-visible absorption spectrum of the solution, as shown in figure A.4.

The photoproduct from this reaction was isolated by column chromatography (silica gel, chloroform eluent) and its UV-visible and fluorescence spectra are shown in figure A.5.
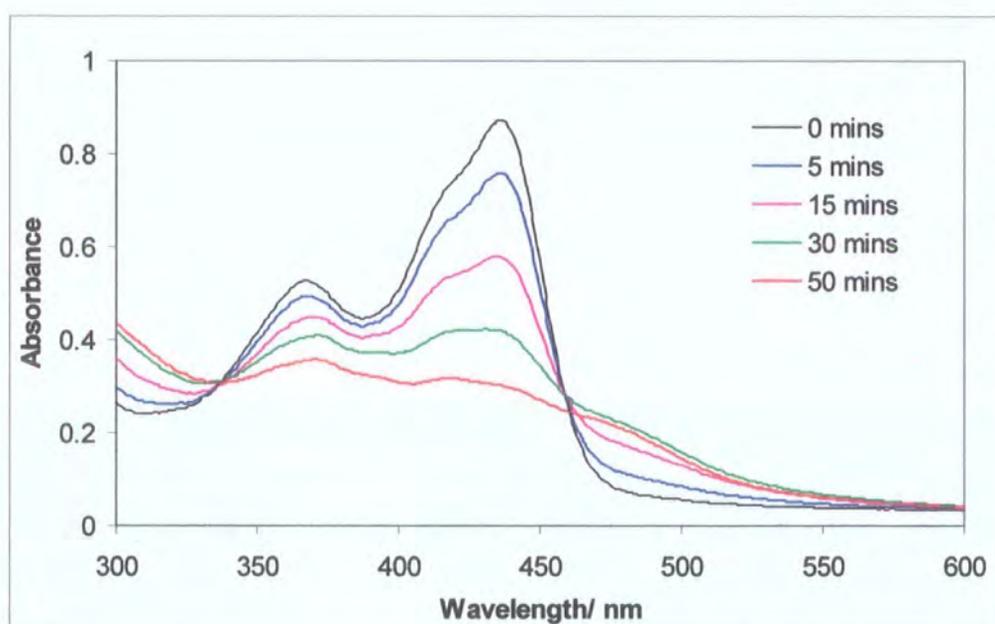
Figure A.4. UV-visible spectra of TTFAQ in aerated chloroform after various irradiation times.
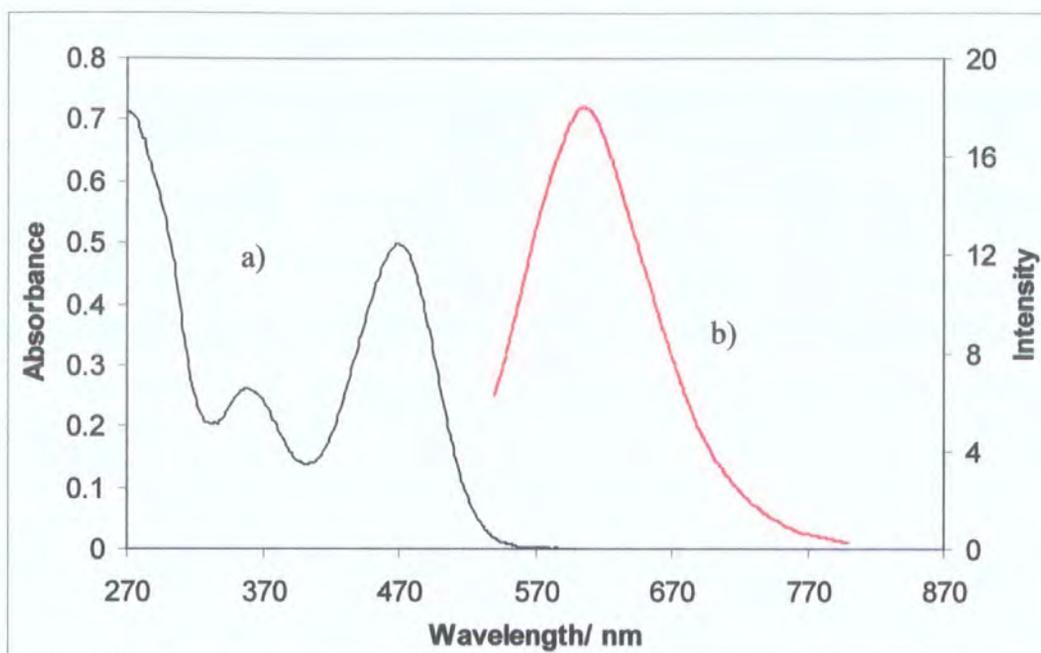
Figure A.5. UV-visible absorption (a) and corrected fluorescence emission spectrum
(b) of the ketone photodecomposition product in chloroform. An excitation
wavelength of 460 nm was used to record the emission spectrum.

This product is unambiguously identified as the ketone decomposition product, on the basis that its melting point, TLC behaviour, mass spectrum, ^{1}H NMR and UV-visible spectrum were identical to those of an authentic sample of the ketone synthesised from the anthrone[12]. Significantly, the UV-visible spectrum of the ketone is markedly different from that of the dication, $TTFAQ^{2+}$. Irradiation of TTFAQ in degassed chloroform solution also resulted in a change in the UV-visible spectrum, consistent with the formation of the $TTFAQ^{2+}$ dication, see figure A.6. There was no evidence for the formation of the ketone under these conditions.
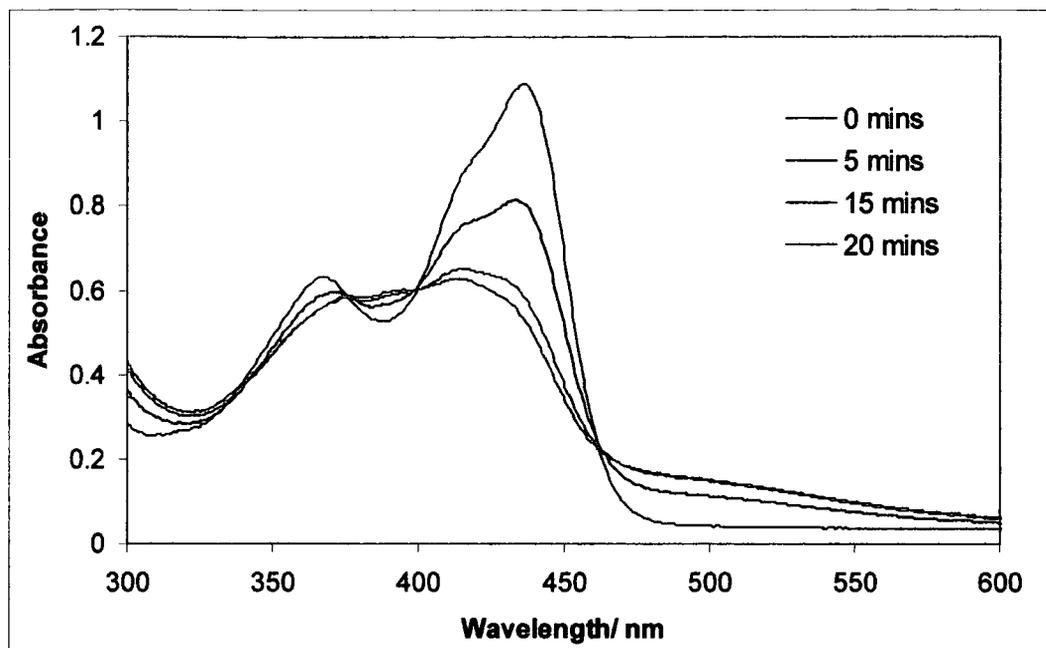
Figure A.6. UV-visible spectra of TTFAQ in degassed chloroform irradiated for various times using the filtered output of a xenon lamp (320-650 nm).

A.3.3. Singlet Oxygen Measurements

In an attempt to elucidate the mechanism of the formation of the ketone we investigated the role of singlet oxygen. Time-resolved near-IR luminescence experiments showed no evidence for the production of singlet oxygen, $\Phi_\Delta < 0.001$, by TTFAQ, the ketone product, or the dication, $TTFAQ^{2+}$. However, we did observe that in toluene solution TTFAQ rapidly quenches the singlet oxygen produced by an added photosensitiser (tetraphenylporphyrin) and degrades to form the ketone with a rate constant of $2.9\pm0.1 \times 10^7$ $dm^3mol^{-1}s^{-1}$. Figure A.7 shows the Stern-Volmer plot used to determine the singlet oxygen quenching rate constant.
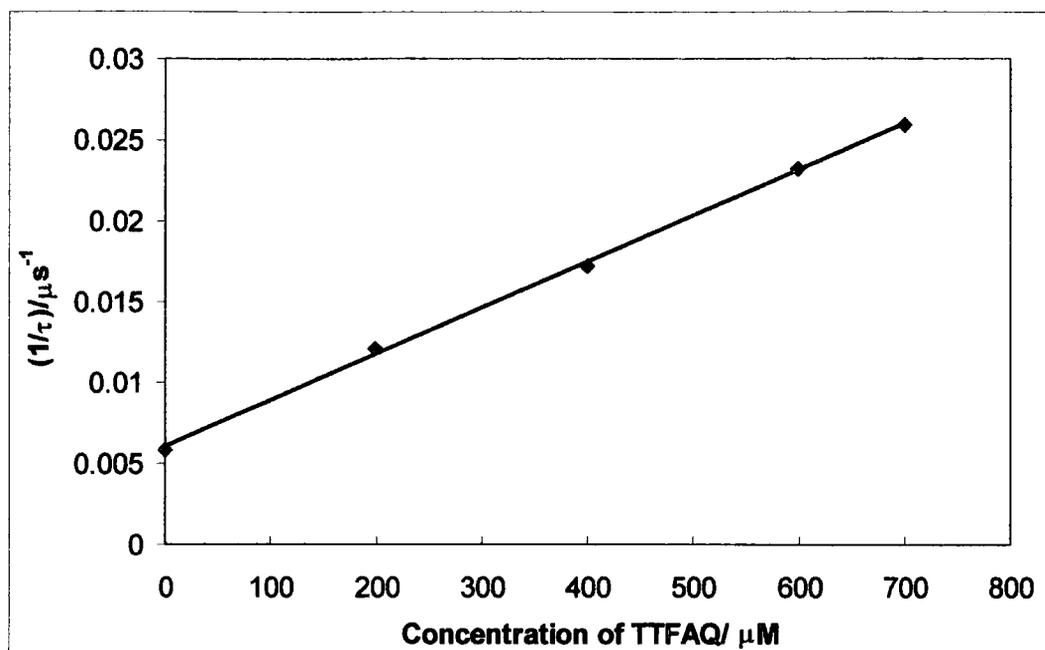
Figure A.7. Stern-Volmer plot for the quenching of singlet oxygen by TTFAQ in toluene.

A.3.4. Time-resolved Studies

Flash photolysis (λ_{ex} = 266 nm or 355 nm) of TTFAQ in degassed chloroform revealed a transient species with an absorption band centred at 650 nm, see figure A.8. This spectrum is consistent with that obtained by Guldi *et al.*[25] for TTFAQ$^{+\bullet}$ generated by the pulse radiolysis of TTFAQ in oxygenated chloroform. This transient absorption decays via a non-exponential function as shown in figure A.9. The signal to noise ratio obtained during the course of the experiments did not allow us to differentiate between a double exponential or a second order decay. Under the conditions used the transient absorption decayed to half its initial intensity over a period of *ca.* 80 μs and the decay was not significantly affected by aeration of the solution. This indicates that the transient species is unlikely to be an excited triplet electronic state of the parent TTFAQ. The same species was also observed in dichloromethane solution, but could not be observed when propionitrile or tetrahydrofuran were used as solvents. Based on these observations it is proposed that the transient absorption arises from the radical cation TTFAQ$^{+\bullet}$, formed by the monophotonic photoionisation of neutral TTFAQ.
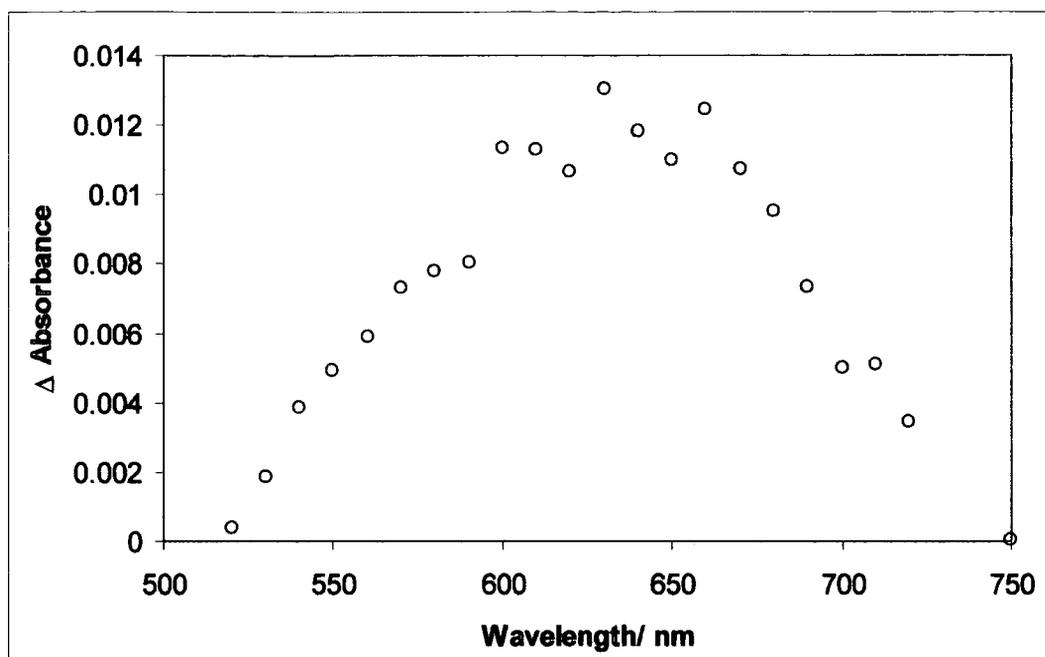
Figure A.8. Transient absorption spectrum obtained following 266 nm irradiation of

TTFAQ in degassed chloroform solution.

The halogenated solvents play an important role by acting as a sink for the ejected photoelectrons according to the mechanism in equation A.1.

$$CH_nCl_{4-n} + e^- \longrightarrow CH_nCl_{3-n}{}^\bullet + Cl^- \qquad\qquad \text{Equation A.1}$$
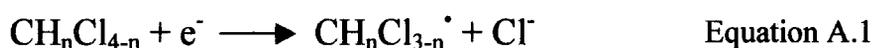
In aerated solutions the halomethyl radicals may further oxidise to form $CH_nCl_{3-n}O_2{}^\bullet$, although the suggestion that this peroxyhalomethyl radical can oxidise TTFAQ to $TTFAQ^{+\bullet}$, as suggested by Guldi *et al.* is in doubt, since we observe no evidence for the enhancement of the transient bands in aerated solutions. Attempts to determine the quantum yield of radical cation formation were prevented due to the photodecomposition of the samples during the course of the measurements.
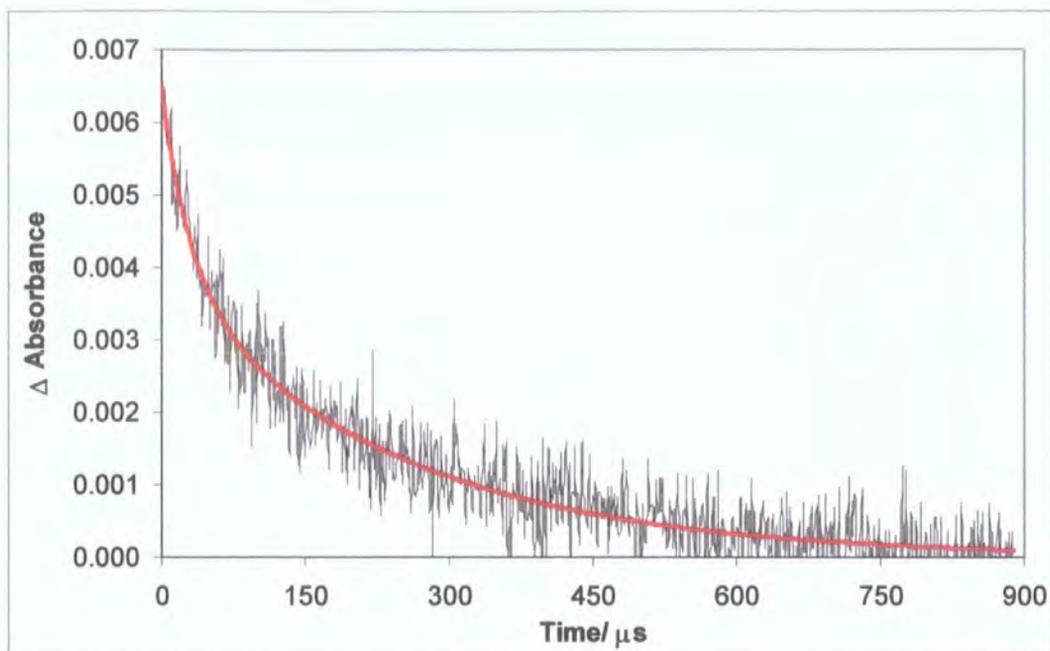
***Figure A.9. Transient absorption decay at 630 nm produced upon irradiation of a
degassed solution of TTFAQ in chloroform. The decay is non-exponential and has a
trendline added as a guide.***

A.3.5. Raman Spectroscopy

The resonance Raman spectrum of TTFAQ was recorded using a probe wavelength of
488 nm. Attempts to record the resonance Raman spectrum of $TTFAQ^{2+}$ failed due to
its fluorescence. Using a 266 nm excitation source and a 650 nm laser probe the time
resolved resonance Raman spectrum of $TTFAQ^{+\bullet}$ was obtained which differs
somewhat from that of the neutral TTFAQ species, as shown in figure A.10. The
spectrum of neutral TTFAQ is dominated by three intense bands at ~1480, ~1520 and
~1580 cm^{-1} and this profile has similarities to the non-resonant Raman spectrum of
anthracene[28]. These bands are assigned to phenyl C=C stretching modes. Formation
of $TTFAQ^{+\bullet}$ changes the spectral profile and yields a much richer array of bands. The
highest resonant Raman band is observed at ~1540 cm^{-1} and this wavenumber value is
less than for a typical aromatic C=C stretch and reflects a lowering of the aromatic
C=C bond order following the loss of an electron from the bonding MO. The key
question of interest is whether $TTFAQ^{+\bullet}$ is planar and if so forms a 'pseudo-quinoid'

type structure, that is the two dithiolylidene groups form a π-conjugated network with the central anthracene group and the bridging carbon-carbon bonds develop partial double bond character. In a recent investigation on the radical cation of an ethylene bridged thiophene based oligomer an intense band is observed at 1411 cm^{-1} which in the neutral oligomer is observed at ~1430 cm^{-1}.[32] These values (1340 to 1430 cm^{-1}) are typical for CC modes in the thio-ring (e.g. thiophene) systems and it is likely that the broad feature at 1390 cm^{-1} resembles such a stretch. However, in resonance Raman spectra specific enhancement (Frank-Condon, A-term resonance enhancement) occurs for modes associated with the particular chromophore responsible for the electronic absoprtion at the laser wavelength chosen. The richness of the spectrum as well as the intensity of the bands probably indicates a very delocalised chromophore system supporting a 'quinoid' type framework. Future investigations will be directed towards establishing this.
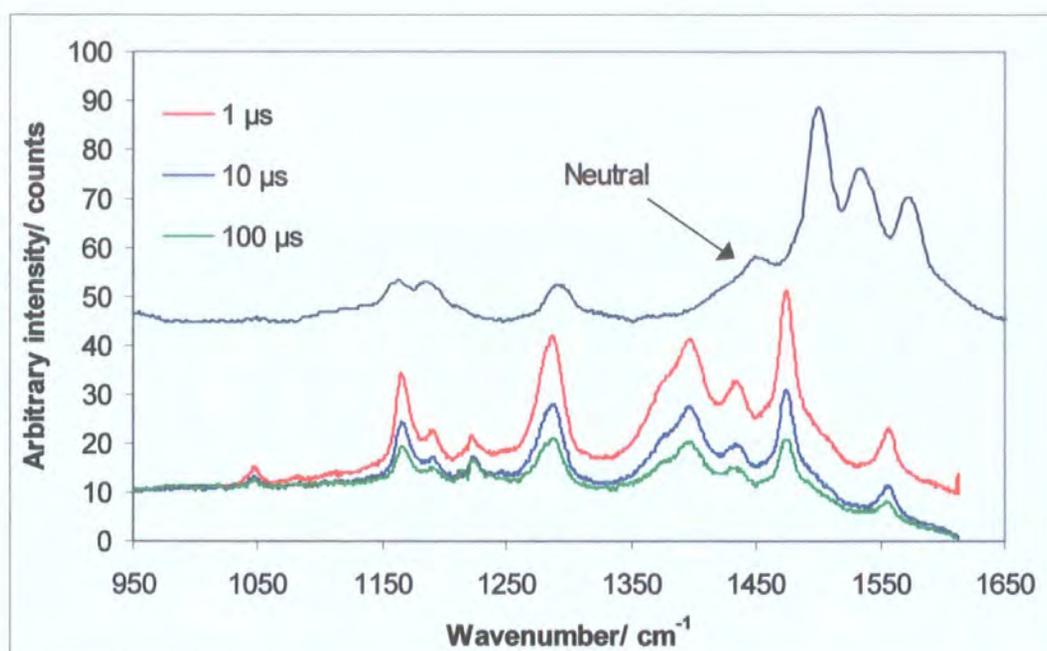
Figure A.10. Time-resolved resonance Raman spectrum of TTFAQ and TTFAQ$^{+•}$. Ground state Raman spectrum taken at 630 nm and time resolved resonance Raman spectrum taken using $\lambda_{pump} = 266$ nm, $\lambda_{probe} = 630$ nm. Spectra of TTFAQ^{2+} are corrected by subtracting ground state and solvent bands (probe only).

Attempts to probe the formation of TTFAQ^{2+} using a pump/probe combination of 266/514 nm, respectively, failed to yield Raman spectra due to fluorescence from the samples. However, it was found that the intensity of the fluorescence signal increased with the delay time between the pump and probe pulses. Figure A.11 shows the increase in absorption intensity at 680 nm with time (0-200 μs) consistent with the formation of the dication species TTFAQ^{2+}. The spectra of authentic TTFAQ^{2+} and the ketone are shown offset for reference.

Furthermore, the spectral profile of this fluorescence (λ_{max} 680 nm) was clearly characteristic of the dication TTFAQ^{2+}, by comparison with the electrochemically generated sample. The fluorescence from the ketone, whilst much more intense, has a shorter λ_{max} value (630 nm).

Figure A.11. Fluorescence spectra obtained by pump (266 nm) – probe (514 nm) on TTFAQ in degassed chloroform solution. The spectra of authentic TTFAQ^{2+} and the ketone are shown offset for reference.

This observation is consistent with the disproportionation of the radical cation according to equation A.2.

$$TTFAQ^{+\bullet} + TTFAQ^{+\bullet} \longrightarrow TTFAQ + TTFAQ^{2+}$$

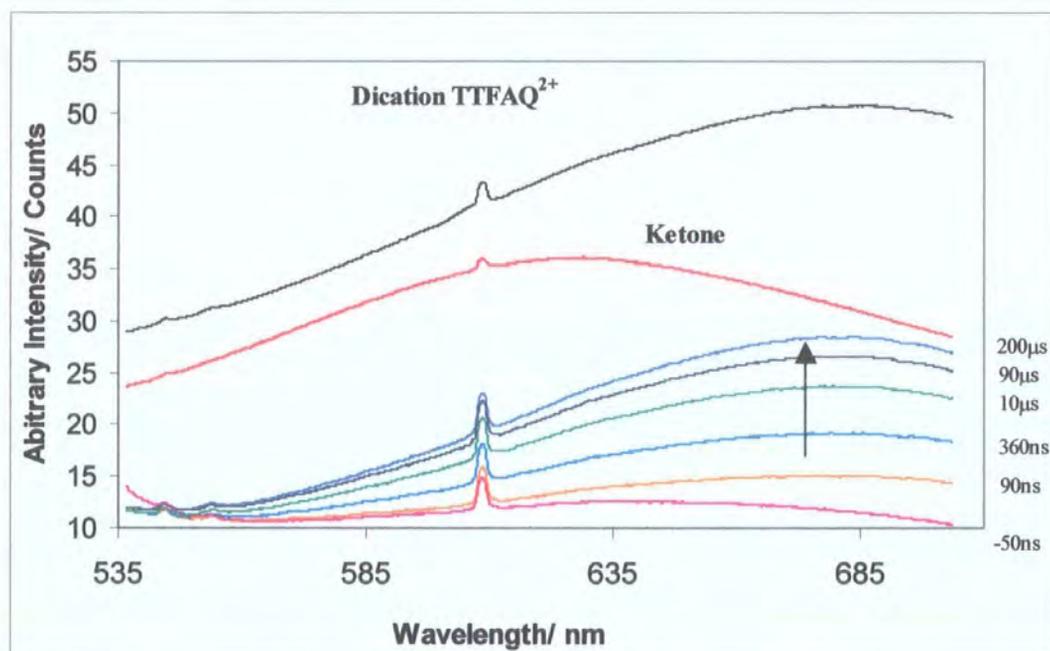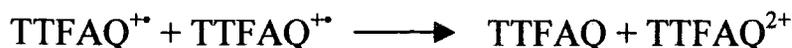<div align="right">Equation A.2.</div>

Thus, the non-fluorescent radical cation, which is formed immediately upon irradiation by the 266 nm pump pulse forms the fluorescent dication, $TTFAQ^{2+}$ *in degassed solution* and this process occurs over a period of tens of microseconds. In contrast, *in aerated solution*, $TTFAQ^{2+}$ is not observed: the ketone is the only detectable product.

A.4. Conclusions

The work described above has provided evidence for the first time of the radical cation, $TTFAQ^{+\bullet}$, formed by the photoionisation of the parent in chlorinated hydrocarbon solutions. This radical cation has been characterised by transient absorption and resonance Raman spectroscopies. In degassed solution this species appears to disproportionate to give the known dication $TTFAQ^{2+}$, a species that has been characterised by spectroelectrochemical techniques and the crystal structure determined. Aerated solutions of TTFAQ also show the presence of the radical cation, but the photodegradation product observed in these solutions is the ketone. There was no evidence for the formation of the dication in the aerated solutions although the mechanism of the formation of the ketone remains uncertain.

A.5. References

1. Wudl F., G.M. Smith and E. Hufnagel (1970) Bis-1,3-dithiolium Chloride: An unusually stable organic radical cation. *J. Chem. Soc. Chem. Comm.*, 1453-1454.

2. Hünig S., G. Kiesslich, H. Quast and D. Scheutzow (1973) Tetrathioethylenes and their higher oxidation levels. *Liebigs Ann. Chem.*, 310-323.

3. Bryce M. R. (2000) Functionalised tetrathiafulvalenes: new applications as versatile π-electron systems in materials chemistry. *J. Mater. Chem.*, **10**, 589-598.

4. Hansen T.K. and J. Becher. (1993) Applications of the 1,3-dithiole unit in a post-ttf era. *Adv. Mater.*, **5**, 288-292.

5. Sugimoto T., H. Awaji, I. Sugimoto, Y. Misaki, T. Kawase, S. Yoneda and Z. Yoshida (1989) Ethylene analogues of tetrathiafulvalene and tetraselenafulvalene: New donors for organic metals. *Chem. Mater.*, **1**, 535-547.

6. Bryce M.R., A.J. Moore, B.K. Tanner, R. Whitehead, W. Clegg, F. Gerson, A. Lamprecht and S. Pfenninger (1996) Vinylogous tetrathiafulvalene (TTF) π-electron donors and derived radical cations: ESR spectroscopic, magnetic and X-ray structural studies. *Chem. Mater.*, **8**, 1182-1188.

7. Moore A.J., M.R. Bryce, A.S. Bastanov, A. Green, J.A.K. Howard, M.A. McKervey, P. McGuigan, I. Ledoux, E. Ortí, R. Viruela, P.M. Viruela and B. Tarbit (1998) New 1,3-dithiol-2-ylidene donor-π-acceptor chromophores with intramolecular charge-transfer properties, and related donor-π-donor molecules: synthesis, electrochemistry, X-ray crystal structures, non-linear optical properties and theoretical calculations. *J. Mater. Chem.*, **8**, 1173-1184.

8. Yamashita Y., M. Tomura, M.B. Zaman, and M. Imaeda (1998) Synthesis and properties of novel tetrathiafulvalene vinylogues. *Chem. Commun.*, 1657-1658.

9. Yamada J., H. Nishikawa and K. Kikuchi (1999) Newly modified TTF and DSDTF donors for developing molecular-based organic metals. *J. Mater. Chem.*, **9**, 617-628.

10. Yamashita Y., Y. Kobayahsi and T. Miyashi (1989) *p*-Quinodimethane analogues of tetrathiafulvalene. *Angew. Chem. Int. Ed. Engl.*, **28**, 1052-1053.

11. Moore A.J. and M R. Bryce (1991) Highly conjugated π-electron donors for organic metals − synthesis and redox chemistry of new 1,3-dithiole and 1,3-selenathiole derivatives. *J.Chem. Soc. Perkin Trans. 1*, 157-168.

12. Bastanov A.S., M.R. Bryce, M.A. Coffin, A. Green, R.E. Hester, J.A.K. Howard. I.K. Lednev, N. Martín, A.J. Moore, J.N. Moore, E. Ortí, L. Sánchez, M. Savíron, P.M. Viruela, R. Viruela and T-Q. Ye (1998) Donor-π-acceptor species derived from functionalised 1,3-dithiol-2-ylidene anthracene donor units exhibiting photoinduced electron transfer properties: Spectroscopic, electrochemical, X-ray crystallographic and theoretical studies. *Chem. Eur. J.*, **4**, 2580-2592.

13. Bryce M.R., M.A. Coffin, M.B. Hursthouse, A.I. Karaulov, K. Müllen and H. Scheich (1991) Synthesis, X-ray crystal structure and multistage redox properties of a severely distorted tetrathiafulvalene donor. *Tetrahedron Lett.*, **32**, 6029-6033.

14. Bryce M.R., T. Finn, A.S. Bastanov, R. Kataky, J.A.K. Howard and S.B. Lyubchik (2000) 2,6-dialkoxy-9,10-bis(1,3-dithiole-2-ylidene)-9,10-dihydroanthracene derivatives: Synthesis, electrochemistry and X-ray crystal structures of neutral and dication species. *Eur. J. Org. Chem.*, 1199-1205.

15. Hünig S. and H. Berneth (1980) Two step reversible redox systems of the Weitz type. *Top. Curr. Chem.*, **92**, 1-44.

16. Bryce M.R., T. Finn, A.J. Moore, A.S. Bastanov, and J.A.K. Howard (2000) Syntheses and X-ray crystal structures of functionalised 9,10-bis(1,3-dithiole-2-ylidene)-9,10-dihydroanthracene derivatives. *Eur. J. Org. Chem.*, 51-60.

17. Bryce M.R., A.S. Bastanov, T. Finn, T.K. Hansen, A.J. Moore, J.A.K. Howard, M. Kamenjicki I.K. Lednev and S.A. Asher (2000) Molecular Saddles Part 5: Crown-annelated 9,10-bis(1,3-dithiol-2-ylidene)-9,10-dihydroanthracene derivatives as cation sensors: synthesis, X-ray crystal structures, voltammetric and spectroscopic monitoring of metal complexation. Submitted to *Eur. J. Org. Chem.*

18. Bryce M.R., A.J. Moore, M. Haslan, G.J. Ashwell, A.T. Fraser, W. Clegg, M.B. Hursthouse and A.I. Karaulov (1990) Electrical and magnetic properties and X-ray crystal structures of a highly conductive 4-1 complex of tetracyanoquinodimethane and a tetrathiafulvalene derivative. *Angew. Chem. Int. Ed. Engl.*, **29**, 1450-1452.

19. Triki S., L. Ouahab, D. Lorcy and A. Robert (1993) Structure of anthracenediylidene - bis - (1,3 - dithiole) - tetracyanoquinodimethane - bis - (cyanoformyl) phenyl-malononitrile ylide monohydrate (EXT-TTF^{2+})•TCNQ•(Y-)$_2$•H$_2$0. *Acta Cryst.*, **C49**, 1189-1192.

20. Martín N., L. Sánchez, C. Seoane, E. Ortí, P.M. Viruela and R. Viruela (1998) Synthesis, properties and theoretical characterization of largely π-extended tetrathiafulvalene derivatives with quinoid structures. *J. Org. Chem.*, **62**, 1268-1279.

21. Herranz M.A., N.L. Martín, L. Sánchez, J. Garín, J. Orduna, R. Alcalá, B. Villacampa and C. Sánchez, (1998) Synthesis and characterization of novel NLO-phores from π-extended tetrathiafulvalene (TTF) derivatives. *Tetrahedron*, **54**, 11651-11658.

22. Herranz M.A. and N.L. Martín (1999) A new building block for Diels-Alder reactions in extended tetrathiafulvalenes: Synthesis of a novel electroactive C60-based dyad. *Org. Lett.*, **1**, 2005-2007.

23. Christensen C.A., M.R. Bryce, A.S. Bastanov, J.A.K. Howard, J.O. Jeppesen and J. Beecher (1999) The first Diels-Alder reaction of a 9.10-bis(1,3-dithiole-2-ylidene)-9,10-dihydroanthracene derivative: synthesis and crystal structure of a novel donor-π-anthraquinone dyad. *Chem. Commun.*, 2433-2434.

24. Martín N., L. Sánchez and D.M. Guldi (2000) Stabilisation of charge-separated states via gain of aromaticity and planarity of the donor moiety in C-60 based dyads. *Chem. Commun.*, 113-114.

25. Guldi D.M., L. Sánchez and N. Martín, (2000) Radiolytic formation and characterisation of the π-radical cation and dication of π-extended-TTF's, Pre-print.

26. Duff C.M. and G.A. Heath (1991) Stepwise ligand-additivity effects on electrode potentials and charge transfer spectra in hexahalide, mixed halide, nitrile, and hexakis(nitrile) complexes of ruthenium (IV), ruthenium (III) and ruthenium (II). *Inorg. Chem.*, **30**, 2528-2535.

27. Beeby A. and A.E. Jones (2000) The photophysical properties of menthyl anthranilate: A UV-A sunscreen. *Photochem. Photobiol.*, **72(1)**, 10-15.

28. Schrader B. (1989) *Raman:Infrared Atlas of Organic Compounds*,VCH Verlaggesellschaft, Weinheim.

29. *SMART & SAINT*, Area detector control and integration software, Ver. 6.01. Bruker Analytical X-Ray Systems, Madison, Wisconsin, U.S.A, 1999.

30. Sheldrick G.L., (1998) *SADABS*: Program for scaling and correction of area detected data. University of Göttingen, Germany.

31. *SHELXTL*, An integrated system for solving, refining and displaying crystal structures from diffraction data, Ver. 5.10. Bruker Analytical X-Ray Systems, Madison, Wisconsin, U.S.A, 1997.

32. Casada J., V. Hernández, Y. Kanemitsu and J.Y. López Navarrete (2000) Infrared and Raman spectra of a new radical cation charged defect created on a well-barrier-well thiophene-based oligomer. *J. Raman. Spec.*, **31**, 565-570.

Appendix B

Publications, Presentations,

Courses and Seminars

B.1. Publications and Presentations

B.1.1. Publications

"The Photophysical Properties of Menthyl Anthranilate: A UV-A Sunscreen"

Andrew Beeby and Allison E. Jones.

Photochem. Photobiol., 2000, **72(1)**, 10-15.

"Molecular Saddles Part 6: Photochemistry of the π-Extended 9,10-Bis(1,3-dithiol-2-ylidene)-9,10-dihydroanthracene System: Generation and Characterisation of the Radical Cation, Dication and Derived Products."

Allison E. Jones, Christian A. Christensen, Dmitrii F. Perepichka, Andrei S. Batsanov, Andrew Beeby, Paul Low, Martin R. Bryce and Anthony W. Parker.

Accepted by *Chem. Eur. J.*, October 2000.

"ns-TR[3] Study of TTF-Anthraquinone Hybrids"

A. Beeby, M.R. Bryce, A.E. Jones, C. Christensen, P.J. Low, D.F. Peripechka, A.W. Parker and I.P Clark.

CRC Rutherford Appleton Laboratory Central Laser Facility Annual Report, 1999-2000, **RAL-TR-2000-034**, 119.

.

B.1.2. Presentations
B.1.2.1. Poster Presentations

"The Use of Infrared Spectroscopy for the Detection and Analysis of Sunscreens",

Allison E. Jones and Andrew Beeby.

ICI Poster Competition, University of Durham, 21st December 1998.

"The Photophysical Properties of Anthranilate Esters"

Allison E. Jones and Andrew Beeby.

FRIS 1999, Lisbon, Portugal, 29th August – 1st September 1999.

"The Photophysics of Anthranilate Esters"

Allison E. Jones and Andrew Beeby.

ICI Poster Competition, University of Durham, 20th December 1999.

"The Photophysical Properties of N-acetyl-menthyl Anthranilate "

Allison E. Jones and Andrew Beeby.

FRIS 2000, Durham, UK, 27th – 30th August 2000.

B.1.2.2. Oral Presentations

"The Photochemistry of Sunscreens"

Graduate Symposia 2000, University of Durham, 21st June 2000.

B.2. Conferences

Royal Society of Chemistry, 1998 National Congress and Young Researchers Meeting, University of Durham, 6th-9th April 1998.

FRIS 1999, Lisbon, Portugal, 29th August – 1st September 1999.

FRIS 2000, Durham, UK, 27th – 30th August 2000.

B.3. Courses

Department of Chemistry, University of Durham

PG6   Advanced Mass Spectrometry, Dr. M. Jones and Dr. C.A. Woodward

PG7   Experimental Design and Instrumentation , Professor J.P.S. Badyal

PG8   Molecular Modelling, Dr. M. Wilson

B.4. Seminars

B.4.1. 1997-1998

1. "Spectroscopy of Liquid Interfaces: From Bio-organic Chemistry to Atmospheric Chemistry". Dr. J. Frey, *University of Southampton.*

2. "A Random Walk in Polymer Science". Professor R.W. Richards, *University of Durham.*

3. "Energy Transfer and Optical Harmonics in Molecular Systems". Professor D. Andrews, *University of East Anglia.*

4. "What's in a Formula? Some Chemical Controversies of the 19th Century". Professor J. Brooke, *University of Lancaster.*

5. "Aspects of Metal and Carbon Cluster Chemistry". Professor D. Cardin, *University of Reading.*

6. "The Synthesis of dendrimers using highly selective chemical reactions". Dr. S. Rannard, *Courtaulds Coatings, Coventry.*

7. "Classical and Non-classical Fullerenes". Professor P. Fowler, *University of Exeter.*

8. "Surprises in the Photochemistry of Tropospheric Ozone". Professor G. Hancock, *University of Oxford.*

9. "How to make Phthalocyanine Films and what to do with them". Professor M.J. Cook, *University of East Anglia.*

10. "Raman Microscopy of Molecular materials: Confocal, Direct Imaging and Scanning Near Field". Professor D. Batchelder, *University of Leeds.*

11. "Experiments with Singlet Oxygen". Dr. Tamas Vidoczy, *Central Research Institute for Chemistry, Budapest.*

B.4.2. 1998-1999

1. "New Perspectives on Interfacial Processes using Dynamic Electrochemistry". Prof. P. Unwin, *University of Warwick.*

2. "In Search of Hypervalent Free Radicals and Carbocations". Prof. J.C. Scaiano, *University of Ottawa.*

3. "Tailoring Solid Surfaces". Prof. J.P.S. Badyal, *University of Durham.*

4. "New methodology for the asymmetric transfer hydrogenation of ketones". Dr. M. Wills, *University of Warwick.*

5. "Polymer Electronics". Dr. I. Samuel, *University of Durham.*

6. "Multi-nuclear Solid-state Magnetic Resonance Studies of Nano-crystalline Oxides and Glasses". Dr. M. Smith, *University of California, Berkeley.*

7. "Luminescence of large molecules: from conducting polymers to coral reefs:. Dr. A. Jones, *University of Edinburgh.*

8. "Surfactant Adsorption and Marangoni Flow at expanding liquid surfaces". Dr. C. Bain, *University of Oxford.*

9. "Microelectrode techniques for the study of immobilised enzymes and nucleic acids". Dr. B. Horrocks, *University of Newacstle.*

10. "Biomolecular Damage by Free Radicals: New Insights through ESR spectroscopy". Prof. B. Gilbert, *University of York.*

11. "Crystalline Schiff base Complexes of the Lanthanide Series". Dr. K. Binnemans, *Katholieke University Leuven, Herverlee, Belguim.*

12. "Ozone Holes and Ozone Hills". Prof. J. Sodeau, *University of Cork.*

13. "The Synthesis and Characterisation of Liquid-Crystalline Transition Metal Complexes". Prof. D. Bruce, *University of Exeter.*

B.4.3. 1999-2000

1. "Chocolate for the Next Millenium". Dr. S. Beckett, *Nestle, UK.*

2. "Aspects of Complexation and Supramolecular Chemistry". Prof. S. Lincoln, *University of Adelaide.*

3. "Improving Organic LEDs by Molecular, Optical and Device Design". Dr. I. Samuel, *University of Durham.*

4. "Trace Evidence – a Challenge for the Forensic Scientist". Prof. B. Caddy, *University of Strathclyde.*

5. "Controlled Growth of Inorganic and Organic Semi-conductor Thin Films". Prof. T. Jones, *Imperial College, London.*

6. "Miniaturised Chemical Analysis (Lab-on-a-Chip): Functional or Merely Fashionable?". Dr. P.R. Fielden, *UMIST, Manchester.*

7. "A Little Light Relief". Prof. D. Phillips O.B.E., *Imperial College, London.*

8. "The Flow of Polymer Blends". Dr. N. Clarke, *UMIST, Manchester.*

9. "Computer Simulation of Interfaces: fact and friction". Prof. D. Tildsely, Head of Reasearch, *Unilever.*

10. "Chiral NMR in Liquid Crystals". Prof. J. Courtieu, *Universite de Paris-Sud, Orsay.*

11. "Ultrafast Molecular and Protein Dynamics seen through their vibrations". Prof. R. Hochstrasser, *University of Pennsylvania.*

12. "Fakes, Forensics and Failures". Dr. R. Lehrle, *University of Birmingham.*

13. "Carbon Toys". Dr. P.J. Low, *University of Durham.*